General Disclaimer

One or more of the Following Statements may affect this Document

- This document has been reproduced from the best copy furnished by the organizational source. It is being released in the interest of making available as much information as possible.

- This document may contain data, which exceeds the sheet parameters. It was furnished in this condition by the organizational source and is the best copy available.

- This document may contain tone-on-tone or color graphs, charts and/or pictures, which have been reproduced in black and white.

- This document is paginated as submitted by the original source.

- Portions of this document are not fully legible due to the historical nature of some of the material. However, it is the best reproduction available from the original submission.

von KARMAN INSTITUTE

FOR FLUID DYNAMICS

LECTURE SERIES 3 - Part 5

AGARD-VKI LECTURE SERIES ON

MECHANICS OF BOUNDARY LAYER TRANSITION

January 15 - 19, 1968

BOUNDARY-LAYER STABILITY THEORY IN INCOMPRESSIBLE AND COMPRESSIBLE FLOW

Leslie M. MACK

RHODE-SAINT-GENESE, BELGIUM

JANUARY 1968

Boundary-Layer Stability Theory in Incompressible and Compressible Flow

Leslie M. Mack

Jet Propulsion Laboratory
California Institute of Technology
Pasadena, California

December 1967

Notes prepared for the VKI-AGARD Lecture Series:

Mechanics of Boundary-Layer Transition

von Karman Institute for Fluid Dynamics
Rhode-Saint-Genese, Belgium

January 15-19, 1968

These notes represent, in part, the results of one phase of research carried out at the Jet Propulsion Laboratory, California Institute of Technology, under Contract No. NAS7-100, sponsored by the National Aeronautics and Space Administration.

PART A. INCOMPRESSIBLE FLOW

1. Introduction

The purpose of the stability theory of the laminar boundary layer is to determine whether a small disturbance introduced into the boundary layer will amplify or damp. If the disturbance damps, the boundary layer should remain laminar. If the disturbance amplifies, and by a sufficient amount, then transition to turbulence should eventually take place. The stability theory cannot predict the location of transition. What it can do is to establish those states of the boundary layer which are most likely to lead to transition, to identify those frequencies which are the most dangerous, and to indicate how the external parameters can best be changed to avoid transition.

It will be the purpose of these lectures to give the fundamentals of the stability theory, to establish its chief results, and to give an idea of the physical mechanisms at work. Detail, except for a few topics felt to be of particular importance, will be left to the numerous references. Of the latter, there now exist a number of review articles and two books. The articles are by Shen (1964), Stuart (1963), Reid (1965), and Drazin and Howard (1966). The latter is devoted exclusively to the inviscid theory. The article by Reid is particularly complete on the asymptotic theory. The books are by Lin (1955) and Betchov and Criminale (1967). An older review article that can still be read with profit is Prandtl (1935). The well-known book of Schlichting (1960) on boundary-layer theory includes two chapters on boundary-layer stability.

There has always been a certain air of mystery about stability theory for many people. This is probably a result of the elaborate mathematical procedures that were necessary to arrive at any results. The well-developed inviscid stability theory suffered the embarrassment of predicting complete stability for two of the most common flows, the Blasius boundary layer and flow in a pipe. The viscous theory was of such a complexity that almost no general results could be established. In spite of the many difficulties, the instability of the incompressible Blasius boundary layer was worked out by Tollmien (1929), and this theory received confirmation in its essential aspects in the classic experiment of Schubauer and Skramstad (1947).

Since about 1960, the approach to stability theory has been considerably modified by the modern high-speed digital computer. Instead of the painful extraction of a handful of numerical results from elaborate and time-consuming calculations of dubious accuracy, the computer can produce an immense quantity of accurate numerical results directly from the differential equations. The ease of producing these results makes it possible to not only solve any specific problem, but also to fill in the gaps in our understanding which still exist because of the difficulty of analysis. For example, the theory deals almost exclusively with disturbances of neutral stability, which from a practical standpoint are of limited interest. The computer permits the study of the much more interesting disturbances of maximum amplification, which can be obtained as easily, indeed more easily, than the neutral disturbances.

In spite of the limitations of the theory in producing numerical results, it is still essential for our understanding of boundary-layer stability and as a guide to the formulation and use of the computer programs. For this reason, it will be covered in these lectures, and will provide the motivation for the entire subject. The computer will elaborate and provide the main body of numerical results.

Before we get into the main body of the subject, a few words are in order to orient those who are new to this field. The stability theory considers individual sinusoidal disturbances whose amplitude is small enough so that a linear theory can be used. The wave number in the free-stream direction is $\alpha (= 2\pi/\lambda$, where λ is the wave length). The wave may be two-dimensional, with the normal to the wave front parallel to the free-stream direction, or it may be oblique, with the wave normal at an angle ψ to the free-stream direction. The disturbance propagates in the downstream direction with phase velocity c_r. The phase velocity is always less than the free-stream velocity, U_1, so that at some point in the boundary layer the mean velocity is equal to c_r. This point is called the critical point, and it plays a central role in the mathematical theory.

At a given distance from the origin of the boundary layer, or better, at a given Reynolds number R_x ($= U_1 x/\nu$, where ν is the kinematic viscosity), the disturbance may be in one of three states: damped, neutral, or amplified. The numerical results obtained from the stability theory are often presented in the form of neutral-stability diagrams which show graphically which state a given disturbance is in at each Reynolds number. There are two general kinds of neutral-stability diagrams to be found, as is shown in Fig. 1.1.

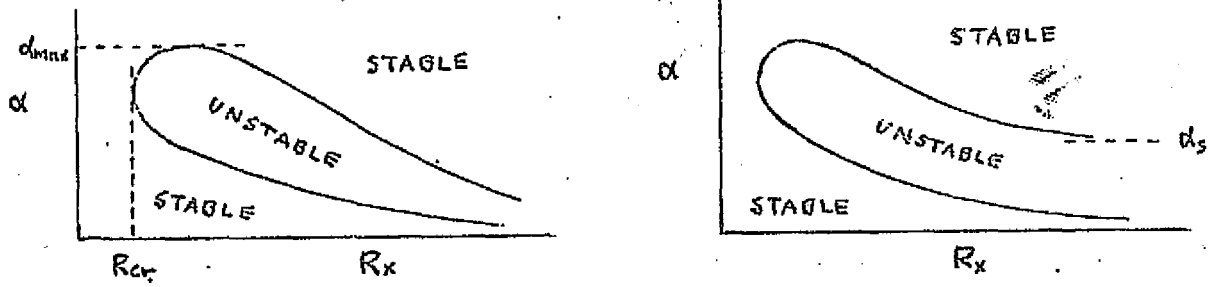

(a) Inviscid stability (Blasius type)

(b) Inviscid instability (inflexion point)

Fig. 1.1. Typical curves of neutral stability

In these diagrams, α is plotted against R_x. Disturbances are neutral at those values of α and R_x which lie on the contour marked neutral; they are amplified inside of the contour; and they are damped outside of the contour. With a neutral-stability curve of type (a), all wave numbers are damped at sufficiently high Reynolds numbers. In this case, the mean flow is said to have inviscid stability. Since decreasing Reynolds number, or increasing viscosity, can lead to instability, it is apparent that viscosity does not act solely to damp out disturbances, but actually can have a destabilizing influence. The flat plate, or Blasius, boundary layer is an example of a flow which is unstable only through the action of viscosity. With a neutral-stability curve of type (b), wave numbers smaller than α_s, the neutral wave number at infinite Reynolds number, remain unstable no matter how large the Reynolds number becomes. A mean flow with a type (b) neutral-stability curve is said to have inviscid instability. The boundary layer in an adverse pressure gradient is an example of a flow of this kind.

In both cases (a) and (b), all disturbances with $\alpha < \alpha_{max}$ are unstable for some range of Reynolds numbers. The Reynolds number, R_{cr} below which no amplification at all is possible, is called the critical Reynolds number. It is often an objective of the stability theory to compute R_{cr}, although it must be cautioned that it has a limited significance and is often not the best indicator of the relative instability of various mean flows.

Although the wave number is a useful quantity in developing the theory, the frequency, which is equal to αc_r, is more useful in practice. A disturbance which is introduced into the boundary layer with a particular frequency will preserve that frequency as it progresses downstream, while the wave number will change. A frequency f which crosses the unstable region

will be damped from the leading edge up to R_L, the first neutral point. Between R_L and R_U, the second neutral point, it will be amplified; downstream of R_U it will be damped again. If the magnitude of the disturbance becomes large enough before R_U is reached, then the nonlinear processes which eventually lead to transition will take over, and the disturbance will continue to grow even though the linear theory says it should damp.

The theory can be used to calculate amplification and damping rates as well as the wave number, Reynolds number and phase velocity of neutral disturbances. For example, it is possible to compute the amplification rate as a function of frequency at a given R_X. The neutral-stability curve only identifies the range of unstable frequencies, but the calculation of the amplification rates tells how fast each frequency is growing, and which frequency is growing the most. Perhaps even more useful than the amplification rate is the overall growth of a disturbance of constant frequency as it travels through the unstable region. This result can be obtained from the theory as a supplemental calculation once the amplification rates are known. Consequently, it is possible to identify, for each initial spectrum, the frequency which has the largest amplitude at each Reynolds number. It is presumably one of these frequencies which, when it reaches some critical amplitude, triggers the whole transition process.

2. Derivation of Stability Equations

2.1 Formulation of theory

The conventional form of the theory will be used throughout these lectures. That is, the actual boundary layer is replaced by a parallel flow having the same velocity profile as the boundary layer at a particular Reynolds number. A single Fourier component is considered as the disturbance. It extends to infinity both upstream and downstream and grows or damps in time, not in space. However, the physical problem suggests a disturbance growing in space, and the theory could be carried through for this type of disturbance.

The Navier-Stokes equations of a viscous incompressible fluid are:

$$\frac{\partial u}{\partial t} + u\frac{\partial u}{\partial x} + v\frac{\partial u}{\partial y} + w\frac{\partial u}{\partial z} = -\frac{1}{\rho}\frac{\partial p}{\partial x} + \nu\left(\frac{\partial^2 u}{\partial x^2} + \frac{\partial^2 u}{\partial y^2} + \frac{\partial^2 u}{\partial z^2}\right) \tag{2.1}$$

$$\frac{\partial v}{\partial t} + u\frac{\partial v}{\partial x} + v\frac{\partial v}{\partial y} + w\frac{\partial v}{\partial z} = -\frac{1}{\rho}\frac{\partial p}{\partial y} + \nu\left(\frac{\partial^2 v}{\partial x^2} + \frac{\partial^2 v}{\partial y^2} + \frac{\partial^2 v}{\partial z^2}\right) \tag{2.2}$$

$$\frac{\partial w}{\partial t} + u\frac{\partial w}{\partial x} + v\frac{\partial w}{\partial y} + w\frac{\partial w}{\partial z} = -\frac{1}{\rho}\frac{\partial p}{\partial z} + \nu\left(\frac{\partial^2 w}{\partial x^2} + \frac{\partial^2 w}{\partial y^2} + \frac{\partial^2 w}{\partial z^2}\right) \tag{2.3}$$

$$\frac{\partial u}{\partial x} + \frac{\partial v}{\partial y} + \frac{\partial w}{\partial z} = 0 \tag{2.4}$$

The x axis can be considered to be in the direction of the free-stream velocity; the y axis is normal to the surface; and the z axis is normal to the x and y axes. The velocities u , v , w are in the x, y, z directions, respectively. The density is ρ , the pressure p , and the kinematic viscosity $\nu = \mu/\rho$. The first three equations are the x, y, z momentum equations; the fourth equation the equation of continuity.

2.2 Linearization of equations

All flow quantities are divided into a mean flow term and a fluctuation term:

$$q(x, y, z, t) = Q(x, y, z) + q'(x, y, z, t) \tag{2.5}$$

The mean-flow terms (denoted by capital letters) satisfy the boundary-layer equations, which are

$$U \frac{\partial U}{\partial x} + V \frac{\partial U}{\partial y} + W \frac{\partial U}{\partial z} = -\frac{1}{\rho} \frac{\partial P}{\partial x} + \nu \frac{\partial^2 U}{\partial y^2} \tag{2.6}$$

$$0 = -\frac{1}{\rho} \frac{\partial P}{\partial y} \tag{2.7}$$

$$U \frac{\partial W}{\partial x} + V \frac{\partial W}{\partial y} + W \frac{\partial W}{\partial z} = -\frac{1}{\rho} \frac{\partial P}{\partial z} + \nu \frac{\partial^2 W}{\partial y^2} \tag{2.8}$$

$$\frac{\partial U}{\partial x} + \frac{\partial V}{\partial y} + \frac{\partial W}{\partial z} = 0 \tag{2.9}$$

In the linear case it will not be necessary to distinguish between the undisturbed mean flow and the mean flow in the presence of a disturbance. The replacement for (2.6) in the nonlinear case is given in Section 10 by (10.6). When the expressions (2.5) are substituted into (2.1)-(2.4); the negligible mean-flow terms (by the boundary-layer approximation) dropped; the mean boundary-layer equations subtracted out; and the nonlinear terms neglected; there remains the following system of equations:

$$\frac{\partial u'}{\partial t} + u' \frac{\partial U}{\partial x} + U \frac{\partial u'}{\partial x} + v' \frac{\partial U}{\partial y} + V \frac{\partial u'}{\partial y} + w \frac{\partial U}{\partial z} + W \frac{\partial u'}{\partial z} = -\frac{1}{\rho} \frac{\partial p'}{\partial x} + \nu \left(\frac{\partial^2 u'}{\partial x^2} + \frac{\partial^2 u'}{\partial y^2} + \frac{\partial^2 u'}{\partial z^2} \right) \tag{2.10}$$

$$\frac{\partial v'}{\partial t} + u' \frac{\partial V}{\partial x} + U \frac{\partial v'}{\partial x} + v' \frac{\partial V}{\partial y} + V \frac{\partial v'}{\partial y} + w' \frac{\partial V}{\partial z} + W \frac{\partial v'}{\partial z} = -\frac{1}{\rho} \frac{\partial p'}{\partial y} + \nu \left(\frac{\partial^2 v'}{\partial x^2} + \frac{\partial^2 v'}{\partial y^2} + \frac{\partial^2 v'}{\partial z^2} \right) \tag{2.11}$$

$$\frac{\partial w'}{\partial t} + u' \frac{\partial W}{\partial x} + U \frac{\partial w'}{\partial x} + v' \frac{\partial W}{\partial y} + V \frac{\partial w'}{\partial y} + w' \frac{\partial W}{\partial z} + W \frac{\partial w'}{\partial z} = -\frac{1}{\rho} \frac{\partial p'}{\partial z} + \nu \left(\frac{\partial^2 w'}{\partial x^2} + \frac{\partial^2 w'}{\partial y^2} + \frac{\partial^2 w'}{\partial z^2} \right) \tag{2.12}$$

$$\frac{\partial u'}{\partial x} + \frac{\partial v'}{\partial y} + \frac{\partial w'}{\partial z} = 0 \tag{2.13}$$

2.3 Reduction to parallel-flow equations

The above equations are still too complicated and must be reduced further. If it is assumed that all velocity fluctuations are of the same order of magnitude, and all derivatives of velocity fluctuations are of the same order of magnitude (but possibly different from the fluctuations), then the application of the boundary-layer relations to the mean flow quantities will result in the desired simplification. These relations are:

$$V << U, W \qquad \frac{\partial}{\partial y} >> \frac{\partial}{\partial x}, \frac{\partial}{\partial z} \tag{2.14}$$

The terms with velocity fluctuations are compared separately, and those with derivatives of the fluctuations are also compared separately. The equations reduce to

$$\frac{\partial u'}{\partial t} + U \frac{\partial u'}{\partial x} + v' \frac{\partial U}{\partial y} + W \frac{\partial u'}{\partial z} = -\frac{1}{\rho} \frac{\partial p'}{\partial x} + \nu \nabla^2 u' \tag{2.15}$$

$$\frac{\partial v'}{\partial t} + U\frac{\partial v'}{\partial x} + v'\frac{\partial V}{\partial y} + W\frac{\partial v'}{\partial z} = -\frac{1}{\rho}\frac{\partial p'}{\partial y} + \nu\nabla^2 v' \qquad (2.16)$$

$$\frac{\partial w'}{\partial t} + U\frac{\partial w'}{\partial x} + v'\frac{\partial W}{\partial y} + W\frac{\partial w'}{\partial z} = -\frac{1}{\rho}\frac{\partial p'}{\partial z} + \nu\nabla^2 w' \qquad (2.17)$$

$$\frac{\partial u'}{\partial x} + \frac{\partial v'}{\partial y} + \frac{\partial w'}{\partial z} = 0 \qquad (2.18)$$

Now a close inspection reveals that the coefficients of the v' terms in (2.15) and (2.17) are an order of magnitude larger than the coefficients of the $\partial/\partial x$ and $\partial/\partial z$ terms on the right-hand sides, while in (2.16) the coefficient of v' is of the same order as the other two terms. Since $v' << U, W$ for the linearization to be valid, the $v'\,\partial V/\partial y$ term can be dropped from (2.16). In (2.15) and (2.17), although $\partial U/\partial y$ and $\partial W/\partial z$ are an order of magnitude larger than U and W, the $v'\partial U/\partial y$ and $v'\partial W/\partial y$ terms are not necessarily larger than the terms immediately preceding and following, because although v' is always small, the derivatives of u' and v' do not have to be small. Consequently, (2.16) is replaced by

$$\frac{\partial v'}{\partial t} + U\frac{\partial v'}{\partial x} + W\frac{\partial v'}{\partial z} = -\frac{1}{\rho}\frac{\partial p'}{\partial y} + \nu\nabla^2 v' \qquad (2.16a)$$

and (2.15) and (2.17) remain as given. The final approximation is to consider that for disturbances for which the wavelength is not too long, the mean-flow quantities will be slowly varying functions of x and z compared with the fluctuations. Therefore, U and W can be taken as functions of y alone, and the stability of the velocity profile at a given x is considered independently of the rest of the boundary layer.

The final system of equations (2.15), (2.16a), (2.17), (2.18) is the same as would have been obtained by making the assumption of parallel flow at the outset. This assumption is

$$U = U(y) \quad , \quad W = W(y) \quad , \quad V = 0 \tag{2.19}$$

The argument given above that led to these equations is far from rigorous and is included mainly to point out the terms that are neglected in the parallel-flow equations. These equations are the basis of almost all stability investigations. They are exact for the flow in a channel, but are only an approximation for other flows. Their adequacy is best tested by comparison of the results with experiment. Also the magnitudes of the neglected terms can be checked a posteriori, and it is hoped that some day a more exact theory will be available for comparison.

2.4 Nondimensional equations

Before proceeding further, the equations will be written in dimensionless form. The characteristic velocity is U_1^*, the free-stream velocity in the x^* direction; the characteristic length is δ, the boundary-layer thickness; and the characteristic pressure is p_1^*, the free-stream pressure. If the dimensional quantities are designated by asterisks (except for the boundary-layer thickness), the nondimensional quantities are

$$u' = \frac{u^{*'}}{U_1^*} \quad , \quad v' = \frac{v^{*'}}{U_1^*} \quad , \quad U = \frac{U^*}{U_1^*} \quad , \quad W = \frac{W^*}{U_1^*}$$

$$x = \frac{x^*}{\delta} \quad , \quad y = \frac{y^*}{\delta} \quad , \quad z = \frac{z^*}{\delta} \quad , \quad t = \frac{t^*}{\delta} U_1^* \tag{2.20}$$

$$p = \frac{p^*}{p_1^*}$$

and the Reynolds number is defined as

$$R_\delta = \frac{u_1^* \delta}{\nu^*} \tag{2.21}$$

We define the boundary-layer thickness to be equal to y^* at the point where $u^* = 0.999\, u_1^*$. For the Blasius boundary layer $\delta\sqrt{R_x} / x^* = 6.0$. The dimensionless equations are the same as (2.15)-(2.18) except for the coefficient of the pressure terms and the replacement of ν by $1/R_\delta$. The pressure is nondimensionalized with respect to the free-stream pressure rather than the more usual $\rho^* u_1^{*2}$ in order to make the development here correspond more closely to the derivation for compressible flow to be given later. The dimensionless equations are

$$\frac{\partial u'}{\partial t} + u\frac{\partial u'}{\partial x} + w\frac{\partial u'}{\partial z} + v'\frac{du}{dy} = -\frac{p_1^*}{\rho^* u_1^{*2}}\frac{\partial p'}{\partial x} + \frac{1}{R_\delta}\nabla^2 u' \tag{2.22}$$

$$\frac{\partial v'}{\partial t} + u\frac{\partial v'}{\partial x} + w\frac{\partial v'}{\partial z} = -\frac{p_1^*}{\rho^* u_1^{*2}}\frac{\partial p'}{\partial y} + \frac{1}{R_\delta}\nabla^2 v' \tag{2.23}$$

$$\frac{\partial w'}{\partial t} + u\frac{\partial w'}{\partial x} + w\frac{\partial w'}{\partial z} + v'\frac{dw}{dy} = -\frac{p_1^*}{\rho^* u_1^{*2}}\frac{\partial p'}{\partial z} + \frac{1}{R_\delta}\nabla^2 w' \tag{2.24}$$

$$\frac{\partial u'}{\partial x} + \frac{\partial v'}{\partial y} + \frac{\partial w'}{\partial z} = 0 \tag{2.25}$$

2.5 Boundary conditions

The boundary conditions are that the no-slip condition applies to the disturbance velocities at the wall,

$$u'(0) = 0, \quad v'(0) = 0, \quad w'(0) = 0 \tag{2.26}$$

and that the disturbances go to zero as $y \to \infty$.

$$u'(y) \to 0, \quad v'(y) \to 0, \quad w'(y) \to 0 \quad \text{as} \quad y \to \infty \tag{2.27}$$

Since all of the boundary conditions are homogeneous, it can be expected that solutions will exist only for particular combinations of R_δ and the parameters of the disturbance (α_δ, β_δ, c; see next paragraph). That is, the stability problem is an eigenvalue problem. The values of α_δ, β_δ, c and R_δ for which the boundary conditions can be satisfied are eigenvalues, and the corresponding amplitude functions are eigenfunctions.

2.6 Introduction of Fourier components

The final form of the differential equations, where the coefficients are functions only of y, and x, z, t appear only as derivatives, suggests the following type of disturbance.

$$q(x, y, z, t) = q(y) \exp\left[i(\alpha_\delta x + \beta_\delta z - \alpha_\delta c\, t \right] \tag{2.28}$$

In (2.20), $q(y)$ is a typical complex amplitude function; α_δ and β_δ are the dimensionless wave numbers, $\alpha_\delta = 2\pi\delta/\lambda_x^*$, $\beta_\delta = 2\pi\delta/\lambda_z^*$, where λ_x^* and λ_z^* are the wavelengths in the x and z directions, respectively, and δ is the boundary-layer thickness. If α_δ and β_δ are real, then a complex c will give a disturbance that grows in time. With

$$c = c_r + i c_i \tag{2.29}$$

the phase velocity is c_r. The dimensionless frequency ω is $\alpha_\delta c_r$, and $\alpha_\delta c_i$ is the time derivative of the logarithm of the amplitude,

$$\frac{1}{|q|}\frac{d|q|}{dt} = \alpha_s c_i \qquad (2.30)$$

We shall refer to $\alpha_s c_i$ as the time rate of amplification. It is also possible to take α_s complex and $\alpha_s c$ real, thus providing a disturbance that grows in space. All results to be presented here will be for real α_s and complex c. In (2.28), only the real part of q is to be considered to have physical meaning.

$$\text{Real } q = e^{\alpha_s c_i t}\left[q_r \cos(\alpha_s x + \beta_s z - \alpha_s c_r t) - q_i \sin(\alpha_s x + \beta_s z - \alpha_s c_r t)\right] \qquad (2.31)$$

Equation (2.30) gives the time rate of amplification, but we also need to know the space rate of amplification in order to compute the overall growth of a disturbance as it travels through the boundary layer. The space rate can be obtained from the time rate only if the proper propagation velocity is known. When a wave packet made up of individual waves of the form

$$\exp i(\alpha x - \omega t)$$

propagates through a dispersive medium, i.e., a medium, such as the boundary layer, where the frequency ω is a function of α, each frequency advances with the phase velocity

$$c_r = \frac{\omega}{\alpha} \qquad (2.32)$$

but an overall quantity such as the energy of the wave packet advances with the group velocity

$$c_g = \frac{d\omega}{d\alpha} \tag{2.33}$$

It seems reasonable that the propagation velocity needed to obtain a space rate of amplification from (2.30) would be the group velocity rather than the phase velocity. Therefore, we write

$$\frac{1}{|q|}\frac{d|q|}{dx} = \frac{\alpha_\delta c_i}{c_g} \tag{2.34}$$

In terms of R_δ,

$$\frac{1}{|q|}\frac{d|q|}{dR_\delta} = 2\frac{\alpha_\delta c_i}{c_g} \tag{2.35}$$

and the ratio of the amplitudes at two Reynolds numbers is

$$\frac{|q|_2}{|q|_1} = 2\int_{R_1}^{R_2}\frac{\alpha_\delta c_i}{c_g}\,dR_\delta \tag{2.36}$$

where the integration will normally be carried out for a constant dimensionless frequency. A commonly used form of the dimensionless frequency which varies as the frequency for a constant free stream is

$$F = \frac{\omega^* \nu^*}{U_1^{*2}} = \frac{\alpha_\delta c_r}{R_\delta} \tag{2.37}$$

Equation (2.34) has been demonstrated by Gaster (1963) to be correct for small amplification rates. Unfortunately the group velocity requires some additional calculations to be made, and it is difficult to resist the

temptation to simply replace it with the phase velocity. This temptation is all the more attractive in that c_r rarely differs from c_g by more than about 15%, and, perhaps more important, excellent agreement is obtained with experiment by using c_r. Another difficulty with the group velocity is that if there is a region of anomalous dispersion ($d\omega/d\alpha$ changes sign), the group velocity no longer represents the velocity of energy propagation in this region. In the compressible stability theory, we will find that just such regions can actually occur.

3. Reduction of Equations to Two-Dimensional Form

Inspection of (2.22)-(2.25) reveals that w' and W occur only in $\partial/\partial z$ terms except in the z momentum equation. Consequently, if the disturbances have the form (2.28), and the x, z axes are rotated about the y axis so that the new z axis is parallel to the wave front, the z derivatives in the new coordinate system must be zero, and the w' and W terms will drop out of (2.22), (2.23) and (2.25). This special coordinate system is called the tilde system. If, further, the reference velocity is changed from U_1^* to $\tilde{U}_1^* = U_1^* \cos\psi$, where ψ is the angle between the wave normal and the x axis, then the renormalized equations in the tilde coordinate system are

$$\frac{\partial \tilde{u}'}{\partial \tilde{t}} + \tilde{U}\frac{\partial \tilde{u}'}{\partial \tilde{x}} + \tilde{v}'\frac{d\tilde{U}}{dy} = -\frac{p_1^*}{\rho^* \tilde{U}_1^{*2}}\frac{\partial p'}{\partial \tilde{x}} + \frac{1}{\tilde{R}_\delta}\left(\frac{\partial^2 \tilde{u}'}{\partial \tilde{x}^2} + \frac{\partial^2 \tilde{u}'}{\partial y^2}\right) \tag{3.1}$$

$$\frac{\partial \tilde{v}'}{\partial \tilde{t}} + \tilde{U}\frac{\partial \tilde{v}'}{\partial \tilde{x}} = -\frac{p_1^*}{\rho^* \tilde{U}_1^{*2}}\frac{\partial p'}{\partial y} + \frac{1}{\tilde{R}_\delta}\left(\frac{\partial^2 \tilde{v}'}{\partial \tilde{x}^2} + \frac{\partial^2 \tilde{v}'}{\partial y^2}\right) \tag{3.2}$$

$$\frac{\partial \tilde{w}'}{\partial \tilde{t}} + \tilde{U}\frac{\partial \tilde{w}'}{\partial \tilde{x}} + \tilde{v}'\frac{d\tilde{W}}{dy} = \frac{1}{\tilde{R}_\delta}\left(\frac{\partial^2 \tilde{w}'}{\partial \tilde{x}^2} + \frac{\partial^2 \tilde{w}'}{\partial y^2}\right) \tag{3.3}$$

$$\frac{\partial \tilde{u}'}{\partial \tilde{x}} + \frac{\partial \tilde{v}'}{\partial y} = 0 \tag{3.4}$$

where

$$\tilde{t} = t\cos\psi\,, \quad \tilde{R}_\delta = R_\delta \cos\psi\,, \quad \tilde{u}' = \frac{\tilde{u}'}{\tilde{U}_1^*}\,, \quad \tilde{v}' = \frac{v'}{\tilde{U}_1^*}\,, \quad \tilde{w}' = \frac{\tilde{w}'}{\tilde{U}_1^*} \tag{3.5}$$

and

$$\tilde{U}_1^* = U_1^* \cos\psi \quad , \quad \tilde{R}_\delta = R_\delta \cos\psi \tag{3.6}$$

The original and tilde coordinate systems are shown in Fig. 3.1.

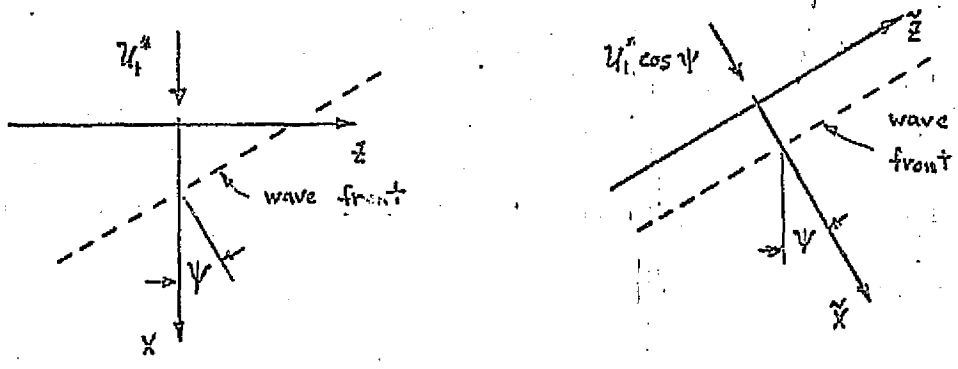

Fig. 3.1. Original and tilde coordinate systems

The system of equations (3.1), (3.2) and (3.4) is identical in all respects to the equations for a two-dimensional disturbance in the boundary layer $\tilde{U}(y)$ at Reynolds number $\tilde{R}_\delta$. The transformation formulas are

$$\begin{aligned}
\tilde{u} &= u + w\tan\psi & \tilde{w} &= -u\tan\psi + w \\
\tilde{u}' &= u' + w'\tan\psi & \tilde{w}' &= -u'\tan\psi + w' \\
\tilde{v}' &= v'/\cos\psi & & \\
x' &= x\cos\psi + z\sin\psi & \tilde{z} &= -x\sin\psi + z\cos\psi
\end{aligned} \tag{3.7}$$

The dimensional normal velocity is unchanged by the transformation, but the dimensionless normal velocity must change because of the change in

the reference velocity. The transformation is, of course, only valid for disturbances of the type (2.28) with a wave front at a fixed angle. The relations between the wave numbers and wave velocities in the two coordinate systems are

$$\tilde{\alpha} = (\alpha_\delta^2 + \beta_\delta^2)^{1/2} = \alpha_\delta / \cos\psi \quad , \quad \tilde{c} = c \tag{3.8}$$

Although the dimensional phase velocity in the $\tilde{x}$ direction is $c^* \cos\psi$, the dimensionless phase velocity $\tilde{c}$ is the same as c because of the difference in the reference velocities in the two cases.

Since $\tilde{U}(y)$ is different for each ψ, a different eigenvalue problem must be solved for each ψ. The only simplification is that a lower order system of differential equations can be used. However, to obtain the disturbance velocities u' and w' in the original coordinate system, it is necessary to know $\tilde{w}'$, which means that the $\tilde{z}$ momentum equation

$$\frac{\partial \tilde{w}'}{\partial \tilde{t}} + \tilde{U} \frac{\partial \tilde{w}'}{\partial \tilde{x}} + \tilde{v}' \frac{d\tilde{W}}{dy} = \frac{1}{\tilde{R}_\delta} \left(\frac{\partial^2 \tilde{w}'}{\partial \tilde{x}^2} + \frac{\partial^2 \tilde{w}'}{\partial y^2} \right) \tag{3.9}$$

must be solved. Note that because of the term $\tilde{v}' d\tilde{W}/dy$, there will always be a $\tilde{w}'$ component as long as there is a $\tilde{W}$ component. A normal fluctuation velocity always gives rise to a fluctuation in any quantity which has a normal gradient.

If $W = 0$ in the original coordinate system, x, y, z, i.e., the boundary layer is two-dimensional, $\tilde{U}$ is identical to U, and the transformed equations for a three-dimensional disturbance at angle ψ are precisely the equations for a two-dimensional disturbance at a lower

Reynolds number $R_\delta \cos\psi$. This is the content of the celebrated theorem of Squire (1935). Consequently, if the minimum Reynolds number for instability of two-dimensional disturbances is R_{cr}, then it follows that the minimum unstable Reynolds number for three-dimensional disturbances at wave angle ψ is $R_{cr}/\cos\psi$. It is in this sense that the statement is made that the most unstable disturbance is a two-dimensional disturbance. Obviously, if the complete stability characteristics are known for two-dimensional disturbances, then the stability characteristics of all oblique waves can be obtained. For a wave at angle ψ and Reynolds number R_δ with wave numbers α_δ and β_δ, the time rate of amplification is equal to $\tilde{\alpha}_\delta c_i \cos\psi$, where $\tilde{\alpha}_\delta = \alpha_\delta/\cos\psi$ is the wave number of a two-dimensional disturbance at Reynolds number $\tilde{R}_\delta = R_\delta \cos\psi$. It is possible, depending on the exact shape of the unstable region in an α_δ, R_δ plane, that an α_δ, R_δ which is stable for $\psi = 0$ is unstable for some range of non-zero ψ. Since the stability characteristics of a three-dimensional wave can be deduced from those of a two-dimensional wave, the subsequent analysis will be for a two-dimensional wave.

4. Special Forms of the Stability Equations

4.1 Orr-Sommerfeld equation

The Fourier components of the flow quantities are defined to be

$$u'(x, y, t) = f(y)\, e^{i\alpha_s (x - c t)}, \quad v'(x, y, t) = \alpha\, \varphi(y)\, e^{i\alpha_s (x - c t)}$$
$$p'(x, y, t) = \pi(y)\, e^{i\alpha_s (x - c t)} \tag{4.1}$$

(If φ is replaced by $-i\bar{\varphi}$, then $\bar{\varphi}$ is the amplitude function of the stream function. This procedure is the usual one, but the present derivation is chosen to correspond with the course followed in compressible flow.) Substitution of these relations into (2.22), (2.23) and (2.25) yields

$$i(U - c) f + U' \varphi = -\frac{p_1'}{\rho^* U_1'^2}\, i\pi + \frac{1}{\alpha_s R_s} (f'' - \alpha_s^2 f) \tag{4.2}$$

$$i\alpha^2 (U - c)\varphi = -\frac{p_1'}{\rho^* U_1'^2}\, \pi' + \frac{\alpha_s}{R_s} (\varphi'' - \alpha_s^2 \varphi) \tag{4.3}$$

$$i f + \varphi' = 0 \tag{4.4}$$

The primes now refer to differentiation with respect to y. If (4.2) is differentiated with respect to y and π' and f eliminated, a single 4th-order differential equation is obtained for φ.

$$(U - c)(\varphi'' - \alpha_s^2 \varphi) - U'' \varphi = -\frac{i}{\alpha_s R_s} (\varphi^{IV} - 2\alpha_s^2 \varphi'' + \alpha_s^4 \varphi) \tag{4.5}$$

This is the Orr-Sommerfeld equation. The boundary conditions are

$$g(0) = 0 \quad , \quad g'(0) = 0$$

$$g(y) \to 0 \quad , \quad g'(y) \to 0 \quad \text{as} \quad y \to \infty \tag{4.6}$$

4.2 Four first-order equations

It is also possible to write (4.2)-(4.4) as four first-order equations in terms of f , f' , π and g . In order to correspond with the compressible-flow theory, these are written as

$$Z_1 = f \ , \ Z_2 = f' \ , \ Z_3 = g \ , \ Z_4 = \frac{p_1^*}{\rho^* u_1^{*2}} \pi \tag{4.7}$$

The four equations are

$$Z_1' = Z_2 \tag{4.8}$$

$$Z_2' = \left[i \alpha_s R_s (u - c) + \alpha_s^2 \right] Z_1 + \alpha_s R_s u' Z_3 + i \alpha_s R_s Z_4 \tag{4.9}$$

$$Z_3' = -i Z_1 \tag{4.10}$$

$$Z_4' = -\frac{i \alpha_s}{R_s} Z_2 - \alpha_s^2 \left[i (u - c) + \frac{\alpha_s}{R_s} \right] Z_3 \tag{4.11}$$

with the boundary conditions

$$Z_1(0) = 0 \ , \quad Z_3(0) = 0$$

$$Z_1(y) \to 0 \ , \quad Z_3(y) \to 0 \quad \text{as} \quad y \to \infty \tag{4.12}$$

4.3 Simplified forms of the Orr-Sommerfeld equation

4.3.1 Free stream

The Orr-Sommerfeld equation will now be applied to three simplified situations: to the free stream, where $U = 1$, $U' = 0$, $U'' = 0$; to inviscid disturbances, where $\alpha_\delta R_\delta \to \infty$; and to viscous layers within the boundary layer.

In the free stream, (4.5) can be written

$$i\alpha_\delta R_\delta (1-c)\left(\frac{d^2}{dy^2} - \alpha_\delta^2\right)\varphi = \left(\frac{d^2}{dy^2} - \alpha_\delta^2\right)^2 \varphi \qquad (4.13)$$

Since this equation has constant coefficients, the solutions must have the form

$$\varphi(y) = A e^{\lambda y} \qquad (4.14)$$

When this form is substituted into (4.13), a quartic equation for the characteristic value λ is obtained (the term eigenvalue is reserved for those combinations of α_δ, R_δ, c which provide solutions of the Orr-Sommerfeld equation and boundary conditions).

$$i\alpha_\delta R_\delta (1-c)(\lambda^2 - \alpha_\delta^2) = (\lambda^2 - \alpha_\delta^2)^2 \qquad (4.15)$$

The four solutions can be written down by inspection, and are

$$\lambda = \pm \alpha_\delta \quad , \quad \lambda = \pm\left[\alpha_\delta^2 + i\alpha_\delta R_\delta (1-c)\right]^{1/2} \qquad (4.16)$$

Only two of these characteristic values satisfy the boundary conditions at infinity. They will be called λ_1 and λ_3.

$$\lambda_1 = -\alpha_\delta \quad , \quad \lambda_3 = -\left[\alpha_\delta^2 + i\alpha_\delta R_\delta (1-c)\right]^{1/2} \tag{4.17}$$

The corresponding characteristic vectors $A^{(n)}$ are, from (4.8), (4.9), (4.10), (4.11), and leaving out $A_2^{(n)}$,

$$\begin{aligned} A_1^{(1)} &= -i\alpha_\delta \\ A_3^{(1)} &= 1 \\ A_4^{(1)} &= i\alpha_\delta (1-c) \end{aligned} \tag{4.18}$$

and

$$\begin{aligned} A_1^{(3)} &= -1\left[\alpha_\delta^2 + i\alpha_\delta R_\delta (1-c)\right]^{1/2} \\ A_3^{(3)} &= 1 \\ A_4^{(3)} &= 0 \end{aligned} \tag{4.19}$$

The vector $A^{(1)}$ is the inviscid solution, and is just the linearized inviscid solution over a wavy wall of wavelength $2\pi/\alpha_\delta$. The second vector $A^{(2)}$ is the viscous solution, and represents a viscous decay.

4.3.2 Inviscid equation

The inviscid solution in the free stream is obtained from the inviscid equation

$$\varphi'' - \alpha_\delta^2 \varphi = 0 \tag{4.20}$$

which is the free-stream form of the complete inviscid equation

$$\varphi'' - \alpha_\delta^2 \varphi - \frac{U''}{U-c}\varphi = 0 \qquad (4.21)$$

(4.21) is obtained from the complete Orr-Sommerfeld equation by taking the limit $\alpha_\delta R_\delta \to \infty$.

Since (4.21) is only a second-order equation and the Orr-Sommerfeld equation is fourth order, only two instead of four boundary conditions can be satisfied. These two conditions are

$$\varphi(0) = 0 \;, \quad \varphi(y) \to 0 \quad \text{as} \quad y \to \infty \qquad (4.22)$$

As is usual in inviscid flow, the normal velocity at $y = 0$ is zero, but the no-slip condition is not satisfied.

4.3.3 Simplified viscous equation

Since instability occurs at large Reynolds numbers, $\alpha_\delta R_\delta$ will be large and, consequently,

$$\lambda_3 \approx -\left[i\alpha_\delta R_\delta (1-c)\right]^{1/2} \qquad (4.23)$$

It is interesting to observe that the version of the Orr-Sommerfeld equation that leads to (4.23) is

$$(U-c)\varphi'' = -\frac{i}{\alpha_\delta R_\delta}\varphi^{IV} \qquad (4.24)$$

Both (4.21) and (4.24) are the basis for important further developments.

5. Inviscid Theory

The inviscid equation, (4.21), is important for two reasons. First, it is possible that there are situations where viscosity is of little importance in the stability problem, except as it establishes the mean flow, and a purely inviscid stability theory is applicable. Second, the asymptotic viscous theory, where $\alpha_\delta R_\delta$ is large, uses the inviscid solutions as two of the necessary four independent solutions. It is important to clearly distinguish between these two separate uses of the inviscid solutions. Since the inviscid equation is much simpler than the Orr-Sommerfeld equation, an extensive inviscid theory has been developed, mainly by Rayleigh (see list of references in Betchov and Criminale (1967)), with important additions by Tollmien (1935) and Lin (1945). A comprehensive review of the inviscid theory may be found in the article by Drazin and Howard (1966).

5.1 Rayleigh theorems

As a first step in the inviscid theory, some important results of a general nature will be established. Multiply (4.21) by φ^*, the complex conjugate of φ.

$$\varphi''\varphi^* - \alpha_\delta^2 \varphi\varphi^* - \frac{U''}{|U-c|^2}(U-c^*)\varphi\varphi^* = 0 \tag{5.1}$$

Subtract from this equation its complex conjugate. Then

$$\frac{d}{dy}(\varphi'\varphi^* - \varphi^{*\prime}\varphi) - i\frac{2U''c_i}{|U-c|^2}|\varphi|^2 = 0 \tag{5.2}$$

When (5.2) is integrated from $y = 0$ to infinity, the first term is zero by the boundary conditions. Hence

$$c_i \int_0^\infty \frac{U'' |\varphi|^2}{|U-c|^2} \, dy = 0 \qquad (5.3)$$

It follows from (5.3) that if $c_i \neq 0$, U'' must change sign in the interval $0 < y < \delta$. Consequently, a necessary condition for an amplified disturbance is that the boundary-layer velocity profile must have an inflection point. This result was first obtained by Rayleigh. It has subsequently been proved by Tollmien (1935) that for certain velocity profiles, which include the boundary-layer profile, this condition is also sufficient. A stronger result was obtained by Høiland (1953). He proved that an amplified solution can exist only if $U''(U-U_c)$ is negative between $y = 0$ and $y = \delta$. Consequently, the vorticity U' must have a maximum at y_c. This condition rules out certain velocity profiles for which $U_c'' = 0$, but where U_c' is a minimum.

It can also be proved that an inflection point is necessary for a neutral disturbance. Let

$$W = \frac{i}{2}(\varphi \varphi^{*\prime} - \varphi' \varphi^*) \qquad (5.4)$$

It follows from (5.2) that with $c_i = 0$, W must be constant except possibly at the critical point. A result of Rayleigh for which the proof will not be given establishes that the critical point y_c will always lie between the wall and free stream. When (5.2) is integrated across the boundary

layer, the only contribution to the integral for $c_i \to 0$ comes from near $y = y_c$.

$$W(y_c + \varepsilon) - W(y_c - \varepsilon) = \frac{U_c''}{U_c'} |\varphi_c|^2 \lim_{c_i \to 0} \int_{U(y_c-\varepsilon)}^{U(y_c+\varepsilon)} \frac{c_i}{(U - c_r)^2 + c_i^2} \, dU \qquad (5.5)$$

The integration variable has been changed from y to U. In the limit of $c_i \to 0$, the integral of (5.5) acts like a delta function. Consequently,

$$W(y_c + \varepsilon) - W(y_c - \varepsilon) = \pi \frac{U_c''}{U_c'} |\varphi_c|^2 \qquad (5.6)$$

Since by the boundary conditions, $W(y_c + \varepsilon)$ and $W(y_c - \varepsilon)$ are both zero, U_c'' must also be zero, and it has been proven that a neutral disturbance can only exist if the velocity profile has a point of inflection. It further follows from (5.5) that the phase velocity of the neutral disturbance is equal to the mean velocity at the inflection point.

5.2 Analytic solutions

The chief analytic feature of the inviscid equation is the singularity at $U = c$, a singularity which is not present in the Orr-Sommerfeld equation. This singularity is called the critical point, and its location is denoted by y_c. Since c is complex, so is y_c. The mean velocity U is real, of course, but it may be analytically continued onto the complex plane. The continuation may be carried out by a power series expansion of U.

5.2.1 Method of Frobenius

Two approaches have been used to find analytic solutions of the inviscid equation. The first approach applies the method of Frobenius, and was used by Tollmien (1929). The two solutions are

$$\varphi_1(y) = (y-y_c) P_1(y-y_c) \tag{5.7}$$

$$\varphi_2(y) = P_2(y-y_c) + \frac{U_c''}{U_c'} (y-y_c) P_1(y-y_c) \log (y-y_c) \tag{5.8}$$

where

$$\begin{aligned} P_1(y-y_c) &= 1 + \frac{U_c''}{2U_c'} (y-y_c) + (U_c'' + \alpha^2)(y-y_c)^2 + \cdots \\ P_2(y-y_c) &= 1 + \left(\frac{U_c''}{2U_c'} - \frac{U_c''}{U_c'^2} + \frac{1}{2}\alpha^2 \right)(y-y_c)^2 + \cdots \end{aligned} \tag{5.9}$$

The first solution, φ_1, is regular, but because of the logarithmic term, φ_2 is not regular near y_c. Also, there is an ambiguity about which branch of the logarithm to use for $y < y_c$, $+\pi i$ or $-\pi i$. The resolution of this ambiguity is discussed in Section 5.4.

5.2.2 Power series in α^2

The second method of solution of (4.21) is due to Heisenberg (1924). In this method, the solutions are obtained as convergent power series in α^2. These series were reintroduced into the stability problem by Lin (1945), and form the basis of his computational procedure. They have the further advantage of permitting simple approximate formulas to be developed for such things as the critical Reynolds number. Their drawback

is that they are only convenient to use for small values of α_s , and they do not show the analytic nature of the solutions as clearly as do Tollmien's solutions. The two solutions are

$$\hat{\varphi}_1(y) = (U-c)\left[1 + \alpha_s^2 h_2(y) + \alpha_s^4 h_4(y) + \cdots\right] \tag{5.10}$$

$$\hat{\varphi}_2(y) = (U-c)\left[h_1(y) + \alpha_s^2 h_3(y) + \alpha_s^4 h_5(y) + \cdots\right] \tag{5.11}$$

where

$$h_0(y) = 1$$

$$h_n(y) = \int_0^y \frac{1}{(U-c)^2}\,dy \int_0^y (U-c)^2 h_{n-2}(y)\,dy \tag{5.12}$$

$$h_1(y) = \int_0^y \frac{1}{(U-c)^2}\,dy \tag{5.13}$$

$$h_n(y) = \int_0^y \frac{1}{(U-c)^2}\,dy \int_0^y (U-c)^2 h_{n-2}(y)\,dy$$

The path of integration to be followed in the evaluation of these integrals is under the singularity.

5.3 Numerical integration of inviscid equation

Neither of the analytic methods described above are really adequate for producing numerical solutions of the inviscid equation. Only direct numerical integration of (4.21) can produce solutions accurately and quickly. There are two basic methods available. In the first, which was developed by Conte and Miles (1959), the integration is restricted to the real axis

and the Tollmien solutions are used to carry the solution across the critical point. In the second method, which was developed by Zaat (1958), the solution is produced entirely by numerical integration. This is made possible by use of an indented contour in the complex plane, and the calculation is performed on this contour just as easily as if the path of integration were the real axis. This same method will be applied in Part B to the integration of the compressible inviscid equation.

5.4 Use of inviscid solutions in asymptotic theory

Since U_2'' must be zero for an inviscid neutral disturbance, the second inviscid solution (5.8) is regular in this case. However, for a viscous neutral solution, which is constructed in part from the two inviscid solutions ϕ_1 and ϕ_2, U_2'' is not zero and the logarithmic term of (5.8) must be dealt with. The question to answer is, which branch of the logarithm does one use for $y < y_c$, $-i\pi$ or $+i\pi$? Tollmien (1929) provided the answer by obtaining a viscous correction to ϕ_2 in the region around the critical point, and requiring that this viscous correction match ϕ_2 away from the critical point. This comparison gives $-i\pi$ as the proper branch of the logarithm, which means the path of integration for the inviscid solution must pass under the critical point. The viscous correction which provides this result is derived in Section 6.6.

5.5 Amplified and damped inviscid solutions as complex conjugates

Now we continue with the inviscid theory itself. Since $U' > 0$ for a boundary layer, it follows that when $c_i > 0$, the critical point lies above the real y axis ($y_{c_i} > 0$), and when $c_i < 0$, it is below the real axis ($y_{c_i} < 0$). When $c_i = 0$, the singularity is on the real axis, but thanks to $U_c'' = 0$, the logarithmic term drops out of (5.8) and there is no problem. For amplified and damped solutions, the singularity is off of the real axis, and it would seem that there is also no problem in these two cases. Indeed it can be seen by manipulating the inviscid equation, (4.21), that if $\phi_r + i\phi_i$ is a solution for $c_r + i c_i$, then $\phi_r - i\phi_i$ is a solution for $c_r - i c_i$. Thus amplified and damped solutions are complex conjugates, and the existence of one implies the existence of the other. From this point of view the criterion for instability is that c is complex; the only stability is neutral stability with c real. Equation (5.3) applies for $c_i < 0$ as well as $c_i > 0$, so unless there is a point of inflection, neither amplified nor damped solutions can exist. Since the Blasius boundary layer has no inflection point, this argument says that no inviscid disturbances are possible: amplified, neutral or damped. But viscous disturbances exist; what happens in the limit as $R \to \infty$?

5.6 Amplified and damped inviscid solutions as $R \to \infty$ limit of viscous solutions

The clarification of this point is due to Lin (1945), who showed that if the inviscid solutions are regarded as the infinite Reynolds number limit of viscous solutions, a consistent inviscid theory can be

constructed in which damped disturbances exist and are not complex conjugates of amplified disturbances. To achieve this result, something must be surrendered, namely the existence of the damped solutions everywhere on the real y axis. What this amounts to is that even though viscosity is zero in the limit, the region over which it acts also goes to zero, so an integrated effect remains and the inviscid solution must break down somewhere. Lin's arguments were physical and heuristic, but a rigorous justification was given by Wasow (1948).

It is also possible to arrive at Lin's results from a strictly numerical point of view, which is the procedure to be followed here. To apply the method of direct numerical integration, (4.21) is replaced by two first-order equations for $Z_3 (= \varphi)$ and $Z_4 (= (p'/\rho U_1^2)\pi)$. These equations are

$$Z_3' = \frac{U'}{U-c} Z_3 + \frac{1}{U-c} Z_4 \tag{5.14}$$

$$Z_4' = -i\alpha_s^2 (U-c) Z_3 \tag{5.15}$$

The analytic solutions in the free stream,

$$Z_3 = \frac{1}{\alpha_s} e^{-\alpha_s y} \quad , \quad Z_4 = -(1-c) e^{-\alpha_s y} \tag{5.16}$$

are used to start the integration which then proceeds to the wall for selected values of α and $c_r + i c_i$. To obtain an inviscid solution, the boundary condition $Z_3(0) = 0$ is satisfied by a linear perturbation of any two of α, $c_r + i c_i$.

The main question to decide is how to indent the contour of integration. The two possibilities are shown in Fig. 5.1.

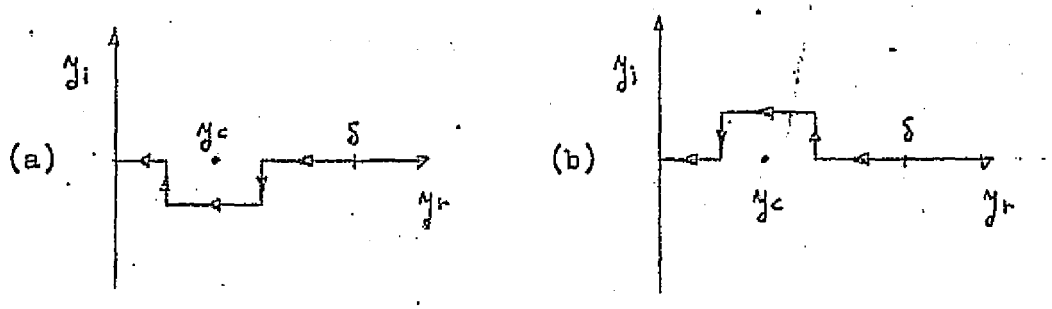

Fig. 5.1. Alternate contours of integration for inviscid equation

i) For an inviscid neutral solution, $c_i = 0$; Z_3 is pure imaginary and Z_4 is real. It makes no difference if the contour is indented below, as in (a), or above as in (b).

ii) When the inviscid solutions are used in the computation of a viscous neutral solution, $c_i = 0$, but $Z_3(0) \neq 0$ since the boundary condition is to be satisfied by the inviscid solution plus a viscous solution. The solutions are complex and path (a) under the singularity must be used as shown by Heisenberg (1924) and Tollmien (1929).

iii) If $c_i \neq 0$, the integration can be restricted to the real axis. However, then the Rayleigh theorem applies, and unless $U'' = 0$ there are no amplified solutions (or their complex conjugates, the damped solutions). But if contour (a) is used for damped solutions, and contour (b) for amplified solutions, both of these solutions exist even with $U'' \neq 0$. Some eigenvalues computed for the Blasius velocity profile are shown in

Table 5.1.

Contour	α_s	c_r	c_i
(a)	0.226	0.100	- 0.00057
(b)	0.226	0.100	+ 0.00057
(a)	0.529	0.200	- 0.00717
(b)	0.529	0.200	+ 0.00717

Table 5.1. Inviscid eigenvalues for Blasius velocity profile with indented contours.

As can be verified from (5.14) and (5.15), the solutions with $c_r - i c_i$ and contour (a) are related to the solutions with $c_r + i c_i$ and contour (b) by

$$\begin{aligned} Z_{3r}^{(a)} + i Z_{3i}^{(a)} &= Z_{3r}^{(b)} - i Z_{3i}^{(b)} \\ Z_{4r}^{(a)} + i Z_{4i}^{(a)} &= - Z_{4r}^{(b)} + i Z_{4i}^{(b)} \end{aligned} \qquad (5.17)$$

Which option does one pick? Since the neutral-stability curve for the Blasius profile is as shown in Fig. 1.1a, the viscous solutions at all α become damped in the limit $R \to \infty$. With the inviscid solutions required to be the limiting viscous solutions, it is evident that contour (a) is to be used, just as in the asymptotic theory and in agreement with Lin. There are no amplified inviscid solutions. For a profile with $U'' = 0$ at y_s, both amplified and damped solutions exist for each contour, unlike the Blasius case. The neutral solution is α_s, and can be obtained with either contour. With contour (a) the amplified solutions have $\alpha < \alpha_s$,

the damped solutions $\alpha > \alpha_s$. Contour (b) gives the opposite results. Comparison with the viscous neutral-stability curve, which will be of the type shown in Fig. 1.1b, shows contour (b) must be rejected.

The damped solutions with contour (a) do not exist everywhere on the real axis. According to the theory, there is a length of real axis where viscosity will always have an effect and the inviscid solution does not apply. The numerical integration produces a perfectly reasonable looking solution everywhere except at y_{c_r}, but for sufficiently large $-c_i$ the numerical solution ceases to be an analytic function of c. This matter may need further investigation as physically it is difficult to imagine how in the limit $R \to \infty$ viscosity could continue to have an effect over a length of the real axis and not just at a point (or several points).

Figure 5.2 gives $-\alpha_s c_i$, the time rate of damping, as a function of α_s for a Blasius velocity profile.

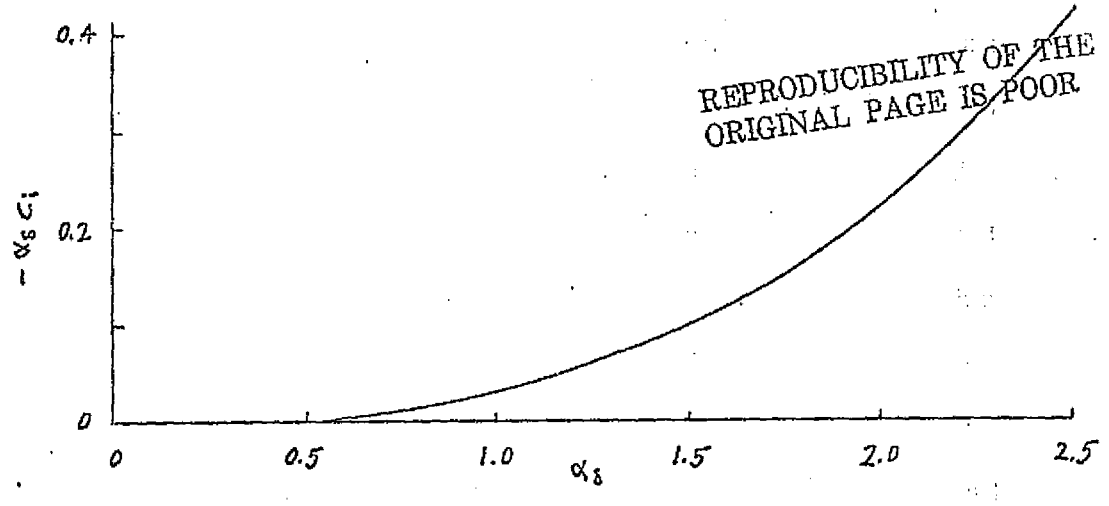

Fig. 5.2. Inviscid damping rate as function of wave number for Blasius velocity profile.

6. Asymptotic Viscous Theory

6.1 General ideas

We now turn our attention to finding four linearly independent solutions of the Orr-Sommerfeld equation at large but finite Reynolds numbers, which means that an asymptotic theory in αR is indicated. If a simple expansion is made in inverse powers of αR ($\varphi = \varphi^{(0)} + (\alpha R)^{-1}\varphi^{(1)} + \cdots$), the first term will satisfy the inviscid equation, and thus this approach yields only two of the necessary four solutions. However, the inviscid solution designated by $\bar{\varphi}$ ($= z_3$), which is the solution that behaves as $e^{-\alpha y}$ in the free stream and is a combination of φ_1 and φ_2, or of $\hat{\varphi}_1$ and $\hat{\varphi}_2$, goes a long way towards solving the whole problem. It satisfies the boundary condition at infinity; it is an adequate solution over the large part of the boundary layer where viscosity is unimportant; and the device of following an indented contour under the singularity at $U = c$ properly accounts for the effect that the action of viscosity in the region of the critical point has on the solution between the critical point and the wall. What remains is to determine the influence of viscosity in the region immediately adjacent to the wall. A true inviscid solution can only satisfy one boundary condition at the wall, and indeed, as we have seen, only damped inviscid solutions are possible for the Blasius boundary layer. To satisfy both boundary conditions, we must use a combination of the inviscid solution which satisfies the boundary condition at infinity and a viscous correction. With the viscous correction designated by φ_3, and the subscript w used for conditions at the wall,

the boundary conditions at the wall are

$$\begin{aligned} \bar{\Phi}_w + A\,\varphi_{3w} &= 0 \\ \bar{\Phi}'_w + A\,\varphi'_{3w} &= 0 \end{aligned} \tag{6.1}$$

where A is a complex constant. Because these two equations are homogeneous, solutions can only exist when the determinant is zero. Hence

$$\frac{\bar{\Phi}_w}{\bar{\Phi}'_w} = + \frac{\varphi_{3w}}{\varphi'_{3w}} \tag{6.2}$$

The left-hand side is a function of α_s and c, and the right-hand side is a function of α_s, c, and R_s. Thus (6.2) is the secular equation, or equation for the determination of the eigenvalues. Once the eigenvalues are known, the constant A is found from either one of the equations of (6.1), and the eigenfunctions can be computed over that portion of the boundary layer for which $\bar{\Phi}$ and φ_3 are adequate approximations. Most of the rest of this section is devoted to finding a form of φ_3 which will provide reliable numerical results. The viscous correction φ_3 is obtained from the simplified Orr-Sommerfeld equation (4.24), which was indicated in Section 4.3.3 to be the appropriate viscous equation for large $\alpha_s R_s$. This equation is, when rewritten slightly,

$$\varphi^{iv} - i\,\alpha_s R_s (u-c)\,\varphi'' = 0 \tag{6.3}$$

The physical reasoning behind (6.3) is that viscosity is important for the disturbances only where large disturbance velocity gradients exist. A first-order viscous theory need only retain the largest viscous term (right-hand side) and largest inviscid term (left-hand side) of the complete Orr-Sommerfeld equation (4.5).

6.2 Length scales of the viscous regions

There are two regions of the boundary layer where viscosity is of importance for the disturbances. The first of these regions is near the wall. Since the eigenvalues are computed from (6.2), which involves only wall values of $\bar{\phi}$ and ϕ_3, the asymptotic theory is devoted primarily to developing solutions which are adequate near the wall. The second viscous region is near the critical point, where viscosity is brought into play by the singularity of the inviscid equation. As already mentioned, the effect of viscosity near the critical point has been included in the inviscid solution by the device of integrating along an indented contour under the singularity. However, the function $\bar{\phi}$ does not correctly represent the solution in the vicinity of the critical point, and if the critical point is close to the wall, the use of $\bar{\phi}$ in the eigenvalue equation will not be correct. The development of the viscous correction to $\bar{\phi}$ near y_c is given in Section 6.6.

It is useful to have available estimates of the thickness of the viscous regions. If the thickness of the wall viscous region is small compared with y_c, the distance from the wall to the critical point, then (6.3) simplifies to

$$\varphi^{IV} + i\alpha_s R_s c\,\varphi'' = 0 \tag{6.4}$$

The solution of (6.4) which decreases with increasing y_s is

$$\varphi_s(y_1) = \varphi_s(0)\, e^{-(1-i)\sqrt{\frac{\alpha_s R_s c}{2}}\, y} \tag{6.5}$$

This solution decreases to $1/e$ of its wall value in the distance

$$\varepsilon_w = \left(\frac{2}{\alpha_s R_s c}\right)^{1/2} \tag{6.6}$$

We can use ε_w as an estimate of the scale of the wall viscous region. As φ_s decreases, it also oscillates with a "wavelength" of $2\pi\varepsilon_w$. A definition of the thickness of the viscous region which is more comparable to the usual definition of a boundary-layer thickness would give a result closer to $2\pi\varepsilon_w$ than to ε_w. The viscous solution (6.5), which will reappear in Section 11.1 when we discuss the viscous instability mechanism, is not adequate for the eigenvalue problem.

The reason for the inadequacy of 6.5 is that the assumption $u \ll c$ is too drastic. Two methods have been developed to solve (6.3) without making this assumption. The first solves (6.3) by the WKB method and is discussed in the following section. The second takes advantage of the fact that the velocity profile in many instances is almost linear between the wall and y_c, and uses (6.3) in the form

$$\varphi^{IV} - i\alpha_s R_s u'_c (y - y_c)\varphi'' = 0 \tag{6.7}$$

This equation can be regarded either as the viscous equation in the

immediate vicinity of y_c , or as an approximate form of (6.3) which is valid when the velocity profile is almost linear. It is the latter view that is appropriate for the wall viscous region. The Blasius velocity profile constitutes a particularly favorable case for this assumption since U'' is equal to zero at $y = 0$. With a nearly linear $U(y)$, solutions of (6.7) will be valid from the wall to beyond the critical point. In particular, these solutions will be valid even when the critical point is too close to the wall for the WKB method to be accurate. It is the latter case which exists over much of the unstable region of practical importance.

The solutions of (6.7) are functions of the variable ζ , where

$$\zeta = (\alpha_s R_s U_c')^{1/3} (y - y_c) \tag{6.8}$$

Hence a new viscous length scale

$$l_v = \text{const.} \times \varepsilon_c \tag{6.9}$$

has appeared, where

$$\varepsilon_c = (\alpha_s R_s U_c')^{-1/3} \tag{6.10}$$

The behavior of the solutions of (6.7) is complicated and it is not easy to assign a meaningful numerical value to the constant in (6.9). Inspection of the actual solutions, which are presented later (Figs. 6.1 and 6.2), shows that in the wall viscous region φ_3 is reduced to $1/e$ of its wall value when y increases by 1 to 2 units of ε_c . For the

viscous correction to $\bar{Q}$ near y_c, the major effect of viscosity extends over a distance of about two units of ε_c on each side of the critical point. Consequently, a length scale of $2\varepsilon_c$ would be a reasonable estimate of the half-thickness of the viscous region near y_c, and also of the wall viscous region when (6.7) is the governing equation.

To get an idea of typical magnitudes of ε_w and ε_c and their relationship to y_c, we take two points from the neutral-stability curve of the Blasius boundary layer:

i) upper branch: $R_\delta = 3500,\ \alpha_\delta = 1.25,\ c_r = 0.37,\ U_c' = 1.91$

$$\varepsilon_w = 0.035, 2\varepsilon_c = 0.098,\ y_c = 0.187 \tag{6.11}$$

ii) lower branch: $R_\delta = 3500,\ \alpha_\delta = 0.60,\ c_r = 0.32,\ U_c' = 1.94$

$$\varepsilon_w = 0.053, 2\varepsilon_c = 0.126,\ y_c = 0.162 \tag{6.12}$$

6.3 WKB solutions

The WKB method is a standard method of obtaining solutions of equations of the type (6.3), and was first applied to the stability problem by Heisenberg (1924). It will provide solutions which are valid far from y_c. Let

$$\varphi(y) = \exp\left(\int g(y)\, dy\right) \tag{6.13}$$

and expand $g(y)$ in the series

$$g(y) = (i\alpha_\delta R_\delta)^{1/2} g_0(y) + g_1(y) + \cdots \tag{6.14}$$

Substitute (6.13) and (6.19) in (6.3) and equate equal powers of $(\alpha_s R_s)^{1/2}$. The following two equations are obtained for g_0 and g_1.

$$g_0^4 = (u-c)\, g_0^2$$

$$4 g_0^3 g_1 + 6 g_0^2 g_0' = (u-c)(g_0'' + 2 y_0 g_1) \tag{6.15}$$

The solutions of these equations are

$$g_0 = \pm (u-c)^{1/2} \quad , \quad g_1 = -\frac{5}{4}\,\frac{u'}{u-c} \tag{6.16}$$

If more terms in g are desired, it is necessary to return to the complete Orr-Sommerfeld equation, but to the above order of approximation (6.3) and the complete equation are the same.

With (6.16) we find the two WKB solutions to be

$$\varphi_3(y) = (u-c)^{-5/4} \exp\left[-(\alpha_s R_s)^{1/2}\, Q(y)\right] \tag{6.17}$$

$$\varphi_4(y) = (u-c)^{-5/4} \exp\left[+(\alpha_s R_s)^{1/2}\, Q(y)\right] \tag{6.18}$$

where

$$Q(y) = \int_{y_c}^{y} \left[i\,(u-c)\right]^{1/2} dy \tag{6.19}$$

The point y_c, where $u = c$, is a branch point for these solutions. Just as for the inviscid solutions it is necessary to select the proper

branch by specifying the path of integration. The correct path, which is determined by comparison with the solution of (6.7) to be obtained in Section 6.4, is the same as for the inviscid solution, i.e., under the singularity. Consequently, when c is real,

$$\begin{aligned} u - c &= |u-c|, \quad \arg Q = \tfrac{\pi}{4} \quad \text{for} \quad y > y_c \\ u - c &= |u-c| e^{-\pi i}, \quad \arg Q = -\tfrac{5}{4}\pi \quad \text{for} \quad y < y_c \end{aligned} \tag{6.20}$$

Of the two WKB solutions, φ_3 decreases exponentially (and oscillates) with increasing y. Since φ_4 increases exponentially, it is not suitable for the boundary-layer stability problem and need not be considered further. φ_3 is a maximum at $y = 0$ and with increasing y it oscillates with rapidly decreasing magnitude.

With (6.15), the ratio $\varphi_3'(y) / \varphi_3(y)$ is found to be

$$\frac{\varphi_3'(y)}{\varphi_3(y)} = -\left[i\alpha_s R_s (u-c)\right]^{1/2} - \frac{5}{4}\frac{u'}{u-c} \tag{6.21}$$

and, at $y = 0$,

$$-\frac{\varphi_{3w}'}{\varphi_{3w}} = (\alpha_s R_s c)^{1/2} e^{-\frac{\pi i}{4}} - \frac{5}{4}\frac{u_w'}{c} \tag{6.22}$$

The right-hand side becomes a function of a single variable if (6.22) is multiplied by c/u_w'.

$$-\frac{c}{u_w'}\frac{\varphi_{3w}'}{\varphi_{3w}} = \frac{1}{2}^{3/2} e^{-\frac{\pi i}{4}} - \frac{5}{4} \tag{6.23}$$

The single variable is

$$\bar{z} = (\alpha_3 R_3 U_w')^{1/3} \frac{c}{U_w'} \tag{6.24}$$

It can be noted that for a velocity profile which is linear from the wall to the critical layer, $U_w' = U_c'$ and $c/U_w' = y_c$. In this case, $\bar{z}$ is equal to the variable $-\zeta_w$ which is defined by (6.8).

We can now write the boundary condition (6.2) as

$$E(\alpha, c) = \bar{F}(\bar{z}) \tag{6.25}$$

where

$$E(\alpha, c) = -\frac{U_w'}{c} \frac{\bar{\Phi}_w}{\bar{\Phi}_w'} \tag{6.26}$$

and

$$\bar{F}(\bar{z}) = \left(\bar{z}^{3/2} e^{\frac{\pi i}{4}} - \frac{5}{4} \right)^{-1} \tag{6.27}$$

The left-hand side of (6.25), $E(\alpha, c)$, is determined entirely by the inviscid solution $\bar{\Phi}$. The right-hand side, $\bar{F}(\bar{z})$, is determined entirely by the viscous solution φ_3. Further, it is a universal function of $\bar{z}$ and does not depend on the particular boundary-layer profile. Equation (6.25) is the equation for the determination of the eigenvalues α_3, c, R_3, or as it is often called, the secular equation. It is easily solvable

by a graphical procedure devised by Tollmien (. 29) in which the functions $\bar{F}(\bar{z})$ and $E(\alpha, c)$ are both plotted in the complex plane. The intersection point of the two curves determine α_s, c and $\bar{z}$ and hence R_s from (6.24), the definition of $\bar{z}$. An example of this procedure, using the Tietjens function instead of $\bar{F}(\bar{z})$, is given in Section 7.1.

The only thing wrong with the method just outlined is that it gives poor numerical results except for $\bar{z}$ greater than about 7. It could have been expected to fail on the lower branch because the wall viscous region occupies more of the distance between the wall and y_c there, and φ_3 is not valid near y_c , but it is somewhat of a disappointment that it is not really adequate on the upper branch either until very high Reynolds numbers are reached.

6.4 Hankel function solutions

The second method of obtaining viscous solutions replaces (6.3) by (6.7) and will be valid when y_c is a much smaller multiple of ε_w than is permissible with the WKB method. The independent variable is ζ , given by (6.8) and repeated here for convenience,

$$\zeta = (y - y_c)/\varepsilon_c = (\alpha_s R_s U_c')^{1/3}(y - y_c) \tag{6.28}$$

With the solutions designated by $\chi_n(\zeta)$, (6.7) becomes

$$\chi_n^{iv} - i\zeta\chi_n'' = 0 \tag{6.29}$$

Four solutions of this equation are

$$\chi_1 = \zeta \tag{6.30}$$

$$\chi_2 = 1 \tag{6.31}$$

$$\chi_3 = \int_{\infty}^{\zeta} d\zeta \int_{\infty}^{\zeta} \zeta^{1/2} H_{1/3}^{(1)} \left[\tfrac{2}{3}(i\zeta)^{3/2}\right] d\zeta \tag{6.32}$$

$$\chi_4 = \int_{-\infty}^{\zeta} d\zeta \int_{-\infty}^{\zeta} \zeta^{1/2} H_{1/3}^{(2)} \left[\tfrac{2}{3}(i\zeta)^{3/2}\right] d\zeta \tag{6.33}$$

where $H_{1/3}^{(1)}$ and $H_{1/3}^{(2)}$ are modified Hankel functions of order 1/3 of the first and second kind, respectively. These solutions, which were first used in this problem by Heisenberg (1924), are usually expressed in most recent work (e.g., Reid (1965)) in terms of Airy functions in order to make use of the highly developed asymptotic theory of second-order differential equations.

A tabulation of the function χ_3 and its first two derivatives is given by Stuart (1963) from the paper of Holstein (1950). The real and imaginary parts of χ_3, and also $|\chi_3|$, are plotted in Fig. 6.1 as functions of ζ; the real and imaginary parts of χ_3', and $|\chi_3'|$, are given in Fig. 6.2. The critical point is always at $\zeta = 0$, and the wall is at some particular value of $-\zeta$. It is seen that $|\chi_3|$, unlike $|\chi_3'|$, does not decrease monotonically with increasing ζ. The asymptotic expansion of χ_3, given below by (6.34), is not valid until $\zeta \approx -8$.

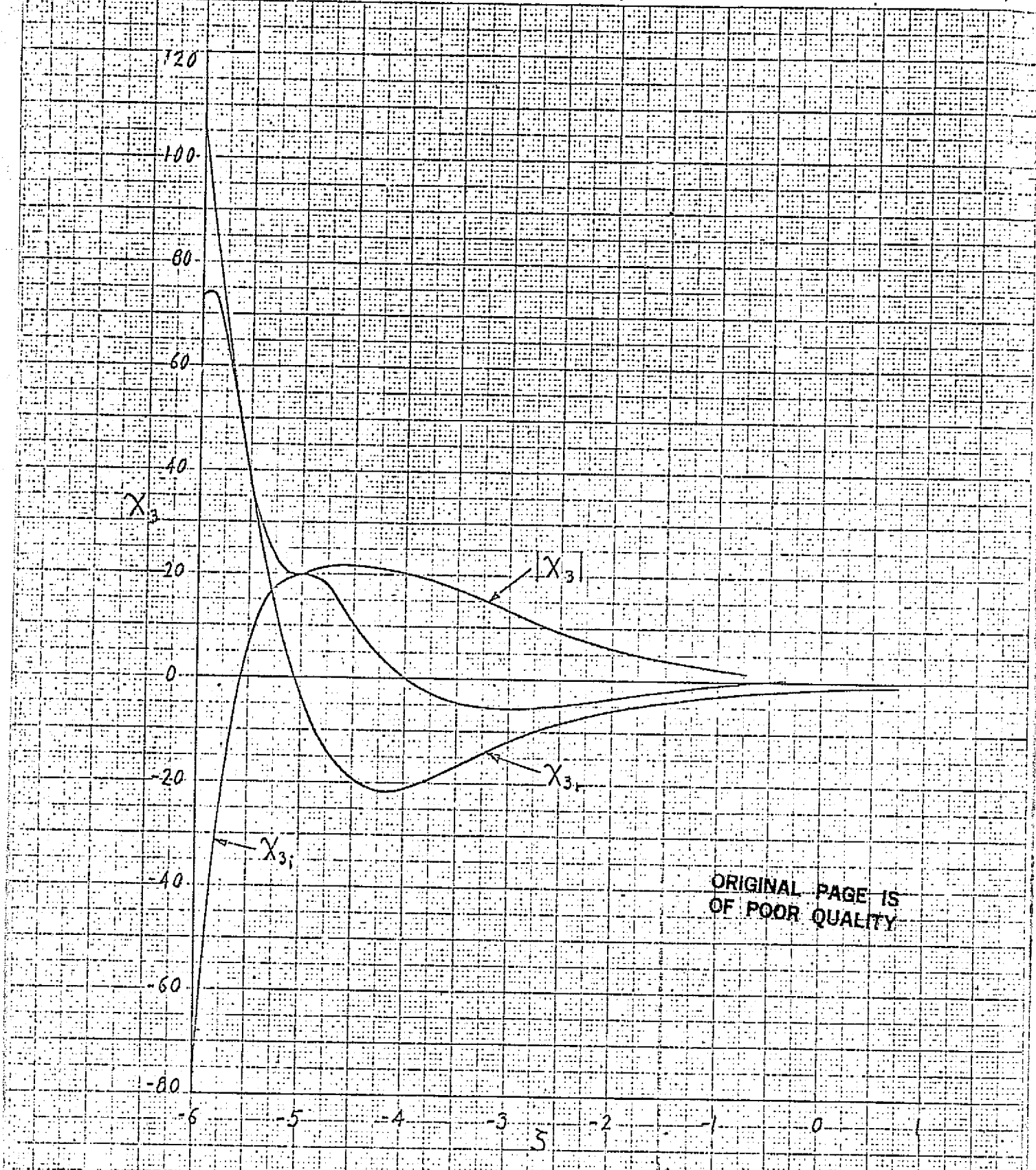

Fig. 6.1 Viscous correction function in wall region

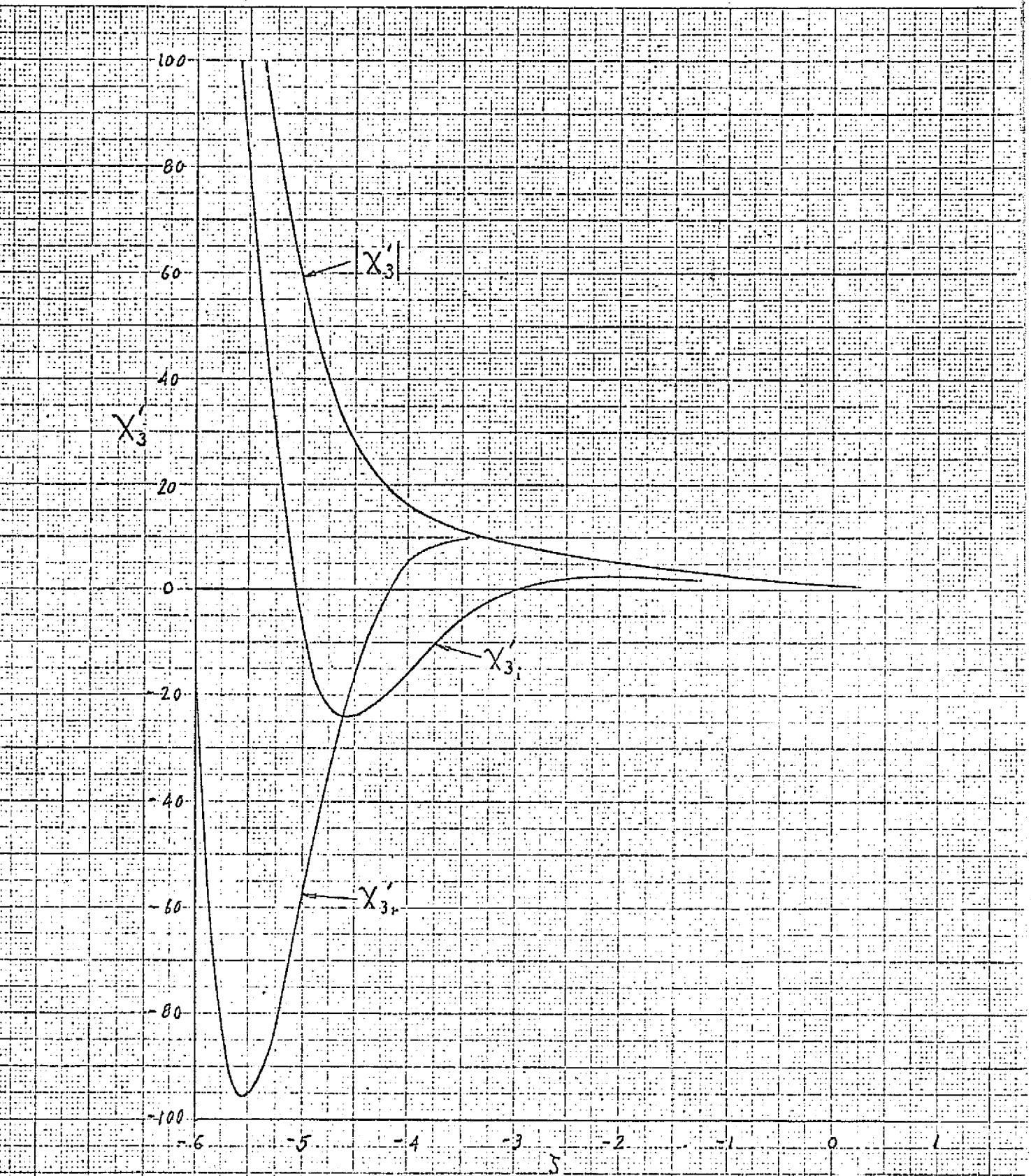

Fig. 6.2 Derivative of viscous correction function in wall region

The first two solutions, (6.30) and (6.31), are the leading terms of the inviscid solutions (5.7) and (5.8). The two Hankel function solutions, (6.32) and (6.33), can be identified with the WKB solutions φ_3 and φ_4. The asymptotic expansions of (6.32) and (6.33) for large ζ are

$$\chi_3 \sim \zeta^{-5/4} \exp\left(\tfrac{2}{3}\zeta^{3/2} e^{-\frac{5}{4}\pi i}\right) \tag{6.34}$$

$$\chi_4 \sim \zeta^{-5/4} \exp\left(\tfrac{2}{3}\zeta^{3/2} e^{\frac{1}{4}\pi i}\right) \tag{6.35}$$

If in the WKB solutions, (6.17) and (6.18), $Q(y)$ is replaced by

$$Q(y) = \int_{y_c}^{y} \left[i(U-c)\right]^{1/2} dy \approx (iU_c')^{1/2} \tfrac{2}{3}(y-y_c)^{3/2} \tag{6.36}$$

then

$$\varphi_{3,4} = \left[U_c'(y-y_c)\right]^{-5/4} \exp\left[\mp \tfrac{2}{3}(i\alpha_s R_s U_c')^{1/2}(y-y_c)^{3/2}\right] \tag{6.37}$$

and, since $\zeta = (\alpha_s R_s U_c')^{1/3}(y-y_c)$, $i^{1/2} = e^{\pi/4}$, and $(-i)^{1/2} = e^{-\frac{5}{4}\pi}$, φ_3 can be identified with χ_3, and φ_4 with χ_4. It is this identification that establishes the integration path for the WKB solutions to be under the singularity, because the asymptotic expansions, (6.34) and (6.35), of the Hankel functions are only valid in regions traversed by such a path, and not in the regions traversed by a path above the singularity. This whole question of the proper path to follow and the regions

of validity of the asymptotic expansions is highly complicated. For more detailed discussions, it is necessary to consult Lin's book, and, for the complete rigorous theory, the paper by Wasow (1948). A good discussion is given by Reid (1965).

6.5 Tollmien's improved viscous solutions

The WKB solutions are valid for $|y-y_c| \gg \varepsilon_c$, and the Hankel function solutions are strictly valid for $|y-y_c| = O(\varepsilon_c)$, since in general $U(y)$ is not linear from $y=0$ to y_c. Tollmien (1947) gave a pair of solutions for real c which are valid everywhere. Similar solutions were obtained for complex c by Wasow (1953). The form of these solutions is suggested by a simple argument of Lin (1955). In the comparison of the WKB solutions with the asymptotic expansions of the Hankel function solutions, the arguments of the exponentials were shown to be identical when $U-c$ in $Q(y)$ was expanded in a series about y_c and only the first term retained. If the two arguments are identified without the expansion,

$$\frac{2}{3}\tilde{\zeta}^{3/2} e^{\frac{5}{4}\pi i} = -(\alpha_s R_s)^{1/2} Q \qquad (6.38)$$

then

$$\tilde{\zeta} = (\alpha_s R_s)^{1/3}\left[\frac{3}{2}\int_{y_c}^{y}(U-c)^{1/2}\,dy\right]^{2/3} \qquad (6.39)$$

With the variable ζ of (6.32) and (6.33) reinterpreted to be (6.39) instead of (6.28), and with a suitable factor placed outside of the

integral signs, the viscous solutions are

$$\hat{\chi}_3 = \left(\frac{\hat{\zeta}}{U-c}\right)^{5/4} \int_{\infty}^{\zeta} d\zeta \int_{\infty}^{\zeta} \zeta^{1/2} H_{1/3}^{(1)}\left[\tfrac{2}{3}(i\zeta)^{3/2}\right] d\zeta \qquad (6.40)$$

$$\hat{\chi}_4 = \left(\frac{\hat{\zeta}}{U-c}\right)^{5/4} \int_{-\infty}^{\zeta} d\zeta \int_{-\infty}^{\zeta} \zeta^{1/2} H_{1/3}^{(2)}\left[\tfrac{2}{3}(i\zeta)^{3/2}\right] d\zeta \qquad (6.41)$$

These are Tollmien's solutions. Their asymptotic expansions for large $\hat{\zeta}$ are equal to the WKB solutions; for $y \to y_c$, they reduce to (6.32) and (6.33) (except for an unimportant constant factor). Tollmien proved that these solutions differ from two solutions of the Orr-Sommerfeld equation by an error of order ε_c for all y.

6.6 Improved inviscid solutions

The viscous solution χ_3 discussed in Section 6.4, and $\bar{\phi}$, the solution of the inviscid equation, are adequate to solve the eigenvalue problem. However, for the calculation of the eigenfunctions it is necessary to get rid of the singularity in the inviscid solution at y_c. This singularity does not exist in the Orr-Sommerfeld equation, and it can be removed from the inviscid solution by adding a viscous correction.

The first two of the four solutions of the simplified viscous equation (6.7), which are given by (6.30) and (6.31), are the first terms of the analytic series solution for ϕ_1 and ϕ_2. They are actually solutions of the equation $\phi'' = 0$, which may be regarded as the inviscid equation with the $\alpha_s^2 \phi$ and $U''\phi/(U-c)$ terms neglected. Now the improved inviscid solution must come from a balance of the main viscous term $i\phi^{IV}/\alpha_s R_s$, the convection term $(U-c)\phi''$, and the term $U''\phi$, which in the absence

of viscosity is responsible for the singularity. Hence, the equation for the viscous correction is

$$\varphi^{iv} - i\alpha_\delta R_\delta (U-c)\varphi'' + i\alpha_\delta R_\delta U''\varphi = 0 \qquad (6.42)$$

Since the scale of the viscous region in the vicinity of y_c is proportional to $\varepsilon_c = (\alpha_\delta R_\delta U_c')^{-1/3}$, the variable ζ given by (6.28) is the proper one to use. The solutions sought have the form

$$\chi_1(\zeta) = \chi_1^{(0)}(\zeta) + \varepsilon_c \chi_1^{(1)}(\zeta) \qquad (6.43)$$

$$\chi_2(\zeta) = \chi_2^{(0)}(\zeta) + \varepsilon_c \chi_2^{(1)}(\zeta) \qquad (6.44)$$

When these are substituted into (6.42) and equal powers of ε_c are equated, it is found that $\chi_1^{(0)}$ and $\chi_2^{(0)}$ satisfy the simplified viscous equation (6.29), and are given by (6.30) and (6.31). $\chi_1^{(1)}$ and $\chi_2^{(1)}$ satisfy the equation

$$\chi_{1,2}^{(1)\,iv} - i\zeta\chi_{1,2}^{(1)\,''} = \frac{1}{2} i\zeta^2 \frac{U_c''}{U_c'} \chi_{1,2}^{(0)\,''} - i\frac{U_c''}{U_c'}\chi_{1,2}^{(0)} \qquad (6.45)$$

or, since $\chi_{1,2}^{(0)\,''} = 0$,

$$\chi_{1,2}^{(1)\,iv} - i\zeta\chi_{1,2}^{(1)\,''} = -\frac{U_c''}{U_c'}\chi_{1,2}^{(0)} \qquad (6.46)$$

For $\chi_1^{(1)}$ the proper solution is

$$\chi_1^{(1)} = \frac{1}{2}\frac{U_c''}{U_c'}\zeta^2 \qquad (6.47)$$

since, with (6.47),

$$\chi_1 = \chi_1^{(0)} + \varepsilon_c \chi_1^{(1)} = \zeta + \varepsilon_c \frac{U_c''}{2U_c'} \zeta^2 \tag{6.48}$$

and agrees with the first two terms of the regular inviscid solution as given by (5.7).

The second solution of (6.46), $\chi_2^{(0)}$, cannot be written down in a simple form. It is determined from (6.46) by the requirement that its asymptotic form for large ζ behave as $(U_c''/U_c')\zeta(\log\zeta + \log\varepsilon_c)$, the first singular term of (5.8). The solution $\chi_2^{(0)}$ has been calculated and tabulated by Holstein (1950). The tabulation may also be found in Stuart (1963). The first derivatives of $\chi_{2r}^{(0)}$ and $\chi_{2i}^{(0)}$, which are proportional to the real and imaginary parts of f, the amplitude function of the longitudinal disturbance velocity u', are plotted in Fig. 6.3. Also shown is the real part of the singular term of φ_2, which is also the asymptotic form of $\chi_{2r}^{(0)\prime}$. It will be recalled from Section 5.4 that the proper branch of the logarithm to use in φ_2 for $y < y_c$ could not be established within the framework of the inviscid theory. The imaginary part of $\chi_2^{(0)\prime}$, as seen from Fig. 6.3, clearly establishes the correct branch to be $-\pi i$.

According to Tollmien (1947), the improved second inviscid solution can be immediately written down as

$$\varphi_2(y) = P_2(y-y_c) + \varepsilon_c P_1(y-y_c)\chi_2^{(1)}(\zeta) \tag{6.49}$$

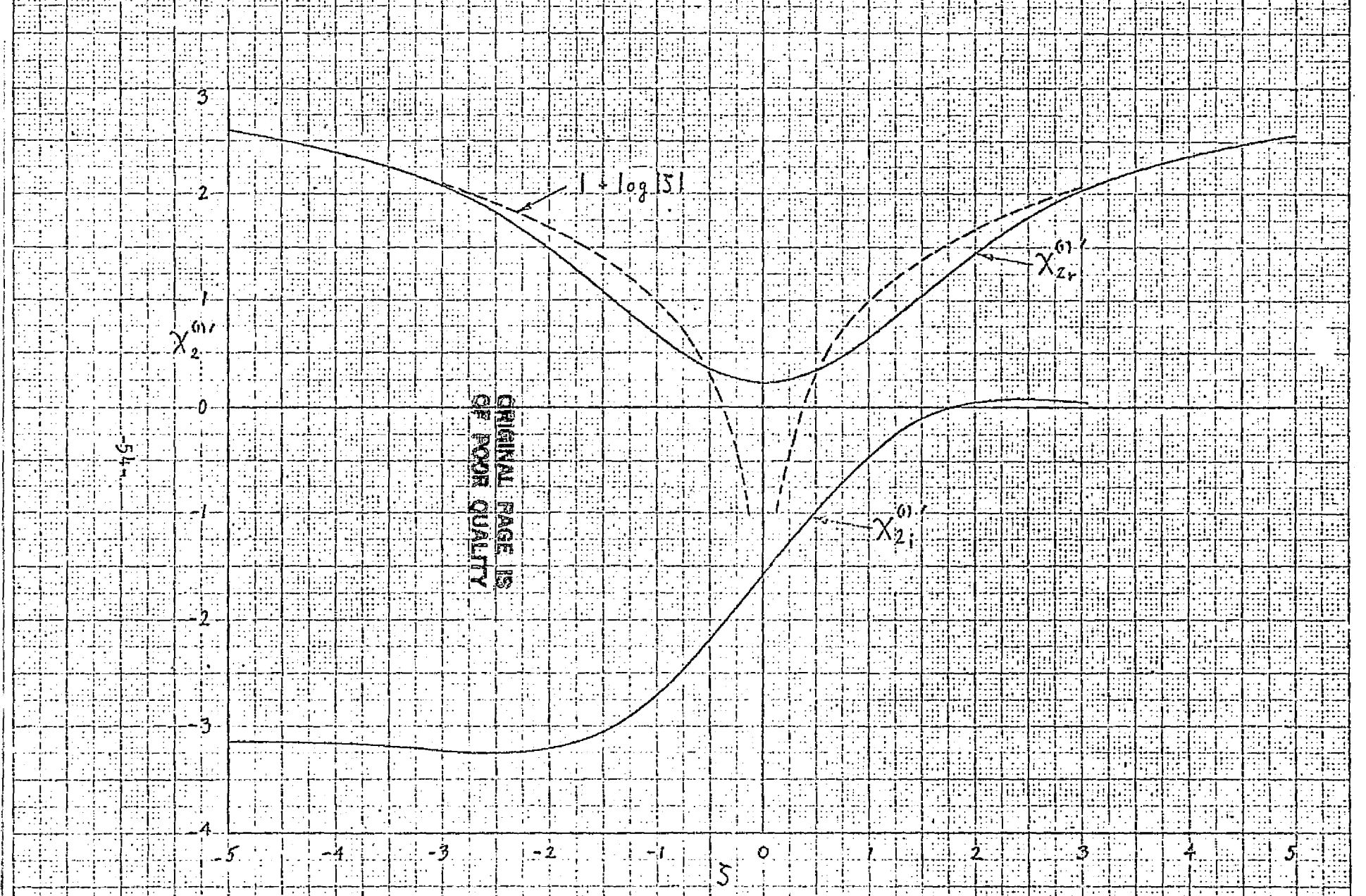

Fig. 6.3 Derivative of viscous correction function in region of critical point

where P_1 and P_2 are still given by (5.9). However, according to Reid (1965), $\chi_2^{(1)}$ can only correct the first singular term of $\varphi_2(y)$ and higher-order corrections would have to be obtained to remove the higher-order singularities. Reid gives for φ_2,

$$\varphi_2(y) = P_2(y-y_c) + \varepsilon_c \chi_2^{(1)}(\zeta) + \frac{U_c''}{U_c'}(y-y_c)\left[P_1(y-y_c)-1\right]\log(y-y_c) \tag{6.50}$$

in which the most important singularity is $(y-y_c)^2\log(y-y_c)$. If y_c is close enough to the wall so that $\chi_2^{(1)}(\zeta)$ differs from its asymptotic form $(U_c''/U_c')(\log\zeta + \log\varepsilon_c)$ at $y=0$, then the viscous correction will affect the eigenvalues. No calculations have yet been made with either (6.49) or (6.50) used in place of (5.8) for φ_2.

6.7 Tietjens function and the secular equation

The ratio φ_3'/φ_3, when χ_3 in the form (6.32) is used for φ_3, is

$$\frac{\varphi_3'}{\varphi_3} = (\alpha_3 R_3 U_c')^{1/3} \frac{\int_\infty^\zeta d\zeta\, H_{1/3}^{(1)}\left[\frac{2}{3}(i\zeta)^{3/2}\right] d\zeta}{\int_{+\infty}^{\zeta} d\zeta \int_{+\infty}^{\zeta} \zeta^{1/2} H_{1/3}^{(1)}\left[\frac{2}{3}(i\zeta)^{3/2}\right] d\zeta} \tag{6.51}$$

This ratio is to be evaluated at $y=0$ to provide the right-hand side of (6.2). In order to have a positive variable, ζ_w is replaced by $-z$.

$$z = -\zeta_w = (\alpha_3 R_3 U_c')^{1/3} y_c \tag{6.52}$$

The ratio at $y=0$ is expressed by Tietjens function, which is defined to be,

$$F(z) = \frac{\int_{\infty}^{-z} ds \int_{\infty}^{s} s^{1/2} H_{1/3}^{(1)}\left[\frac{2}{3}(is)^{3/2}\right] ds}{-z\int_{\infty}^{-z} s^{1/2} H_{1/3}^{(1)}\left[\frac{2}{3}(is)^{3/2}\right] ds} \tag{6.53}$$

Then the function which in the WKB method could be expressed as a universal function of z, is

$$-\frac{c}{U_w'}\frac{\varphi_{3w}'}{\varphi_{3w}} = \frac{c}{U_w'}\frac{1}{y_c}\frac{1}{F(z)} \tag{6.54}$$

Define

$$1 + \lambda(c) = \frac{U_w'}{c} y_c \tag{6.55}$$

If the velocity profile is linear from $y = 0$ to y_c, the quantity λ will be zero. In any case it can be expected to be a small quantity and could well be ignored. The secular equation, (6.2), now takes the form

$$\frac{U_w'}{c}\frac{\overline{\Phi}_w}{\overline{\Phi}_w'} = -\frac{U_w'}{c}\frac{\varphi_{3w}}{\varphi_{3w}'} = (1+\lambda) F(z) \tag{6.56}$$

or

$$\frac{1}{1+\lambda} E(\alpha_s, c) = F(z) \tag{6.57}$$

This equation is the counterpart of (6.25) in the WKB method. The right-hand side is a universal function of $\hat{z}$ and is independent of the velocity profile, and the left-hand side is a function of α_δ and c and depends on the velocity profile.

When the Tollmien viscous solution (6.40) is used for φ_3 a secular equation of the form (6.57) is also obtained. However, the variable $\hat{z}$ and the function λ have different interpretations. They are

$$\hat{z} = (\alpha_\delta R_\delta)^{1/3} \left[\frac{3}{2} \int_0^{y_c} |U - c|^{1/2} \, dy \right]^{2/3} \tag{6.58}$$

$$1 + \hat{\lambda} = \frac{U_w'}{c^{3/2}} \, \frac{3}{2} \int_0^{y_c} |U - c|^{1/2} \, dy \tag{6.59}$$

The Tietjens function, first introduced by Tietjens (1925) in the form $\hat{z} F(\hat{z})$, is perhaps the most computed function in fluid mechanics. The paper of Holstein (1950) includes tabulations of the results of his own computation plus the results of five other authors. The most recent and extensive computation is by Miles (1960). The Tietjens function is equivalent to the function $\bar{F}(\bar{z})$ of the WKB method, but has an entirely different behavior except for large $\hat{z}$. The same graphical procedure as described in Section 6.3 can be used to solve (6.57). The use of the Tollmien solutions requires the computation of the integral appearing in (6.58) and (6.59) as a supplementary calculation.

7. Numerical Examples of Asymptotic Method

7.1 Calculation of neutral-stability points

After all of the theoretical development, we can take a brief respite by working out some numerical examples. The first example will consist of the calculation, by Tollmien's graphical procedure, of the upper and lower branch points of neutral stability for the Blasius velocity profile and $c_r = 0.360$. The calculation proceeds as follows:

a) From a tabulation of the Tietjens function, such as given by Miles (1960) or Mack (1960), $F_i(z)$ is plotted against $F_r(z)$ to give the curve labelled Tietjens function in Fig. 7.1.

b) From a computer program that integrates the inviscid equation, the function $E(\alpha_\delta, c)/(1+\lambda)$ of the left-hand side of the secular equation (6.56) is computed for $c_r = 0.360$, $c_i = 0$ and several values of α_δ. E_i is plotted against E_r on the same graph as $F(z)$. The result is the curve labelled inviscid in Fig. 7.1.

c) The intersection point of the two curves establishes α_δ and z for the two neutral-stability points.

The numerical results are (with $\delta\sqrt{R_x}/x = 6.0$):

$$\eta_c = 0.1823, \qquad U'_c = 1.922 \qquad \text{for} \qquad c_r = 0.360$$

Lower Branch	Upper Branch
$\alpha_\delta = 0.7290$, $z = 2.642$	$\alpha_\delta = 1.204$, $R_\delta = 3.965$

Since $z = (\alpha_\delta R_\delta U'_c)^{1/3} \eta_c$

$\alpha_\delta R_\delta = 1584$	$\alpha_\delta R_\delta = 5350$
$R_\delta = 2173$	$R_\delta = 4444$

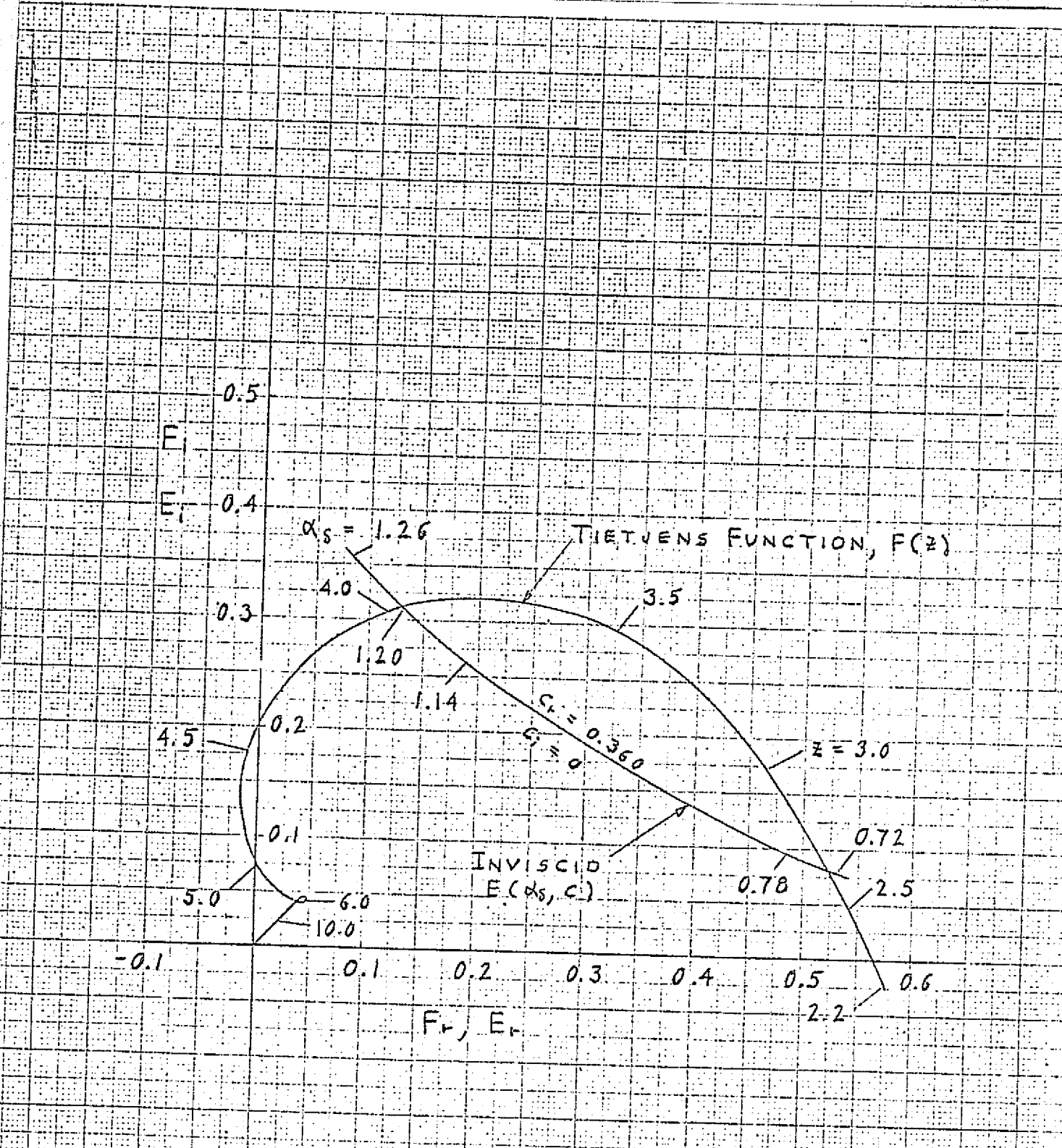

Fig. 7.1 Tietjens function and sample calculation

These results may be compared with those obtained by Kaplan (1964) from the numerical integration of the Orr-Sommerfeld equation.

$$\alpha_\delta = 0.765, \quad R_\delta = 2360 \qquad\qquad \alpha_\delta = 1.20, \quad R_\delta = 4360$$

The close agreement on the upper branch is probably a lucky accident. The differences on the lower branch are about what one would expect.

If the calculations are performed with the Tollmien viscous solution of Sectio.. 6.5, the values of α_δ remain unchanged because the left-hand side of the secular equation is unchanged except for the unimportant function $\lambda(c)$ (λ changes from 1.009 to 1.0055). Only the definition of $\hat{z}$, and hence R_δ , changes. According to (6.57),

$$\hat{z} = (\alpha_\delta R_\delta)^{1/3} \left[\frac{3}{2} \int_0^{\eta_c} |U - c|^{1/2} \, d\eta \right]^{2/3}$$

For $c_r = 0.360$,

$$\hat{z} = 0.2292 \, (\alpha_\delta R_\delta)^{1/3}$$

and

$$\alpha_\delta R_\delta = 1555 \qquad\qquad \alpha_\delta R_\delta = 5245$$

$$R_\delta = 2133 \qquad\qquad R_\delta = 4356$$

The already good agreement on the upper branch is made even better; the discrepancy on the lower branch becomes a bit greater. The Tollmien solution is an unnecessary refinement for the Blasius velocity profile,

since $u(y)$ is so nearly linear. However, it should offer a distinct improvement over the simpler solution for those profiles where $u(y)$ is far from linear.

7.2 Thickness of viscous regions

We can compute the viscous length scales ε_w and ε_c from their definitions (6.6) and (6.10).

$$\varepsilon_w = 0.0592 \qquad \varepsilon_w = 0.0322$$

$$2\varepsilon_c = (2)(0.0690) = 0.138 \qquad 2\varepsilon_c = (2)(0.0440) = 0.0880$$

Since the functions χ_3' and $\chi_2^{(1)\prime}$ are available to us, we may examine the extent of the viscous regions directly from Figs. 6.1 and (6.2). The wall values are

$$|\chi_{3w}'| = 7.30 \qquad |\chi_{3w}'| = 15.40$$

χ_3' is reduced to $1/e$ of its wall value at

$$\zeta = -1.0 \qquad \zeta = -2.1$$

Hence, in terms of y the thicknesses of the viscous regions are

$$y_v = (2.64 - 1.00)\,\varepsilon_c \qquad y_v = (3.96 - 2.10)\,\varepsilon_c$$

$$= 0.113 \qquad = 0.082$$

and

$$y_v/y_c = 0.62 \qquad y_v/y_c = 0.45$$

These values for y_v are not too far from the value of $2\varepsilon_c$ computed above. It is apparent that ε_w gives a considerable underestimate of the thickness. However, it should be noted that the ratio of y_v at the two neutral points is proportional to neither the ratio of ε_w or ε_c .

By reference to Fig. 6.3 for the correction function $\chi_2^{(1)\prime}$, we are able to check directly whether the critical-point viscous region extends to the wall. For the upper-branch point ($\bar{z} = 3.96$), it is evident that this region does not extend to the wall, although it does overlap the wall viscous region. However, for the lower-branch point ($\bar{z} = 2.64$), $\chi_{2r}^{(1)\prime}$ is still $2\frac{1}{2}\%$ below its asymptotic value at $y = 0$. It is not known how much of an effect this small difference would have on the eigenvalues, but we can expect any effect to be well within the order of accuracy of the method.

7.3 Calculation of an eigenfunction

The final step in the computation is to obtain the eigenfunctions, and we shall partially indicate how this is done for the longitudinal velocity fluctuation at the upper-branch point calculated above. The inviscid amplitude function $F = i\bar{\Phi}'$ is plotted in Fig. 7.2. It is valid for y greater than $y_c + 3\varepsilon_c$ ($3\varepsilon_c = 0.132$). For $y_c - 3\varepsilon_c < y < y_c + 3\varepsilon_c$ it must be corrected by $\chi_2^{(1)\prime}$, and for $y < y_c$ it must also be corrected by χ_3' . Consequently, for $y < y_c$ these two corrections must be applied simultaneously.

The first step is to compute the complex constant A (actually iA here) from the second equation of (6.1).

We obtain F_r and F_i from the output of the computer program for $c_r = 0.360$, $c_i = 0$, $\alpha_s = 1.204$ The χ'_{3_r} and χ'_{3_i} are taken from Stuart's (1963) table, with the second derivatives used to calculate the values listed here.

$$F_r(0) = -5.217 \qquad F_i(0) = -1.915$$

$$\chi'_{3_r}(0) = 6.09 \qquad \chi'_{3_i}(0) = -14.14$$

With these values, we find

$$A_r = 0.0198, \qquad A_i = 0.360$$

The corrected amplitude function $f(y)$ is found from

$$f(y) = F(y) + A\chi'_3(y)$$

and is shown in Fig. 7.2.

In Fig. 7.2 the viscous correction in the critical-point region is applied only to the imaginary part of F. This is done quite simply by multiplying χ''_{1_i} by a constant C such that $C\chi''_{1_i}(y_c - 0.132) = F_i(y_c - 0.132)$ and then continuing F_i beyond $y = y_c - 0.132$ with $C\chi''_{1_i}$. To correct F_r it is first necessary to separate $1 + \log \zeta$ from F_r and this has not been done. A complete description of the correction procedure may be found in Schlichting (1935), where the inviscid solution through the entire boundary layer is obtained from the series expansions in powers of $y - y_c$.

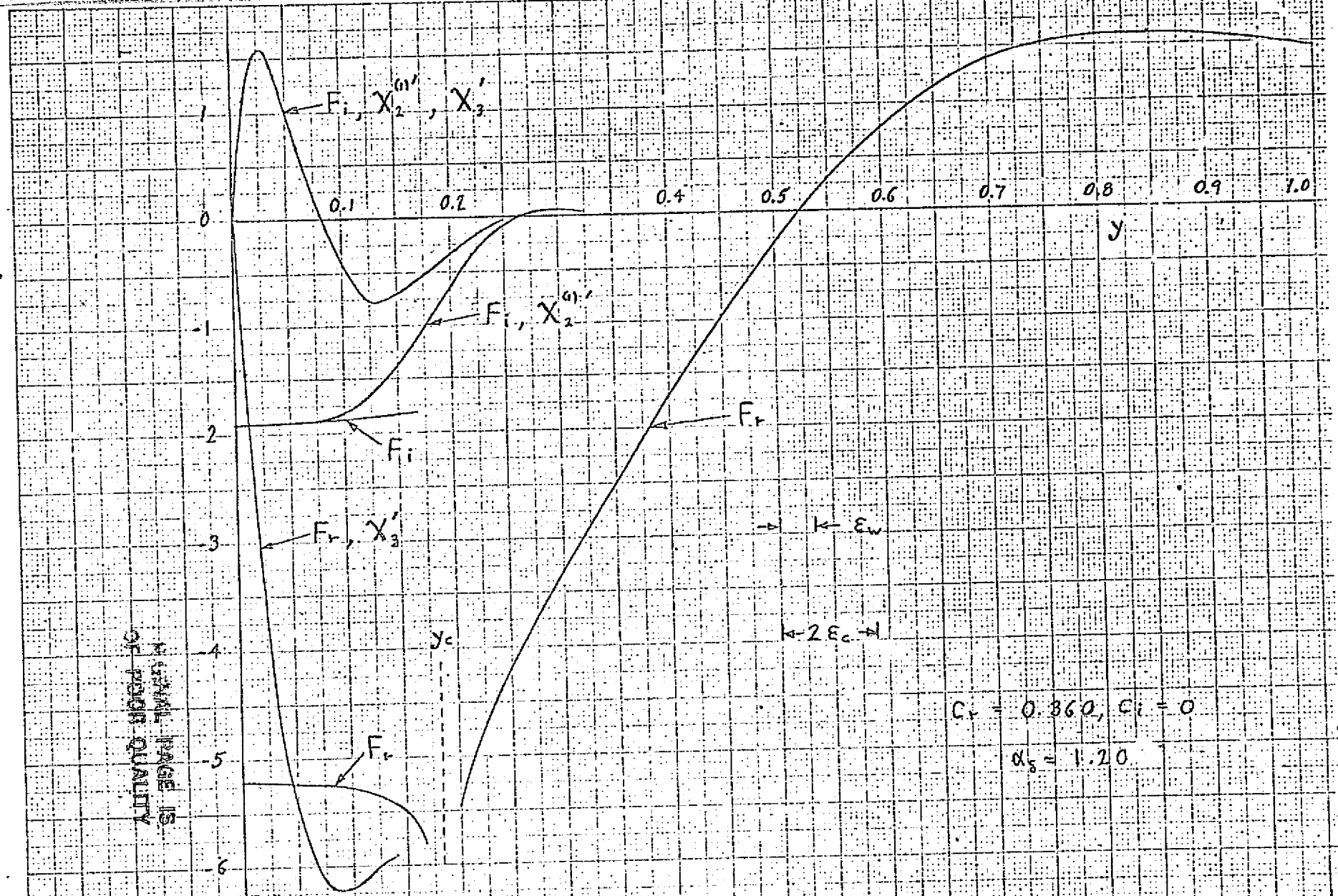

Fig. 7.2 Application of viscous corrections to inviscid eigenfunction

8. Numerical Integration of Orr-Sommerfeld Equation

The asymptotic method described in the previous section provides eigenvalues of neutral disturbances with reasonable accuracy. However, for the best results it is necessary to have available a computer program for calculating exact numerical inviscid solutions, and, in the absence of computations of the Tietjens function for complex $\bar{z}$, amplified and damped solutions must be obtained by a different method which involves a perturbation of the neutral solutions (Schlichting (1933b), Shen (1954)). Because of these limitations, attention has turned in the last few years to obtaining all numerical results from exact numerical solutions of the Orr-Sommerfeld equation itself. The task of developing suitable numerical methods was not an easy one because in the Orr-Sommerfeld equation the highest-order derivative φ is multiplied by a small quantity, $1/\alpha_s R_s$. This circumstance, which is the source of the non-regular nature of the inviscid and WKB solutions, is also a source of great difficulties in the numerical integration.

The WKB solutions clearly demonstrate the reason for this difficulty. It can be seen from the solutions φ_3 and φ_4, given by (6.17) and (6.18), that regardless of whether the integration proceeds in the + y or - y direction, there will always be a solution present which grows roughly as $\exp\left[(\alpha_s R_s)^{1/2} \Delta y^{3/2}\right]$. Any eigensolution of the Orr-Sommerfeld equation is of order one throughout the boundary layer, and it is the task of the numerical integration to produce this solution in the presence of solutions φ_3 and φ_4. Since every numerical integration scheme has some inherent

errors, and the growth of these errors will be determined by the most rapidly growing solution, it can easily happen that after the integration proceeds a certain distance, the error will overwhelm the solution.

The available numerical integration methods fall into three main types. The earliest in time (for channel flow) was by Thomas (1953), where the forward integration method was abandoned at the outset. Instead, a finite-difference approach was used where the Orr-Sommerfeld equation was simultaneously solved at a large number of y stations, and the eigenvalues obtained by the inversion of a large matrix. This method was later successfully applied by Kurtz and Crandall (1962) to the Blasius boundary layer. The second approach is that of Brown (1954, 1959). He used a straightforward forward integration method and errors were controlled by restriction to low values of $\alpha_i R_\delta$, or by an increase in the number of significant figures (use of double-precision arithmetic). The third approach was initiated by Kaplan (1964). In this method, the integration starts in the free stream and proceeds to $y = 0$. Two linearly independent solutions are produced. The first solution, which for $y > \delta$ is equal to the viscous solution (4.19), is integrated first. It becomes large and offers no problem. The second solution, which for $y > \delta$ is equal to the inviscid solution (4.18), grows much less than the first solution and is in danger of being "contaminated" by it. To avoid this, a quantity proportional to the first solution is subtracted from the second solution after a few integration steps, and a condition

is applied which forces the second solution to remain small. This process was called "purification" by Kaplan, and a version of the method is described in detail in Betchov and Criminale (1967). A rigorous version of Kaplan's method was provided by Bellman and Kalaba (1965) and applied to the boundary layer by Wazzan, Okamura, and Smith (1966). In this method, the standard Gram-Schmidt orthonormalization technique is used to assure that the second solution is linearly independent of the rapidly growing solution and of magnitude unity. Another method along these lines that is worthy of mention is the quasilinearization method of Radbill and Van Driest (1966).

The method of Kurtz and Crandall and the forward integration method with single-precision arithmetic (8 digits) are limited to growth factors of the rapidly growing solution of about 10^8. Double precision in the forward integration method extends this growth factor to about 10^{18}. In contrast, according to Betchov and Criminale (1967), the growth factor in Kaplan's method can be 10^{40}, and in Wazzan, Okamura, and Smith's method it can be 10^{80}. Both of these methods use only single precision arithmetic. The latter method can be considered to solve the problem of integrating the Orr-Sommerfeld equation under almost any conceivable circumstances. For example, the latter authors have computed the eigenvalues of neutral and amplified disturbances for the Blasius boundary layer up to $R_x = 2.5 \times 10^9$, where R_x is the x Reynolds number. Instability first appears at $R_x = 2.5 \times 10^5$, and transition, even for a free stream of very low turbulence level, occurs by $R_x = 3 \times 10^6$. Therefore, this method more than covers the range of Reynolds numbers of interest for the transition problem, and could be used

to study such things as the approach of finite-Reynolds number damped solutions to the inviscid limit with increasing Reynolds number.

No details of any of these methods will be given here. In Section 14.2, a brief description is presented of a forward integration method which provides automatic calculation of the eigenvalues and eigenfunctions of the compressible stability equations.

9. Numerical Results

9.1 Review of existing calculations

A considerable body of numerical results has been accumulated over the years from both the asymptotic method and from direct numerical integration of the Orr-Sommerfeld equation. These results, while extensive, did not begin to be comprehensive until the computer came into use. The earlier investigators usually contented themselves with the computation of the neutral-stability curve. A notable exception was the calculation of Pretsch (1941), where amplified as well as neutral solutions were obtained for a family of velocity profiles. After the development of approximate formulas by Lin (1945), it became the somewhat unfortunate custom to compute only the critical Reynolds number, i.e., the lowest Reynolds number for instability. Such calculations, as has been emphasized by Kaplan (1964), are of limited usefulness. In order to have an accurate picture of the comparative instability of two different boundary-layer profiles, it is necessary to calculate the neutral-stability curve and the amplification rates. In the following summary, only those calculations are mentioned in which at least a neutral-stability curve has been obtained.

The neutral-stability curve of the Blasius boundary layer has been computed, using the asymptotic method, by Tollmien (1929), Schlichting (1933a), Pretsch (1941), Lin (1945), Lees (1947), and Shen (1954); and, using numerical integration, by Brown (1959), Kurtz and Crandall (1962), Kaplan (1964), Betchov (1965), Wazzan, Okamura and Smith (1966), and Radbill and Van Driest (1966). The effect of pressure gradient was first

considered by Schlichting (1940) for the Howarth profiles $U_1 - ax$. Neutral-stability curves for the Falkner-Skan family, $U_1 \sim x^m$, have been computed by Pretsch (1941), Kaplan (1964), and Wazzan, Okamura and Smith (1966). Neutral-stability curves for 6th-degree polynomials have been computed for various values of the Pohlhausen parameter by Schlichting and Ulrich (1942) and by Timman, Zaat and Burgerhout (1956).[1] The boundary layer with suction was computed by Pretsch (1942), Bussmann and Münz (1942), Freeman (unpublished, but see Chiarulli and Freeman (1948)), and Hughes and Reid (1965). Contour lines of constant non-zero c_i, from which the amplification rate may be obtained, have been computed for various flows from the asymptotic theory by Schlichting (1933b) and Shen (1954) for the Blasius boundary layer, and by Pretsch (1941) for the Falkner-Skan family of profiles. Such calculations are usually performed as a matter of course when the method of numerical integration is used. Eigenfunctions have been computed by Schlichting (1935) and Holstein (1950) from the asymptotic method, and are normally obtained along with the eigenvalues in the numerical integration methods.

Some results for the Blasius boundary layer will be found in Section 12, where the experimental confirmation of the theory is presented. The calculations performed for the Falkner-Skan family of velocity profiles are of particular interest because these profiles provide examples where

[1] Doubt has recently been expressed about the validity of calculations made from the parallel-flow theory for the case of a favorable pressure gradient by Morkovin and Donaldson (private communications).

inviscid instability is important, and thus the results serve as background for the stability of the compressible boundary layer to be presented later. A short discussion of these results is given in the next section.

9.2 Falkner-Skan velocity profiles

The Falkner-Skan family of boundary-layer velocity profiles correspond to free-stream velocity distributions of the form

$$u_1(x) = k\, x^m \tag{9.1}$$

The boundary-layer equations reduce to ordinary differential equations for these profiles. These equations were solved for various values of m by Hartree (1937), and more exactly and with more detailed results by Smith (1954). The similarity variable which replaces y is

$$\eta = \frac{y}{x}\left(\frac{2}{2-\beta}\right)^{1/2}(R_x)^{1/2} \tag{9.2}$$

where

$$\beta = \frac{2m}{m+1} \tag{9.3}$$

The value $\beta = 0$ corresponds to the Blasius boundary layer; with $\beta > 0$ there is a favorable pressure gradient; with $\beta < 0$ there is an adverse pressure gradient. The value $\beta = -0.1988$ corresponds to the separation profile, where $u'_w = 0$.

According to the theorems presented in Section 5.1, the necessary and sufficient condition for neutral and amplified inviscid solutions is that U'' must be zero somewhere in the boundary layer. For $\beta \geq 0$, $U'' < 0$ everywhere (except at $y = 0$ for the Blasius boundary layer). However, for $\beta < 0$, U'' will always be zero at some y. Consequently, for $\beta < 0$ the Falkner-Skan profiles have inviscid instability and the curves of neutral stability will be of the type shown in Fig. 1.1b. These profiles are of interest because they provide an example where there is a steady evolution from a profile where viscous instability is dominant ($\beta = 0$) to profiles where inviscid instability becomes increasingly important. In Part B, we shall find that a similar evolution takes place with increasing Mach number for the compressible boundary layer on an insulated flat plate.

Table 9.1 gives some numerical results for the Falkner-Skan profiles with adverse pressure gradient.[1] In the table, η_s is the similarity variable as defined by (9.2) evaluated at y_s, which is

β	η_s	c_s	$(\alpha_s^* c_i)_s$	$(\alpha_s^* c_i)_{max}$	η_b	δ^*
0	0	0	0	4.4×10^{-3}	6.0	1.7
- 0.05	-	0.32	0.30	5.9×10^{-3}	-	1.8
- 0.10	1.3	0.43	0.46	1.0×10^{-2}	6.5	2.0
- 0.14	2.1	0.49	0.64	1.6×10^{-2}	6.7	2.2
- 0.1988	3.3	0.50	1.31	6.3×10^{-2}	7.8	3.2

Table 9.1. Numerical results for Falkner-Skan velocity profiles. Adverse pressure gradient.

[1] These results, and Fig. 9.1, were obtained from material kindly furnished to me by Mr. A. M. O. Smith of McDonnell-Douglas Corp, Long Beach, Calif. and computed by Wazzan, Okamura, and Smith (1966).

the η where $U'' = 0$. The third column, c_s , is the phase velocity of the inviscid neutral disturbance, and is equal to the mean velocity at η_s as was shown in Section 5.1. The fourth column gives the corresponding wave number $(\alpha_{\delta^*})_s$ referenced here to displacement thickness, as obtained from the upper branch of the neutral-stability curve at high but finite Reynolds number. It could be computed exactly from (4.21) for $c_r = c_s$, $c_i = 0$. The fifth column of Table 9.1 gives the maximum time rate of amplification (at finite Reynolds number except for $\beta = -0.1988$), again referenced to displacement thickness. The final two columns give the boundary-layer thickness and the displacement thickness, both in the η coordinate.

It is seen from Table 9.1 that with increasing negative values of β , the quantities η_s , c_s , $(\alpha_{\delta^*})_s$ and $(\alpha_{\delta^*} c_i)_{max}$ increase. Thus, instability increases as the inflection point moves away from the wall. The amplification rates of Table 9.1 for $\beta < 0$ contrast strongly with the maximum amplification rate of the Blasius boundary layer. It is evident that a velocity profile with an inflection point located well away from the wall has much stronger instability than a profile with no inflection point. The most unstable profile of all is the separation profile.

The neutral-stability curves and contours of c_i = const. are of great interest. Figures 9.1 and 9.2 give these results for $\beta = -0.14$ and -0.1988 (separation profile), respectively. Figure 9.1 clearly shows that in spite of the large inviscid instability, there is still a small

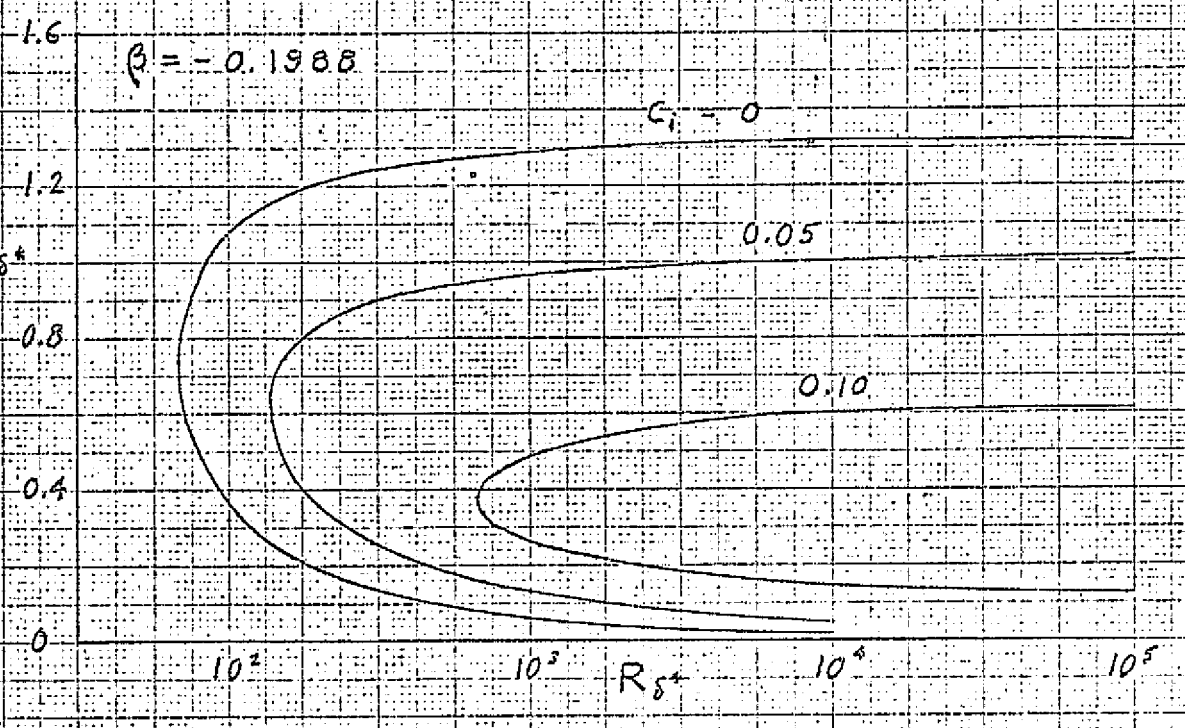

Fig. 9.2 Neutral-stability curve and contours of c_i = const. Falkner-Skan separation profile. β = - 0.1988

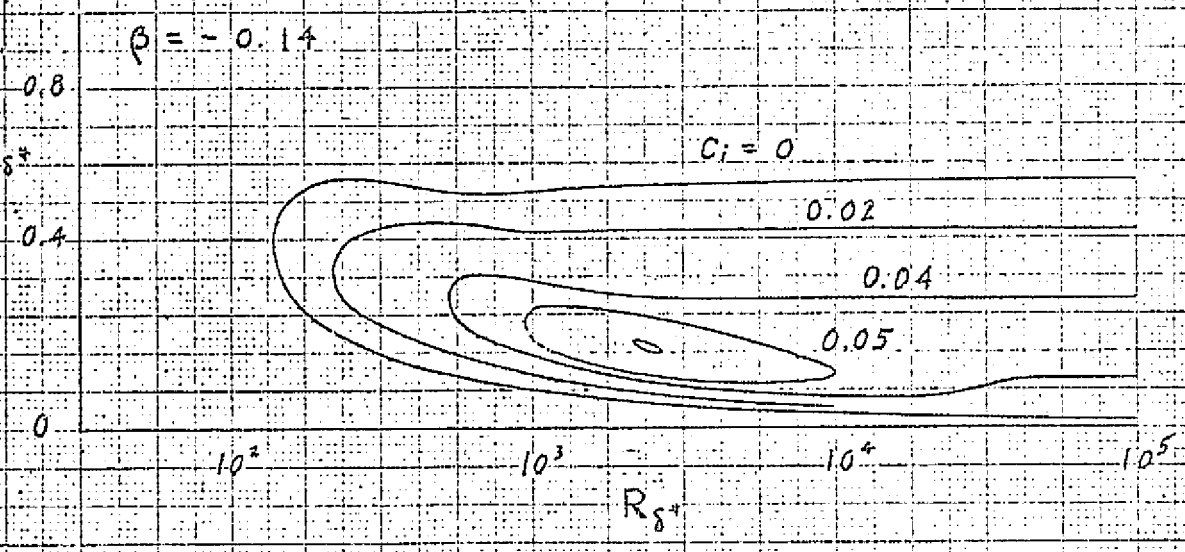

Fig. 9.1 Neutral-stability curve and contours of c_i = const. Falkner-Skan profile. β = - 0.14

destabilizing effect of viscosity.[1] The maximum amplification rate at a fixed R_{δ^*} increases about 15% as R_{δ^*} decreases from infinity to about 10^3. Note that the maximum amplification rate is nearly constant until R_{δ^*} is reduced below 10^4. Most of the c_i = const. contours are open for $\beta = -0.14$, i.e., the upper and lower branches extend to infinity. Only those contours with $c_i > 0.04$ form closed loops. In contrast, for the Blasius profile ($\beta = 0$) all of the contours except for $c_i = 0$ close at some finite Reynolds number.

Figure 9.2, for the separation profile, shows the final stage in the evolution of the c_i = const. contours. Here none of the contours are closed, and they all extend to infinity. Also the upper branches are all either parallel to the R_{δ^*} axis or have a positive slope. As a result, the maximum amplification rate at $R \to \infty$ is the highest amplification rate that is possible for this velocity profile. The destabilizing effect of viscosity has completely disappeared, and viscosity serves only to damp the disturbances. These disturbances are formed by the inviscid instability mechanism associated with the inflection point. Neutral-stability curves of this type are common for free-shear flows, where the inviscid amplification rates are even larger than for the separation profile. We shall find in Part B that they are characteristic of the compressible boundary layer at a sufficiently high Mach number even in the absence of a pressure gradient.

---

[1] We use the term "destabilizing effect of viscosity" to mean that the maximum (with respect to α_δ at a fixed R_δ) amplification rate increases with decreasing Reynolds number over some portion of the Reynolds number range.

10. Kinetic-Energy Equation

Some of the earliest attempts at a stability theory were carried out on the basis of energy methods. These methods were aimed primarily at a calculation of the critical Reynolds number, but were not very successful even in this limited objective, as the Reynolds numbers obtained were always extremely low. This was a direct result of the fact that the disturbances used in these analyses were not required to be solutions of the differential equations. Consequently, the conditions necessary to secure stability of all disturbances had to be more severe than those necessary to insure the stability of only hydrodynamically possible disturbances. For our purposes the energy method will be useful in shedding some light on the physical basis of the stability theory. Up to now, the discussion has been mainly mathematical, and the time has come to bring out some of the physical mechanisms at work.

This section is devoted to a derivation of an equation for the kinetic energy of a disturbance. The dimensional x-momentum equation is, in two dimensions,

$$\frac{\partial u}{\partial t} + u\frac{\partial u}{\partial x} + v\frac{\partial u}{\partial y} = -\frac{1}{\rho}\frac{\partial p}{\partial x} + \nu\left(\frac{\partial^2 u}{\partial x^2} + \frac{\partial^2 u}{\partial y^2}\right) \tag{10.1}$$

When the flow quantities are split into a steady mean component and a disturbance, the resulting equation is

$$\frac{\partial u'}{\partial t} + U\frac{\partial u'}{\partial x} + u'\frac{\partial u'}{\partial x} + v'\frac{\partial U}{\partial y} + v'\frac{\partial u'}{\partial y} + U\frac{\partial U}{\partial x} + V\frac{\partial U}{\partial y}$$
$$= -\frac{1}{\rho}\frac{\partial p'}{\partial x} - \frac{1}{\rho}\frac{\partial P}{\partial x} + \nu\left(\frac{\partial^2 u'}{\partial x^2} + \frac{\partial^2 u'}{\partial y^2} + \frac{\partial^2 U}{\partial y^2}\right) \tag{10.2}$$

Three mean-flow terms have been dropped by the boundary-layer approximation, but nonlinear terms have been retained. These terms can be transformed as follows with the use of the continuity equation.

$$u' \frac{\partial u'}{\partial x} + v' \frac{\partial u'}{\partial y} = \frac{\partial}{\partial y}(u'v') + \frac{\partial}{\partial x}\frac{u'^2}{2} \tag{10.3}$$

The disturbance is assumed to be periodic in x and growing in time. Thus an x average taken over a wavelength at a particular time has a definite meaning. Since such an average of periodic terms is zero, only nonlinear and mean-flow terms remain when the equation is averaged.

$$U \frac{\partial U}{\partial x} + V \frac{\partial U}{\partial y} + \frac{\partial}{\partial y}(\overline{u'v'}) = \frac{1}{\rho}\frac{\partial p}{\partial x} + \nu \frac{\partial^2 U}{\partial y^2} \tag{10.4}$$

The quantity

$$\tau = -\rho \overline{u'v'} \tag{10.5}$$

is the Reynolds stress. It is a momentum transfer caused by the disturbance, and acts in addition to the mean-flow stress $\mu \partial U/\partial y$. If (10.4) is written in the form

$$\rho U \frac{\partial U}{\partial x} + \rho V \frac{\partial U}{\partial y} = -\frac{\partial p}{\partial x} + \frac{\partial}{\partial y}\left(\mu \frac{\partial U}{\partial y} - \rho \overline{u'v'}\right) \tag{10.6}$$

we recognize it as the mean flow boundary-layer equation with an additional stress term. Consequently, when nonlinear terms are included, the mean flow in the presence of a periodic disturbance cannot be the same as the mean flow with no disturbance (see Stuart (1956)).

The next step is to subtract the mean-flow equation from (10.2), and then to multiply the remaining equation by u' in order to form part of a kinetic energy equation. This equation is

$$\left(\frac{\partial}{\partial t} + U\frac{\partial}{\partial x}\right)\left(\frac{u'^2}{2}\right) + u'v'\frac{\partial U}{\partial y} + u'\frac{\partial}{\partial y}(u'v') + u'\frac{\partial u'^2}{\partial x}$$

$$u'\frac{\partial}{\partial y}(\overline{u'v'}) = -\frac{1}{\rho}u'\frac{\partial p'}{\partial x} + \nu u'\nabla^2 u' \qquad (10.7)$$

When the same procedure is applied to the y momentum equation, except for multiplication by v' instead of u', and the resulting equation is added to (10.7), we have

$$\left(\frac{\partial}{\partial t} + U\frac{\partial}{\partial x}\right)\left(\frac{u'^2+v'^2}{2}\right) + u'v'\frac{\partial U}{\partial y} + u'\frac{\partial}{\partial y}(u'v') + v'\frac{\partial}{\partial y}(u'v')$$

$$+ u'\frac{\partial u'^2}{\partial x} + v'\frac{\partial v'^2}{\partial y} - u'\frac{\partial}{\partial y}(\overline{u'v'}) - v'\frac{\partial^2\overline{v'^2}}{\partial y^2} \qquad (10.8)$$

$$= -\frac{1}{\rho}\left(u'\frac{\partial p'}{\partial x} + v'\frac{\partial p'}{\partial y}\right) + \nu\left(u'\nabla^2 u' + v'\nabla^2 v'\right)$$

The last two terms of the first line can be converted into energy fluxes.

$$u'\frac{\partial}{\partial y}(u'v') = -u'\frac{\partial}{\partial x}\left(\frac{u'^2}{2}\right) + v'\frac{\partial}{\partial y}\left(\frac{u'^2}{2}\right)$$

$$v'\frac{\partial}{\partial x}(u'v') = u'\frac{\partial}{\partial x}\left(\frac{v'^2}{2}\right) - v'\frac{\partial}{\partial y}\left(\frac{v'^2}{2}\right) \qquad (10.9)$$

The energy equation then becomes

$$\left(\frac{\partial}{\partial t} + u\frac{\partial}{\partial x}\right)\left(\frac{u'^2+v'^2}{2}\right) + u'\frac{\partial}{\partial x}\left(\frac{u'^2+v'^2}{2}\right) + v'\frac{\partial}{\partial y}\left(\frac{u'^2+v'^2}{2}\right)$$

$$- u'\frac{\partial}{\partial y}(\overline{u'v'}) - v'\frac{\partial \overline{v'^2}}{\partial y} + u'v'\frac{\partial u}{\partial y} \qquad (10.10)$$

$$= -\frac{1}{\rho}\left(u'\frac{\partial p'}{\partial x} + v'\frac{\partial p'}{\partial y}\right) + \nu(u'\nabla^2 u' + v'\nabla^2 v')$$

At this point we integrate (10.10) over a volume which extends one wavelength λ in the x direction and to infinity in the y direction. The terms with a single fluctuation quantity, or an x derivative of a fluctuation times a mean-flow quantity, are zero by periodicity. There are two terms of the type $u'\partial G/\partial x + v'\partial G/\partial y$. Their integrals can be shown to be zero as follows:

$$\int_0^\infty \int_x^{x+\lambda} u'\left(\frac{\partial G}{\partial x} + v'\frac{\partial G}{\partial y}\right) dx\, dy = \int_0^\infty \left(u'G\Big|_x^{x+\lambda} - \int_x^{x+\lambda} G\frac{\partial u'}{\partial x}\, dx\right) dy$$

$$+ \int_x^{x+\lambda}\left(v'G\Big|_0^\infty - \int_0^\infty G\frac{\partial v'}{\partial y}\, dy\right) dx \qquad (10.11)$$

From periodicity and the boundary condition at $y \to \infty$ on v', we have

$$\iint\left(u'\frac{\partial G}{\partial x} + v'\frac{\partial G}{\partial y}\right) dx\, dy = -\iint G\left(\frac{\partial u'}{\partial x} + \frac{\partial v'}{\partial y}\right) dx\, dy \qquad (10.12)$$

This integrand on the right-hand side is zero by the continuity equation. The viscous terms of (10.10) can be transformed into

$$u'\nabla^2 u' + v'\nabla^2 v' = u'\frac{\partial \zeta'}{\partial y} - v'\frac{\partial \zeta'}{\partial x} \qquad (10.13)$$

where

$$\zeta' = \frac{\partial u'}{\partial y} - \frac{\partial v'}{\partial x} \tag{10.14}$$

is the disturbance vorticity. The integral of (10.13) gives, after integration by parts,

$$\iint \left(u' \frac{\partial \zeta'}{\partial y} - v' \frac{\partial \zeta'}{\partial x} \right) dx\, dy = -\iint \zeta' \left(\frac{\partial v'}{\partial x} - \frac{\partial u'}{\partial y} \right) dx\, dy = -\iint \zeta'^2 dx\, dy \tag{10.15}$$

An alternate form of this integral, which is perhaps more easily identifiable as the viscous dissipation, is

$$\begin{aligned} -\iint \zeta'^2 dx\, dy = 2 \iint \left[\left(\frac{\partial u'}{\partial x} \right)^2 + \left(\frac{\partial v'}{\partial y} \right)^2 \right] dx\, dy \\ + \iint \left(\frac{\partial u'}{\partial y} + \frac{\partial v'}{\partial x} \right)^2 dx\, dy \end{aligned} \tag{10.16}$$

With these reductions, the remaining terms in the energy equation are

$$\rho \frac{\partial}{\partial t} \iint \left(\frac{u'^2 + v'^2}{2} \right) dx\, dy = -\rho \iint u'v' \frac{\partial \bar{u}}{\partial y} dx\, dy + \mu \iint \zeta'^2 dx\, dy \tag{10.17}$$

Now,

$$-\rho \frac{1}{\lambda} \int_x^{x+\lambda} u'v' dx = -\rho \overline{u'v'} = \tau \tag{10.18}$$

where the bar refers to an x average, and τ has already been identified as the Reynolds stress. Hence, (10.17) can be written, with asterisks introduced again to identify dimensional quantities,

$$\boxed{\frac{\partial \bar{E}^*}{\partial t^*} = P^* - D^*} \tag{10.19}$$

where

$$\bar{E}^* = \rho^* \int_0^\infty \frac{\overline{u^{*\prime 2}} + \overline{v^{*\prime 2}}}{2} \, dy^* \tag{10.20}$$

is the disturbance kinetic energy in the volume of fluid,

$$P^* = \int_0^\infty \tau^* \frac{\partial \bar{u}^*}{\partial y^*} \, dy^* \tag{10.21}$$

is the energy production term, and

$$D^* = \mu^* \int_0^\infty \overline{\zeta^{*\prime 2}} \, dy^* \tag{10.22}$$

is the energy dissipation term.

If all quantities are made dimensionless in the usual manner, with u_1^* as the velocity scale, and δ as the length scale, then the integrated kinetic-energy equation becomes

$$\frac{\partial \bar{E}}{\partial t} = P - \frac{1}{R_\delta} D \tag{10.23}$$

where

$$\begin{aligned} \bar{E} &= \int_0^\infty \frac{\overline{u'^2} + \overline{v'^2}}{2} \, dy \\ P &= \int_0^\infty \tau \frac{\partial \bar{u}}{\partial y} \, dy \\ D &= \int_0^\infty \overline{\zeta'^2} \, dy \end{aligned} \tag{10.24}$$

and

$$\tau = -\overline{u'v'} \tag{10.25}$$

are the dimensionless counterparts of (10.20), (10.21), (10.22) and (10.18).

Equation (10.23) is exact in the sense that no further approximations were made beyond the boundary-layer approximation. It holds for nonlinear as well as linear disturbances, although, as already mentioned, in the latter case U must be interpreted as the mean velocity in the presence of a disturbance and differs from the disturbance-free mean flow. For a linear disturbance, as seen from (10.6), U is the same with a disturbance as without one. The nonlinear and pressure-gradient terms of (10.10) contribute nothing to the integrated energy balance. They serve only to redistribute the energy within the boundary layer.

The term P of (10.23) represents the interaction of the mean flow with the disturbance. If the disturbance results in a Reynolds stress such that $P > 0$, then energy will pass from the mean flow into the disturbance. The dissipation term represents kinetic energy lost by the irreversible viscous work and is necessarily positive. Consequently, the conditions for damped, neutral, and amplified disturbances are, respectively,

$$P < \frac{1}{R_\delta} D \qquad P = \frac{1}{R_\delta} D \qquad P > \frac{1}{R_\delta} D \tag{10.26}$$

The purpose here is not to construct a stability theory based on (10.23). The eigensolutions of the Orr-Sommerfeld equation already provide complete information about the stability characteristics. Rather, (10.23) can serve to point out the direction to go in increasing our understanding of the physical mechanisms which are at work to produce instability. It is clear from (10.23) that a decisive role is played by the Reynolds stress and it is to this quantity that we must turn our attention.

11. Distribution of Reynolds Stress

11.1 Prandtl's analysis of wall region

Prior to 1921 it had been accepted doctrine that a flow which was stable in the absence of viscosity could only be made more stable by the presence of viscosity. Although an earlier, and in this connection evidently unnoticed, paper by Taylor (1915) pointed out the possible destabilizing influence of viscosity, it remained for Prandtl (1921) to clearly demonstrate the mechanism by which a stable inviscid flow can be made unstable by viscosity. It was this discovery which led to the elaboration of the stability theory in later years by Prandtl's students and colleagues. In view of the importance of this discovery, it is of interest to quote a few lines from Prandtl's paper (my translation).

"Previous mathematical investigations on the origin of turbulence have led to the opinion that small disturbances of a viscous, laminar flow between two walls are always damped...In order to learn how turbulence actually originates, I had built at Göttingen an open channel... and observed the flow by the Ahlborn method (sprinkled lycopodium powder) ...wave forms with slowly increasing amplitude were occasionally observed ...these waves of increasing amplitude completely contradicted the dogma of the stability of laminar motion with respect to small disturbances, so that at first I tended to believe that I had not seen this infrequent phenomenon completely right."

"We now applied outselves to the theoretical treatment, and, to anticipate a little, we found, contrary to the dogma, an instability of the small disturbances."

Prandtl's argument was later repeated in a different form by Lin (1954, 1955), but we shall follow essentially the original derivation here. The viewpoint adopted here is the same as that used in Section 6.2 to derive viscous solutions near the wall, i.e., it is assumed that $U(y) \approx 0$. With this assumption, the x-momentum equation, from (3.1), simplifies to

$$\frac{\partial u'}{\partial t} = -\frac{\partial p'}{\partial x} + \frac{1}{R_\delta}\frac{\partial^2 u'}{\partial y^2} \tag{11.1}$$

where the term $v' dU/dy$ has also been dropped. Outside of the wall viscous region, (11.1) reduces further to

$$\frac{\partial u'}{\partial t} = -\frac{\partial p'}{\partial x} \tag{11.2}$$

The velocity u' consists of two parts: an inviscid part u_i' which satisfies (11.2), and a viscous part u_v' which satisfies the difference between (11.1) and (11.2) and together with u_i' the no-slip boundary condition.

$$\frac{\partial u_v'}{\partial t} = \frac{1}{R_\delta}\frac{\partial^2 u_v'}{\partial y^2} \tag{11.3}$$

The solution of (11.3) is, for $c_i = 0$ and hence ω real,

$$u_v'(y) = -u_i'(0)\, e^{-(1-i)\left(\frac{\omega R_\delta}{2}\right)^{1/2} y}\, e^{i(\alpha x - \omega t)} \tag{11.4}$$

where the boundary conditions that $u'(0) = u_i'(0) + u_v'(0) = 0$ and $u'(y) \to u'(y_s)$ outside of the viscous layer have been applied.

The additional longitudinal disturbance velocity u_v', which is needed to satisfy the no-slip condition, induces an additional normal disturbance velocity v_v' through the continuity equation,

$$v_v'(y) = -\int_0^y \frac{\partial u_v'}{\partial y}\, dy \tag{11.5}$$

which yields, upon substitution of (11.4),

$$v_v'(y) = (1-i)\,\alpha_s\, u_i'(0)\, \frac{1}{(2\omega R_s)^{1/2}} \left[e^{-(1-i)\left(\frac{\omega R_s}{2}\right)^{1/2} y} - 1 \right] e^{i(\alpha_s x - \omega t)} \tag{11.6}$$

Outside of the viscous region v_v' is independent of y.

$$v_v' = -(1-i)\, \frac{\alpha_s\, u_i'(0)}{(2\omega R_s)^{1/2}}\, e^{i(\alpha_s x - \omega t)} \tag{11.7}$$

and u_v' is zero.

The consequences of (11.7) for the Reynolds stress are as follows. We have noted in Section 10 that the Reynolds stress is given by $\tau = -\overline{u'v'}$ (in dimensionless form). For an inviscid neutral disturbance u' and v' are 90° out of phase and τ is zero. However, for any other disturbance u' and v' are correlated and there is a Reynolds stress. Since u_v' is zero outside of the wall viscous layer, it can contribute nothing to τ outside of the layer. However, v_v' persists for some distance outside of the wall layer, and, since it is shifted in phase 135° with respect

to u_i' , it will produce a Reynolds stress. This Reynolds stress must equal the Reynolds stress set up by the flow in the vicinity of the critical layer, and which, in the absence of the wall viscous region, would extend to the wall. This stress is discussed in Section 11.2.

The formula for the Reynolds stress at the edge of the wall viscous region can be derived from (11.7). If we recall that it is necessary to take the real parts of u_i' and v_v' before multiplying and averaging, we find

$$\tau_e = -\overline{u_i' v_v'} = \frac{1}{2} \frac{\alpha_s}{(2\omega R_s)^{1/2}} \left[u_i'(0)\right]^2 \tag{11.8}$$

where $\omega = \alpha c_r$. If the ratio $\tau_e / \overline{v'^2}$ is formed, we have

$$\frac{\tau_e}{\overline{v'^2}} = \frac{1}{2\alpha_s} \left(\frac{2}{\omega R_s}\right)^{1/2} \tag{11.9}$$

A general expression for τ in the wall viscous region can be obtained from (11.4) and (11.6), and this expression would give the increase of τ from zero at the wall to the value given by (11.9) at the edge of the viscous region. Equation (11.9) establishes that τ is positive and, according to (10.2), energy will be transferred from the mean flow to the disturbance. Consequently, the wall viscous region, which is formed to satisfy the no-slip boundary condition, also has the effect of creating a Reynolds stress which acts to destabilize the flow. This mechanism must be present to some extent for all disturbances, but whether a particular disturbance is actually amplified or damped will depend on the distribution of the Reynolds stress through the entire boundary layer

and on the dissipation term.

As a note of caution, it must be recalled that the preceding analysis rests on the neglect of $\mathcal{U}$ in the wall viscous region. Consequently, we can expect the results to be valid only at high values of $\alpha_s R_s$, where the wall viscous region will be thin compared to the boundary-layer thickness, and for values of y_c large compared to the thickness of the wall viscous region.

11.2 Reynolds stress distribution from the inviscid theory

The inviscid theory can also provide us with a formula for the Reynolds stress which will apply to all of the boundary layer except the two viscous regions. First, we need a general expression for the Reynolds stress. Since

$$u' = i\varphi' e^{i(\alpha_s x - \omega t)} \quad , \quad v' = \alpha_s \varphi e^{i(\alpha_s x - \omega t)} \tag{11.10}$$

we find

$$\tau = \frac{1}{2}\alpha_s (\varphi_r \varphi_i' - \varphi_r' \varphi_i) e^{2\alpha_s c_i t} \tag{11.11}$$

It is easy to verify that the quantity W defined by (5.4) is equal to the part of (11.11) which is in parentheses.

$$W = \frac{i}{2}(\varphi \varphi^{*\prime} - \varphi^* \varphi') = \varphi_r \varphi_i' - \varphi_r' \varphi_i \tag{11.12}$$

Therefore, the Reynolds stress can be written

$$\tau = \frac{1}{2}\alpha_s W e^{2\alpha_s c_i t} \tag{11.13}$$

We have, from (5.2),

$$\frac{dW}{dy} = \frac{c_i U''}{|U-c|^2} |\phi|^2 \tag{11.14}$$

and it follows from (11.10) that

$$\overline{v'^2} = \frac{1}{2} \alpha_s^2 |\phi|^2 e^{2\alpha_s c_i t} \tag{11.15}$$

Consequently, the derivative of the Reynolds stress is

$$\frac{d\tau}{dy} = \frac{\overline{v'^2}}{\alpha_s} \frac{c_i U''}{|U-c|^2} \tag{11.16}$$

This equation was first derived by Foote and Lin (1950).

For a neutral disturbance, $d\tau/dy$ is zero everywhere except at $U=c$ where, by the same derivation that led to (5.6), τ has a discontinuity given by

$$\tau(y_c + 0) - \tau(y_c - 0) = \frac{\pi}{\alpha_s} \overline{v_c'^2} \frac{U_c''}{U_c'} \tag{11.17}$$

We can now sketch the expected Reynolds stress distribution in the boundary layer for a neutral viscous disturbance.

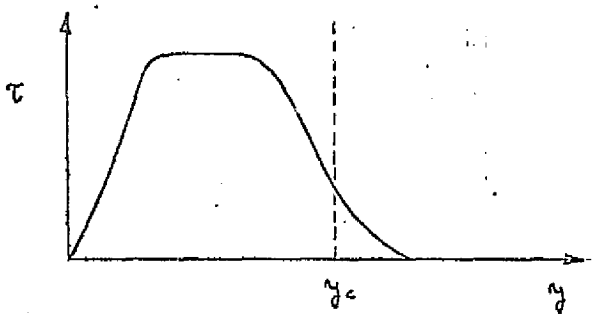

Fig. 11.1

The Reynolds stress builds up in the wall viscous region to the constant value given by (11.9) which, for consistency, must be equal to the value given by (11.17) with $\tau(y_c+0)=0$. The action of viscosity near y_c smooths out the discontinuity in τ. The integral of $\tau\, d\mathcal{U}/dy$ must be equal to $\mathcal{D}/R_\delta$, the integral of the dissipation terms.

The results obtained in Section 5.1 concerning the importance of an inflection point in the inviscid theory also follow directly from (11.16) and (11.17). Since there is no dissipation in an inviscid fluid, the Reynolds stress must be zero throughout the boundary layer for a neutral inviscid disturbance. Equation (11.17) shows immediately that $\mathcal{U}_c''$ must be zero. For an amplified disturbance, integration of (11.16) from $y=0$ to $y\to\infty$ and application of the boundary conditions on τ yields the result that $\mathcal{U}''$ must be zero somewhere in the boundary layer.

12. Experimental Confirmation of Stability Theory - Schubauer-Skramstad Experiment

No account of the laminar stability theory is complete without a mention of the classic experiment of Schubauer-Skramstad (1947). Up to the time this experiment was performed there was · experimental evidence to confirm Tollmien's theory of the stability of the Blasius boundary layer. Indeed what evidence there was indicated that the size of the disturbance was the controlling factor. The general attitude towards the theory was one of skepticism, and most people probably agreed with Taylor (1938) in thinking that the theory had little or no connection with boundary-layer transition. Only in Germany does there seem to have been general acceptance of the theory.

This picture was radically changed by the Schubauer-Skramstad experiment which provided a complete demonstration of the validity of the theory, and also firmly established the connection of the amplified oscillations with transition. This demonstration was unmistakable in spite of the fact that the calculations in existence at that time were not very accurate. The exact numerical calculations of recent years have only strengthened the demonstration. The experiment was performed during 1940 and 1941, but security restrictions prevented its publication in the open literature until 1947.

Experimental techniques will be discussed elsewhere in this course and we are only interested here in the results. It will suffice to say

that the disturbances were produced artificially in the boundary layer by means of a vibrating ribbon, which thus provided a means of controlling the amplitude and frequency of the disturbances. A hot-wire anemometer was used to follow the disturbance as it travelled downstream. The amplitude and phase of u' were the primary quantities measured.

The three main results of the experiments were: (i) the neutral-stability curve, (ii) the amplification rate as a function of wave number at three fixed Reynolds numbers, and (iii) the distribution with y of the amplitude of u'. The comparison of the experimental neutral-stability points with the neutral-stability curve computed by Kurtz (1961) is shown in Fig. 12.1. The agreement is very good except near the critical Reynolds number where there is a great deal of scatter.

In the comparison of the amplification rates, it has for some reason been customary to plot c_i rather than αc_i. Figure 12.2 gives c_i vs. α_{δ^*} at $R_{\delta^*} = 2200$ as measured and as computed by Kaplan. What was actually measured is the spatial amplification rate, which is transformed into a temporal amplification rate by (2.26). Schubauer-Skramstad used the phase velocity instead of the group velocity and achieved the remarkable agreement shown in Fig. 12.2. The agreement at the other two Reynolds numbers is not as good, and at the lowest Reynolds number there is a factor of two difference in the maximum amplification rate between theory and experiment (use of the group velocity would in every case worsen the agreement).

The third comparison is given in Fig. 12.3 where experimental measurement of the amplitude of u' as a function of η is plotted along with an eigenfunction calculated by Kaplan. Again the agreement is remarkable.

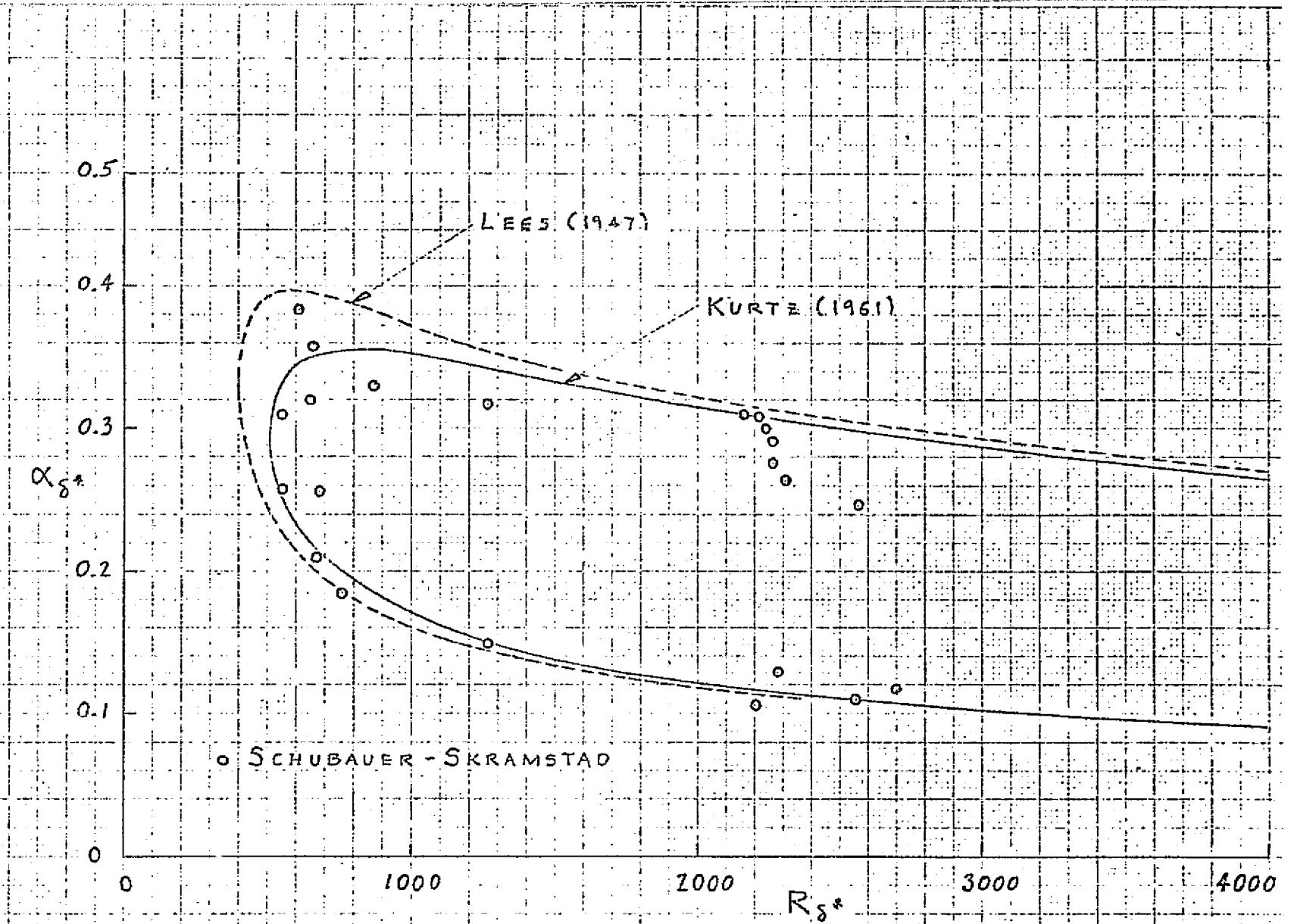

Fig. 12.1 Comparison of theoretical and experimental neutral-stability curves for Blasius boundary layer.

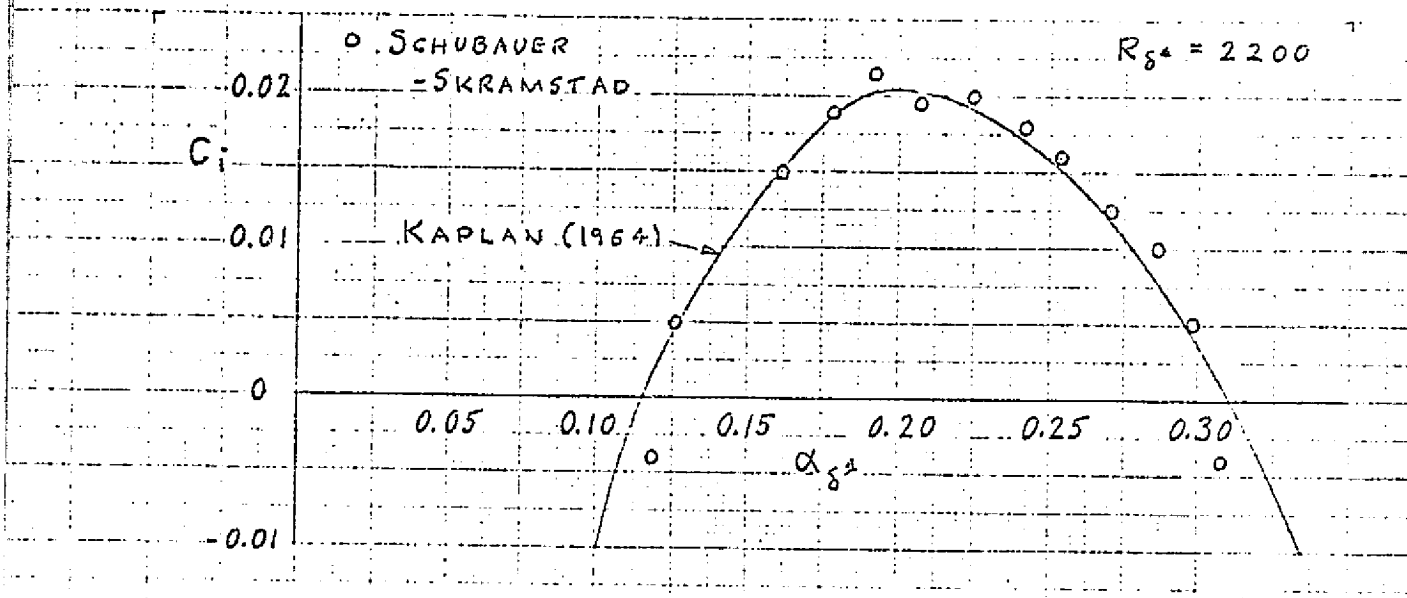

Fig. 12.2 Theoretical and experimental amplification factors for Blasius boundary layer.

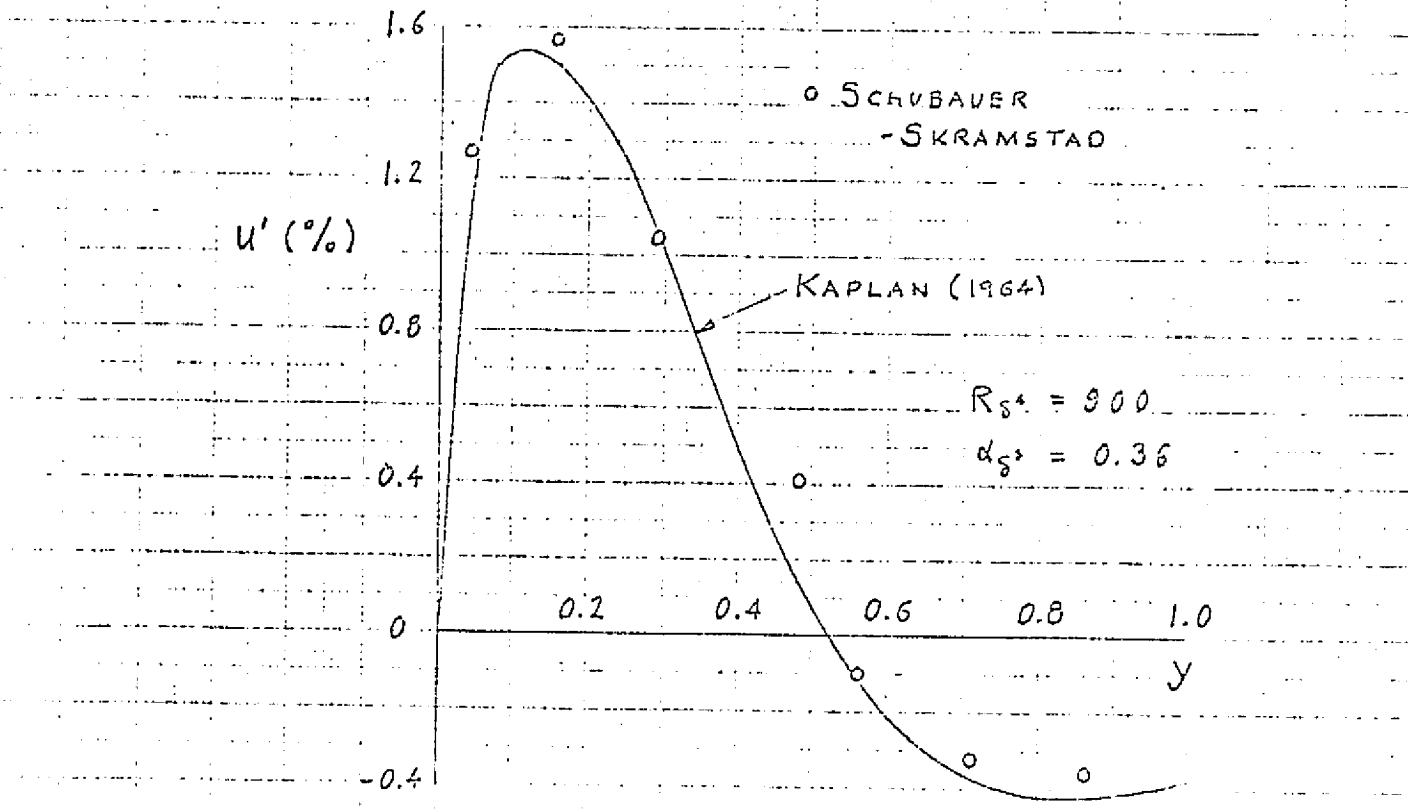

Fig. 12.3 Amplitude of longitudinal velocity fluctuation according to theory and experiment for Blasius boundary layer.

13. Derivation of Equations

13.1 Introductory remarks

The theory of the stability of a compressible boundary layer differs sufficiently from the incompressible boundary layer to warrant being treated as an entirely separate subject. Many of the general ideas are the same, and for this reason the incompressible theory can be regarded as an indispensable prelude, but there are at least three main differences. First, the asymptotic theory, which served to give an adequate account for incompressible flow, has had only a limited success for supersonic flow. Almost all results will have to be derived from numerical integration of the stability equations. Second, the inviscid theory has a much greater relevance than it had for incompressible flow, where it served mainly as a source of two solutions for the asymptotic theory. Although we shall concentrate entirely on the zero pressure-gradient boundary layer, the inviscid theory even here will be of great usefulness. Third, the existence of regions of supersonic flow relative to the phase velocity of the disturbance permits waves of an entirely different type than those found in incompressible flow.

The compressible theory has been developed by fewer people than was the case for the incompressible theory. Aside from an early investigation by Kuchemann, the theory can be considered to have started with a report by Lees and Lin (1946). In this work, the inviscid theory was considered in some detail and the elements of the asymptotic theory were worked out.

A subsequent work of Lees (1947) carried out calculations of neutral-stability curves up to $M_1 = 1.3$, and also included the famous prediction that cooling the wall would act to stabilize the boundary layer. The next study was by Dunn (1953) and Dunn and Lin (1955), where the asymptotic theory was worked out in a less approximate form than by Lees and Lin, and three-dimensional disturbances were also considered. Neutral-stability curves were computed at $M_1 = 1.3$, 1.6 and 2.2 by Mack (1960) on the basis of the Dunn-Lin theory, with the inviscid solutions being obtained with improved accuracy. The next step was by Reshotko (1960) and Lees and Reshotko (1962). The asymptotic theory was retained, but both the inviscid and viscous solutions were obtained by numerical integration. The viscous equations used contained higher-order terms than in the usual approximation.

Direct numerical integration of the compressible stability equations was first carried out by Brown (1961, 1962), first for the simplified equations of Dunn and Lin and then for the complete linearized equations. More recently, Brown (1967) has integrated a more complicated system of equations which include the mean normal boundary-layer velocity and are valid for three-dimensional disturbances. I started my own work on the numerical integration of the stability equations in 1961. The numerical method is described in Mack (1965a), and results for two-dimensional disturbances are presented in Mack (1965b).

13.2 Linearized, parallel flow equations

A comprehensive account of the theory must start, as it did in Part A, with the derivation of the governing equations. The dimensionless

Navier-Stokes equations for a viscous, heat-conducting perfect gas are as follows

$$\frac{\partial u_i^*}{\partial t^*} + u_j^* \frac{\partial u_i^*}{\partial x_j^*} = -\frac{1}{\rho^*} \frac{\partial \tau_{ij}^*}{\partial x_j^*} \tag{13.1}$$

$$\frac{\partial \rho^*}{\partial t^*} + \frac{\partial}{\partial x_j^*}(\rho^* u_j^*) = 0 \tag{13.2}$$

$$\rho^* c_v^* \frac{\partial T^*}{\partial t^*} + u_j^* \frac{\partial T^*}{\partial x_j^*} = \frac{\partial}{\partial x_j^*}\left(k^* \frac{\partial T^*}{\partial x_j^*}\right) + \tau_{ij}^* e_{ij}^* \tag{13.3}$$

$$p^* = \rho^* R^* T^* \tag{13.4}$$

where

$$e_{ij}^* = \frac{1}{2}\left(\frac{\partial u_i^*}{\partial x_j^*} + \frac{\partial u_j^*}{\partial x_i^*}\right)$$

$$\tau_{ij}^* = 2\mu^* e_{ij}^* + \left[\frac{1}{3}(\lambda^* - \mu^*) e_{kk}^* - p^*\right] \delta_{ij} \tag{13.5}$$

The summation notation has been adopted for economy, and the asterisks refer to dimensional quantities. The equations are, respectively, momentum, continuity, energy and state. The quantities which did not appear in the incompressible equations are T^*, the temperature; k^*, the coefficient of thermal conductivity; R, the gas constant; c_v^*, the specific heat at constant volume, which will be assumed constant; and λ^*, the coefficient of second viscosity (= 1.5x bulk viscosity coefficient).

The stability equations are obtained from the Navier-Stokes equations by the same procedure that was used for incompressible flow. All quantities are divided into mean flow and disturbance terms, the equations

are linearized, the mean-flow terms are subtracted out, and, finally, the parallel-flow assumption is made. The resulting equations are then made dimensionless with respect to u_1^*, the velocity scale, δ, the length scale, and free-stream quantities serving as reference quantities for all state variables and transport coefficients. The exception is k^*, which is referred to $c_p^* \mu_1^*$. The x-momentum equation is

$$\rho\left(\frac{\partial u'}{\partial t} + u\frac{\partial u'}{\partial x} + v'\frac{du}{dy} + w\frac{\partial u'}{\partial z}\right) = -\frac{1}{\gamma M_1^2}\frac{\partial p'}{\partial x}$$
$$+ \frac{1}{R_\delta}\left[2\mu\frac{\partial^2 u'}{\partial x^2} + \mu\left(\frac{\partial^2 u'}{\partial y^2} + \frac{\partial^2 v'}{\partial x \partial y} + \frac{\partial^2 u'}{\partial z^2} + \frac{\partial^2 w'}{\partial x \partial z}\right)\right.$$
$$+ \frac{2}{3}(\lambda-\mu)\left(\frac{\partial^2 u'}{\partial x^2} + \frac{\partial^2 v'}{\partial x \partial y} + \frac{\partial^2 w'}{\partial x \partial z}\right) + \frac{d\mu}{dT}\frac{dT}{dy}\left(\frac{\partial u'}{\partial y} + \frac{\partial v'}{\partial x}\right)$$
$$\left. + \frac{d\mu}{dT}\left(\frac{d^2 u}{dy^2}T' + \frac{du}{dy}\frac{\partial T'}{\partial y}\right) + \frac{d^2\mu}{dT^2}\frac{dT}{dy}\frac{du}{dy}T'\right] \qquad (13.6)$$

The y-momentum equation is

$$\rho\left(\frac{\partial v'}{\partial t} + u\frac{\partial v'}{\partial x} + w\frac{\partial v'}{\partial z}\right) = -\frac{1}{\gamma M_1^2}\frac{\partial p'}{\partial y} + \frac{1}{R_\delta}\left[2\mu\frac{\partial^2 v'}{\partial y^2}\right.$$
$$+ \mu\left(\frac{\partial^2 v'}{\partial x^2} + \frac{\partial^2 u'}{\partial x \partial y} + \frac{\partial^2 v'}{\partial z^2} + \frac{\partial^2 w'}{\partial y \partial z}\right) + \frac{2}{3}(\lambda-\mu)\left(\frac{\partial^2 u'}{\partial x \partial y} + \frac{\partial^2 v'}{\partial y^2}\right.$$
$$\left. + \frac{\partial^2 w'}{\partial y \partial z}\right) + \frac{d\mu}{dT}\left(2\frac{dT}{dy}\frac{\partial v'}{\partial y} + \frac{du}{dy}\frac{\partial T'}{\partial x} + \frac{dw}{dy}\frac{\partial T'}{\partial z}\right)$$
$$\left. + \frac{2}{3}\left(\frac{d\lambda}{dT} - \frac{d\mu}{dT}\right)\frac{dT}{dy}\left(\frac{\partial u'}{\partial x} + \frac{\partial v'}{\partial y} + \frac{\partial w'}{\partial z}\right)\right] \qquad (13.7)$$

The z-momentum equation is

$$\rho\left(\frac{\partial w'}{\partial t} + v'\frac{dW}{dy} + u\frac{\partial w'}{\partial x} + w\frac{\partial w'}{\partial z}\right) = -\frac{1}{\gamma M_1^2}\frac{\partial p'}{\partial z}$$

$$+ \frac{1}{R_s}\left[2\mu\frac{\partial^2 w'}{\partial z^2} + \mu\left(\frac{\partial^2 w'}{\partial y^2} + \frac{\partial^2 w'}{\partial x^2} + \frac{\partial^2 v'}{\partial y\,\partial z} + \frac{\partial^2 u'}{\partial x\,\partial z}\right)\right.$$

$$+ \frac{2}{3}(\lambda-\mu)\left(\frac{\partial^2 u'}{\partial x\,\partial z} + \frac{\partial^2 v'}{\partial y\,\partial z} + \frac{\partial^2 w'}{\partial z^2}\right) + \frac{d^2\mu}{dT^2}\frac{dT}{dy}\frac{dW}{dy}T'$$

$$\left. + \frac{d\mu}{dT}\left(\frac{dT}{dy}\frac{\partial w'}{\partial y} + \frac{dW}{dy}\frac{\partial T'}{\partial y} + \frac{dT}{dy}\frac{\partial v'}{\partial z} + \frac{d^2W}{dy^2}T'\right)\right] \qquad (13.8)$$

The continuity equation is

$$\frac{\partial \rho'}{\partial t} + \rho\left(\frac{\partial u'}{\partial x} + \frac{\partial v'}{\partial y} + \frac{\partial w'}{\partial z}\right) + v'\frac{d\rho}{dy}$$

$$+ u\frac{\partial \rho'}{\partial x} + w\frac{\partial \rho'}{\partial z} = 0 \qquad (13.9)$$

The energy equation is

$$\rho\left(\frac{\partial T'}{\partial t} + u\frac{\partial T'}{\partial x} + v'\frac{dT}{dy} + w\frac{\partial T'}{\partial z}\right) = -(\gamma-1)\left(\frac{\partial u'}{\partial x} + \frac{\partial v'}{\partial y} + \frac{\partial w'}{\partial z}\right)$$

$$+ \frac{\gamma}{\sigma R_s}\left[\mu\left(\frac{\partial^2 T'}{\partial x^2} + \frac{\partial^2 T'}{\partial y^2} + \frac{\partial^2 T'}{\partial z^2}\right) + \frac{d\mu}{dT}\frac{d^2T}{dy^2}T' + 2\frac{d\mu}{dT}\frac{dT}{dy}\frac{\partial T'}{\partial y}\right.$$

$$\left. + \frac{d^2\mu}{dT^2}\left(\frac{dT}{dy}\right)^2 T'\right] + \gamma(\gamma-1)\frac{M_1^2}{R_s}\left[2\mu\frac{du}{dy}\left(\frac{\partial u'}{\partial y} + \frac{\partial v'}{\partial x}\right)\right.$$

$$\left. + 2\mu\frac{dW}{dy}\left(\frac{\partial v'}{\partial z} + \frac{\partial w'}{\partial y}\right) + \frac{d\mu}{dT}\left(\frac{du}{dy}\right)^2 T' + \frac{d\mu}{dT}\left(\frac{dW}{dy}\right)^2 T'\right] \qquad (13.10)$$

The equation of state is

$$p' = \rho T' + \rho' T \tag{13.11}$$

Additional quantities which appear in these equations are M_1 , the free-stream Mach number; γ , the ratio of specific heats; and $\sigma = c_p' \mu_1' / k_1'$ is the Prandtl number and is assumed constant.

The boundary conditions at $y_g = 0$ are

$$u'(0) = 0 , \quad v'(0) = 0 , \quad w'(0) = 0 , \quad T'(0) = 0 \tag{13.12}$$

The condition on the temperature fluctuation is suitable for a gas flowing over a solid wall. For almost any frequency of the gas, it is not possible for the wall to do other than remain at its mean temperature. The conditions at infinity are that as $y_g \to \infty$, the disturbances must at least be bounded. This condition is less restrictive than requiring that the disturbances go to zero. In supersonic flow, waves may propagate to infinity and we wish to include those that do so with constant amplitude.

13.3 Reduction of equations to near two-dimensional form

We now specialize the disturbance to a wave of the same form as in Part A.

$$q'(x, y, z, t) = q(y) \exp\left[i (\alpha_1 x + \beta_1 z - \alpha_1 c t) \right] \tag{13.13}$$

With the disturbance in this form, we inspect (13.6)-(13.11) to see to what extent they simplify in the tilde coordinate system, i.e., the

coordinate system where the z axis is parallel to the wave front. It is evident that with $\partial/\partial\tilde{z} = 0$, all $\tilde{w}'$ and $\tilde{W}$ terms drop out of the $\tilde{x}$ and y momentum equations and the continuity equation. When, further, the reference velocity is changed to $U_1^* \cos\psi$, where ψ is the angle between the wave normal and U_1^*, these three equations are identical to the equations for a two-dimensional disturbance in the mean flow $\tilde{U}(y)$ with Mach number $\tilde{M}_1 = M_1 \cos\psi$ and Reynolds number $\tilde{R}_\delta = R_\delta \cos\psi$. If the boundary layer in the original x, z coordinates is two-dimensional, then $\tilde{U}(y) = U(y)$. However, there is an important difference here from the situation in incompressible flow. In the latter case, the transformed flow corresponded to a real flow. Here, $U(y)$ is the boundary-layer velocity profile for the free-stream Mach number M_1, not $\tilde{M}_1$. Consequently, even if the energy equation can be reduced to two-dimensional form, the tilde equations do not represent a real flow. The tilde coordinate system thus serves only to simplify the equations, not, as in the incompressible case, to relate all three-dimensional disturbances to the solution of the same flow for two-dimensional disturbances.

It is evident from an inspection of the energy equation, (13.10), that even with $\partial/\partial\tilde{z} = 0$ all terms which include $\tilde{w}'$ and $\tilde{W}$ do not drop out. Two dissipation terms with $\tilde{w}'$ and $\tilde{W}$ remain. This result, that the three-dimensional stability equation cannot be transformed into two-dimensional equations, has been known to most workers in stability theory for a long time although it is rarely mentioned in the literature. I first learned of it from Prof. M. Finston at M.I.T. in about 1948. It is mentioned by

Dunn and Lin (1955) in the introduction of their paper, but the first explicit demonstration seems to be by Reshotko (1962). This transformation is usually discussed by working with the equations for the amplitude functions and the physical significance is obscured by the manner in which the derivation is carried out. The type of derivation used here was first given by Dunn and Lin (1955), although they too reverted to the older derivation to obtain their final equations. The complete derivation along these lines was first carried through by Shen (1964), but only for the simplified equations of Dunn and Lin where the dissipation terms of the energy equation are neglected.

The dissipation terms of the energy equation are

$$\tilde{D} = \gamma(\gamma-1)\frac{\tilde{M}_1^2}{\tilde{R}_s}\left\{2\mu\frac{d\tilde{U}}{dy}\left(\frac{\partial\tilde{u}'}{\partial y}+\frac{\partial\tilde{v}'}{\partial x}\right)\right.$$

$$\left.+\frac{d\mu}{dT}\left[\left(\frac{d\tilde{U}}{dy}\right)^2+\left(\frac{d\tilde{W}}{dy}\right)^2\right]T'+2\mu\frac{d\tilde{W}}{dy}\frac{\partial\tilde{w}'}{\partial y}\right\} \tag{13.14}$$

The second group of terms has a term with the mean velocity $\tilde{W}$, and this term introduces no essential change from the two-dimensional equations. For a two-dimensional boundary layer, where $\tilde{U}(y) = U(y)$, the second group of terms can be written

$$\frac{d\mu}{dT}\left[\left(\frac{d\tilde{U}}{dy}\right)^2+\left(\frac{d\tilde{W}}{dy}\right)^2\right]T' = \frac{d\mu}{dT}\left(\frac{d\tilde{U}}{dy}\right)^2\frac{T'}{\cos^2\psi} \tag{13.15}$$

However, nothing can be done with the final term, which involves $\tilde{w}'$, the fluctuation parallel to the wave front. That such a fluctuation will

exist is evident from the $\tilde{z}$-momentum equation.

$$\rho\left(\frac{\partial \tilde{w}'}{\partial t} + u\frac{\partial \tilde{w}'}{\partial \tilde{x}} + \tilde{v}'\frac{d\tilde{W}}{dy}\right) = \frac{1}{R_s}\left[\mu\left(\frac{\partial^2 \tilde{w}'}{\partial \tilde{x}^2} + \frac{\partial^2 \tilde{w}'}{\partial y^2}\right)\right.$$
$$\left. + \frac{\lambda^2_\mu}{dT^2}\frac{dT}{dy}\frac{d\tilde{W}}{dy}T' + \frac{d\mu}{dT}\left(\frac{dT}{dy}\frac{\partial \tilde{w}'}{\partial y} + \frac{d\tilde{W}}{dy}\frac{\partial T'}{\partial y} + \frac{d^2\tilde{W}}{dy^2}T'\right)\right] \qquad (13.16)$$

We cannot have $\tilde{w}' = 0$ as a solution, partly because of the source term $\tilde{v}'\, d\tilde{W}/dy$. There is always a source term of this type whenever a normal-velocity fluctuation, $\tilde{v}'$, is combined with a normal gradient of a mean-flow quantity. An example in the Orr-Sommerfeld equation is $v'\, d^2u/dy^2$, which is a vorticity source term (du/dy is the mean vorticity).

With the $\tilde{w}'$ term included in the energy equation, it is necessary to use the $\tilde{z}$-momentum equation, and, as we shall see, the order of the system, which is six for a two-dimensional disturbance, becomes eight. Dunn and Lin (1955) used a simplified system of equations in which all of the dissipation terms are neglected. When this is done, the eigenvalues of three-dimensional disturbances can be found from the two-dimensional equations. However, it is still necessary to use the $\tilde{z}$-momentum equation if the eigenfunctions of the velocity fluctuation components in the x-z plane are to be calculated. An important example of equations with no dissipation terms are the inviscid equations.

13.4 Introduction of Fourier components

With the fluctuations in the form (13.13), the complex amplitude functions for $\tilde{u}'$, $\tilde{v}'$, $\tilde{w}'$, p', ρ' and T' are defined to be $\tilde{f}$, $\tilde{\alpha}\varphi$, $\tilde{\lambda}$, π, τ and θ. (Since $\tilde{v}' = v'/\cos\psi$ and $v' = \alpha\varphi$, $\alpha = \tilde{\alpha}\cos\psi$, we have $\tilde{v}' = \tilde{\alpha}\varphi$). The equations for the amplitude functions are

$$\rho\left[i(\tilde{u}-c)\tilde{f} + \tilde{u}'g\right] = -\frac{i\pi}{\gamma\tilde{M}_1^2} + \frac{\mu}{\tilde{\alpha}\tilde{R}}\left[\tilde{f}'' + \tilde{\alpha}^2(ig' - 2\tilde{f})\right]$$

$$+ \frac{2}{3}\frac{\lambda-\mu}{\tilde{\alpha}\tilde{R}}\tilde{\alpha}^2(ig' - \tilde{f})$$

$$+ \frac{1}{\tilde{\alpha}\tilde{R}}\left[s\tilde{u}'' + s'\tilde{u}' + \mu'(\tilde{f}' + i\tilde{\alpha}^2 g)\right] \tag{13.17}$$

$$\rho\left[i(\tilde{u}-c)g\right] = -\frac{1}{\tilde{\alpha}^2}\frac{\pi'}{\gamma\tilde{M}_1^2} + \frac{\mu}{\tilde{\alpha}\tilde{R}}\left(2g'' + i\tilde{f}' - \tilde{\alpha}^2 g\right)$$

$$+ \frac{2}{3}\frac{\lambda-\mu}{\tilde{\alpha}\tilde{R}}(g'' + i\tilde{f}')$$

$$+ \frac{1}{\tilde{\alpha}\tilde{R}}\left[is\tilde{u}' + 2\mu' g' + \frac{2}{3}(\lambda'-\mu')(g' + i\tilde{f})\right] \tag{13.18}$$

$$\rho\left[i(\tilde{u}-c)\tilde{h} + \tilde{w}'g\right] = \frac{\mu}{\tilde{\alpha}\tilde{R}}\left(\tilde{h}'' - \tilde{\alpha}^2\tilde{h}\right)$$

$$+ \frac{1}{\tilde{\alpha}\tilde{R}}\left[\mu'\tilde{h}' + (s\tilde{w}')'\right] \tag{13.19}$$

$$i(\tilde{u}-c)r + \rho(g' + i\tilde{f}) + \rho' g = 0 \tag{13.20}$$

$$\rho\left[i(\tilde{u}-c)\theta + T'g\right] = -(\gamma-1)(g' + i\tilde{f})$$

$$+ \frac{\gamma}{\tilde{\alpha}\tilde{R}_T}\left[\mu(\theta'' - \tilde{\alpha}^2\theta) + (sT')' + \mu'\theta'\right]$$

$$+ \frac{\gamma(\gamma-1)}{\tilde{\alpha}\tilde{R}}\tilde{M}_1^2\left[s\tilde{u}'^2 + 2\mu\tilde{u}'(\tilde{f}' + i\tilde{\alpha}^2 g) + s\tilde{w}'^2 + 2\mu\tilde{w}'\tilde{h}'\right] \tag{13.21}$$

$$\pi = \frac{r}{\rho} + \frac{\theta}{T} \tag{13.22}$$

where

$$S = \theta \frac{d\mu}{dT} \tag{13.23}$$

The subscript δ has been dropped from α and R. If, whatever length scale, L^*, is used, $(\,)'$ is interpreted to mean differentiation with respect to y^*/L^*, then the corresponding wave number and Reynolds number become α_{L^*}, R_{L^*}. In particular, if

$$L^* = \frac{x^*}{(R_x)^{1/2}} \tag{13.24}$$

where R_x is the x-Reynolds number $U_1^* x^*/\nu_1^*$, then

$$\alpha = \alpha^* \frac{x^*}{(R_x)^{1/2}} \qquad R = \frac{U_1^*}{\nu_1^*} \frac{x^*}{(R_x)^{1/2}} = (R_x)^{1/2} \tag{13.25}$$

and

$$\frac{y^*}{L^*} = \frac{y^*}{x^*}(R_x)^{1/2} = \eta \tag{13.26}$$

Consequently, with the y variable replaced by the Blasius similarity variable η, then α is given by (13.25) and R is simply $(R_x)^{1/2}$. This system permits boundary-layer profiles calculated in terms of the similarity variable to be used directly in the stability equations. However, the boundary-layer thickness, displacement thickness, or momentum thickness can be used equally well as the reference length, with the proper interpretation of α, R, and the independent variable. All of these α's and R's differ only by numerical factors which depend on the Mach number (e.g., $\alpha_\delta = \eta_\delta \alpha$, $\alpha_{\delta^*} = \eta_{\delta^*} \alpha$, $R_\theta = \eta_\theta R$). Since the numerical

results are to be presented in terms of α and R, Table 13.1 is included to give these numerical factors for the insulated flat-plate boundary layer.

M_1	η_δ	η_{δ^*}	η_θ
0	6.0	1.72	0.664
0.7	6.2	1.92	0.660
1.0	6.4	2.13	0.656
1.6	7.0	2.77	0.648
2.0	7.6	3.37	0.644
2.2	8.0	3.72	0.643
3.0	9.8	5.48	0.642
3.8	12.1	7.83	0.644
4.2	13.5	9.22	0.645
4.5	14.6	10.34	0.646
4.8	15.8	11.55	0.646
5.8	20.0	15.73	0.636
6.2	21.7	17.49	0.629
7.0	25.4	21.19	0.616
7.5	27.8	23.62	0.607
8.0	30.3	26.13	0.598
8.5	32.9	28.72	0.590
9.0	35.5	31.38	0.581
9.5	38.2	34.10	0.573
10.0	41.0	36.88	0.565

Table 13.1 Boundary-layer thickness ($u/u_1 = 0.999$), displacement thickness and momentum thickness of insulated-wall boundary layer. (Wind-tunnel temperature conditions)

13.5 System of first-order equations

In order to carry out the numerical integration of the compressible stability equations, it is convenient to reduce them to a system of first-order equations. Following Lees and Lin (1946), we define the dependent variables for this purpose as

$$\begin{aligned} \tilde{Z}_1 &= \tilde{f} \quad , \quad \tilde{Z}_2 = \tilde{f}' \quad , \quad \tilde{Z}_3 = \varphi \quad , \quad \tilde{Z}_4 = \frac{\pi}{\gamma \tilde{M}_1^2} \\ \tilde{Z}_5 &= \theta \quad , \quad \tilde{Z}_6 = \theta' \quad , \quad \tilde{Z}_7 = \tilde{h} \quad , \quad \tilde{Z}_8 = \tilde{h}' \end{aligned} \tag{13.27}$$

The fact that this choice of dependent variable leads to eight first-order equations demonstrates that we have an eighth-order system. The $\tilde{Z}_3'$ equation is obtained from the continuity equation; the $\tilde{Z}_2'$ equation comes from the $\tilde{x}$-momentum equation; the $\tilde{Z}_4'$ equation, after a lengthy manipulation, from the y-momentum equation; the $\tilde{Z}_6'$ equation from the energy equation; and $\tilde{Z}_8'$ equation from the $\tilde{z}$-momentum equation. The resulting eight equations can be written as the product of a matrix $(\tilde{a}_{ij})$ and a column vector $\tilde{Z}$.

$$\tilde{Z}_i' = \sum_{j=1}^{8} \tilde{a}_{ij} \tilde{Z}_j \quad , \qquad i = 1, \ldots, 8 \tag{13.28}$$

The 30 non-zero elements of the 8 x 8 matrix $(\tilde{a}_{ij})$ are listed below. The $\tilde{Z}_1'$ equation has only one non-zero coefficient.

$$\tilde{a}_{12} = 1 \tag{13.29}$$

In the $\tilde{Z}_2'$ equation, six coefficients are non-zero.

$$\tilde{a}_{21} = \frac{i\tilde{\alpha}\tilde{R}}{\mu}\frac{\tilde{u}-c}{T} + \tilde{\alpha}^2 \tag{13.30a}$$

$$\tilde{a}_{22} = -\frac{T'}{\mu}\frac{d\mu}{dT} \tag{13.30b}$$

$$\tilde{a}_{23} = \frac{\tilde{\alpha}\tilde{R}}{\mu}\frac{\mu'}{T} - i\tilde{\alpha}^2\frac{T'}{\mu}\frac{d\mu}{dT} - i\frac{1}{3}(1+2k)\tilde{\alpha}^2\frac{T'}{T} \tag{13.30c}$$

$$\tilde{a}_{24} = \frac{i\tilde{\alpha}\tilde{R}}{\mu} - \frac{1}{3}(1+2k)\gamma\tilde{M}_1^2\tilde{\alpha}^2(\tilde{u}-c) \tag{13.30d}$$

$$\tilde{a}_{25} = \frac{1}{3}(1+2k)\tilde{\alpha}^2\frac{\tilde{u}-c}{T} - \frac{\tilde{u}''}{\mu}\frac{d\mu}{dT} - \frac{\tilde{u}'T'}{\mu}\frac{d^2\mu}{dT^2} \tag{13.30e}$$

$$\tilde{a}_{26} = -\frac{\tilde{u}'}{\mu}\frac{d\mu}{dT} \tag{13.30f}$$

The $\tilde{Z}_3'$ equation has four non-zero coefficients

$$\tilde{a}_{31} = -i \tag{13.31a}$$

$$\tilde{a}_{33} = \frac{T'}{T} \tag{13.31b}$$

$$\tilde{a}_{34} = -i(\tilde{u}-c)\gamma\tilde{M}_1^2 \tag{13.31c}$$

$$\tilde{a}_{35} = i\frac{\tilde{u}-c}{T} \tag{13.31d}$$

The $\tilde{Z}_4'$ equation has six non-zero coefficients. The coefficients are written in terms of the factor L, defined by

$$\frac{1}{L} = \frac{\tilde{R}}{\tilde{\alpha}\mu} + i\frac{2}{3}(2+k)\gamma\tilde{M}_1^2(\tilde{u}-c) \tag{13.32}$$

The coefficients are

$$\tilde{a}_{41} = -\frac{i}{L}\left[2\frac{T'}{\mu}\frac{d\mu}{dT} + \frac{2}{3}(2+k)\frac{T'}{T}\right] \tag{13.33a}$$

$$\tilde{a}_{42} = -\frac{i}{L} \tag{13.33b}$$

$$\tilde{a}_{43} = \frac{1}{L}\left[-\tilde{\alpha}^2 + \frac{2}{3}(2+k)\frac{T'^2}{T}\frac{1}{\mu}\frac{d\mu}{dT} + \frac{2}{3}(2+k)\frac{T''}{T} - \frac{i\tilde{\alpha}\tilde{R}}{\mu}\frac{\tilde{u}-c}{T}\right] \tag{13.33c}$$

$$\tilde{a}_{44} = -i\frac{2}{3}(2+k)\gamma\tilde{M}_1^2\frac{1}{L}\left[(\tilde{u}-c)\frac{T'}{\mu}\frac{d\mu}{dT} + \tilde{u}' + (\tilde{u}-c)\frac{T'}{T}\right] \tag{13.33d}$$

$$\tilde{a}_{45} = \frac{i}{L}\left[\frac{\tilde{u}'}{\mu}\frac{d\mu}{dT} + \frac{2}{3}(2+k)\frac{\tilde{u}-c}{T}\frac{T'}{\mu}\frac{d\mu}{dT} + \frac{2}{3}(2+k)\frac{\tilde{u}'}{T}\right] \tag{13.33e}$$

$$\tilde{a}_{46} = \frac{i}{L}\frac{2}{3}(2+k)\frac{\tilde{u}-c}{T} \tag{13.33f}$$

The $\tilde{Z}_5'$ equation has only a single non-zero coefficient.

$$\tilde{a}_{56} = 1 \tag{13.34}$$

The $\tilde{Z}_6'$ equation has six non-zero coefficients.

$$\tilde{a}_{62} = -2\sigma(\gamma-1)\tilde{M}_1^2\tilde{u}' \tag{13.35a}$$

$$\tilde{a}_{63} = \frac{\tilde{\alpha}\tilde{R}\sigma}{\mu}\frac{T'}{T} - i\,2\sigma(\gamma-1)\tilde{M}_1^2\tilde{\alpha}^2\tilde{u}' \tag{13.35b}$$

$$\tilde{a}_{64} = -\frac{i\tilde{\alpha}\tilde{R}\sigma}{\mu}(\gamma-1)\tilde{M}_1^2(\tilde{u}-c) \tag{13.35c}$$

$$\tilde{a}_{65} = \frac{i\tilde{\alpha}\tilde{R}\sigma}{\mu}\frac{\tilde{u}-c}{T} + \tilde{\alpha}^2 - \frac{T''}{\mu}\frac{d\mu}{dT} - \frac{T'^2}{\mu}\frac{d^2\mu}{dT^2} - \sigma(\gamma-1)\tilde{M}_1^2\frac{1}{\mu}\frac{d\mu}{dT}(\tilde{u}'^2+\tilde{w}'^2) \tag{13.35d}$$

$$\tilde{a}_{66} = -2\frac{T'}{\mu}\frac{d\mu}{dT} \tag{13.35e}$$

$$\tilde{a}_{68} = -2\sigma(\gamma-1)\tilde{M}_1^2\tilde{w}' \tag{13.35f}$$

The $\tilde{Z}_7'$ equation has only a single non-zero coefficient.

$$\tilde{a}_{78} = 1 \tag{13.36}$$

The $\tilde{Z}_8'$ equation has five non-zero coefficients.

$$\tilde{a}_{83} = \frac{\tilde{\alpha}\tilde{R}}{\mu}\frac{1}{T}\tilde{w}' \tag{13.37a}$$

$$\tilde{a}_{85} = -\frac{1}{\mu}\frac{d\mu}{dT}\tilde{w}'' - \frac{1}{\mu}\frac{d^2\mu}{dT^2}T'\tilde{w}' \tag{13.37b}$$

$$\tilde{a}_{86} = -\frac{1}{\mu}\frac{d\mu}{dT}\tilde{w}' \tag{13.37c}$$

$$\tilde{a}_{87} = \tilde{\alpha}^2 + i\,\frac{\tilde{\alpha}\tilde{R}}{\mu}\,\frac{\tilde{u}-c}{T} \tag{13.37d}$$

$$\tilde{a}_{88} = -\frac{1}{\mu}\,\frac{d\mu}{dT}\,T' \tag{13.37e}$$

In these equations,

$$k = \frac{\lambda}{\mu} \tag{13.38}$$

and is a constant.

The boundary conditions are

$$\tilde{Z}_1(0) = 0\ , \quad \tilde{Z}_3(0) = 0\ , \quad \tilde{Z}_5(0) = 0\ , \quad \tilde{Z}_7(0) = 0 \tag{13.39}$$

and at $\eta \to \infty$, the amplitude functions are bounded. Just as for incompressible flow, we have to deal with an eigenvalue problem and can only satisfy the boundary conditions for certain combinations of α, β, c and R.

13.6 First-order equations in free stream

In the free-stream, $\eta > \eta_\delta$, the equations reduce to the following equations with constant coefficients.

$$\tilde{Z}_1' = \tilde{Z}_2 \tag{13.40}$$

$$\tilde{Z}_2' = \left[i\tilde{\alpha}\tilde{R}(1-c) + \tilde{\alpha}^2\right]\tilde{Z}_1 + \left[i\tilde{\alpha}\tilde{R} - \frac{1}{3}(1+2k)\tilde{M}_1^2(1-c)\tilde{\alpha}^2\right]\tilde{Z}_2 + \frac{1}{3}(1+2k)(1-c)\tilde{\alpha}^2\tilde{Z}_5 \tag{13.41}$$

$$\tilde{Z}_3' = -i\,\tilde{Z}_1 - i(1-c)\,\gamma\tilde{M}_1^2\,\tilde{Z}_4 + i(1-c)\,\tilde{Z}_5 \tag{13.42}$$

$$\tilde{Z}_4' = \tilde{\alpha}^2\left[\tilde{\alpha}\tilde{R} + i\,\frac{2}{3}(2+k)\,\gamma\tilde{M}_1^2\,\tilde{\alpha}^2(1-c)\right]^{-1}$$
$$\times\left\{-i\,\tilde{Z}_2 - \left[i\,\tilde{\alpha}\tilde{R}(1-c) + \tilde{\alpha}^2\right]\tilde{Z}_3 + i\,\frac{2}{3}(2+k)(1-c)\,\tilde{Z}_6\right\} \tag{13.43}$$

$$\tilde{Z}_5' = \tilde{Z}_6$$

$$\tilde{Z}_6' = -i\,\tilde{\alpha}\tilde{R}\sigma(\gamma-1)\tilde{M}_1^2(1-c)\,\tilde{Z}_4 + \left[i\,\tilde{\alpha}\tilde{R}\sigma(1-c) + \tilde{\alpha}^2\right]\tilde{Z}_5 \tag{13.44}$$

$$\tilde{Z}_7' = \tilde{Z}_8 \tag{13.45}$$

$$\tilde{Z}_8' = \left[\tilde{\alpha}^2 + i\,\frac{\tilde{\alpha}\tilde{R}}{\mu}(1-c)\right]\tilde{Z}_7 \tag{13.46}$$

The general solution of these equations is of the form

$$\tilde{Z}_i = \sum_{j=1}^{8} C_j\,A_i^{(j)}\,e^{\lambda_j(\eta-\eta_0)}\,, \qquad i = 1,\ldots,8 \tag{13.47}$$

The λ_j are the eight characteristic values of the coefficient matrix, $(\tilde{a}_{ij})$; the $A^{(j)}$ are the 64 components of the eight characteristic vectors $A^{(j)}$; and the eight $C^{(j)}$ are arbitrary constants to be determined by the eight boundary conditions. Equations (13.40)-(13.46) are simple enough so that the λ_j and $A_i^{(j)}$ can be obtained analytically.

A derivation of the λ_j and $A_i^{(j)}$ is given by Mack (1965) for the sixth-order system. The extension to the eighth-order system is obvious. Of the four characteristic values which satisfy the boundary conditions as $\eta \to \infty$, only two have simple forms. They are

$$\lambda_{3,7} = -\left[\tilde{\alpha}^2 + i\,\tilde{\alpha}\tilde{R}(1-c)\right]^{1/2} \tag{13.48}$$

and are identical to λ_3 of (4.17), the characteristic value of the viscous solution for the Orr-Sommerfeld equation in the free stream. In the limit of large $\tilde{\alpha}\tilde{R}$ the four characteristic values are, with the numbering chosen to correspond to the incompressible case,

$$\lambda_1 = -\tilde{\alpha}\left[1 - \tilde{M}_1^2 (1-c)\right]^{1/2} \qquad \text{inviscid compressible wavy wall} \tag{13.49}$$

$$\lambda_3 = -\left[i\tilde{\alpha}\tilde{R}(1-c)\right]^{1/2} \tag{13.50}$$

$$\lambda_5 = -\left[i\tilde{\alpha}\tilde{R}\sigma(1-c)\right]^{1/2} \tag{13.51}$$

$$\lambda_7 = -\left[i\tilde{\alpha}\tilde{R}(1-c)\right]^{1/2} \tag{13.52}$$

viscous type solutions for high Re (viscous decay)

To the same approximation, the characteristic vector $A^{(1)}$ has the components (with $A_2^{(1)}$, $A_6^{(1)}$ and $A_8^{(1)}$ omitted in the listings)

$$A_1^{(1)} = -i\tilde{\alpha} \tag{13.53a}$$

$$A_3^{(1)} = \left[1 - \tilde{M}_1^2 (1-c)^2\right]^{1/2} \tag{13.53b}$$

$$A_4^{(1)} = i\tilde{\alpha}(1-c) \tag{13.53c}$$

$$A_5^{(1)} = i\tilde{\alpha}(\gamma-1)\tilde{M}_1^2(1-c) \tag{13.53d}$$

$$A_7^{(1)} = 0 \tag{13.53e}$$

The characteristic vector $A^{(3)}$ has the components

$$A_1^{(3)} = -i\left[i\tilde{\alpha}\tilde{R}(1-c)\right]^{1/2} \tag{13.54a}$$

$$A_3^{(3)} = 1 \tag{13.54b}$$

$$A_4^{(3)} = A_5^{(3)} = A_7^{(3)} = 0 \tag{13.54c}$$

The characteristic vector $A^{(5)}$ has the components

$$A_1^{(5)} = 0 \tag{13.55a}$$

$$A_3^{(5)} = -\frac{i(1-c)^{1/2}}{(i\tilde{\alpha}\tilde{R}\sigma)^{1/2}} \tag{13.55b}$$

$$A_4^{(5)} = 0 \tag{13.55c}$$

$$A_5^{(5)} = 1 \tag{13.55d}$$

Finally, the components of the characteristic vector $A^{(7)}$ are

$$A_1^{(7)} = A_3^{(7)} = A_4^{(7)} = A_5^{(7)} = 0 \tag{13.56a}$$

$$A_7^{(7)} = 1 \tag{13.56b}$$

The first of these vectors is the compressible wavy-wall inviscid solution; the second is the viscous velocity solution; the third is the

viscous temperature solution; the fourth is a second viscous velocity solution for the non-periodic (in $\tilde{z}$) velocity component parallel to the wave front. The exact counterparts of these solutions provide the initial values for a numerical integration which proceeds from the free stream to the wall.

A discussion of the inviscid equations in the free stream will be given at the end of the next section.

13.7 Inviscid equations

When all of the terms with viscosity and heat conduction are dropped from (13.17)-(13.22), the equations reduce to

$$\rho\left[i(\tilde{u}-c)\tilde{f} + \tilde{u}'\varphi\right] = -\frac{i\pi}{\gamma \tilde{M}_1^2} \tag{13.57}$$

$$\rho\, i\tilde{\alpha}^2(\tilde{u}-c)\varphi = -\frac{\pi'}{\gamma \tilde{M}_1^2} \tag{13.58}$$

$$\rho\left[i(\tilde{u}-c)\tilde{h} + \tilde{w}'\varphi\right] = 0 \tag{13.59}$$

$$i(\tilde{u}-c)r + \rho(\varphi' + i\tilde{f}) + \rho'\varphi = 0 \tag{13.60}$$

$$\rho\left[i(\tilde{u}-c)\theta + T'\varphi\right] = -(\gamma-1)(i\tilde{f} + \varphi') \tag{13.61}$$

$$\pi = \frac{r}{\rho} + \frac{\theta}{T} \tag{13.62}$$

In these equations, as already indicated in Section 13.3, $\tilde{h}$ and $\tilde{w}$ appear only in the $\tilde{z}$-momentum equation, and the other equations are

identical to two-dimensional equations. Consequently, we can obtain the eigenvalues of all inviscid three-dimensional waves from the two-dimensional equations, although in contrast to incompressible flow, separate eigenvalues must be obtained for each wave angle ψ. The amplitude function $\tilde{h}$ can be computed from (13.59) after the eigenvalues are known without an additional integration.

13.7.1 Various forms of inviscid equations

We can easily derive several forms of the inviscid equations which will be useful for various purposes. Substitution of (13.62) into (13.60) yields, with the use of (13.61),

$$\tilde{w} = \frac{i\gamma\,(i\tilde{f} + \varphi')}{\tilde{u} - c} \tag{13.63}$$

When this equation is differentiated and the result substituted into (13.58), and $\tilde{f}$ eliminated from (13.57) and (13.63), the result is

$$\frac{d}{d\eta}\left[\frac{(\tilde{u}-c)\varphi' - \tilde{u}'\varphi}{T - \tilde{M}_1^2(\tilde{u}-c)^2}\right] - \frac{\tilde{\alpha}^2(\tilde{u}-c)}{T}\varphi = 0 \tag{13.64}$$

This is the form of the invscid stability equation derived by Lees and Lin (1946). Since it is a second-order equation, just as for incompressible flow, only two boundary conditions may be satisfied.

$$\varphi(0) = 0\,, \qquad \varphi(\eta) \text{ bounded as } \eta \to \infty \tag{13.65}$$

Equation (13.64) is useful for analytic developments, but it is not suitable for numerical integration because of the denominator $T - \tilde{M}_1^2(\tilde{u}-c)^2$, which, for $c_i = 0$, is zero at the point in the boundary layer where $\tilde{u} - c_r$ is equal to the local speed of sound. From (13.57) and (13.63),

$$\tilde{f} = i\,\frac{T\varphi' - \tilde{u}'(\tilde{u}-c)\tilde{M}_1^2\varphi}{T - \tilde{M}_1^2(\tilde{u}-c)^2} \tag{13.66}$$

Substitution of this equation into (13.63) gives

$$\pi = i\gamma\tilde{M}_1^2\left[\frac{\tilde{u}'\varphi - (\tilde{u}-c)\varphi'}{T - \tilde{M}_1^2(\tilde{u}-c)^2}\right] \tag{13.67}$$

When (13.67) is solved for φ', we find, with the Z notation,

$$\tilde{Z}_3' = \frac{\tilde{u}'}{\tilde{u}-c}\tilde{Z}_3 + i\,\frac{T - \tilde{M}_1^2(\tilde{u}-c)^2}{\tilde{u}-c}\tilde{Z}_4 \tag{13.68}$$

and the y-momentum equation (13.58) is

$$\tilde{Z}_4' = -\frac{i\tilde{\alpha}^2(\tilde{u}-c)}{T}\tilde{Z}_3 \tag{13.69}$$

These equations are the counterparts of (5.14) and (5.15) in Part A. When $\tilde{M}_1 = 0$ and $T = 1$, they reduce to the incompressible equation.

For some purposes it is useful to think of an observer moving with the wave. In order to write the equations in this coordinate system, we introduce

$$\tilde{M}_R = \frac{\tilde{u}-c}{T^{1/2}}\tilde{M}_1 \tag{13.70}$$

For $c_i = 0$, $\tilde{M}_R$ is the local Mach number of the relative flow. Then (13.67) becomes

$$\frac{\pi}{\gamma \tilde{M}_R^2} = -i \frac{1}{1 - \tilde{M}_R^2} \left(\frac{\varphi}{\tilde{u} - c} \right)' \tag{13.71}$$

This equation can be recognized as the linearized pressure-area relation of one-dimensional flow. The quantity $\varphi/(\tilde{u}-c)$ is the amplitude function of the streamline slope.

The other disturbance amplitude functions can also be written in terms of $\varphi/(\tilde{u}-c)$. However, because of the mean normal gradients, the complete expression for the amplitude functions will also involve source terms. We find

$$\tilde{f} = i \left[\tilde{u}' \frac{\varphi}{\tilde{u} - c} + \frac{1}{1 - \tilde{M}_R^2} (\tilde{u} - c) \left(\frac{\varphi}{\tilde{u} - c} \right)' \right] \tag{13.72}$$

$$\theta = i \left[T' \frac{\varphi}{\tilde{u} - c} - (\gamma - 1) \frac{\tilde{M}_R^2}{1 - \tilde{M}_R^2} T \left(\frac{\varphi}{\tilde{u} - c} \right)' \right] \tag{13.73}$$

$$r = i \left[\rho' \frac{\varphi}{\tilde{u} - c} - \frac{\tilde{M}_R^2}{1 - \tilde{M}_R^2} \rho \left(\frac{\varphi}{\tilde{u} - c} \right)' \right] \tag{13.74}$$

When the second terms of these equations are written in terms of π from (13.71), they can be readily recognized as the linearized momentum equation, isentropic temperature-pressure solution, and isentropic density-pressure solution, respectively.

We are able to derive a single second-order equation for $\varphi/(\tilde{u}-c)$. It is

$$\left(\frac{\varphi}{\tilde{u}-c}\right)'' + \left(\log \frac{\tilde{M}_R^2}{1-\tilde{M}_R^2}\right)' \left(\frac{\varphi}{\tilde{u}-c}\right)' - \tilde{\alpha}^2(1-\tilde{M}_R^2)\left(\frac{\varphi}{\tilde{u}-c}\right) = 0 \qquad (13.75)$$

A similar equation can be found for π.

$$\pi'' - \left(\log \tilde{M}_R^2\right)' \pi' - \tilde{\alpha}^2(1-\tilde{M}_R^2)\pi = 0 \qquad (13.76)$$

This equation has been studied by Lighthill (1953) in another connection.

13.7.2 Inviscid equations in free stream

In the free stream, (13.76) reduces to

$$\pi'' - \tilde{\alpha}^2(1-\tilde{M}_{R_1}^2)\pi = 0 \qquad (13.77)$$

where $\tilde{M}_{R_1}$ is a constant and is given by

$$\tilde{M}_{R_1} = (1-c)\tilde{M}_1 \qquad (13.78)$$

The solution of (13.77) which is bounded at infinity is

$$\pi = -\gamma \tilde{M}_{R_1}^2 \exp\left[-\tilde{\alpha}(1-\tilde{M}_{R_1}^2)^{1/2}(\eta-\eta_s)\right] \qquad (13.79)$$

The characteristic value, $-\tilde{\alpha}(1-\tilde{M}_{R_1}^2)^{1/2}$, is equal to the λ_1 of Section 13.6. In order to simplify the notation in the remainder of this section, $\tilde{M}_{R_1}$ will be replaced by M_R and $\tilde{\alpha}$ by α.

When $c_i = 0$ and $M_R < 1$, $\pi \to 0$ as $\eta \to \infty$. We call this case a subsonic neutral disturbance. When $M_R > 1$, we have a supersonic neutral disturbance. The coefficient of $(\eta - \eta_s)$ in (13.79) is pure imaginary and the wave amplitude is independent of η. The whole solution is

$$\pi e^{i\alpha x} = -\gamma M_R^2 \exp\left\{i\alpha\left[x \mp (M_R^2 - 1)^{1/2}(\eta - \eta_s)\right]\right\} \qquad (13.80)$$

It is evident that these waves are Mach waves. There are two cases depending upon the branch of the square root we choose. If $(-1)^{1/2} = +i$, we have the minus sign in (13.80) and the case shown in (a) of Fig. 13.1. If $(-1)^{1/2} = -i$, we have the plus sign and the case shown in (b).

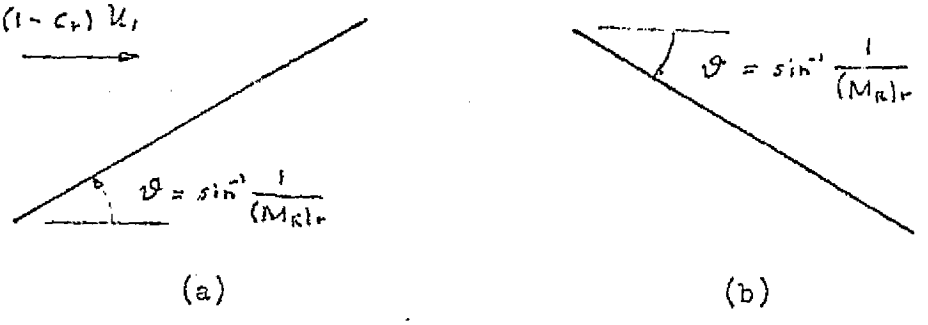

Fig. 13.1 Supersonic neutral disturbances

Case (a) is an outgoing wave; case (b) is an incoming wave. Case (a) appears more appropriate to the boundary-layer stability problem. However, a combination of the two types of waves permits the boundary conditions to

be satisfied for any α and c and we no longer have an eigenvalue problem. But if we restrict ourselves to only one kind of wave, then we still have an eigenvalue problem. Type (a) waves have actually been found, as will be seen in Section 15.6.3.

For amplified and damped waves, $c_i \neq 0$ and M_R will be complex.

$$M_R = (1 - c)\, M_1 = (1 - c_r)\, M_1 - i\, c_i\, M_1 \tag{13.81}$$

The real part of M_R is always positive, but the imaginary part will change sign depending upon whether the wave is amplified ($c_i > 0$) or damped ($c_i < 0$). We can write

$$(1 - M_R^2)^{1/2} \qquad \left[1 - (M_R)_r^2\right]^{1/2} \left[1 - i\, \frac{(M_R)_r\, (M_R)_i}{1 - (M_R)_r^2}\right] \tag{13.82}$$

under the assumption that $(M_R)_i << (M_R)_r$. When $(M_R)_r < 1$, the boundary condition at infinity is always satisfied. The wave fronts of the amplified disturbances are tilted in the upstream direction; the wave fronts of the damped disturbances are tilted in the downstream direction. (The neutral wave fronts are normal to the free-stream direction.) When $(M_R)_r > 0$, there are again two cases to consider. With $(-1)^{1/2} = +i$, we have the outgoing case (a) waves:

$$\exp\left[-\alpha\, (1 - M_R^2)^{1/2} (\eta - \eta_s)\right]$$

$$= \exp\left[\frac{\alpha (M_R)_r\, (M_R)_i}{\left[(M_R)_r^2 - 1\right]^{1/2}} (\eta - \eta_s)\right] \exp\left\{-i\, \alpha \left[(M_R)_r^2 - 1\right]^{1/2} (\eta - \eta_s)\right\} \tag{13.83}$$

With $(-1)^{1/2} = -i$, we have the incoming case (b) waves.

$$\exp\left[-\alpha\left(1-M_R^2\right)^{1/2}(\eta-\eta_\delta)\right]$$

$$= \exp\left[-\frac{\alpha(M_R)_r(M_R)_i}{\left[(M_R)_r^2-1\right]^{1/2}}(\eta-\eta_\delta)\right]\exp\left\{i\alpha\left[(M_R)_r^2-1\right]^{1/2}(\eta-\eta_\delta)\right\} \tag{13.84}$$

We can classify these waves by whether they increase or decrease with increasing η .

	Amplified	Damped
Case (a), outgoing	decrease	increase
Case (b), incoming	increase	decrease

For amplified waves, only the outgoing waves satisfy the boundary condition at infinity. For damped waves ($c_i < \sigma$) , only the incoming waves satisfy the boundary conditions. Hence only two of these solutions can be accepted.

14. Numerical Integration of Stability Equations

14.1 Inviscid equations

Two methods have been devised for the numerical integration of the inviscid stability equations. The first of these is by Reshotko (1960). The second-order linear equation is transformed into a first-order nonlinear equation of the Riccati type. This equation is solved by numerical integration except for the region around the critical point, where generalizations of Tollmien's series solutions are used. Although the numerical integration is performed on a computer, the procedure is not completely automatic because of the matching required between the numerical integration and the series solutions.

The second method is by Mack (1965a) and is a generalization to compressible flow of Zaat's (1958) method. The numerical integration is carried out along an indented contour in the complex plane. The computation of the eigenvalues is completely automatic provided the initial guess is adequate, a condition that can easily be met. The equations that one uses are the two first-order equations (13.68) and (13.69). The integration starts in the free stream and continues to the wall. In the free stream, the equations can be written as a second-order equation for $\bar{Z}_4$ as has already been done in Section 13.7. In the fixed coordinate system this equation is

$$\bar{Z}_4'' - \tilde{\alpha}^2 \left[1 - \tilde{M}_1^2 (1 - c)^2\right] \bar{Z}_4 = 0 \qquad (14.1)$$

The solution which satisfies the boundary condition at infinity is

$$\tilde{Z}_4 = -(1-c)\exp\left\{-\tilde{\alpha}\left[1-\tilde{M}_1^2(1-c)^2\right]^{1/2}(\eta-\eta_\delta)\right\} \tag{14.2}$$

The integration constant has been chosen to make $\tilde{Z}_1(\eta_\delta) = (1,0)$.

The initial conditions at $\eta = \eta_\delta$ for the numerical integration are

$$\tilde{Z}_3(\eta_\delta) = \frac{i}{\tilde{\alpha}}\left[1-\tilde{M}_1^2(1-c)^2\right]^{1/2} \tag{14.3}$$

$$\tilde{Z}_4(\eta_\delta) = -(1-c) \tag{14.4}$$

We must decide which of the indented contours shown in Fig. 5.1 to use. For a neutral disturbance, both contours are satisfactory. For a damped or amplified disturbance, the choice of the correct contour is made on the same basis as in incompressible flow for a velocity profile with an inflection point (p. 34). Table 14.1 gives some eigenvalues for a boundary layer on an insulated flat plate at $M_1 = 3.8$. Contours (a) and (b) are those of Fig. 5.1.

Contour	α	c_r	c_i
a	0.1787	0.8685	-0.005
b	0.1058	0.8317	-0.005
a	0.1058	0.8317	+0.005
b	0.1787	0.8685	+0.005

Table 14.1 Inviscid eigenvalues at $M_1 = 3.8$ for different indented contours.

The eigenvalues of the neutral disturbance are $\alpha_s = 0.1421$, $c_s = 0.8523$. At finite Reynolds numbers, the unstable region lies below the neutral-stability curve; the stable region above it. Consequently, the criterion that the inviscid solutions must be the $R \to \infty$ limit of corresponding viscous solutions selects contour (a) just as it did for incompressible flow.

The numerical integration yields $Z_3(0)$ for specified values of α, c_r and c_i. To find the eigenvalues, one of the three parameters is held constant and the other two perturbed until the boundary condition $Z_3(0) = 0$ is satisfied. With a reasonable initial guess, a linear perturbation is adequate. If a neutral solution is sought, then $c_i = 0$, and α and c_r are perturbed. An initial integration, followed by two more integrations with α then c_r perturbed, yields the following four quantities:

$$\frac{\Delta Z_{3_r}(0)}{\Delta \alpha} \quad , \quad \frac{\Delta Z_{3_i}(0)}{\Delta \alpha}$$

$$\frac{\Delta Z_{3_r}(0)}{\Delta c_r} \quad , \quad \frac{\Delta Z_{3_i}(0)}{\Delta c_r} \qquad (14.5)$$

The new α and c_r are found from

$$\frac{\Delta Z_{3_r}(0)}{\Delta \alpha}\Delta\alpha + \frac{\Delta Z_{3_r}(0)}{\Delta c_r}\Delta c_r = -Z_{3_r}(0) \qquad (14.6)$$

$$\frac{\Delta Z_{3_i}(0)}{\Delta \alpha}\Delta\alpha + \frac{\Delta Z_{3_i}(0)}{\Delta c_r}\Delta c_r = -Z_{3_i}(0) \qquad (14.7)$$

This process is repeated until α and c_r converge to the specified accuracy. If α is held constant, then one integration can be saved by taking advantage of the fact that Z_3 and Z_4 are analytic functions of c. The two derivatives similar to those of (14.5) which are not actually computed are obtained from the Cauchy-Riemann equations. Since there is no serious problem of error buildup with the inviscid equations, single-precision arithmetic and a standard forward-integration method are adequate.

14.2 Complete equations

The numerical integration of the complete compressible stability equations presents the same central difficulty as with the Orr-Sommerfeld equation. Two methods have been successfully applied to this problem. Both methods were first restricted to two-dimensional disturbances, but have since been extended to also handle three-dimensional disturbances. Double-precision arithmetic is used in both methods to control the error build-up. The first method to be developed, just as was the case for the incompressible boundary layer, is by Brown (1961, 1962). In Brown's method, three arbitrary independent solutions (for the sixth-order system) are produced by numerical integration from $\eta = 0$ to $\eta = \eta_\delta$. At η_δ, these solutions are matched to the analytic free-stream solutions. Two of the matching conditions can be immediately satisfied, but the third condition can only be satisfied by searching for a suitable combination of α, c and R. Brown successfully applied his method to several problems.

The second method, which was developed independently shortly after Brown's method is by Mack (1965a). This method is similar in concept to the method described in Section 14.1 for the inviscid equations. The

analytic free-stream solutions provide the initial conditions for four linearly independent solutions (eighth-order system). These solutions are produced by performing four numerical integrations from η_δ to $\eta = o$. Three of the four boundary conditions at $\eta = o$ can be immediately satisfied. The remaining condition, $\bar{z}_5(o) = .o$, is satisfied by the same sort of linear perturbation procedure described in the preceding section. With α and R held constant, only a single perturbation integration (of each of the four independent solutions) is required because the $\bar{z}^{(n)}$ are analytic functions of c . To calculate a neutral solution $(c_i = o)$, c_r is held constant and α and R are perturbed. As is often the case in problems of this kind, the fact that $\bar{z}_5(o)$ is a physical quantity leads to a rapid convergence. Often only a single iteration is needed to give the eigenvalues to three significant figures, and it is rare that more than two iterations are required. Once the eigenvalues are known, then a subsequent integration of a single solution which is formed from the four independent solutions in the proportion determined during the eigenvalue computation will produce the eigenfunctions and whatever related quantities are desired.

On an IBM 7094 computer, this method requires 0.25 sec to integrate the four solutions of the eighth-order system across one integration step; 0.14 sec are required for the three solutions of the sixth-order system. With 160 steps, a common number, and provided only one iteration is needed, it takes two minutes to calculate the eigenvalues of the eighth-order system, and 67 sec for the sixth-order system. At a computer charge of $250/hr., the costs are, respectively, $8.00 and $4.45 for each set of eigenvalues.

These numbers are included here to emphasize that the economics of doing research on a computer is a major consideration.

The method just described has one important drawback. It is limited to maximum values of αR which are not always adequate. Fortunately, as M_1 increases, so does $(\alpha R)_{max}$, but a value of 300 is about the highest one can achieve. The adoption of some version of Kaplan's method, such as the method of Wazzan, Okamura and Smith (1966), would remove this limitation. Also since single-precision arithmetic could then be used, the speed of the program would also increase.

15. Inviscid Theory

15.1 General results

Lees and Lin (1946) have carried out the most complete study to date of the inviscid theory. Their results which are useful for our purposes will be summarized here without proof. Since the equations for a three-dimensional disturbance can be reduced to the two-dimensional equations, only the latter equations will be considered in this section. Lees and Lin classified the disturbances into three groups, depending on whether the phase velocity c_r^* is subsonic, sonic or supersonic with respect to the free-stream velocity U_1^*. In dimensionless terms, this classification is

$$\begin{aligned} c_r &> 1 - \frac{1}{M_1} && \text{subsonic} \\ c_r &= 1 - \frac{1}{M_1} && \text{sonic} \\ c_r &< 1 - \frac{1}{M_1} && \text{supersonic} \end{aligned} \tag{15.1}$$

Lees and Lin's chief results are:

(i) The necessary and sufficient condition for the existence of a neutral subsonic disturbance is that there is some point η_s in the boundary layer where

$$\frac{d}{d\eta}\left(\frac{U'}{T}\right) = 0 \tag{15.2}$$

The phase velocity of this disturbance is c_s, the mean velocity at η_s. (The proof of sufficiency depends upon $T - M_1^2(U-c)^2 > 0$.) This

condition is the generalization of the condition found in Section 5.1 for incompressible flow that there must be an inflection point in the velocity profile for a neutral disturbance to exist. The point η_s, which plays the same role here as the inflection point, will be called the generalized inflection point.

(ii) A sufficient condition for the existence of an amplified disturbance is that

$$\frac{d}{d\eta}\left(\frac{u'}{T}\right) = 0$$

at some η greater than η_0, where η_0 is the point at which $c = c_0 = 1 - 1/M_1$. The proof of this condition also depends upon $T - M_1^2(u-c)^2 > 0$.

(iii) A sonic neutral disturbance is

$$\alpha = 0 \quad , \quad c_0 = 1 - \frac{1}{M_1} \tag{15.3}$$

(iv) If $T - M_1^2(u-c)^2 > 0$, there is a unique wave number α_s corresponding to c_s for the neutral subsonic disturbance. In other words, as long as there is no region in the boundary layer where the local Mach number of the mean flow relative to the wave velocity is supersonic $(M_R < 1)$, a unique α_s exists.

These results are obtained by a direct extension of the methods of proof used for incompressible flow. The necessary condition for a neutral subsonic disturbance is derived from the equation for the discontinuity of the Reynolds stress $-\rho\overline{u'v'}$ at the critical point.

This equation is, for $c_i = 0$,

$$\tau(\eta_c + 0) - \tau(\eta_c - 0) = \frac{1}{2}\alpha\pi\frac{|\varphi_c|^2}{u_c'}\left[\frac{d}{d\eta}\left(\frac{u'}{T}\right)\right]_{\eta_c} \tag{15.4}$$

Since τ is zero at the wall and in the free stream by the boundary conditions for a subsonic disturbance, it follows that $(u'/T)'$ must be zero at η_c. A quantity that appears in the asymptotic viscous theory is

$$v_0(c) = -\pi\frac{u_w' c}{T_w}\frac{T_c^2}{(u_c')^3}\left[\frac{d}{d\eta}\left(\frac{u'}{T}\right)\right]_{\eta_c} \tag{15.5}$$

In terms of $v_0(c)$,

$$\Delta\tau = \frac{1}{2}\alpha\frac{T_w}{u_w' c}\left(\frac{|\varphi_c| u_c'}{T_c}\right)^2 v_0(c) \tag{15.6}$$

The discontinuity in τ is derived from the generalization to compressible flow of the Tollmien series solutions for g_1 and g_2. These solutions are

$$g_1(\eta) = (\eta - \eta_c)\, g_1(\eta - \eta_c) \tag{15.7}$$

$$g_2(\eta) = g_2(\eta - \eta_c) + \frac{T_c^2}{(u_c')^3}\left[\frac{d}{d\eta}\left(\frac{u'}{T}\right)\right]_{\eta_c} g_1(\eta)\log(\eta - \eta_c), \quad \eta > \eta_c \tag{15.8}$$

For $\eta < \eta_c$, $\log(\eta - \eta_c) = \log|\eta - \eta_c| - i\pi$ as for incompressible flow. The leading terms of g_1 and g_2 are U_c' and T_c / U_c' , respectively, so that φ_1 and φ_2 are normalized here in a different manner than in Section 5.2.1. These solutions have been worked out in more detail by Reshotko (1960). Both φ and f have the same analytic behavior as for incompressible flow. What is new here is the existence of a temperature fluctuation. According to Reshotko, it has the behavior

$$\theta \sim \frac{1}{\eta - \eta_c} + \frac{T_c}{U_c'}\left[\frac{d}{d\eta}\left(\frac{U'}{T}\right)\right]_{\eta_c} \log(\eta - \eta_c) + \cdots \tag{15.9}$$

Hence, even for a neutral disturbance, here $(U'/T)'_{\eta_c} = 0$ and φ and f are both regular, θ has a singularity at η_c .

The inviscid solutions in powers of α^2 can also be extended to compressible flow. They are, according to Lees and Lin (1946),

$$\begin{aligned} \varphi_1(\eta) &= (U - c)\sum_{n=0}^{\infty} \alpha^{2n} h_{2n}(\eta) \\ \varphi_2(\eta) &= (U - c)\sum_{n=0}^{\infty} \alpha^{2n} h_{2n+1}(\eta) \end{aligned} \tag{15.10}$$

where

$$\begin{aligned} h_0(\eta) &= 1 \\ h_{2n}(\eta) &= \int_0^{\eta} \frac{T - M_1^2(U-c)^2}{(U-c)^2}\, d\eta \int_0^{\eta} \frac{(U-c)^2}{T} h_{2n-2}(\eta)\, d\eta \end{aligned} \tag{15.11}$$

and

$$k_1(\eta) = \int_0^\eta \frac{T - M_1^2(u-c)^2}{(u-c)^2}\, d\eta$$

$$k_{2n+1}(\eta) = \int_0^\eta \frac{T - M_1^2(u-c)^2}{(u-c)^2}\, d\eta \int_0^\eta \frac{(u-c)^2}{T} k_{2n-1}(\eta)\, d\eta \qquad (15.12)$$

In the course of my numerical studies of the eigenvalues of the complete stability equations, it became evident that (iv) could not be true for $T - M_1^2(u-c)^2 < 0$ $(M_R > 1)$. The consequence of this loss of uniqueness makes the inviscid theory for supersonic free-stream Mach numbers differ greatly from the incompressible theory.

Before going further, we must examine more closely the consequences of the finding that neutral and amplified inviscid disturbances can exist whenever $(u'/T)' = 0$. For the flat plate incompressible boundary layer, u'' is negative everywhere except at $\eta = 0$. However, for a compressible boundary layer on an insulated flat plate $(u'/T)'$ is always zero somewhere in the boundary layer. Consequently, all such boundary layers are unstable to inviscid disturbances. We have seen in Section 9.2 for the Falkner-Skan profiles with $\beta < 0$, that inviscid instability became more important as the inflection point moves away from the wall. Figure 15.1 shows c_s, the mean velocity at the generalized inflection point and the phase velocity of the neutral subsonic disturbance, as a function of M_1. The wall is insulated, and the free-stream temperature, which is a parameter for the exact numerical solutions of the boundary-layer equations used here, is characteristic of wind tunnel conditions. The

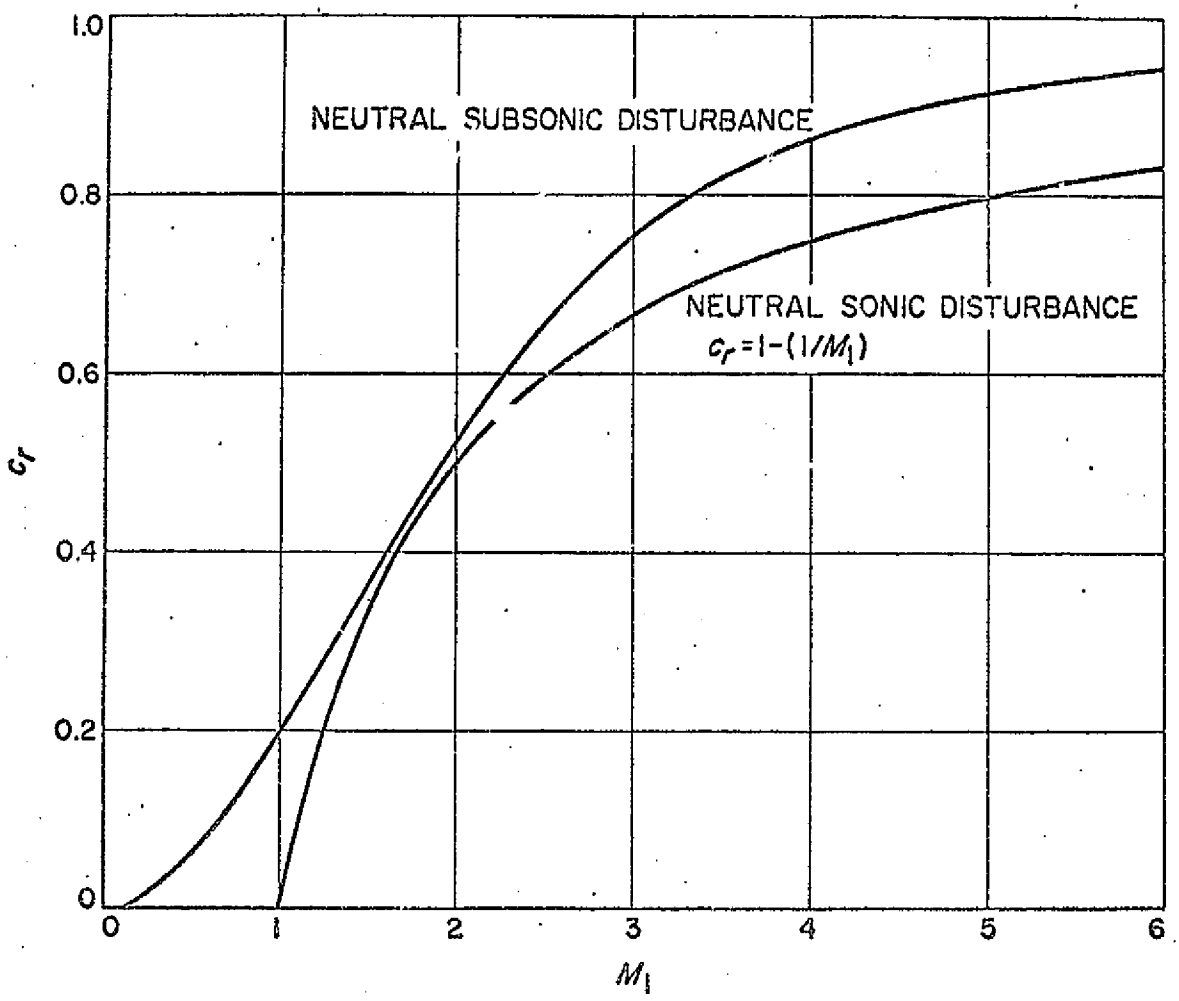

Fig. 15.1 Phase velocity of neutral subsonic disturbance (upper curve) and of neutral sonic disturbance (lower curve) as function of free-stream Mach number

stagnation temperature is held constant at 311°K until, with increasing M_1, the free-stream temperature T_1^* drops to 50°K. For higher Mach numbers, T_1^* is held constant at 50°K. All results to be presented for insulated-wall boundary layers are for this family of boundary-layer profiles unless otherwise noted.

Figure 15.1 also includes a plot of $c_0 = 1 - 1/M_1$. For a disturbance to be subsonic relative to the free stream, and hence have vanishing amplitude at $\eta \to \infty$ even for a neutral disturbance, c_r must be greater than c_0. It is often said that only subsonic disturbances are considered in stability theory, a statement that is not entirely correct. It is true that the neutral subsonic disturbance α_s only exists when $c_s > 1 - 1/M_1$. However, this doesn't rule out amplified or damped disturbances with $c_r < 1 - 1/M_1$, or even neutral supersonic disturbances with a c_r different from c_s. We shall find examples of all of these disturbances, all of which satisfy the boundary conditions at infinity and lead to eigenvalue problems. For $c_i \neq 0$, the amplitudes of outgoing amplified and incoming damped waves vanish at infinity regardless of the value of c_r; for $c_i = 0$, the amplitude will only be bounded at infinity for $c_r < c_0$. What does turn out to be true is that the most unstable disturbances are always subsonic. Further, we shall find that for one class of disturbances, the amplified first-mode waves, $c_0 < c_r < c_s$. This result has important consequences.

15.2 Multiple neutral solutions, two-dimensional disturbances

15.2.1 Neutral subsonic solutions

An important omission in the Lees-Lin inviscid theory was the failure to recognize that for a boundary layer at supersonic free-stream Mach

numbers, there are multiple neutral solutions. It is rather easy to demonstrate the existence of these solutions.[1] The inviscid equation written in terms of π, (13.76), quite evidently has a different character depending upon whether M_R is less than or greater than unity. It is instructive to consider α^2 large enough so that the π' term can be neglected. Then (13.76) reduces to

$$\pi'' - \alpha^2 (1 - M_R^2)\pi = 0 \tag{15.13}$$

When $M_R < 1$, the solutions of (15.13) are elliptic in nature, and it is under this circumstance that Lees and Lin proved the uniqueness of α_s. However, when $M_R > 1$, (15.13) becomes a wave equation, and as in all problems governed by the wave equation we can expect there to be an infinite sequence of wave lengths which will satisfy the boundary conditions.

If we introduce

$$\eta_1 = (\eta)_{M_R = 1} \tag{15.14}$$

then, from (15.13),

$$\pi = \pm \cos\left[\alpha_{sn} \int_0^{\eta} (M_R^2 - 1)^{1/2} d\eta\right] \qquad \eta < \eta_1 \tag{15.15}$$

$$\pi = \exp\left[-\alpha_{sn} \int_{\eta_1}^{\eta} (1 - M_R^2)^{1/2} d\eta\right] \qquad \eta > \eta_1 \tag{15.16}$$

where (15.15) follows from (13.69) and the boundary condition on φ at

[1] Not too long after I found these solutions for the boundary layer, Gill (1965) independently found them during his study of the "top-hat" wake.

$\eta = 0$. We have written α as α_{sn}. The subscript s designates the neutral subsonic solution; the subscript n refers to the multiplicity of solutions. Since we have arbitrarily made π positive for $\eta > \eta_1$, it can have either sign at $\eta = 0$. At $\eta = \eta_1$,

$$\cos\left[\alpha_{sn}\int_0^{\eta_1}(M_R^2 - 1)^{1/2}\,d\eta\right] = \pm 1 \tag{15.17}$$

and

$$\alpha_{sn}\int_0^{\eta_1}(M_R^2 - 1)^{1/2}\,d\eta = n\pi, \qquad n = 1, 2, \ldots \tag{15.18}$$

Because of the approximate nature of (15.15), the magnitude of α_{sn} as given by (15.18) is of little importance. However, the difference between adjacent values of α_{sn}, given by

$$\alpha_{s(n+1)} - \alpha_{sn} = \frac{\pi}{\int_0^{\eta_1}(M_R^2 - 1)^{1/2}\,d\eta} \tag{15.19}$$

turns out to be accurate under many circumstances.

When the numerical integration of (13.68) and (13.69) is carried out with $c_w = c_s$, $c_i = 0$ for the insulated-wall boundary layer, the α_{sn} which are found by the eigenvalue search procedure described in Section 14.1 are shown in Fig. 15.2. The solution for each value of n will be referred to as a mode, with $n = 1$ the first mode, $n = 2$ the second mode, etc. The wave numbers of the first mode were first computed by Reshotko (1960). The second and higher modes appear only for $M_1 > 2$. With $c_w = c_s$ and the family of insulated-wall boundary-layer profiles, a

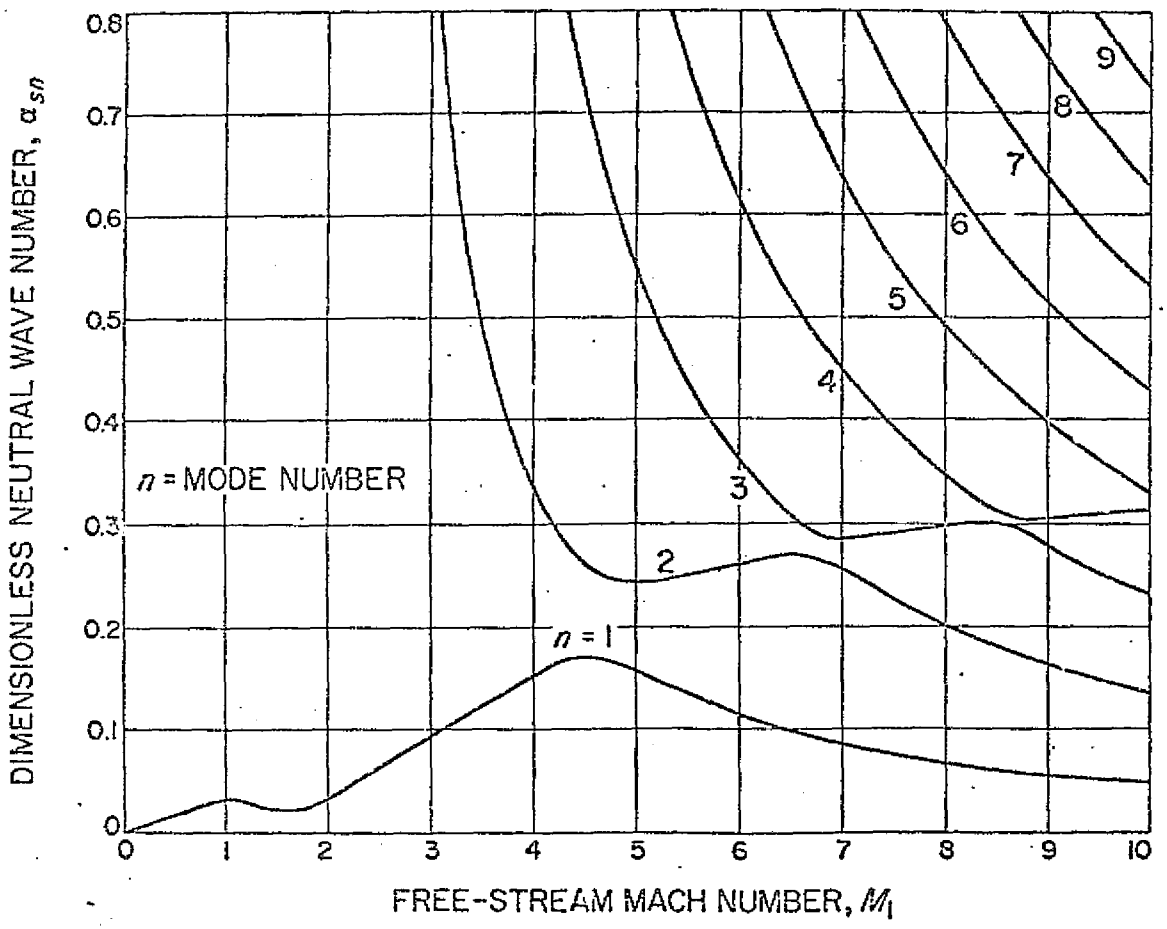

Fig. 15.2 Effect of free-stream Mach Number on neutral wave numbers of two-dimensional disturbances

point η_1 at which $M_R = 1$ first occurs at $M_1 = 2.2$ where $\eta_1 = 0$. With increasing M_1 the point η_1 moves out into the boundary layer. No higher modes could be found numerically for $M_1 < 2.2$, in accord with the theory given above. Also, from (15.18) α_{sn} must be inversely proportional to η_1, the thickness of the relative supersonic layer. As $M_1 \to 2.2$ from above, $\eta_1 \to 0$ and α_{sn} must become infinite, again in agreement with the numerical results.

A curious feature of Fig. 15.2 is that the upward-sloping portion of the first-mode curve between $M_1 = 2$ and 4.5 is in a sense continuous through the other modes; i.e., there is a Mach number range for each mode where the α_{sn} vs M_1 curve has a positive slope. The end point of this region for one mode is close to the starting point of a similar region for the next higher mode. The approach becomes closer as M_1 increases. This upward-sloping portion of each curve has a special significance which will be pointed out later. The same phenomenon will appear in even more emphatic fashion when we take up three-dimensional disturbances in Section 15.5.

The accuracy of the wave number spacing given by (15.19) can be checked from the numerical results, which are given in Table 15.1 for $M_1 = 5.8$ and 10.0.

	$M_1 = 5.8$	$M_1 = 10.0$
Modes	$\Delta\alpha$	$\Delta\alpha$
2-1	0.14	0.09
3-2	0.13	0.10
4-3	0.27	0.08
5-4	0.28	0.02
6-5		0.10
7-6		0.10
8-7		0.10
(15.19)	0.28	0.10

Table 15.1 Comparison of predicted and computed value for wave-number spacing of adjacent modes.

We see that at $M_1 = 5.8$, (15.19) is satisfied starting with the difference between the third and fourth modes; at $M_1 = 10$ it is satisfied approximately for the first three differences, and then exactly starting with the difference between the fifth and sixth modes. The upward-sloping line thus marks an important boundary. Above this line, the spacing solution is satisfied exactly; immediately adjacent to the line, it is not satisfied at all; and below the line it is satisfied approximately at high Mach numbers.

With the eigenvalues of the multiple neutral solutions established, the next step is to examine the eigenfunctions. For this purpose the magnitude of the amplitude function $Z_4 \left(= \pi / \gamma M_1^2 \right)$ is sketched in Fig. 15.3 for the first 8 modes. The first thing to note from this figure is that the number of zeroes in Z_4 is one less than the mode number n. For example, the second mode has one zero, and $Z_4(0)$ is 180° out of phase with $Z_4(\eta_s)$; the third mode has two zeroes and $Z_4(0)$ is in phase with $Z_4(\eta_s)$. The number of zeroes in $Z_4(\eta)$ is the surest identification of the mode under consideration. By keeping track of the phase relation between $Z_4(0)$ and $Z_4(\eta_s)$, it is possible to determine when there is a change from one mode to another.

Second, the appearance of the eigenfunctions in Fig. 15.3 tends to confirm what is suggested by the simple theory given above: there is an infinite sequence of wave lengths in the supersonic relative-flow region which can satisfy the boundary conditions. Third, the magnitude of $Z_4(0)$ is a minimum for the fourth mode. ($Z_4(\eta_s)$ is the same for all modes.) Since the fourth mode at $M_1 = 10$ is on the upward-sloping line of Fig. 15.2,

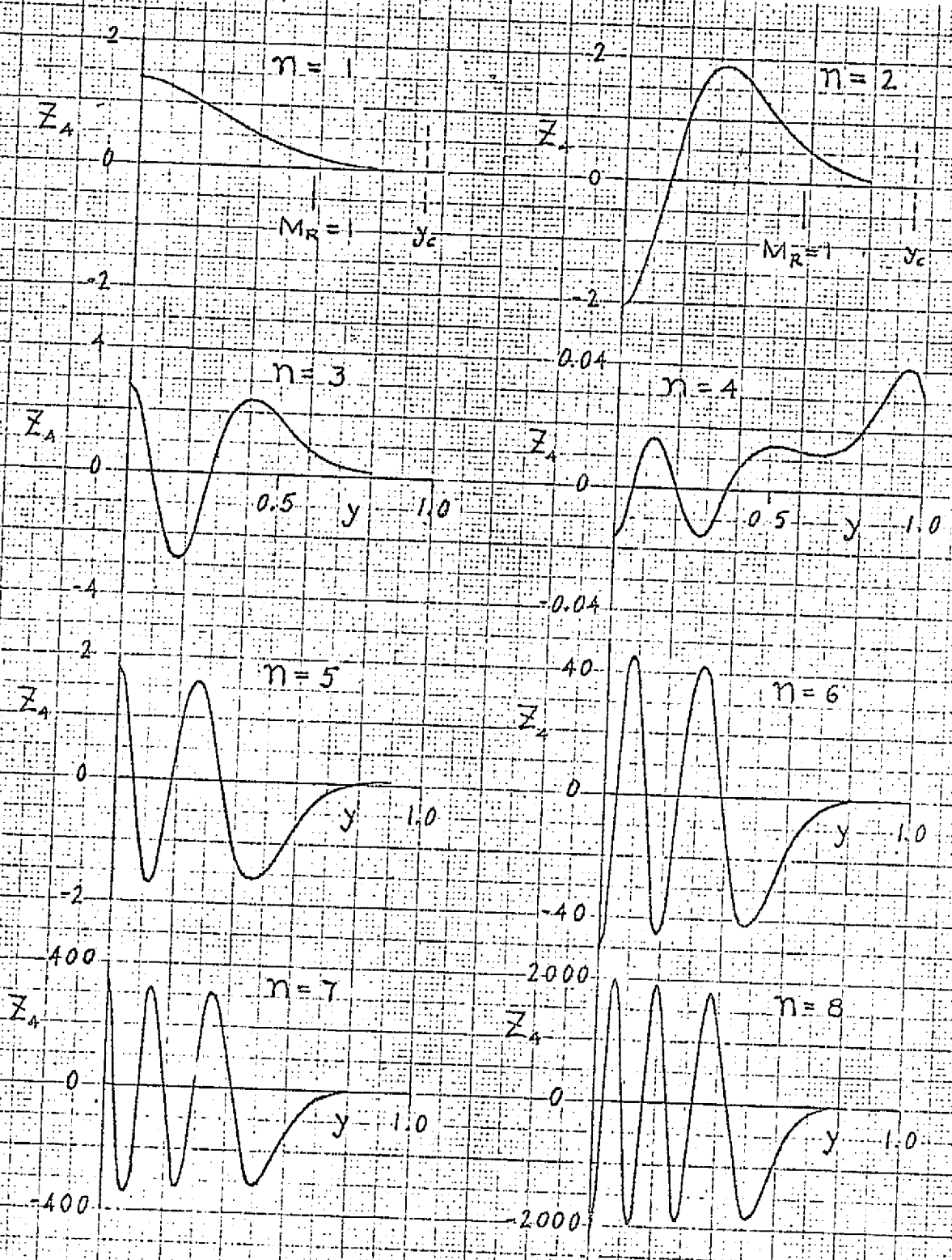

Fig. 15.3 Pressure-fluctuation amplitude function of neutral subsonic solution for first eight modes at $M_1 = 10$.

this is another indication of the special nature of the neutral solutions that make up this line. For other modes, $\pi(o)/\pi(\gamma_s)$ tends to become large away from this line. In particular, this ratio becomes indefinitely large as $n \to \infty$. This same phenomenon will reappear in a slightly different form for three-dimensional disturbances and is illustrated in Fig. 15.13.

15.2.2 Singular neutral solutions

A further consequence of a region of supersonic relative flow in the boundary layer is the existence of another class of neutral disturbances. Although these disturbances are also subsonic, the term neutral subsonic disturbances will always refer to the disturbances associated with the generalized inflection point. The new class of disturbances is called singular because the solutions cannot be computed directly, but are obtained in the limit as $c_i \to 0$ from a family of amplified solutions. In the limit, $c_r \to 1$ and $\pi(o)/\pi(\gamma_s) \to \infty$. That is, these neutral disturbances propagate with the free-stream velocity, and, since for a finite $\pi(o)$ the free-stream pressure fluctuation $\pi(\gamma_s)$ is zero, the disturbance is restricted to the boundary layer. The wave numbers of these solutions are designated by α_{1n}. The first subscript refers to $c_r = 1$, the second is the mode number. The smallest α_{1n} is called the second mode, the next smallest the third mode, etc.

Figure 15.4 gives $|\pi(\gamma)|/|\pi(o)|$ and $\arg \pi(\gamma)$ as functions of γ for almost neutral disturbances of the second and third modes at $M_1 = 5.8$. Both the amplitude ratio and the magnitude of the phase change are nearly independent of c_r near $c_r = 1$, but the location of the phase change in the outer portion of the boundary layer varies somewhat as

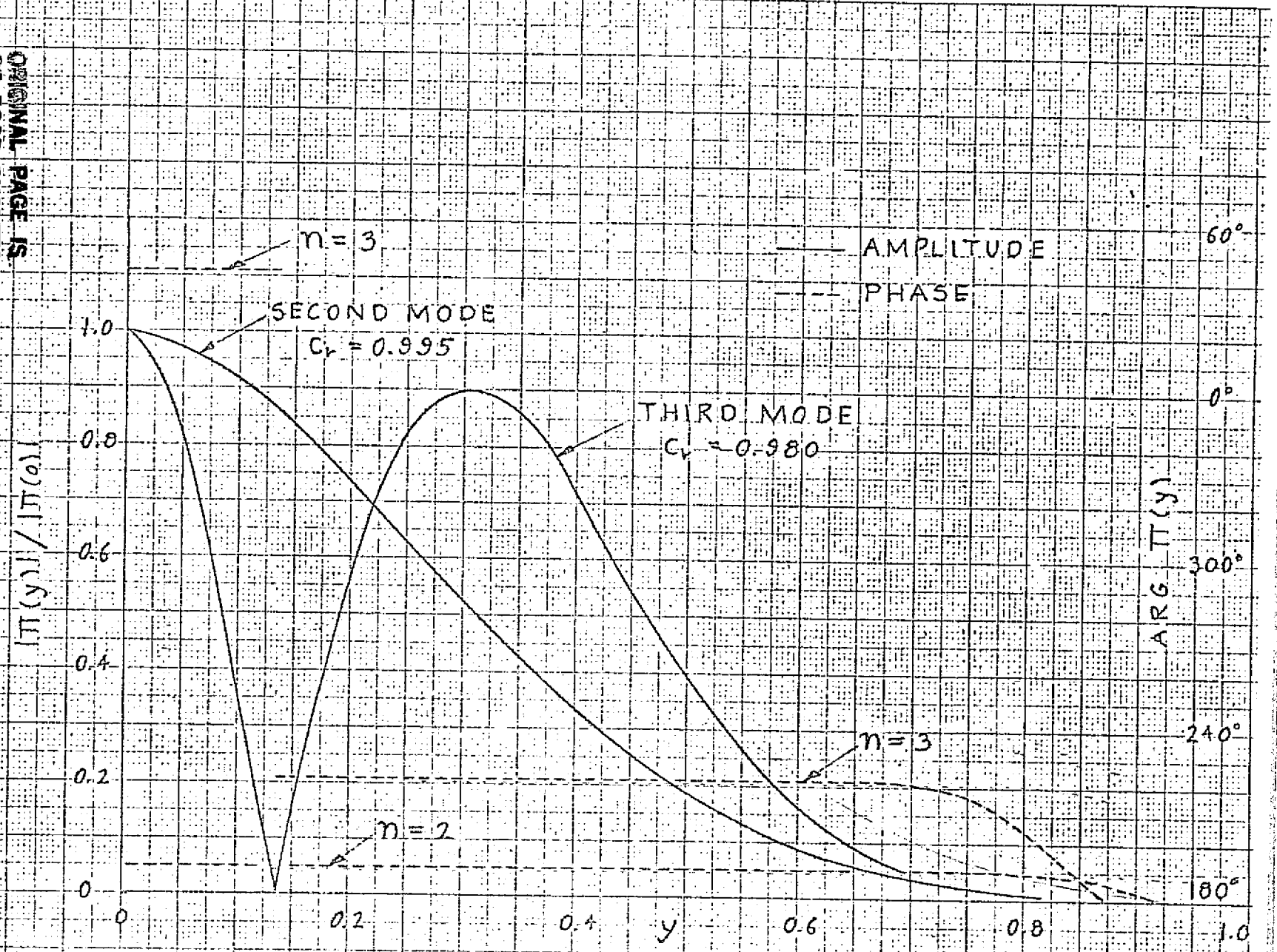

Fig. 15.4 Amplitude and phase solutions of second and third mode singular neutral solutions (approximately) at $M_1 = 5.8$.

$c_r \to 1$. This phase change is always located inside of the critical point. We see that for the second mode the pressure fluctuation undergoes only a 10° phase change, while for the third mode it undergoes a 42° phase change in the outer portion of the boundary layer and a 180° phase change at $y = 0.135$. This 180° phase change is just what is encountered in the second-mode neutral subsonic solution.

15.3 Amplified two-dimensional disturbances

Now that we are acquainted with the main classes of neutral disturbances, we can go on to the much more important amplified disturbances. With the neutral solutions known, it is easy to calculate amplified solutions by letting c_i increase from zero. It will turn out that not all of the neutral subsonic solutions lead to amplified solutions of interest, but at least one always does, as will be seen presently.

It is convenient to plot the eigenvalues of the amplified disturbances in the form of diagrams of α vs c_i and c_r vs c_i. Such diagrams are a necessity in carrying out the calculations. The complete picture of the inviscid solutions requires the damped solutions also, but to simplify the discussion, they will be deferred until Section 17.4, where the behavior of the viscous solutions is discussed.

Figures 15.5, 15.6, and 15.7 give examples of eigenvalue diagrams at three Mach numbers, 3.8, 4.8, and 6.2. At $M_1 = 3.8$, the first two modes are included in the range of α's shown. If the calculations are started at both α_{s1}, c_s and α_{s2}, c_s, the two curves shown in Fig. 15.5 result. The curve which starts from α_{s1}, c_s leads to the sonic neutral solution

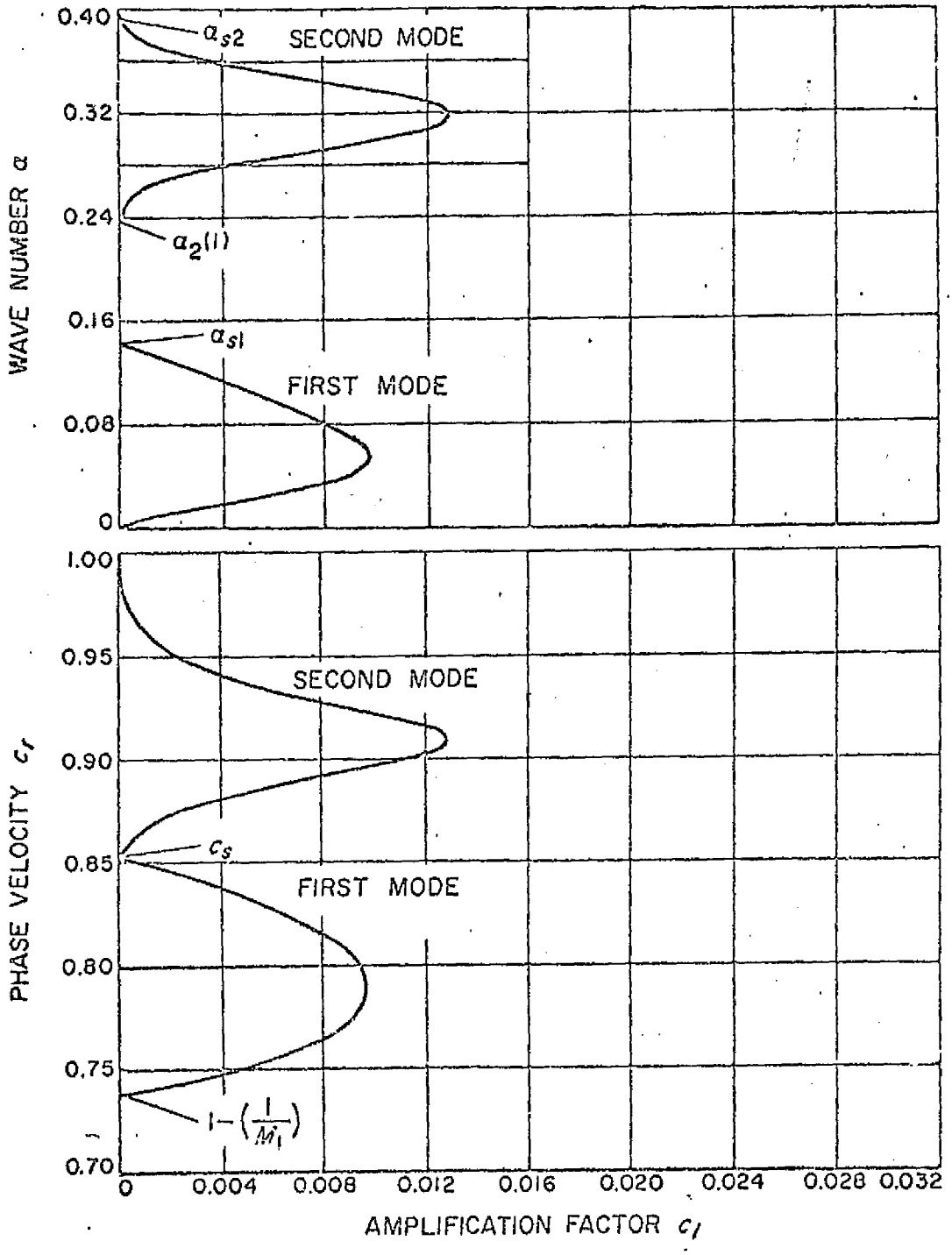

Fig. 15.5 Eigenvalue diagrams at $M_1 = 3.8$

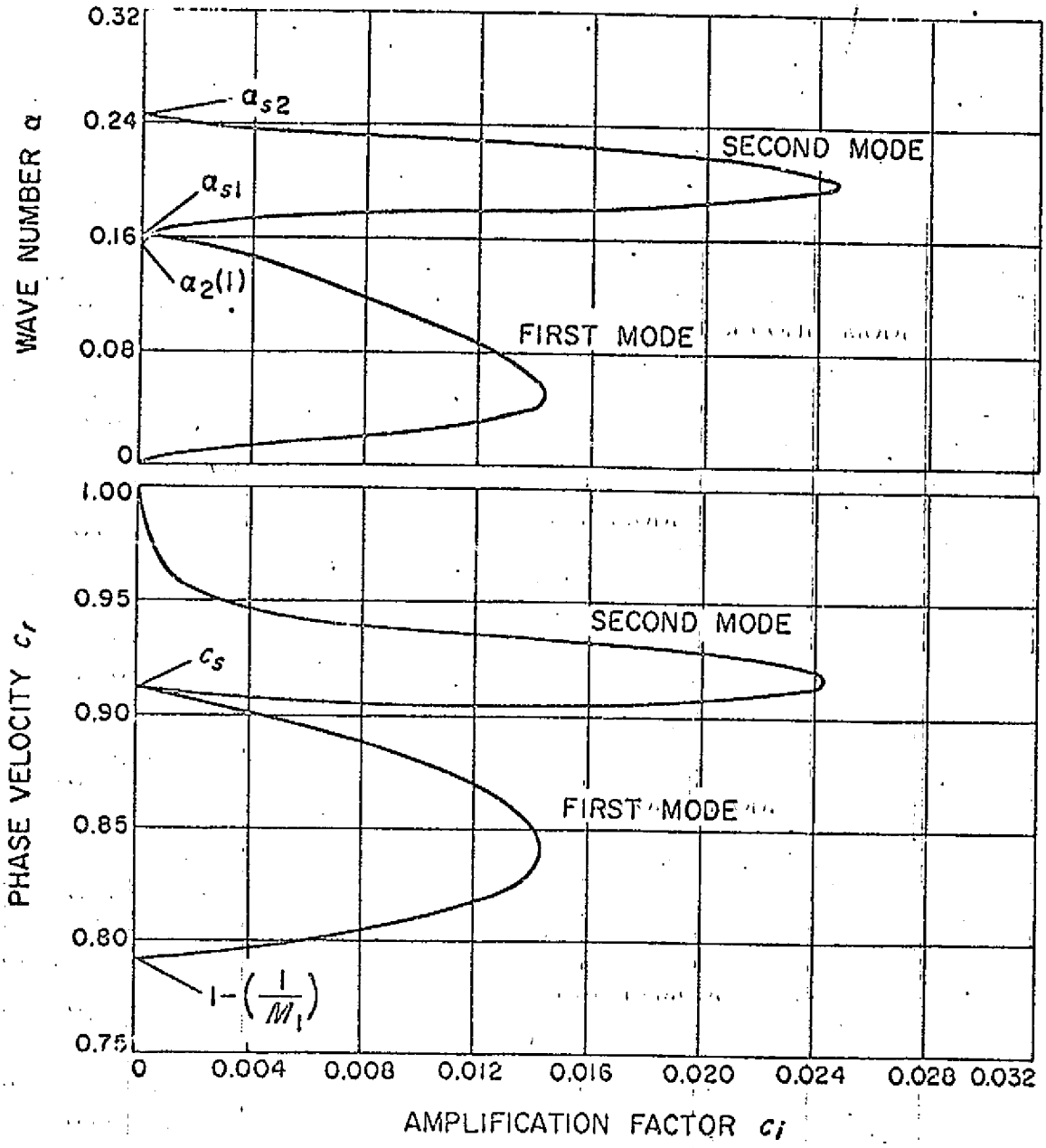

Fig. 15.6 Eigenvalue diagrams at $M_1 = 4.8$

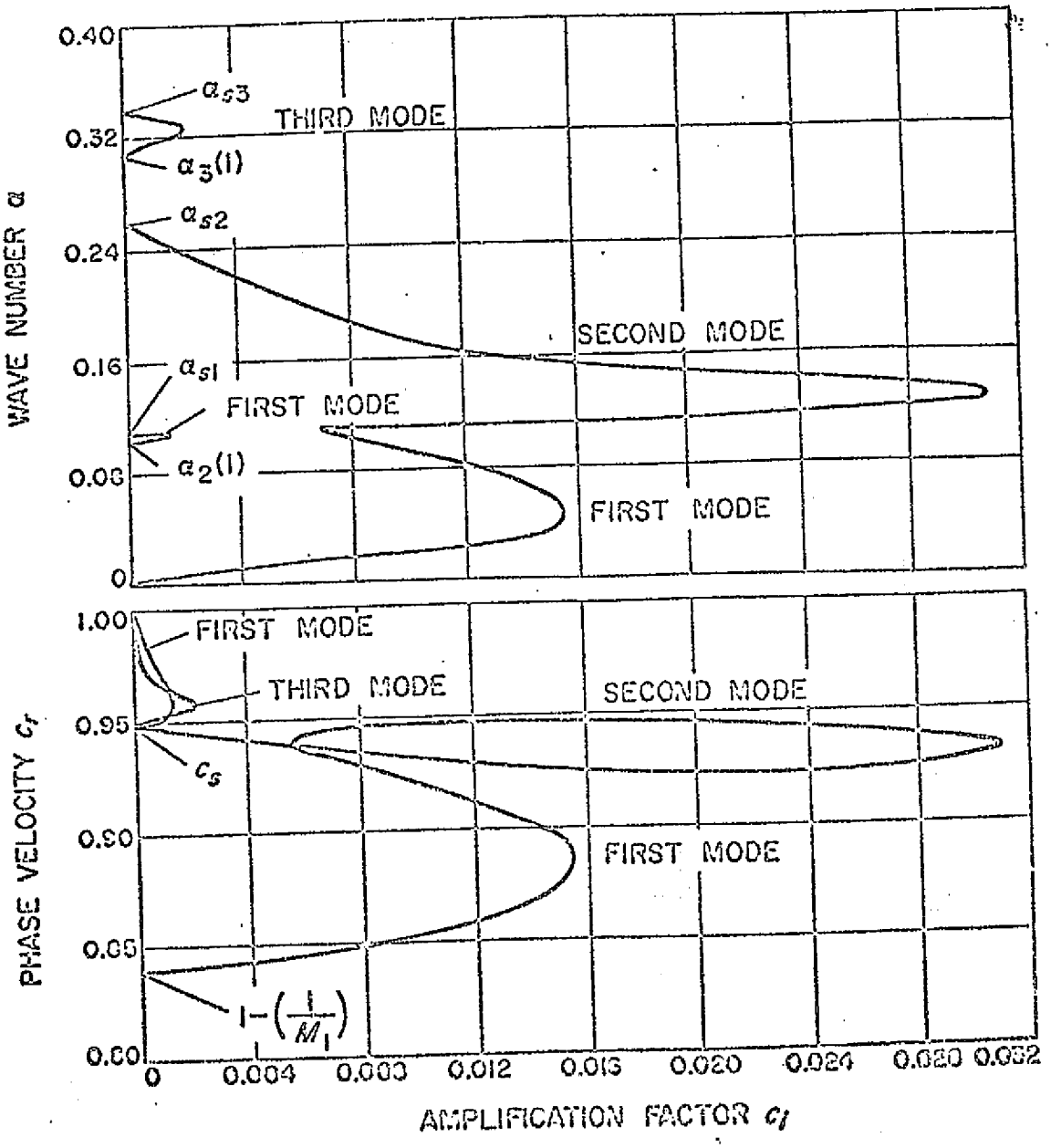

Fig. 15.7 Eigenvalue diagrams at $M_1 = 6.2$

$\alpha = 0$, $c_r = 1 - 1/M_1$. The solutions which lie on this curve have little phase shift in the pressure fluctuation and may be called first-mode amplified solutions. The curve which starts from α_{s_2} , c_s leads to the singular neutral solution α_{12} , $c_r = 1$. The solutions which lie on this curve have a large phase shift in the pressure fluctuation except near the singular neutral solution. They may be called second-mode amplified solutions.

It can be noted in these figures that for the first mode, $c_a < c_r < c_s$. This result is always found for the first mode. For the second mode, as seen from Figs. 15.6 and 15.7, it is possible to have $c_r < c_s$. What is of major importance is that the amplification rate, αc_i , of the second mode is larger than for the first mode, a result which is always true. It is this feature that makes supersonic boundary-layer stability so different from incompressible flow. Not only is there more than one mode of instability, but it is one of the additional modes which is the most unstable.

At $M_1 = 4.8$, Fig. 15.6 shows that α_{12} is smaller than α_{s_1} . This condition persists until $M_1 = 6.0$, after which a marked change occurs as shown in Fig. 15.7 for $M_1 = 6.2$. The eigenvalue curve of the first mode joins the eigenvalue curve of the second mode at $c_i > 0$. As a result, it is not possible to reach α_{s_1} by following the eigenvalue curve which starts at the neutral sonic solution, nor is it possible to reach the singular neutral solution by following the eigenvalue curve which starts at α_{s_2} . Instead, α_{12} is reached by starting at α_{s_1} . By reference to Fig. 15.2, it can be seen that at $M_1 = 6.2$ α_{s_2} lies on the upward-sloping

portion of the α_{s_2} vs. M_1 curve. Although the first-mode neutral subsonic solution still exists, it has ceased to be of importance in the sense that there are no "adjacent" amplified solutions of any consequence. At $M_1 = 6.2$, the magnitude of the ratio $\pi(0)/\pi(\eta_s)$ for the neutral solution α_{s_2}, c_s is 1/8 of the magnitude of $\pi(0)/\pi(\eta_s)$ for the solution α_{s_1}, c_s. An obvious feature of Fig. 15.7 is that nowhere on the combined first- and second-mode curve does c_r exceed c_s.

As M_1 increases beyond 6.2, the eigenvalue diagrams continue to change. At $M_1 = 7.0$, α_{i_3} is less than α_{s_2}, so the second- and third-mode eigenvalue curves cross. At $M_1 = 7.5$, the combined first- and second-mode curve does not lead to α_{s_2}, c_s, but instead joins the third-mode eigenvalue curve at a $c_i > 0$ and leads to α_{s_3}, c_s. Hence, a single eigenvalue curve extends from the neutral sonic solution to the third-mode neutral subsonic solution. Neither of the neutral solutions α_{s_1}, c_s or α_{s_2}, c_s have "adjacent" amplified solutions of importance. It is also true that all along the combined curve, $c_0 < c_r < c_s$.

When there are no longer separate eigenvalue curves for each mode, it can be difficult to identify a particular solution with a definite mode. However, the $\alpha - c_i$ diagram at $M_1 = 6.2$ still retains the appearance of two separate modes. A close investigation shows that there is a rapid change in both the phase difference, $\arg \pi(\eta_s) - \arg \pi(0)$, and in the magnitude of the ratio $\pi(0)/\pi(\eta_s)$ near the "intersection" of two mode curves. These two quantities are shown in Fig. 15.8 as functions of α at $M_1 = 8$, where the first three modes are merged.

With the eigenvalues of the amplified solutions established, the temporal amplification rate αc_i as a function of α follows directly. When, at

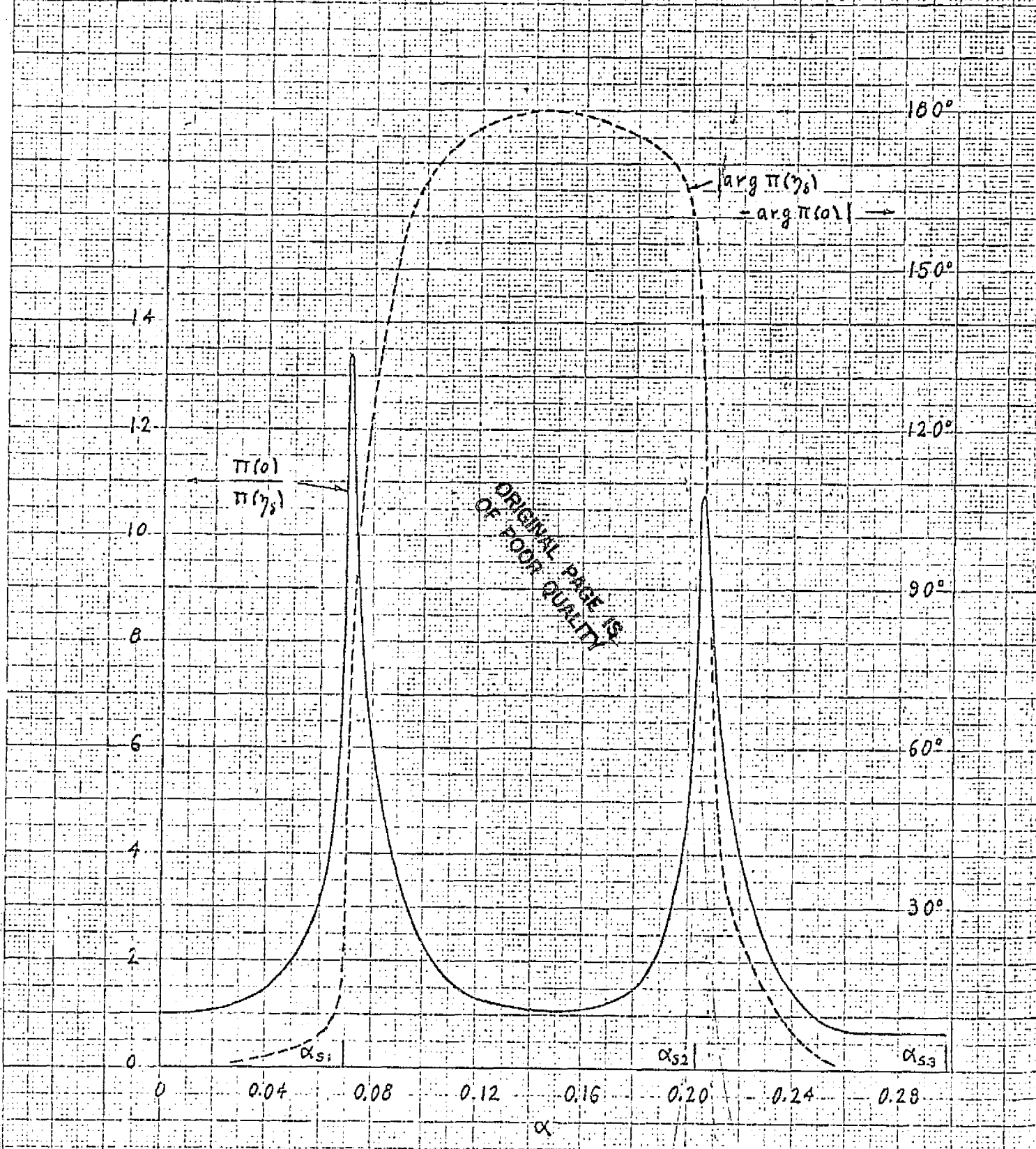

Fig. 15.8 Amplitude and phase relations of $\pi(0)$ for amplified solutions of first three modes at $M_1 = 8$.

several Mach numbers, αc_i is plotted as a function of α for the first four modes, and the maximum amplification rate of each mode is read off, Fig. 15.9 can be constructed. This figure demonstrates that the second mode is always the most unstable mode. For $M_1 > 6.5$, the first mode is not even the second most unstable mode, and at $M_1 = 10$, both the third and fourth modes are more unstable than the first mode. In order to get an idea of how these amplification rates compare to those found for incompressible flow, we recall from Section 9.2 that for the Blasius boundary layer at $M_1 = 0$, $\alpha_\delta c_i = 15 \times 10^{-3}$. The growth of a disturbance in a distance equal to one boundary-layer thickness is

$$\left(\frac{dA}{A}\right)_{\Delta x = \delta} = \frac{\alpha_\delta c_i}{c_r} d\left(\frac{x}{\delta}\right) \tag{15.20}$$

where the group velocity has been replaced by the phase velocity. Table 15.2 gives a few values of $(dA/A)_{\Delta x = \delta}$.

M_1	$(dA/A)_{\Delta x = \delta}$
0, finite R	0.05
0, $\beta = -0.1988$	0.40
3, 2nd mode	0.03
5, 1st mode	0.02
5, 2nd mode	0.10
10, 2nd mode	0.07

Table 15.2 Amplitude growth over one boundary-layer thickness.

Thus for $3.5 < M_1 < 10$, a second-mode disturbance can grow as much over one boundary-layer thickness, according to the inviscid theory, as is

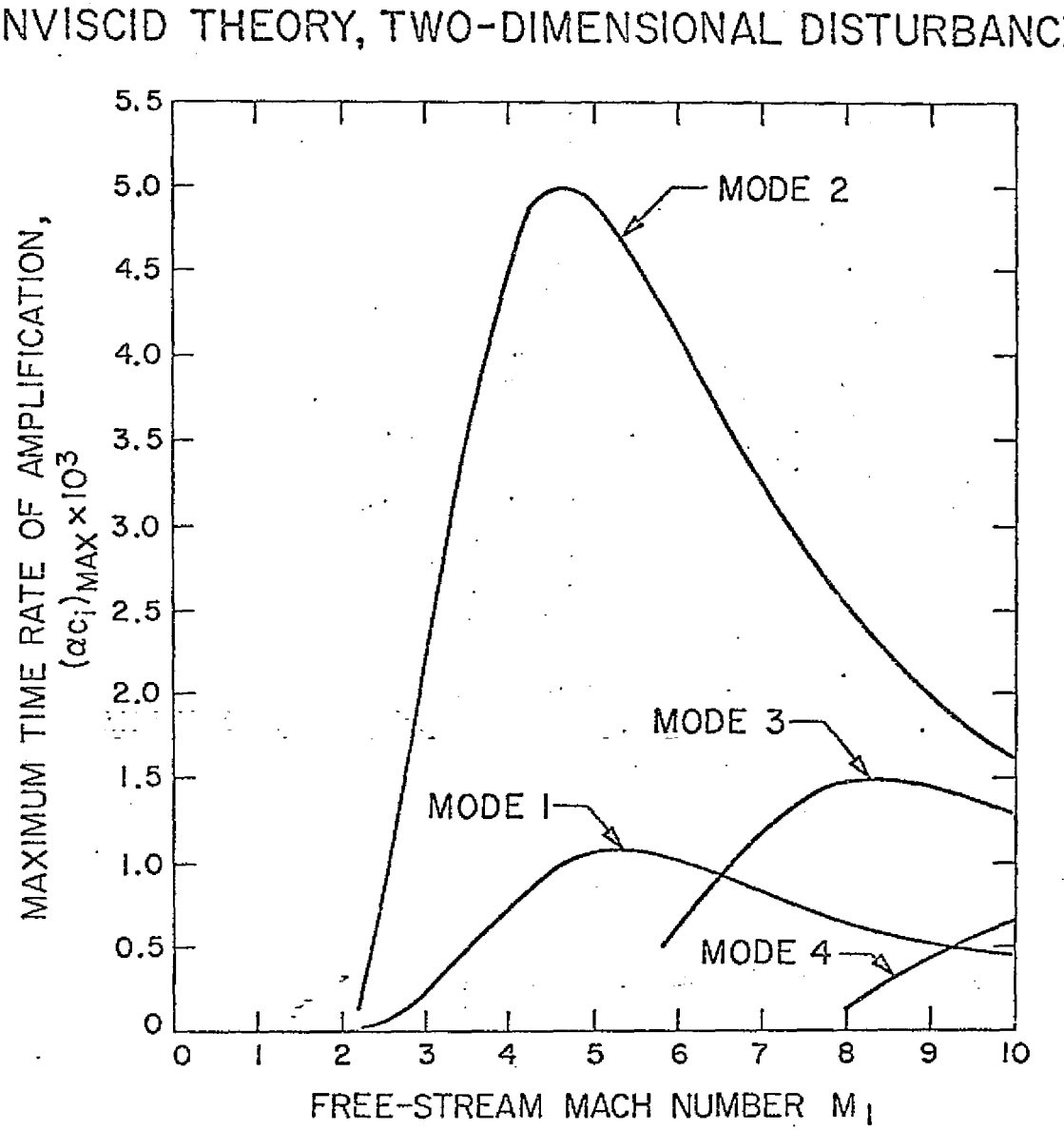

Fig. 15.9 Effect of Mach number on maximum time rate of amplification of first four modes.

possible in the incompressible flat-plate boundary layer. It also follows from Fig. 15.9, that below about $M_1 = 2.3$ the boundary layer is for all practical purposes stable to two-dimensional inviscid disturbances.

Of equal importance with the maximum amplification rate is the frequency of the disturbance which has this amplification rate. It is of no consequence to have a large amplification rate for a particular frequency if the spectrum of an actual disturbance in the boundary layer does not include that frequency. Figure 15.10 gives αc_r $(= \omega)$ as a function of M_1 for the first four modes. The dimensionless (circular) frequency is

$$\omega = \frac{\omega^*}{u_1^*} \frac{x^*}{R} \tag{15.21}$$

Thus for a fixed-frequency disturbance and a constant free stream, the dimensionless frequency varies as $x^{1/2}$, and the disturbance can experience the maximum amplification rate of Fig. 15.9 only at one particular boundary-layer thickness.

As a final observation from Fig. 15.9, we can note that the decrease in $(\alpha c_i)_{max}$ for $M_1 > 4.5$ is almost entirely a result of the increasing thickness of the boundary layer. If $(\alpha_s c_i)_{max}$ were plotted instead of $(\alpha c_i)_{max}$ in Fig. 15.9, the amplification rate for each mode would be but slightly dependent upon M_1 past the peak values of Fig. 15.9.

Now that we are familiar with the results of the inviscid theory for two-dimensional disturbances in the insulated flat-plate boundary layer with wind-tunnel temperature conditions, we are in a position to understand

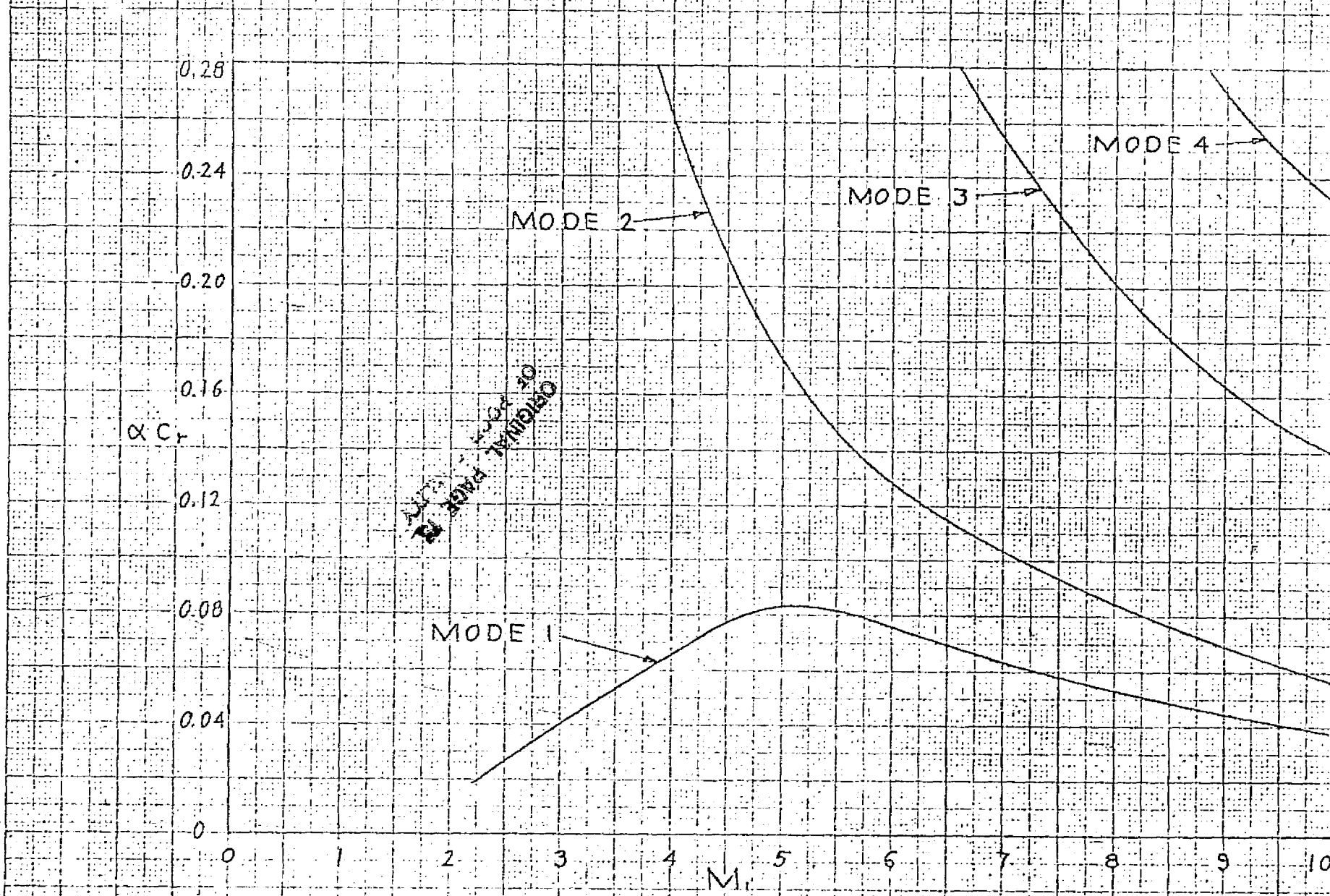

Fig. 15.10 Effect of Mach number on frequency of most unstable two-dimensional disturbance for first four modes.

the changes that occur when any of these restrictions are lifted. Only flat-plate boundary layers have yet been investigated, but in the next three sections we shall find what happens when the free-stream temperature is different from that in the wind tunnel; when the disturbances are no longer two-dimensional, and when the wall is no longer insulated. Unfortunately, except for the numerical results there is a total absence of an inviscid theory for amplified disturbances. As general guides, it will be necessary to make use of two empirical observations for the first mode, and for the higher modes, the result suggested by (15.19), that the wave numbers are inversely proportional to the thickness of the supersonic relative-flow region.

The two empirical results for the first mode are: first, c_i is always between c_0 and c_s ; second, $(\alpha_s c_i)_{max}$ is related to the difference $c_s - c_0$. That is, as $c_s \to c_0$, $(\alpha_s c_i) \to 0$. We can see from Fig. 15.1 that $c_s - c_0$ has a minimum near $M_1 = 1.6$. This difference then increases and finally tends to level off. If $(\alpha_s c_i)_{max}$ for the first mode were to be plotted on a much larger scale than is used in Fig. 15.9, it would be found to have a similar behavior to $c_s - c_0$ with a maximum near $M_1 = 1.5$. This correspondence between $c_s - c_0$ and $(\alpha_s c_i)_{max}$ suggests that anything that changes the relative positions of c_s and c_0 will also have an important effect on the amplification rate of the first mode. Both the free-stream temperature and the ratio of wall temperature to free-stream temperature affect c_s . With three-dimensional disturbances, c_0 will change to $\tilde{c}_0 = 1 - 1/\tilde{M}_1$ because the effective Mach number is the component in the direction of the wave normal. For a sufficiently

oblique wave $\tilde{c}_a$ is equal to zero.

15.4 Effect of free-stream temperature on two-dimensional disturbances

We shall study first the effect of changing the free-stream temperature while keeping the wall insulated. Figure 15.11 is a counterpart of Fig. 15.1. In this figure, there are three curves of c_s (labelled at η_s^u) vs. M_1 for three values of T_1^*, 40°K, 160°K and 300°K. Increasing T_1^* moves the c_s curve closer to the c_0 curve. Consequently, increasing T_1^* will stabilize the first mode. Indeed, for $T_1^* = 300°K$, $c_s < c_0$ between $M_1 = 1.6$ and 2.5, and the first mode will be completely stabilized.

In Fig. 15.12, the maximum amplification rates of the first and second modes are plotted as functions of T_1^* for three Mach numbers, 3.5, 6.0 and 8.0. As expected from Fig. 15.11, increasing T_1^* has a strong stabilizing influence on the first mode. The effect on the second mode is much smaller and can be either stabilizing or destabilizing, depending on the Mach number.

15.5 Three-dimensional disturbances

15.5.1 Neutral solutions

To treat three-dimensional disturbances we must use the tilde coordinate system of Section 13.3 to reduce the three-dimensional equations to two-dimensional equations. In this coordinate system, $\tilde{M}_1 = M_1 \cos\psi$, $\tilde{\alpha} = \alpha/\cos\psi$ and ψ is the angle between the wave normal and the free-stream direction. Since the boundary layers under consideration are two-dimensional, the boundary-layer profiles are independent of ψ. First we shall look at the variation of the neutral wave numbers, $\tilde{\alpha}_{s_n}$, with ψ. Figure 15.13 gives the results at $M_1 = 8$ for the first three modes (ψ is called σ in this figure, and also in Fig. 15.19). We see that with increasing ψ, $\tilde{\alpha}_{s_3}$ and $\tilde{\alpha}_{s_2}$ approach each other closely at $\psi = 35°$,

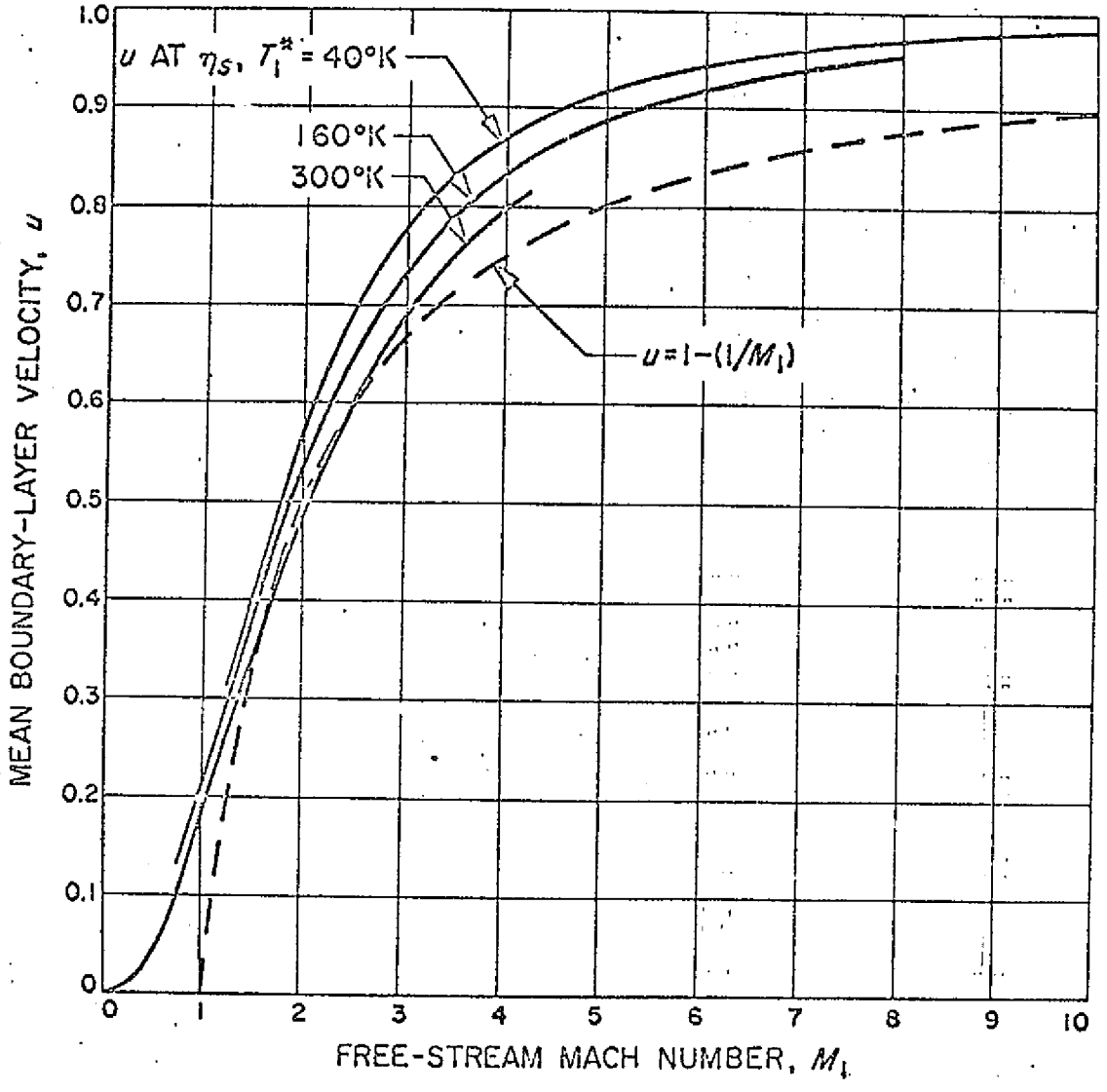

Fig. 15.11 Mean boundary-layer velocity u at the generalized inflection point η_s, and also $1 - (1/M_1)$, vs free-stream Mach number M_1

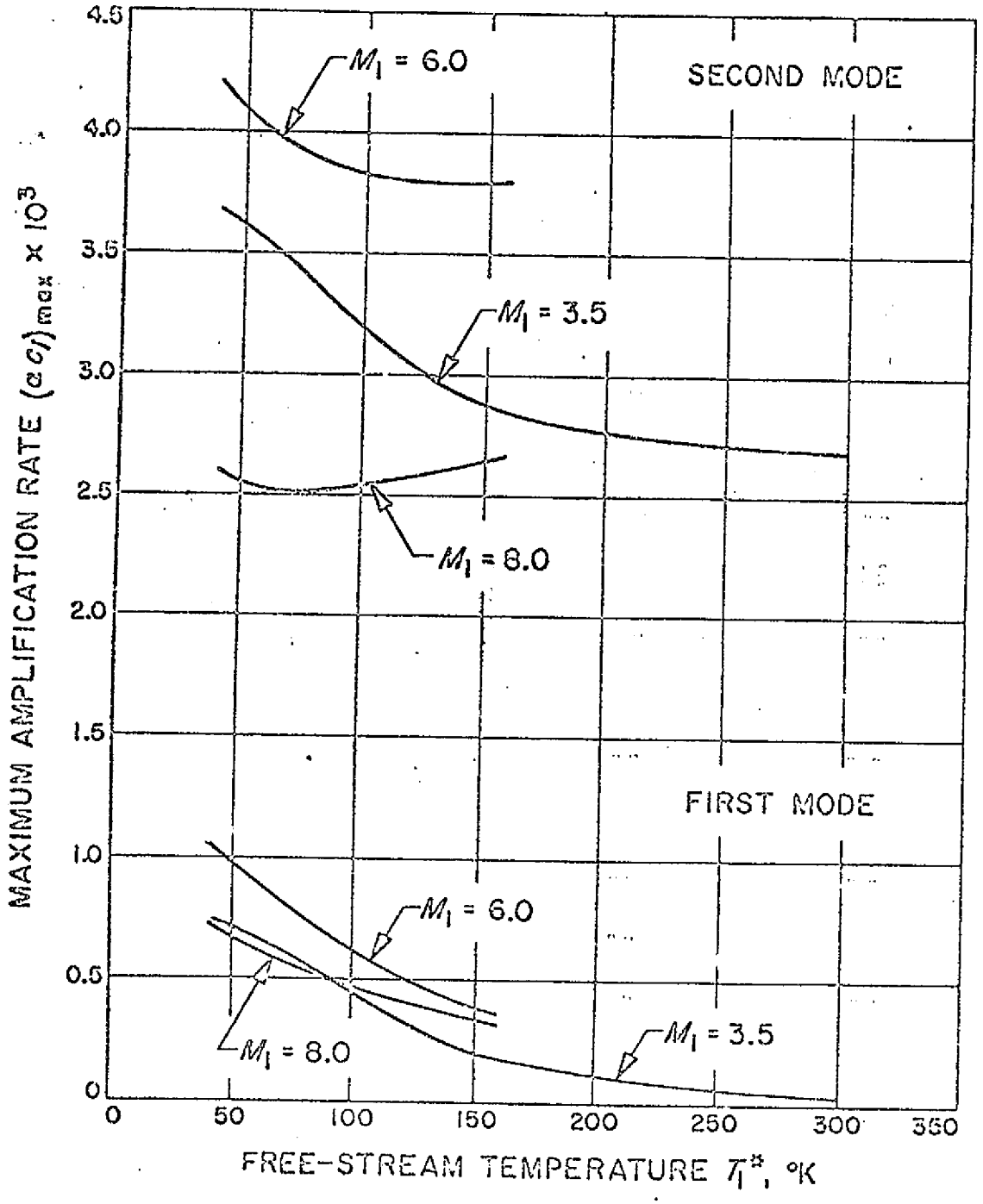

Fig. 15.12 Effect of free-stream temperature T_1^* on the maximum amplification rates of the first and second modes for $M_1 = 3.5$, 6.0, and 8.0

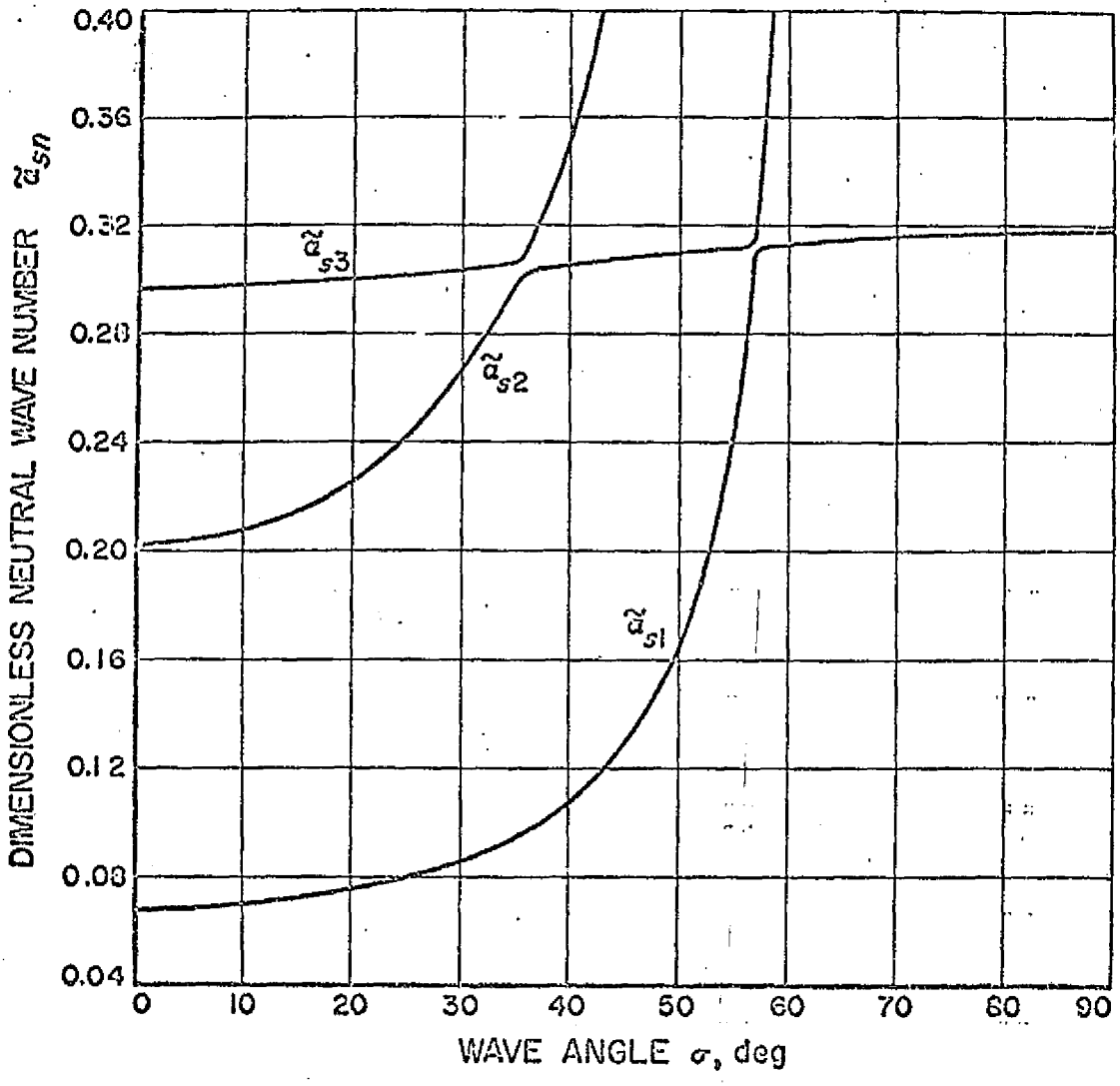

Fig. 15.13 Effect of wave angle on neutral wave numbers at $M_1 = 8.0$

and $\tilde{\alpha}_{s_2}$ and $\tilde{\alpha}_{s_1}$ approach each other even more closely (to within 1%) at $\psi = 56.5^{\circ}$.

The slightly upward-sloping line that starts from $\tilde{\alpha}_{s_4}$ at $\psi = 0$ forms a sort of barrier for $\tilde{\alpha}_{s_2}$. When the $\tilde{\alpha}_{s_2}$ curve reaches the "barrier," it turns away from its previous direction to form a continuation of the upward-sloping line, while the $\tilde{\alpha}_{s_3}$ curve forms a continuation of the $\tilde{\alpha}_{s_2}$ curve. The same thing happens again when the $\tilde{\alpha}_{s_1}$ curve strikes against the "barrier" formed by the $\tilde{\alpha}_{s_2}$ upward-sloping line. At $M_1 = 10$, the first four modes form the same type of pattern. There, it is the curve starting from $\tilde{\alpha}_{s_4}$ at $\psi = 0$ that is almost horizontal (more so than in Fig. 15.13) except for brief interruptions at $\psi = 32^{\circ}$, where it meets α_{s_3}; at 47.2°, where it meets $\tilde{\alpha}_{s_2}$; and at 60.2°, where it meets $\tilde{\alpha}_{s_1}$. At $\psi = 60.2^{\circ}$, $\tilde{\alpha}_{s_1}$ is within less than 0.1% of $\tilde{\alpha}_{s_2}$.

The various modes are easy to identify in these figures by the number of 180° phase changes in the pressure fluctuation. Even though the eigenvalues almost coincide at the angles listed above, the solutions do not. In some limit, probably $c_s \to 1$ as $M_1 \to \infty$, the eigenvalues will be truly degenerate, i.e., two distinct solutions will correspond to one eigenvalue. The wave-number curves will actually intersect, but the mode identity of a given curve will still change beyond the intersection point. On physical grounds, it is necessary for the first-mode wave number to always attain a finite value as $\psi \to 90^{\circ}$, and for all higher-mode wave numbers to go to infinity, with a common asymptote at the angle where the supersonic relative-flow region disappears.

It is of interest to note that Fig. 15.13 bears a resemblance to Fig. 15.2. There the upward-sloping line plays the same role as the more nearly horizontal line of Fig. 15.13. If the angles of closest approach of Fig. 15.13 are converted into component Mach numbers, we can construct Table 15.3. It is apparent from the table that the

	$M_1 = 5.8$	8.0	10.0	2-D
$\tilde{\alpha}_{s1} - \tilde{\alpha}_{s2}$	$M_1 = 3.9$	4.4	5.0	$M_1 = 4.7$
$\tilde{\alpha}_{s2} - \tilde{\alpha}_{s3}$		6.5	6.8	6.7
$\tilde{\alpha}_{s3} - \tilde{\alpha}_{s4}$			8.5	8.6

Table 15.3 Mach numbers in direction of wave normal at which wave numb- - of adjacent modes are most nearly equal.

phenomenon is the same for both two- and three-dimensional disturbances. Whatever the mechanism is that produces these results, it must depend primarily on the Mach number and very little on the boundary-layer profiles.

The same two features that were noted for the upward-sloping line of Fig. 15.2 are also found for the related line of Fig. 15.13. First, it is the mode which is on this line for which the ratio $\pi(0)/\pi(\gamma_s)$ has its minimum value for any particular wave angle, as is shown in Fig. 15.14. Second, it is the wave number of this line which is the end point of the eigenvalue curve of amplified solutions which starts at the neutral sonic solution. This behavior, which for two-dimensional disturbances establishes itself clearly only at high Mach numbers, is

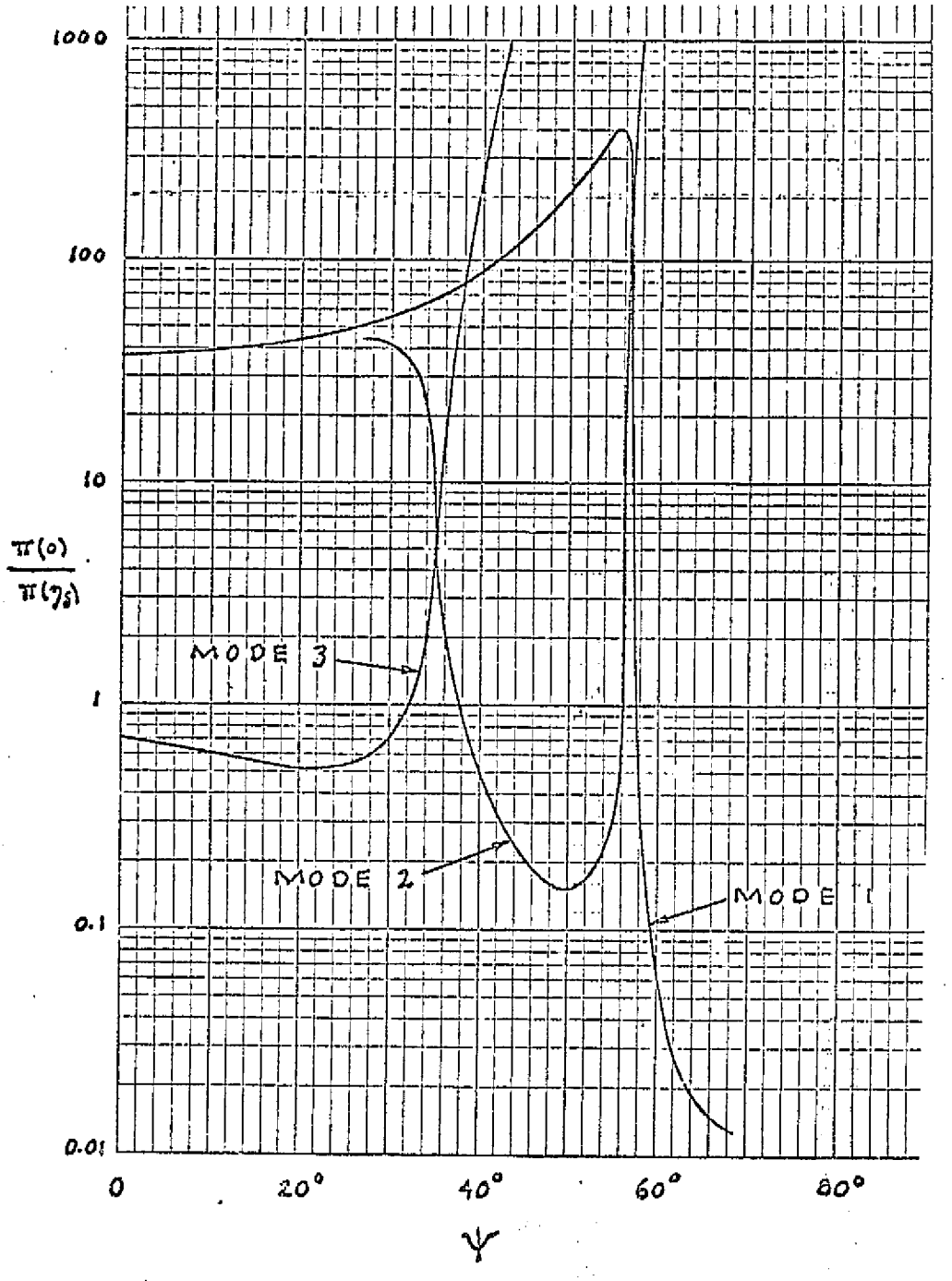

Fig. 15.14 Amplitude ratio of surface pressure fluctuation as function of wave angle for first three modes at $M_1 = 8$.

well defined for three-dimensional disturbances as will be seen in the next section.

15.5.2 Amplified solutions

With the neutral subsonic solutions established, the next step is to consider the amplified solutions. As ψ increases from 0°, $c_0 = 1 - 1/M_1$ decreases, but since the mean velocity and temperature profiles remain fixed, so will c_s. Consequently, the difference $c_s - \tilde{c}_0$ increases and we can expect a destabilization of the first mode. At the same time, the thickness of the supersonic relative-flow region will decrease with $\tilde{M}_1$, and we shall not be surprised to find a stabilization of the second and higher modes.

Figure 15.15 shows the time rate of amplification, αc_i, of the first and second modes at $M_1 = 4.5$ as a function of the dimensionless frequency, αc_r, for several wave angles. The three-dimensional first-mode disturbances are indeed more unstable than the two-dimensional disturbances, and the second-mode three-dimensional disturbances are more stable than the corresponding two-dimensional disturbances. Consequently, the most unstable second-mode disturbance is always two-dimensional. This same result holds for all of the higher modes. The most unstable first-mode disturbance is at an angle of close to 60°, with an amplification rate twice the maximum two-dimensional rate and with a frequency a little over one-half of the frequency of the most unstable two-dimensional disturbance. The maximum in αc_i at a value of ψ between 0° and 90° comes about from the following circumstances. As $c_s - \tilde{c}_0$ increases, the maximum value of c_i also increases. At first this

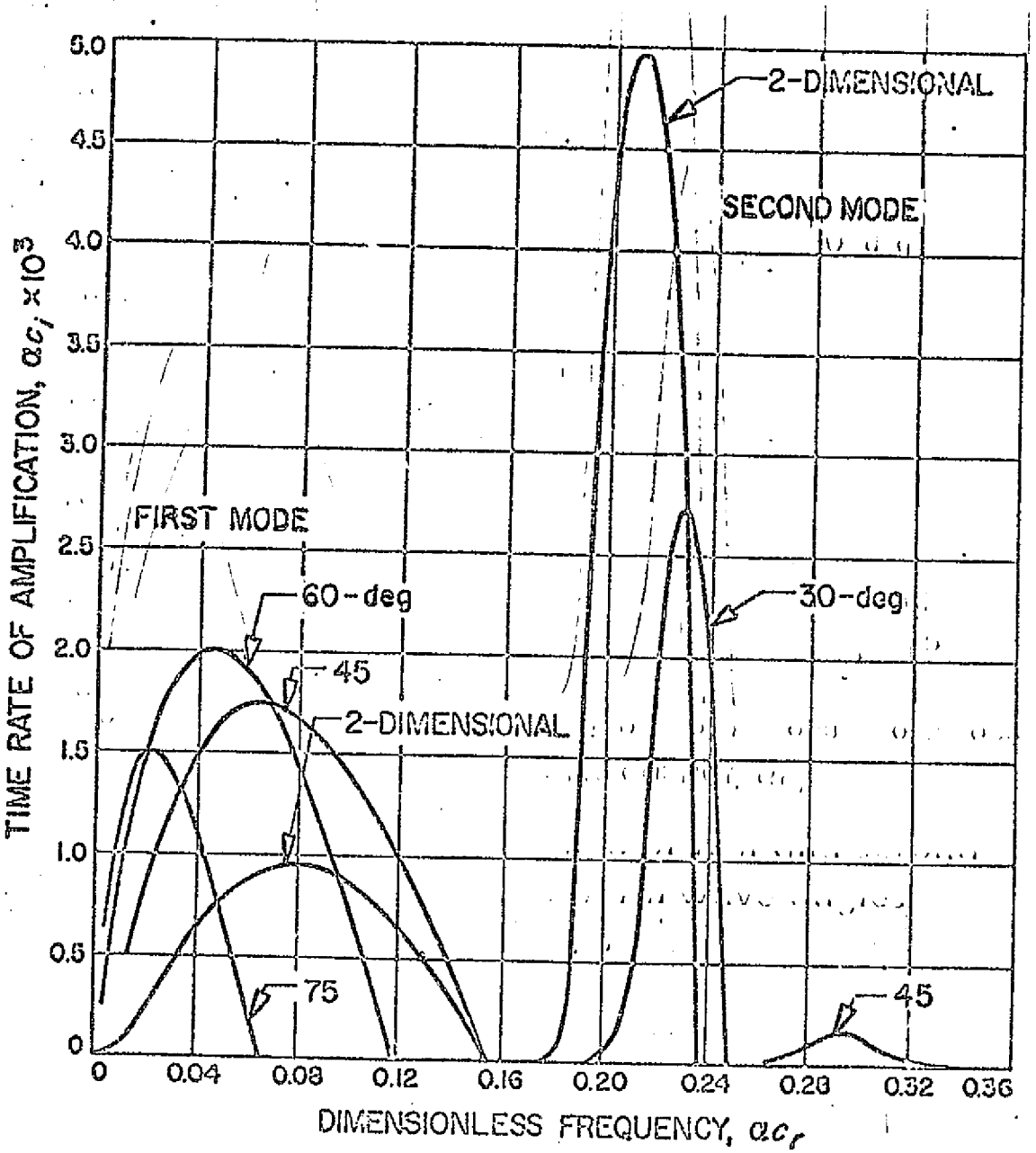

Fig. 15.15 Time rate of amplification of first and second modes vs frequency for several wave angles at $M_1 = 4.5$

increase leads to a corresponding increase in $(\alpha c_i)_{max}$. However, since α (not $\tilde{\alpha}$) must go to zero as $\psi \to 90^\circ$, the decrease in α eventually outweighs the increase in c_i and the amplification rate starts to decrease with further increases of ψ and is zero at $\psi = 90^\circ$.

At $M_1 = 4.5$, the first two modes are completely separate at all wave angles. At $M_1 = 8$, the first three modes are merged for two-dimensional disturbances. Figure 15.16 shows what happens as ψ increases. At $\psi = 30^\circ$, the first three modes are still merged. However, at $\psi = 45^\circ$, only the first two modes are merged. This result is in accord with Fig. 15.13, where the second-mode wave number, $\tilde{\alpha}_{s_2}$, is on the upward-sloping line at $\psi = 45^\circ$ and thus is the end point of the eigenvalue curve for the merged amplified solutions. At $\psi = 50^\circ$, the situation is the same. The next angle, $\psi = 56^\circ$, is of interest because this angle is very near the angle of closest approach for $\tilde{\alpha}_{s_1}$ and $\tilde{\alpha}_{s_2}$. The end point should be α_{s_2} according to Fig. 15.13, and Fig. 15.16 confirms that it is. However, the αc_i vs. α curve in Fig. 15.16 gives no obvious evidence of the second mode as the local maximum in αc_i that has previously always marked the second mode is no longer in evidence. Hence we have an example where it is necessary to examine the phase of the pressure fluctuations in order to make a positive identification of the mode. Figure 15.17 gives the ratio $\pi(0)/\pi(\eta_s)$, and Fig. 15.18 the phase difference $\arg \pi(0) - \arg \pi(\eta)$, as functions of α. These figures show that there is a rapid change from a first-mode disturbance to a second-mode disturbance near $\alpha = 0.16$ even though αc_i continues to decline monotonically. At the next angle, $\psi = 60^\circ$, Fig. 15.13 indicates that α_{s_1} will be the end point of the amplified region

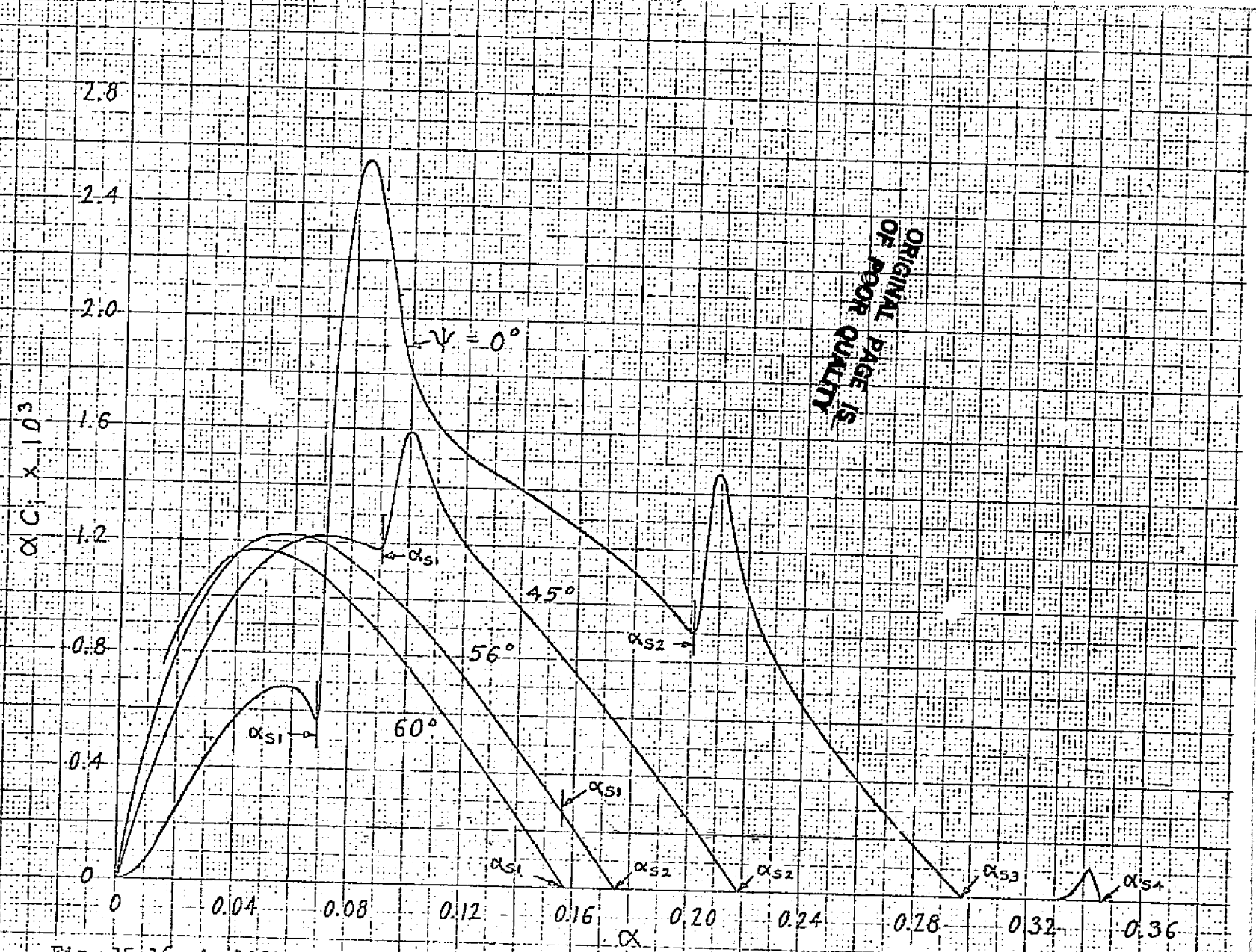

Fig. 15.16 Amplification rate as function of wave number for three-dimensional disturbances at $M_1 = 8$.

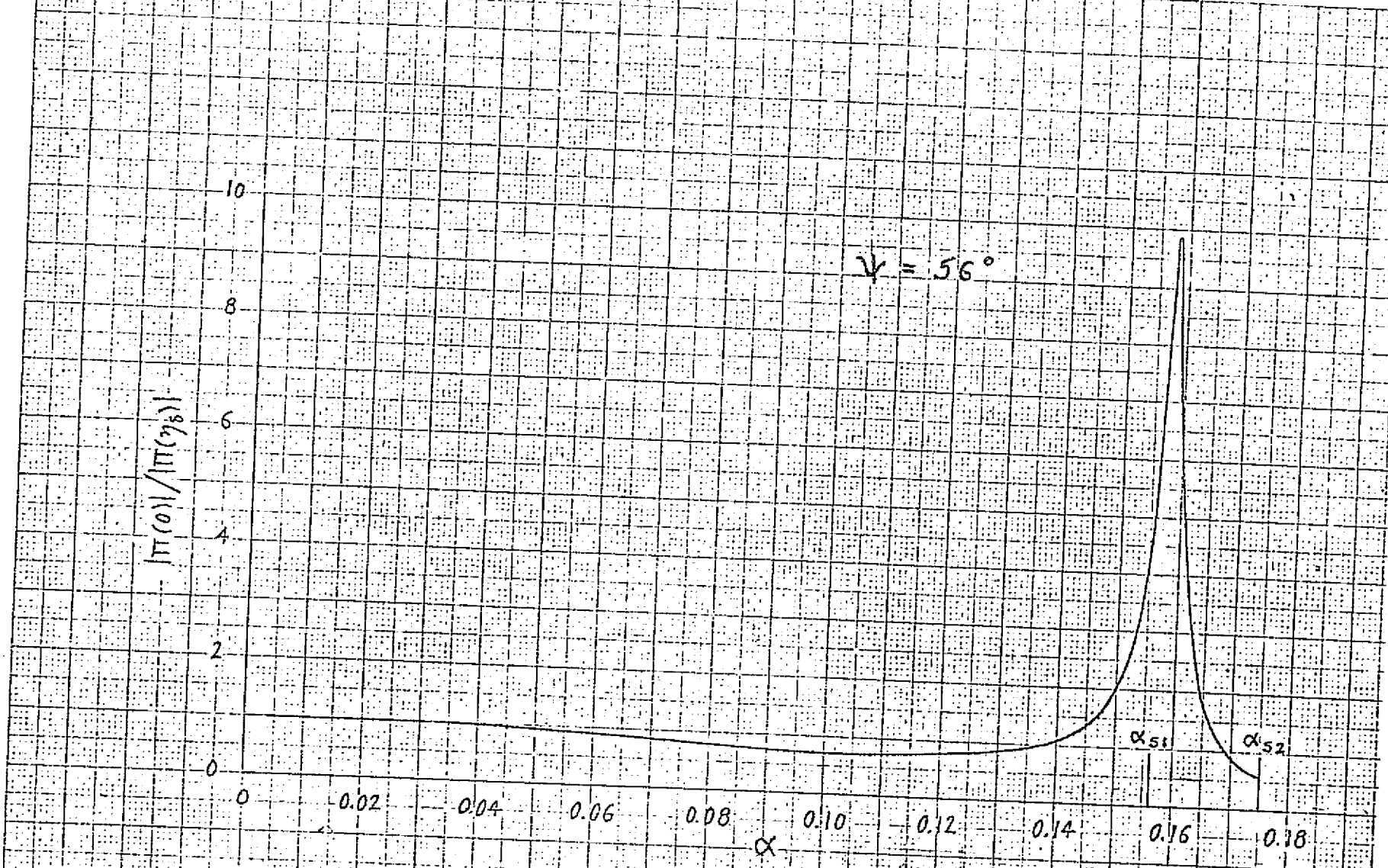

Fig. 15.17 Amplitude of pressure fluctuation of amplified solutions at $\Psi = 56°$, $M_1 = 8$, $T_1^* = 50°K$.

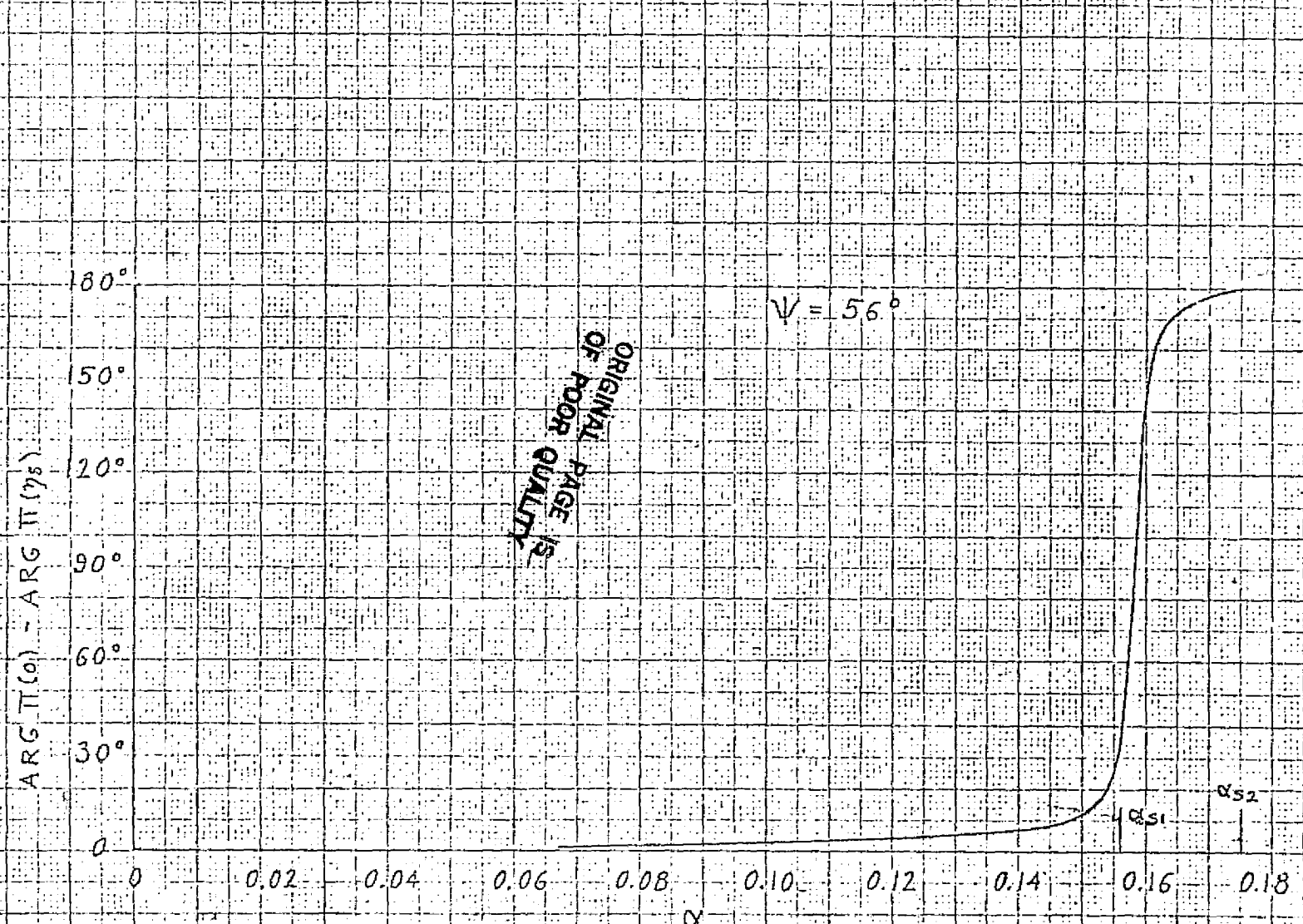

Fig. 15.18 Phase of pressure fluctuation of amplified solutions at $\Psi = 56^{\circ}$, $M_1 = .8$, $T_1 = 50^{\circ}K$.

which will consist entirely of first-mode disturbances. Figure 15.16 and the phase of $\pi(o)$ confirm this to be true. The angle at which the supersonic relative-flow region disappears, and with it the higher modes, is just over 60°.

Once we have found αc_i as a function of αc_r for several values of ψ at a particular Mach number, we can construct Fig. 15.19. In this figure, the maximum temporal amplification rate of the first two modes is plotted against ψ for the four Mach numbers 4.5, 5.8, 8.0 and 10.0. At all of these Mach numbers the most unstable first-mode disturbance is at an angle of between 50° and 60°, and has a maximum amplification rate roughly double the amplification rate of the most unstable two-dimensional disturbance. The two-dimensional second-mode disturbance is the most unstable at all of these Mach numbers, and the decrease of $(\alpha c_i)_{max}$ with increasing ψ is sharpest at the lower Mach numbers.

A summary plot of the first-mode maximum amplification rates appears in Fig. 15.20. The wave angle of the most unstable disturbance (to within 5°) is shown in the figure, and the maximum two-dimensional amplification rates are shown for comparison. An interesting change in the relationship between the two- and three-dimensional amplification rates takes place for $M_1 < 4$. Above this Mach number, $(\alpha c_i)_{max}$ of the three-dimensional disturbances is about double the two-dimensional amplification rate. In contrast, at $M_1 = 3.0$ the ratio of the two amplification rates is 5.8; at $M_1 = 2.2$ it is 33; and at $M_1 = 1.8$ it is 130. We recall from Fig. 15.1 that it is near $M_1 = 1.6$ that the difference $c_3 - c_o$ is the smallest. Therefore, the sonic limit acts as a severe constraint on the two-dimensional

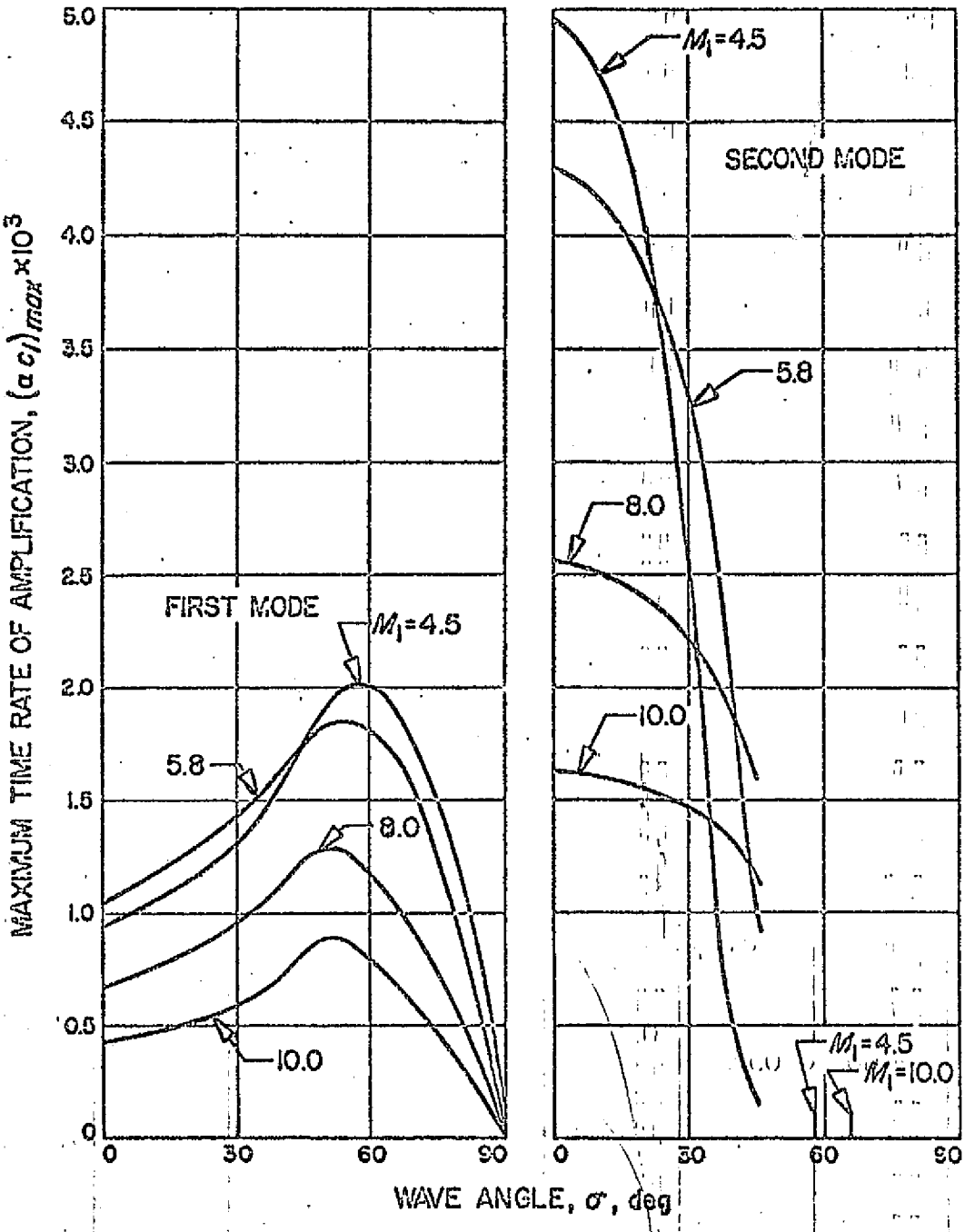

Fig. 15.19 Effect of wave angle on maximum time rate of amplification of first and second modes, at $M_1 = 4.5, 5.8, 8.0,$ and 10.0

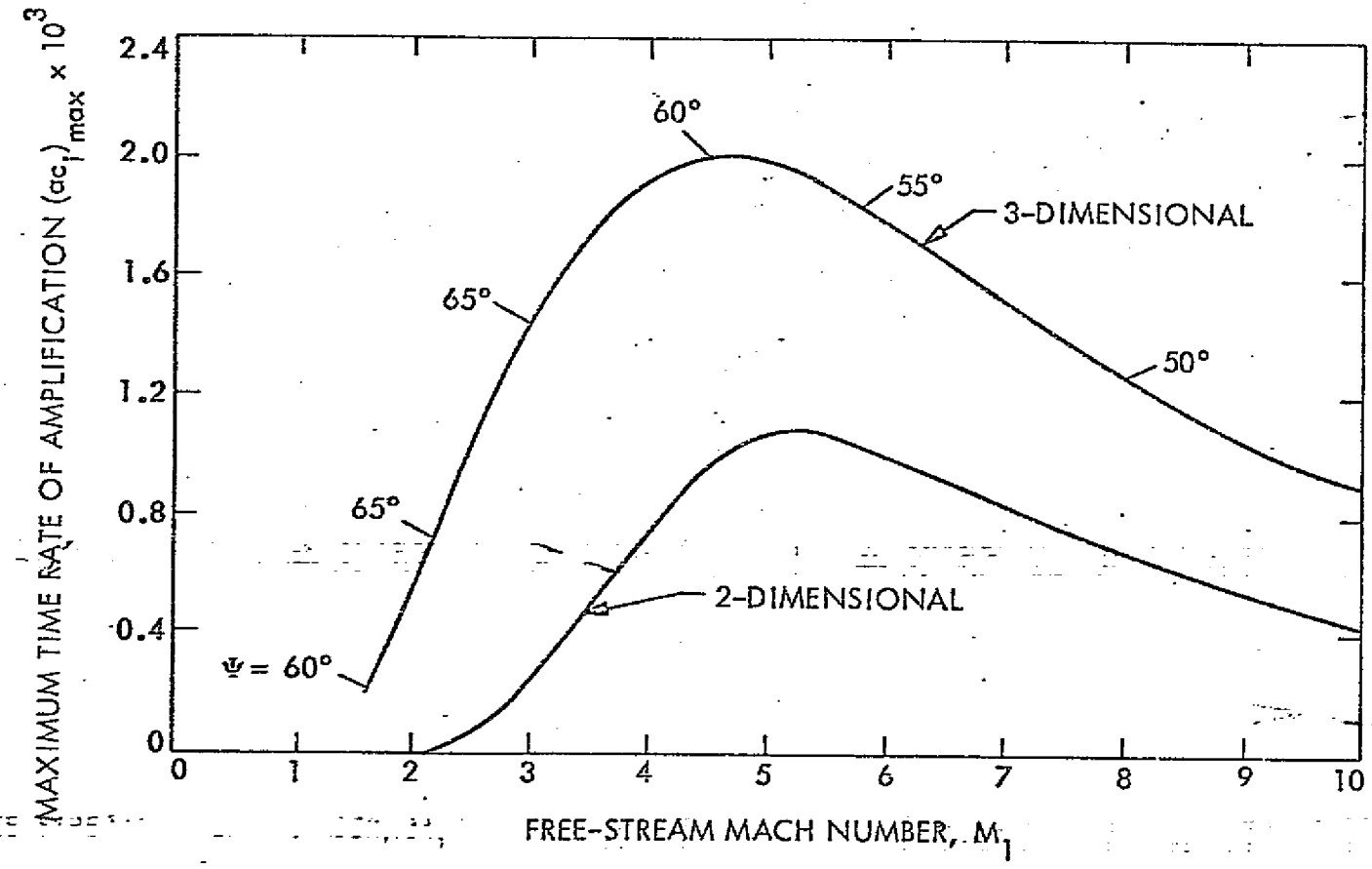

Fig. 15.20 Effect of Mach number on maximum amplification rates of two- and three-dimensional first-mode disturbances. Inviscid theory, insulated wall.

disturbances in the low Mach number range. Indeed the two-dimensional disturbances are almost completely stable even though the generalized inflection point is well out in the boundary layer. When this constraint is removed, as it is for three-dimensional disturbances, the amplification rates increase sharply. We may consider the three-dimensional maximum amplification rate as the one that most clearly reflects the inherent instability of a given boundary-layer profile.

The instability of a compressible flat-plate boundary layer which is due to the generalized inflection point is a weaker instability than the instability of an incompressible boundary-layer profile with an inflection point. In Table 15.4 we compare the growth over one boundary-layer thickness

M_1	$(dA/A)_{\alpha_R=\delta}$
0, β = - 0.14	0.10
0, β = - 0.1988	0.40
1.6	0.005
2.2	0.012
3.0	0.022
4.5	0.036
10.0	0.042

Table 15.4 Comparison of growth of most unstable first-mode inviscid disturbances in insulated flat-plate boundary layers and in Falkner-Skan boundary layers.

of the most unstable three-dimensional first-mode disturbances at a few Mach numbers with the growth of the most unstable inviscid disturbances in two of the Falkner-Skan boundary layers. We see that first-mode disturbances in the compressible boundary layer grow much slower than in the

two Falkner-Skan boundary layers. Indeed the maximum growth rate is smaller than the maximum growth rate of 0.05 (at finite Reynolds numbers) in the incompressible Blasius boundary layer.

15.6 Effect of wall cooling

15.6.1 Two-dimensional disturbances

Perhaps the most celebrated result of the stability theory for compressible boundary layers was the prediction by Lees (1947) that cooling the wall stabilizes the boundary layer. This prediction was made on the basis of the asymptotic theory, and a criterion was provided whereby the ratio of wall temperature to recovery temperature at which the critical Reynolds number becomes infinite can be computed. Although Lees's original calculations contained numerical errors, the temperature ratio for complete stabilization was later computed correctly by a great many authors. The most accurate of these calculations gave the result that complete stability can be achieved for $1 < M_1 < 9$ by sufficient cooling. These calculations can be criticized in two important respects. First, no indication is given as to how the amplification rate varies with wall temperature. Second, and most important, no account is taken of the existence of the higher modes. In this section, we shall see that the inviscid theory can remedy both of these deficiencies.

The first step is to find out how the mean boundary layer changes with wall cooling. In Fig. 15.21, the stability function v_0, which is related to $(U'/T)'$ by (15.5), is given as a function of η at $M_1 = 5.8$ for several values of θ_w, where θ_w is the enthalpy difference ratio $(h_w - h_1)/(h_0 - h_1)$. It is given in terms of some common

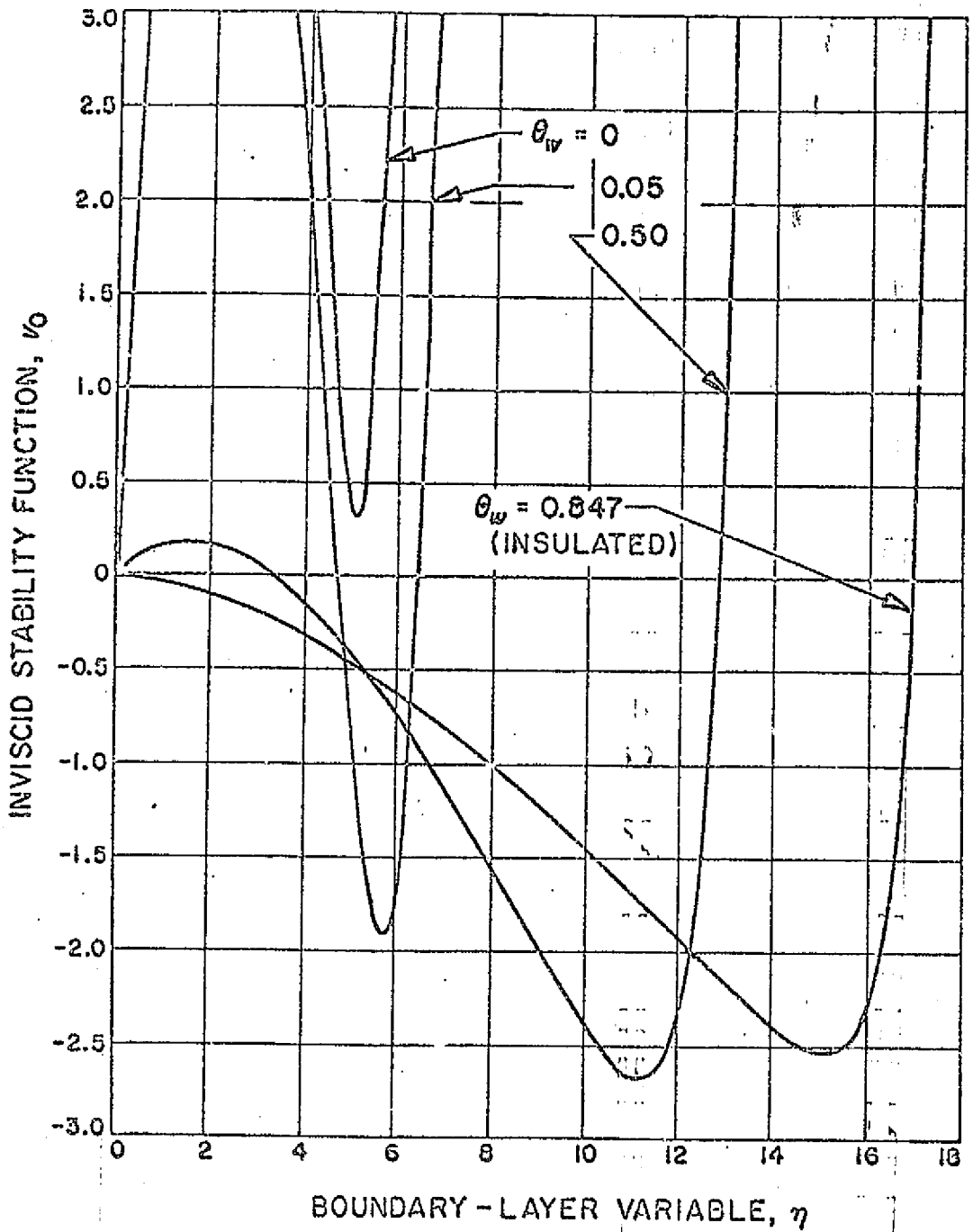

Fig. 15.21 **Distribution through boundary layer of stability function v_0 for four values of θ_w**

temperature ratios at $M_1 = 5.8$ in Table 15.5. In this table T_r is

θ_w	T_w/T_r	T_w/T_1
0.847	1.00	6.7
0.50	0.65	4.4
0.10	0.25	1.7
0.05	0.20	1.3
0.01	0.16	1.1
0	0.15	1.0
-0.10	0.05	0.32

Table 15.5 Temperature ratios as functions of θ_w at $M_1 = 5.8$

the recovery temperature, i.e., the equilibrium or adiabatic wall temperature. In Fig. 15.21 we see that for the insulated wall, $(u'/T)'$ has a single zero located at η_s. For $0.01 < \theta_w < 0.847$, it has two zeroes located at η_{s1} and η_{s2} ($\eta_{s1} > \eta_{s2}$). For $\theta_w < 0.01$, $(u'/T)'$ has no zeroes. The zero at η_{s2} is always below η_o, the point where $u = c_o = 1 - 1/M_1$. The zero at η_{s1} is above η_o provided $\theta_w > 0.05$.

Next we look at the relation of c_s, considered to be the mean velocity at η_{s1}, to c_o. As long as $\eta_{s2} < \eta_o$, there can be no neutral disturbance connected with η_{s2}. It cannot be subsonic because $c_{s2} < 1 - 1/M_1$. It cannot be supersonic because, by (15.4), the Reynolds stress would be zero throughout the boundary layer, a condition incompatible with a neutral supersonic disturbance as we shall see in

Section 15.6.3. Both c_3 and c_0 are shown in Fig. 15.22, where c_3 is plotted as a function of T_w/T_r at $M_1 = 5.8$, 8.0 and 10.0 for $T_1^* = 50^\circ K$, and at $M_1 = 8.0$ for $T_1^* = 80^\circ K$. We see that at $M_1 = 5.8$, c_3 is reduced below c_0 with sufficient cooling, and the first mode can be completely stabilized. However, at $M_1 = 8$ and $M_1 = 10$, c_3 remains greater than c_0 and the first mode cannot be completely stabilized no matter how much the wall is cooled.

In order to find out what happens to the second mode as the wall is cooled, we must look at some eigenvalue diagrams. In Fig. 15.23, α is plotted against c_1 for five values of θ_w at $M_1 = 5.8$. In Fig. 15.24 three of the corresponding c_r vs. c_1 diagrams are given with the two remaining diagrams in Fig. 15.25. Only amplified and neutral solutions are shown. From these diagrams we see that the first mode disappears when η_{s1} moves below η_0 and there can no longer be neutral subsonic solutions. It seems to be a requirement that a family of amplified solutions can exist only if their eigenvalue curve starts at one neutral solution and ends at another. When $\eta_{s1} < \eta_0$, or does not exist, there is still an eigenvalue curve which starts at the neutral sonic solution, but the solutions along this curve are all damped as we shall see in Section 17. When some of the modes are merged for the insulated-wall case, as happens for $M_1 > 6.0$, cooling will separate the modes so that there are distinct eigenvalue curves for each mode just as at lower Mach numbers for the insulated-wall case.

The second mode always has the singular neutral solution as one of its necessary two neutral solutions, just as the first mode always has

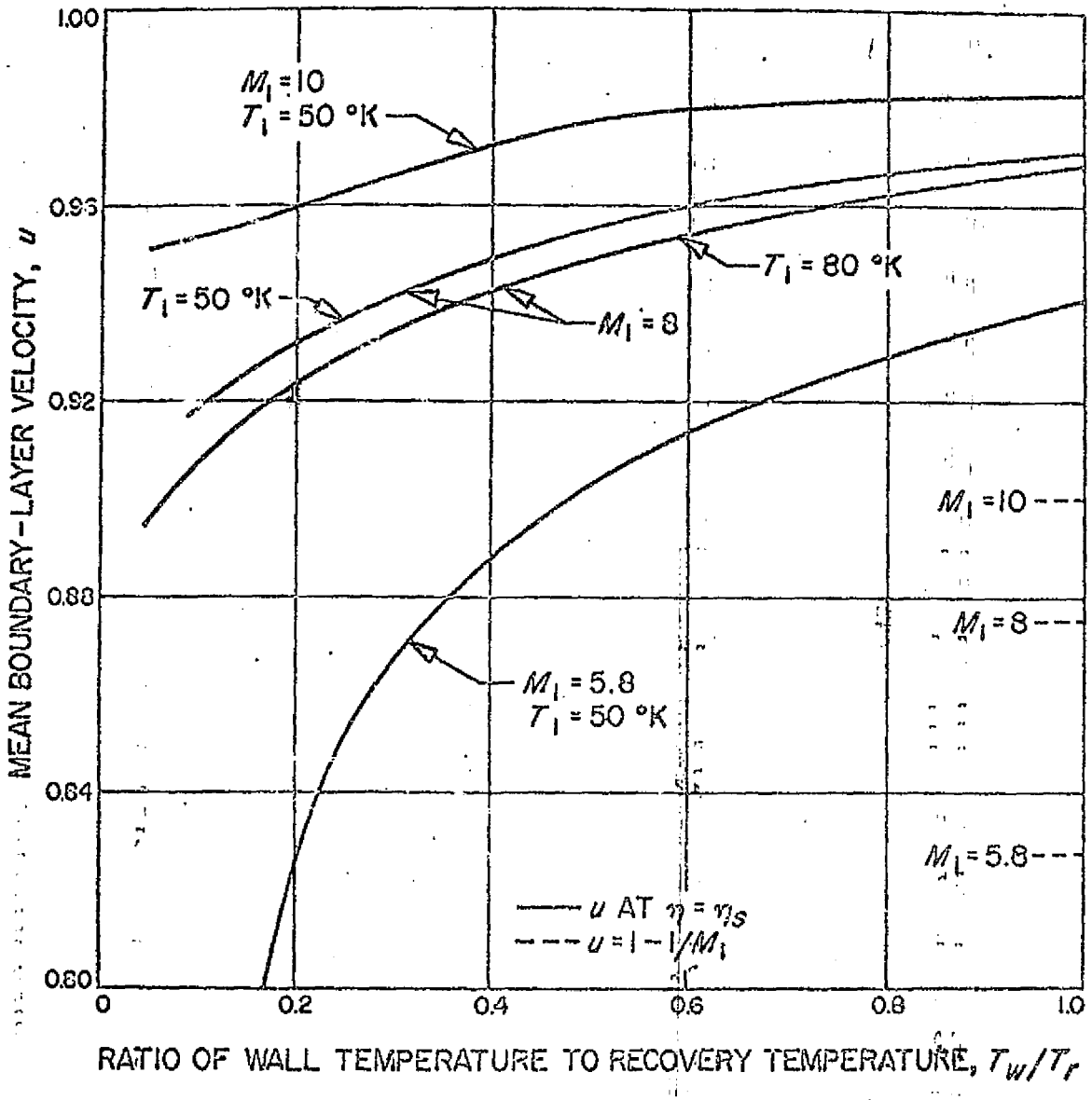

Fig. 15.22 Mean boundary-layer velocity at generalized inflection point as function of ratio of wall temperature to recovery temperature

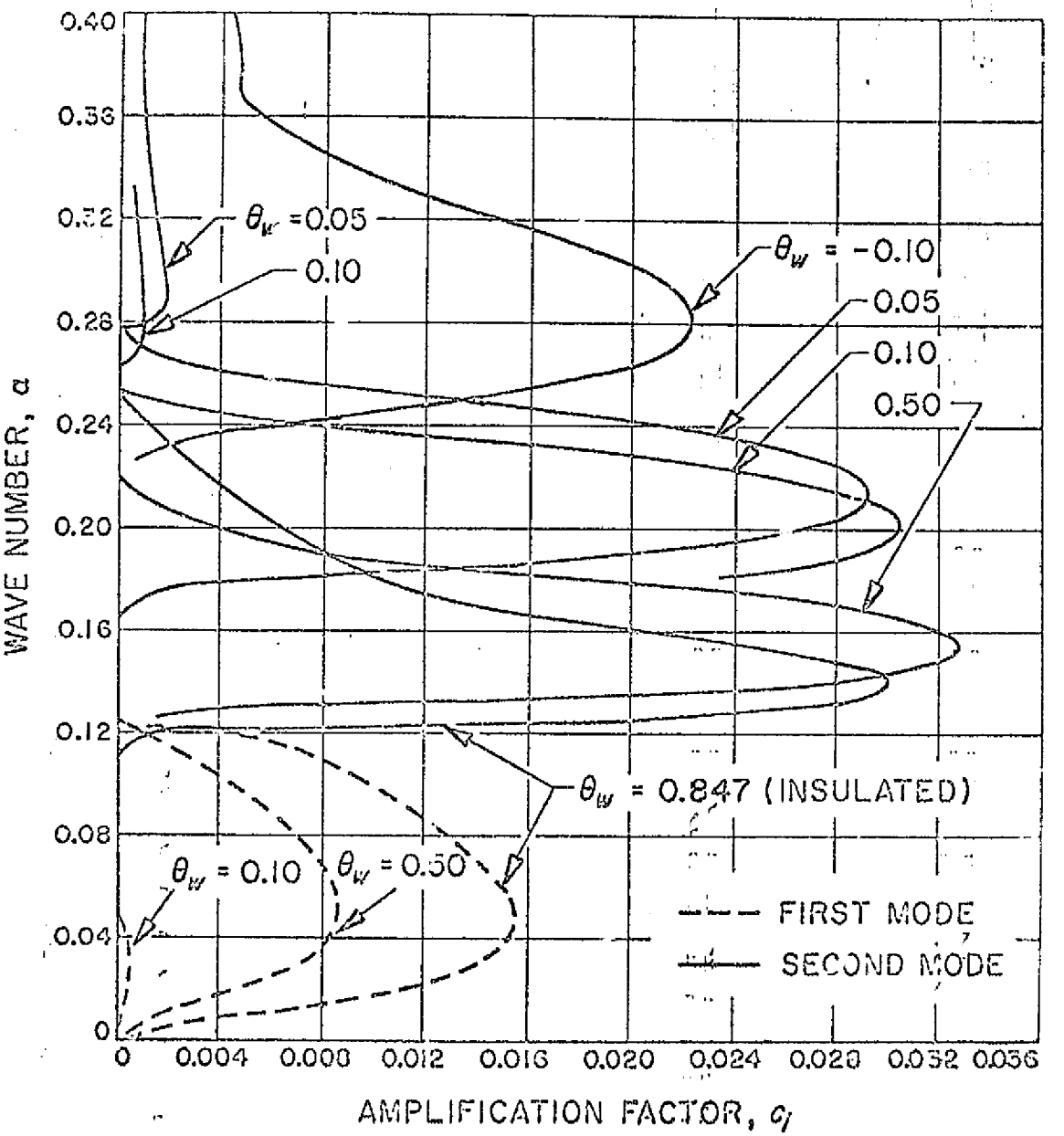

Fig. 15.23 Eigenvalue diagram α vs c_i for θ_w = 0.847 (insulated), 0.50, 0.10, 0.05, and −0.10 at $M_1 = 5.8$

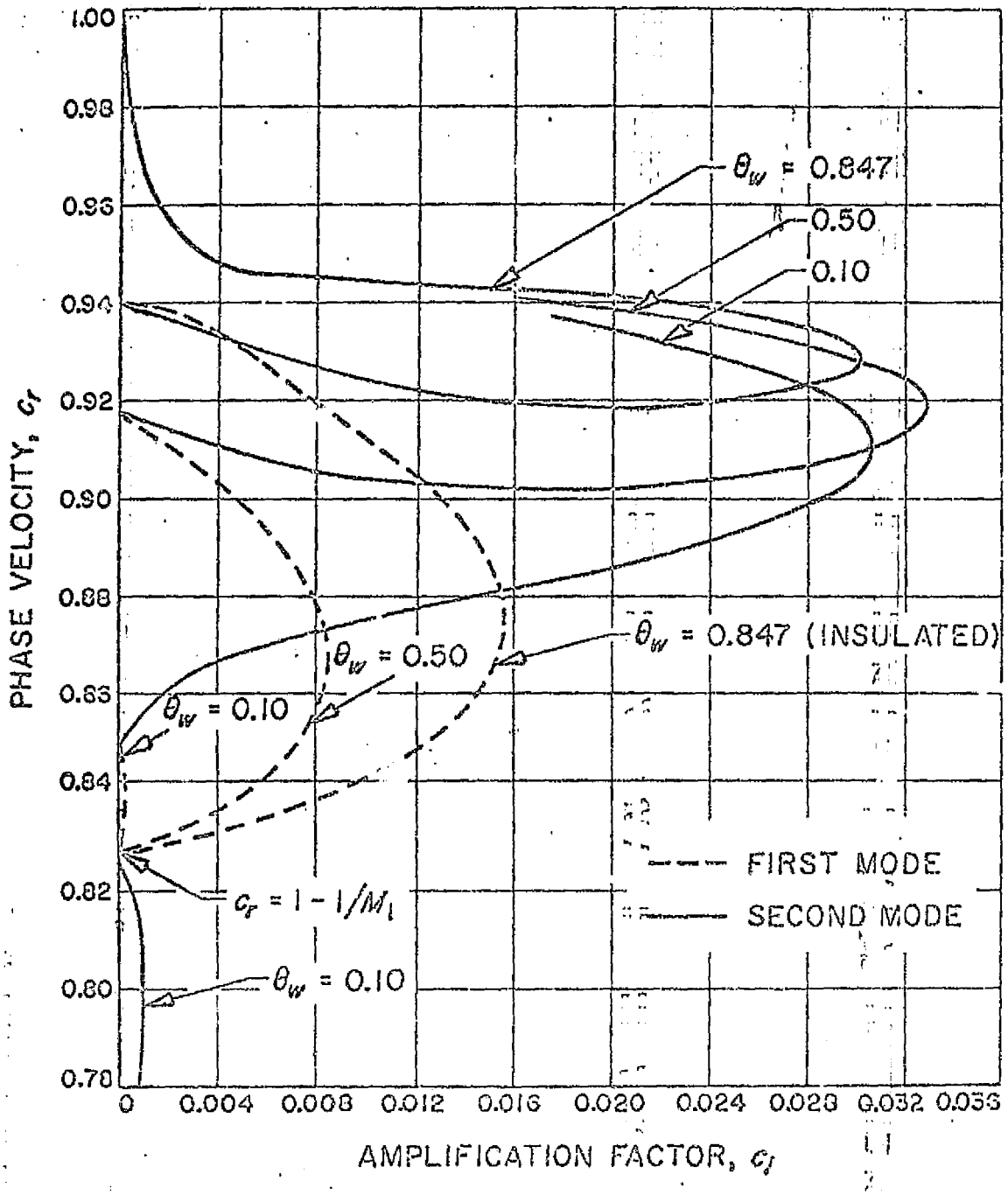

Fig. 15.24 Eigenvalue diagram c_r vs c_i for θ_w = 0.847 (insulated), 0.50, and 0.10 at M_1 = 5.8

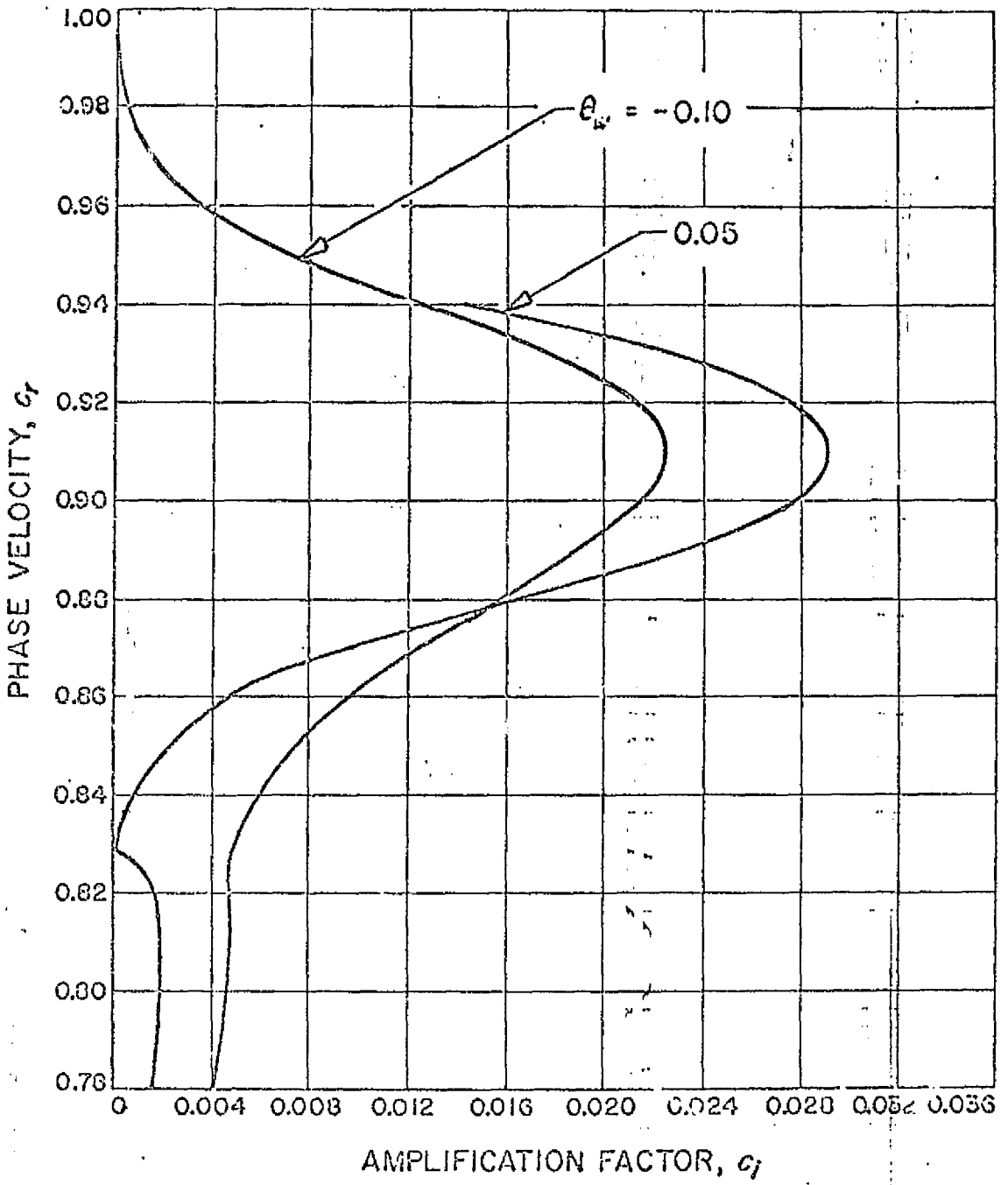

Fig. 15.25 Eigenvalue diagram c_r vs c_i for $\theta_{10} = 0.05$ and -0.10 at $M_1 = 5.8$

the neutral sonic solution. These solutions exist regardless of the temperature boundary condition. All that is required for the singular neutral solution is a region of supersonic relative flow for $c_r = 1$. As the wall is cooled and c_s becomes smaller, the difference $1 - c_s$ increases and there is no tendency to reduce the maximum value of c_i for the second mode as there is for the first mode as a result of the decrease in $c_s - c_0$. Indeed we see from Fig. 15.24 that initially c_i increases. Since α also increases, there is an <u>increase</u> of the maximum amplification rate of the second mode with wall cooling. The increase in the wave number at $(\alpha c_i)_{max}$ is almost entirely a result of the change in the boundary-layer thickness with cooling.

When η_{s1} moves below η_0 and then disappears, it is no longer possible for the second mode eigenvalue curve to have α_{s2} as an end point, since the neutral subsonic solutions no longer exist. Nor is there any possibility of the neutral sonic solution providing the necessary end point as this solution has only first-mode solutions in its neighborhood. If we look at Figs. 15.23 and 15.24, we see that for $\theta_w = 0.10$, where $\eta_{s1} > \eta_0$, there has appeared a new neutral solution together with a family of amplified solutions. For all of these solutions, c_r is less than $1 - 1/M_1$, and is supersonic with respect to the free stream. Consequently, we have a neutral supersonic solution and supersonic amplified solutions of the type discussed in Section 13.7.2. All of these solutions are outgoing waves. It is evident from Figs. 15.23 and 15.25 that when $\eta_{s1} < \eta_0$ or does not exist, the eigenvalue curve of the amplified subsonic solutions joins the eigenvalue curve of the

amplified supersonic solutions at a $c_i > 0$. The end point of this combined eigenvalue curve is another neutral supersonic solution which has not yet been studied, but it appears to be of a singular nature. The important result is that conditions exist by which there can be second-mode amplified solutions regardless of whether or not there is a generalized inflection point in the boundary layer. Cooling the wall does nothing to remove this source of amplification. This same result, of course, applies to all of the higher modes.

If the maximum amplification rate of the first three modes is computed for several T_w / T_r at $M_1 = 5.8$, then Fig. 15.26 can be constructed. We see from this figure that as T_w / T_r decreases, $(\alpha c_i)_{max}$ of the first mode decreases to zero monotonically. In contrast, $(\alpha c_i)_{max}$ of the second mode increases by 50%, and $(\alpha c_i)_{max}$ of the third mode increases by a factor of three. The amplification rate αc_i is the proper one when we wish to make comparisons for a fixed free stream and at a fixed R_x . If we wish to compare disturbance growths over a boundary-layer thickness, then we need $\alpha_\delta c_i$. Table 15.6 gives some

θ_w	T_w / T_r	η_δ	η_i	$(\alpha_\delta c_i)_{max} \times 10^4$
0.847	1.00	20.0	9.4	8.5
0.50	0.65	16.1		8.3
0.25	0.40	13.2	6.0	7.7
0.10	0.25	11.2		7.0
-0.10	0.05	8.5	3.2	5.4

Table 15.6 Maximum second-mode amplification rate based on boundary-layer thickness for cooled-wall boundary layers at $M_1 = 5.8$.

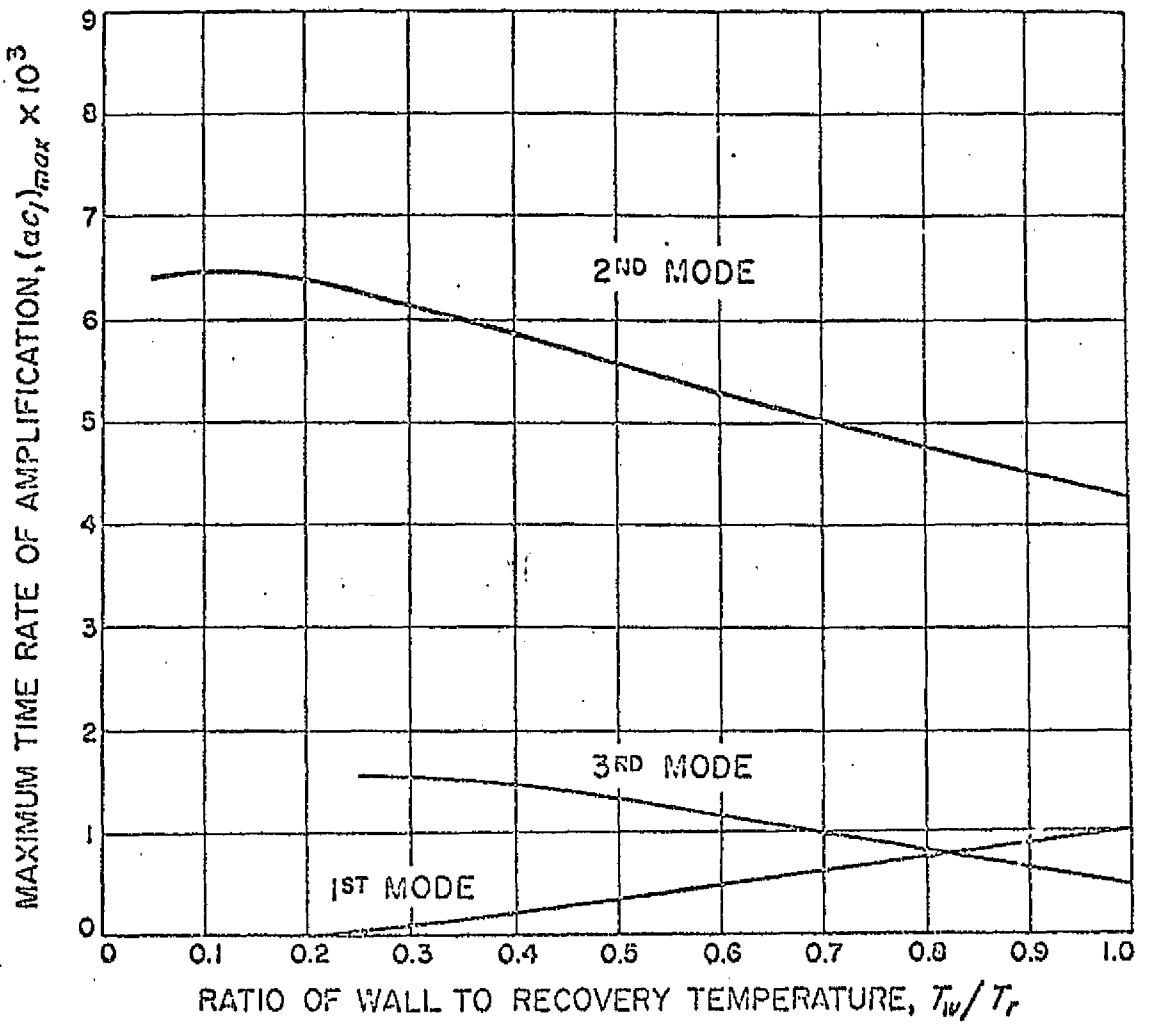

Fig. 15.26 Maximum time rate of amplification of first three modes at $M_1 = 5.8$ as function of ratio of wall to recovery temperature

values of $(\alpha_s c_i)_{max}$ which correspond to the values of $(\alpha c_i)_{max}$ of Fig. 15.26. Also included in the table are some values of η_1, the thickness of the supersonic relative-flow region for the phase velocity of the most unstable disturbance. We see that η_1 decreases a bit more rapidly than η_s as T_w/T_r decreases.

As two final results concerning the effect of cooling on two-dimensional disturbances, we may look at Figs. 15.27 and 15.28, where αc_i is plotted against α at $M_1 = 8$ and $M_1 = 10$ for the insulated wall and for $T_w/T_r = 0.05$. At $M_1 = 8.0$ and $T_1^* = 50^\circ K$, the first three modes are merged for the insulated wall; at $M_1 = 10$ the first four modes are merged. In the highly cooled case, the modes are separate at both Mach numbers. The first mode is slightly unstable at $M_1 = 8.0$, but the amplification rates are too small to show in the figure. At $M_1 = 10.0$, the most unstable first-mode disturbance has an amplification rate equal to 1/3 of its value for the insulated-wall case and a wave number which is larger for the cooled wall than for the insulated wall. At $M_1 = 5.8$, this wave number decreases with increased cooling. The higher modes at both Mach numbers are destabilized and shifted to higher wave numbers, just as at $M_1 = 5.8$. The maximum amplification rate of each higher mode is approximately doubled as a result of the wall cooling. Since the boundary-layer thickness is also cut in half, $(\alpha_s c_i)_{max}$ is virtually unchanged by the cooling.

15.6.2 Three-dimensional disturbances

Cooling the wall stabilizes the first-mode two-dimensional disturbances by moving η_{s1} toward η_0. Since a three-dimensional disturbance at a

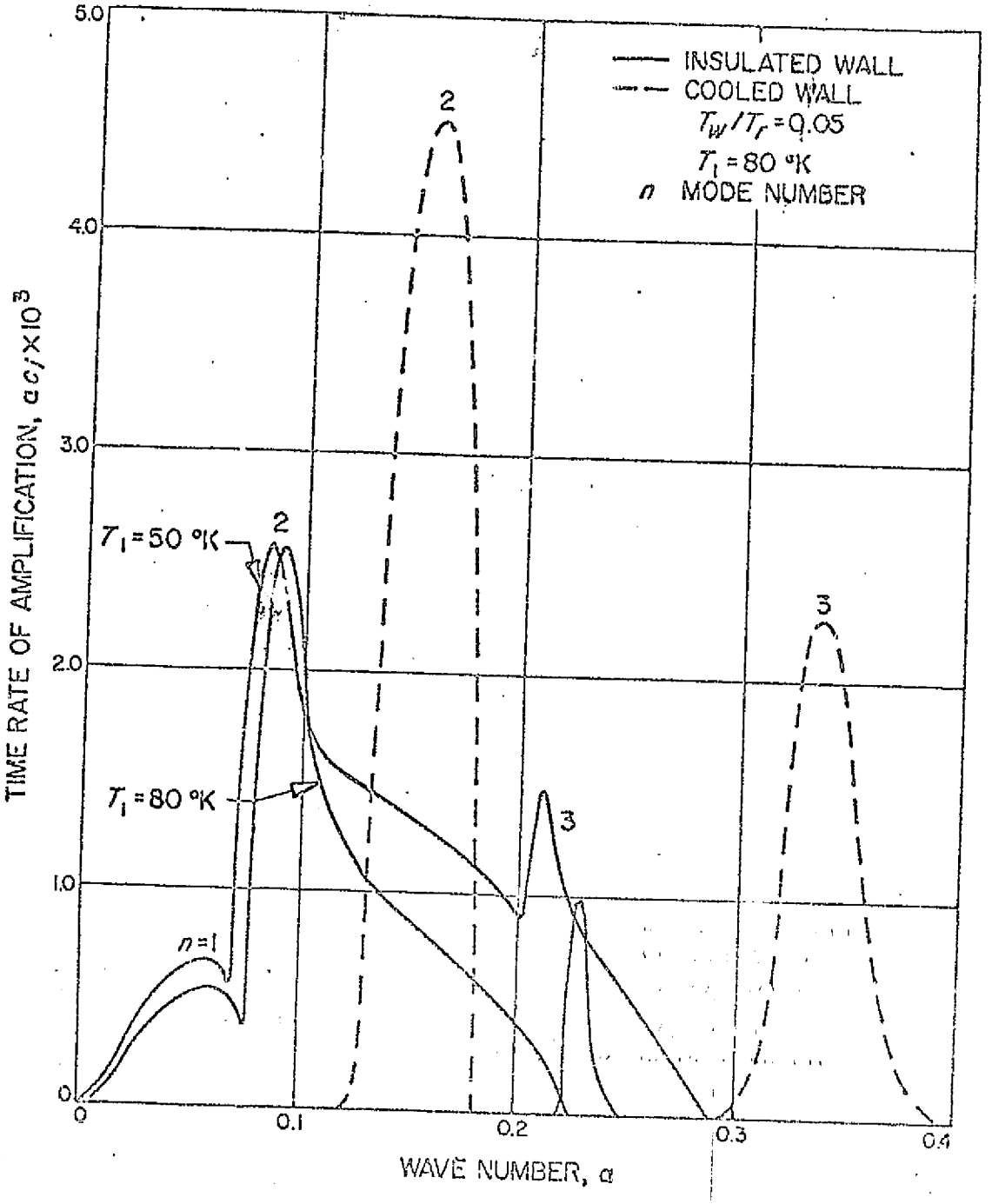

Fig. 15.27 Time rate of amplification vs wave number for first three modes for insulated wall and cooled wall ($M_1 = 8$)

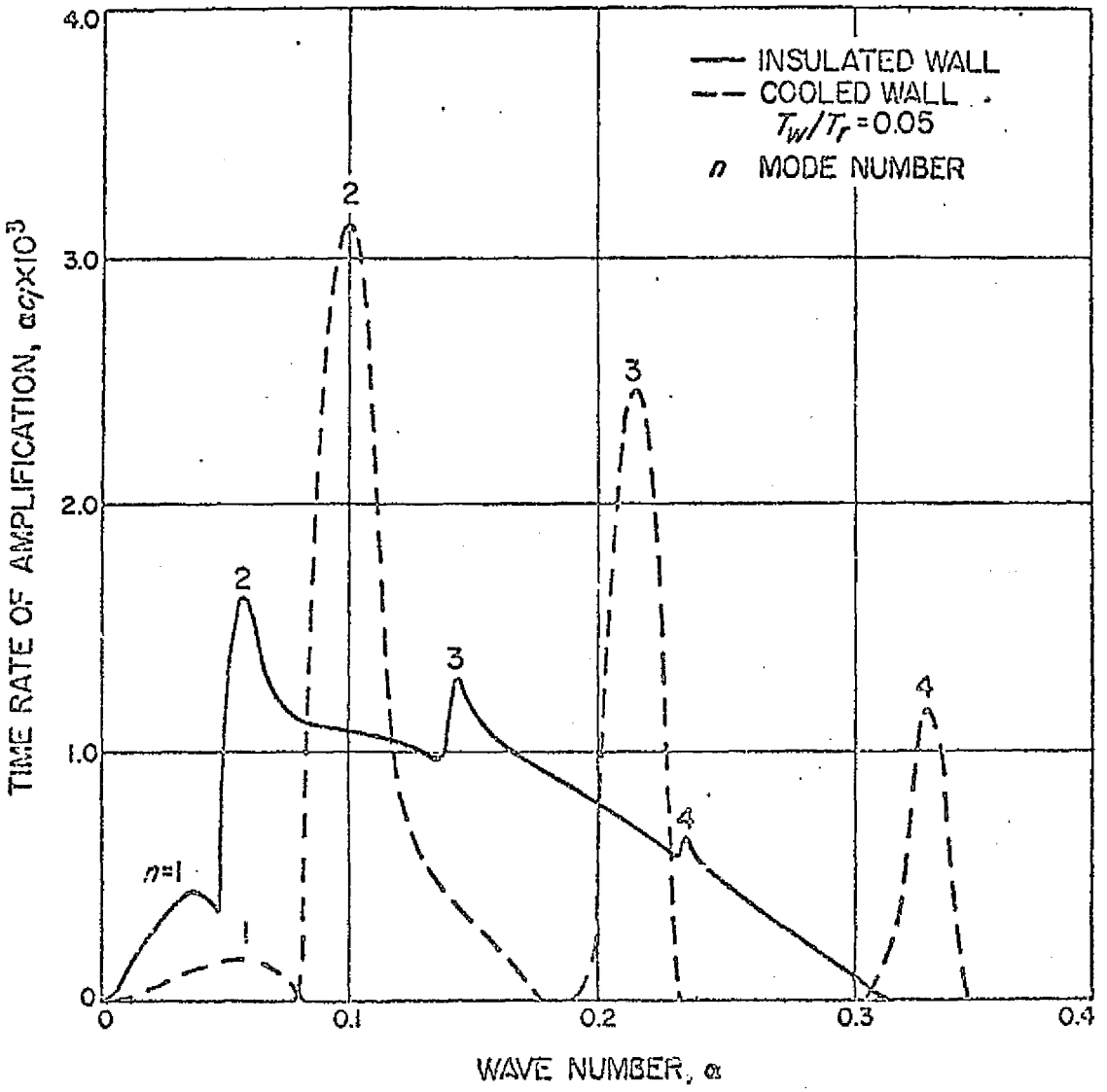

Fig. 15.28 Time rate of amplification vs wave number for first four modes for insulated wall and cooled wall ($M_1 = 10$)

sufficiently large wave angle ψ reduces η_0 well below η_{s1} and makes it impossible for η_{s1} to be less than η_0, we may ask if in this case there also exists a stabilizing mechanism for first-mode three-dimensional disturbances. The answer is yes, and it involves the second generalized inflection point, η_{s2}, which we found to have no significance for two-dimensional disturbances since it was always less than η_0. However, with increasing ψ, η_0 can be made low enough so that $\eta_{s2} > \eta_0$. As soon as this condition is fulfilled, there will be two neutral subsonic solutions, and the eigenvalue curve of the first-mode amplified solutions will be located between those two solutions. As T_w / T_r decreases, $\eta_{s2} \to \eta_{s1}$ and the maximum amplification rate will decrease just as it does for two-dimensional disturbances when $\eta_{s1} \to \eta_0$. At $M_1 = 5.8$, as we see from Fig. 15.21, with sufficient cooling $\eta_{s1} = \eta_{s2}$. Consequently, the first mode is completely stabilized even for three-dimensional disturbances, but at a lower value of T_w / T_r than was required to completely stabilize two-dimensional disturbances. At higher Mach numbers, η_{s1} is greater than η_{s2} regardless of the amount of cooling, and there will always be amplified three-dimensional disturbances. However, the amplification rates of these disturbances will be much less than the amplification rates of the insulated-wall boundary layer.

For second-mode three-dimensional disturbances, the same result holds as for the insulated-wall case: the most unstable disturbance is two dimensional. Complete calculations have not yet been carried out for three-dimensional disturbances in cooled-wall boundary layers, but there has been enough done to establish the above described behavior and also to provide a

curve of $(\alpha c_i)_{max}$ vs. T_w/T_r at $M_1 = 5.8$. (The maximum here is with respect to both α and ψ.) This curve is included in Fig. 19.4.

15.6.3 Neutral supersonic solutions

As already mentioned, a neutral supersonic solution appears in Figs. 15.23 and 15.24 for $\theta_w = 0.10$ ($T_w/T_r = 0.25$). This solution fits the description given in Section 13.7.2. It is a purely outgoing wave, and in the coordinate system fixed relative to the phase velocity it is a Mach wave. Since the wave extends to infinity with undiminished amplitude, it transports energy from the boundary layer to infinity. However, it is a neutral disturbance and the net energy transfer must be zero. The energy carried to infinity is made up by energy production in the boundary layer due to a Reynolds stress which exists in the region $\eta_c < \eta < \eta_s$. This Reynolds stress, as calculated by numerical integration, is shown in Fig. 15.29. This figure agrees with the sketch given by Lees and Lin (1946) for a neutral supersonic disturbance. As noted by Lees and Lin, c_r must be less than c_s in order that the Reynolds stress, which is given by (15.4), is positive. A neutral supersonic solution of this type has also been found at $M_1 = 5.8$ for $\theta_w = 0.15$, but not for $\theta_w = 0.25$.

A plot of the magnitude of the pressure amplitude function, $|\bar{z}_4|$, is given in Fig. 15.30 for the neutral supersonic solution of Fig. 15.29 and also for the second-mode neutral subsonic solution. The two amplitude functions are similar in character, and, because of the single 180° phase shift, we can assign the neutral supersonic solution to the second mode. This result is a reasonable one, in view of the fact that the second-mode amplified solutions join the supersonic amplified solutions when $\eta_{s1} < \eta_0$ or has disappeared.

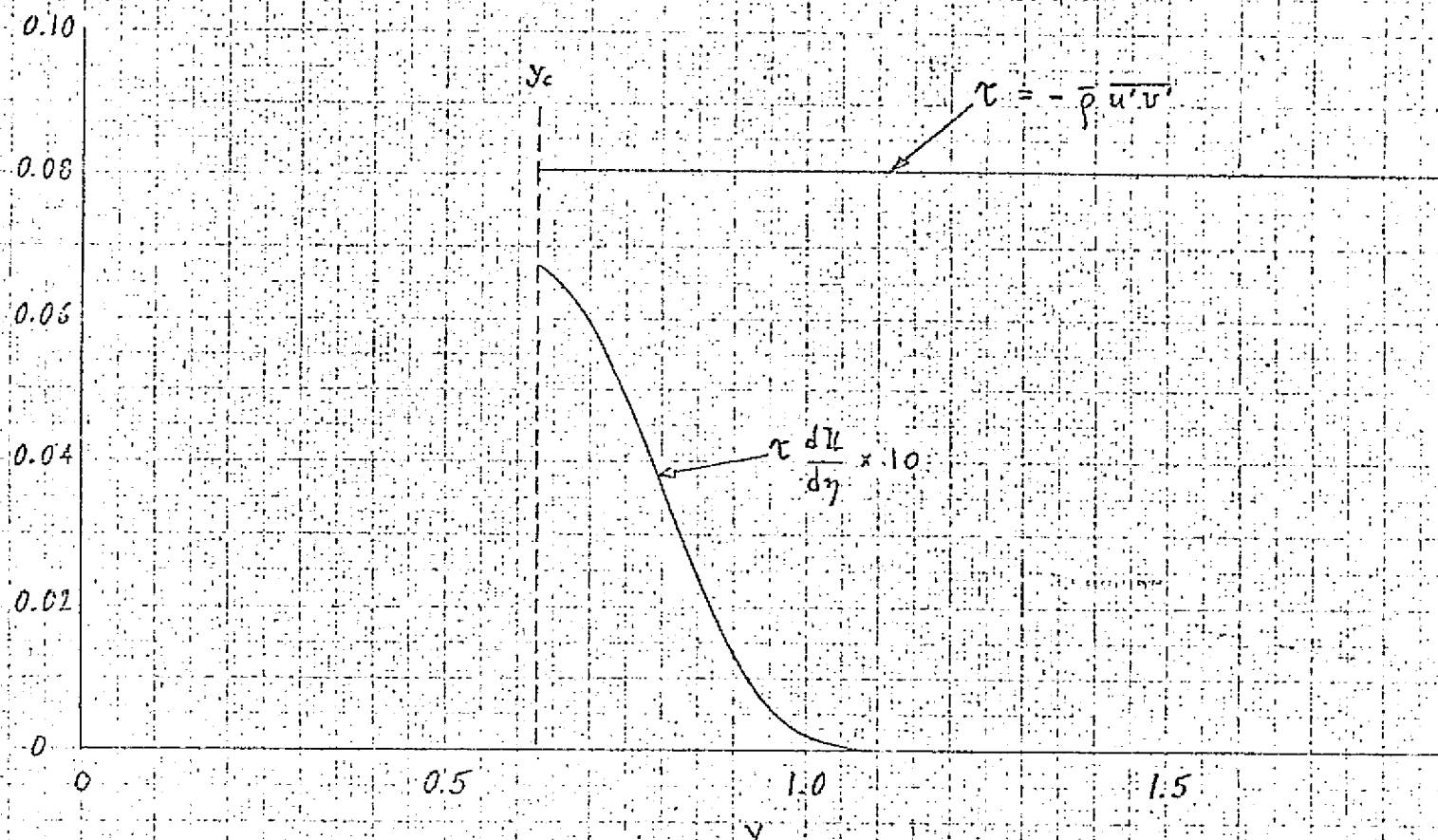

Fig. 15.29 Distribution of Reynolds stress and energy production term for neutral supersonic disturbance. $M_1 = 5.8$, $\theta_w = 0.10$.

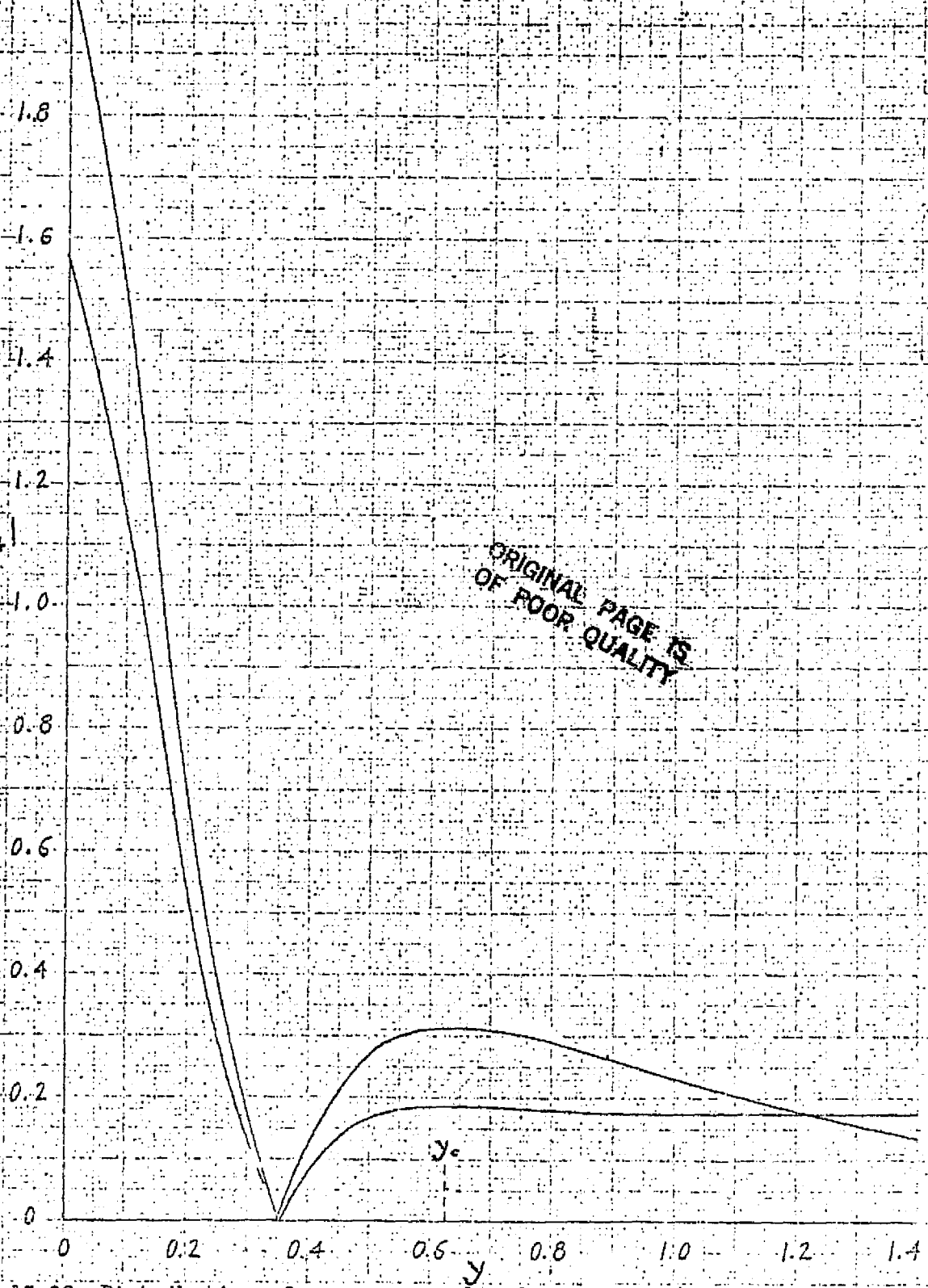

Fig. 15.30 Distribution of pressure amplitude function for neutral supersonic and second-mode neutral subsonic disturbances. $M_1 = 5.8$, $\theta_w = 0.10$.

We may now ask if there are any neutral supersonic solutions which are purely incoming waves instead of the outgoing waves just discussed. No solutions of this type have yet been calculated, but an inspection of complete eigenvalue diagrams which include the damped solutions makes their existence probable. Diagrams of this sort for $T_w / T_r = 0.25$ and 0.05 ($\theta_w = 0.10$ and -0.10) at $M_1 = 5.8$ are included in the figures of Section 19.2. From these diagrams we see that when the eigenvalue curve of the second-mode amplified solutions for $\theta_w = 0.10$ is extended into the damped region, it joins up with the eigenvalue curve of a family of damped supersonic solutions. According to the results obtained in Section 13.7.2, these solutions are incoming waves. At this value of θ_w , there is a neutral supersonic solution and a family of amplified supersonic solutions, all of which are outgoing waves. At $\theta_w = -0.10$, the eigenvalue curve of the second-mode amplified solutions connects up with the previously separate amplified supersonic solutions. By analogy with the situation at $\theta_w = 0.10$, we may speculate that a neutral supersonic solution also exists here, but that it is a purely incoming wave and is associated with a family of damped incoming waves. Obviously, this neutral disturbance receives energy from infinity, and the energy gain must be balanced by an energy loss due to a negative Reynolds stress in the region $\eta_s < \eta < \eta_s$. In order to have a negative Reynolds stress, according to (15.4), c_r must be greater than c_s .

16. Review of Asymptotic Theories

The inviscid theory as presented in the preceding section has given us a large body of numerical results, the applicability of which has not yet been established. To find out where these results can be used, it is necessary to turn to the viscous theory. Historically, the viscous theory was first attacked by the same methods that had proved successful for incompressible flow. A brief account of this theory and its immediate successors is given in this section. Only two-dimensional disturbances are considered.

16.1 Lees-Lin theory

Each form of the asymptotic theory depends upon reducing the complete stability equations of Section 13.5 to a simplified system of equations by means of order-of-magnitude arguments. The inviscid equation provides two of the necessary six solutions. The simplified equations are derived to be valid in a viscous region, and they will provide the four additional solutions needed to solve the eigenvalue problem. The region of validity of the Lees-Lin equations is the immediate neighborhood of the critical point.

A new independent variable ζ is defined, where

$$\zeta = \frac{\eta - \eta_c}{\varepsilon} \tag{16.1}$$

and

$$\varepsilon = (\alpha R)^{-1/3} \tag{16.2}$$

C-3

This variable is essentially the same as the one used in the incompressible theory in Section 6.4. The order-of-magnitude considerations lead to

$$Z_1 = \chi_1 \tag{16.3}$$

$$\varepsilon Z_2 = \chi_2 \tag{16.4}$$

$$\frac{1}{\varepsilon} Z_3 = \chi_3 \tag{16.5}$$

$$\frac{1}{\varepsilon} Z_4 = \chi_4 \tag{16.6}$$

$$Z_5 = \chi_5 \tag{16.7}$$

$$\varepsilon Z_6 = \chi_6 \tag{16.8}$$

where the χ_n are all of the same order and may be considered to be the first terms in a power-series expansion in ε. When these relations are substituted into the complete equations, the mean-flow quantities $u - c$ and T expanded in series about η_c, and only the lowest order terms kept, the equations of Lees and Lin are obtained. They are

$$\chi_1' = \chi_2 \tag{16.9}$$

$$\chi_2' = \frac{u_c'}{\nu_c}(i\zeta\chi_1 + \chi_3) + \frac{iT_c}{\nu_c}\chi_4 \tag{16.10}$$

$$\chi_3' = -i\chi_1 \tag{16.11}$$

$$\chi_4' = 0 \tag{16.12}$$

$$\chi_5' = \chi_6 \tag{16.13}$$

$$\chi_6' = \frac{\sigma}{\nu_c}\left(i u_c' \zeta \chi_5 + T_c' \chi_3\right) \tag{16.14}$$

If (16.10) is differentiated, the following equation is obtained for χ_3

$$\chi_3'' - \frac{i u_c'}{\nu_c} \zeta \chi_3'' = 0 \tag{16.15}$$

Since this equation is the same as (6.29), two viscous solutions are provided by (6.32) and (6.33). From (16.14), the equation for χ_5 is

$$\chi_5'' - \frac{i u_c' \sigma}{\nu_c} \zeta \chi_5 = \frac{\sigma T_c'}{\nu_c} \chi_3 \tag{16.16}$$

Consequently, χ_3 is coupled to χ_5, and velocity fluctuations will bring about temperature fluctuations. The important point of the Lees-Lin theory is that temperature fluctuations do not similarly bring about velocity fluctuations (χ_5 does not occur in the equations for χ_1 and χ_3). The velocity boundary conditions at the wall may be satisfied by the inviscid solution and the proper viscous solution of (16.15). Then solutions of the homogeneous part of (16.16) are simply added to the temperature fluctuations associated with these solutions to satisfy

the temperature boundary condition at the wall. The temperature fluctuations do not enter the eigenvalue problem, which is identical in all essential respects to the eigenvalue problem in incompressible flow.

This form of the theory was used by Lees (1947) to compute neutral-stability curves at $M_1 = 0.5$, 0.7, 0.9, 1.1 and 1.3 for an insulated wall, and at $M_1 = 0.7$ for three cooled-wall cases and one heated-wall case. In a later report, Lees (1952), he computed amplification rates and the overall growth of constant-frequency disturbances at $M_1 = 0.7$ for the insulated-wall case.

The Lees-Lin equations can also be written without expanding U and T in power series. In this form, the equations for f, g and θ are as follows:

$$f''' - \frac{i\alpha R(U-c)}{\nu} f' = 0 \qquad (16.17)$$

$$g' = -if \qquad (16.18)$$

$$\theta'' - \frac{i\alpha R\sigma(U-c)}{\nu}\theta = \frac{\alpha R\sigma T'}{\nu} g \qquad (16.19)$$

where the independent variable is η. The validity of these equations still rests on the supposition that $U-c$ is a small quantity. However, we may also do as in incompressible flow and simply regard these equations as an approximation that is useful when $U-c$ is not small, which is the way the theory is applied in any case. A further step with $U-c$

not considered small is to obtain the counterparts of the Tollmien viscous solutions of Section 6.5. In this form, the theory is an approximation to the Dunn-Lin theory which is discussed in the next section. Neutral-stability curves have been computed by Mack (1960) at $M_1 = 1.3$, 1.6 and 2.2 from this version of the theory. The inviscid solutions were calculated by the same numerical method as used by Lees (1947)(power-series expansion in α^2), except that one additional term was used.

16.2 Dunn-Lin theory

Because the viscous solutions of the Lees-Lin theory are strictly valid only near the critical point, Dunn and Lin (1955) developed an improved theory where the viscous solutions are of the Tollmien type and are valid everywhere. The viscous equations were derived by Dunn (1953) from careful order-of-magnitude arguments applicable in the wall viscous region. In this viscous region, the ordering parameter is $\varepsilon = (\alpha R)^{-1/2}$, the same quantity which appeared in Section 6.2. With $u - c$ no longer considered a small quantity, the viscous equations are

$$f''' - \frac{i\alpha R(u-c)}{\nu} f' = 0 \tag{16.20}$$

$$\varphi' = -if + \frac{i(u-c)}{T}\theta \tag{16.21}$$

$$\theta'' - \frac{i\alpha R\sigma(u-c)}{\nu}\theta = 0 \tag{16.22}$$

When $u-c$ is small, (16.21) reduces to (16.18), and when $u-c$ is not small, (16.19) reduces to (16.22). Equation (16.20) is the same in both the Lees-Lin and Dunn-Lin theories.

There is an important difference between the Dunn-Lin and the Lees-Lin viscous equations. In the Lees-Lin theory, velocity fluctuations induce temperature fluctuations, but temperature fluctuations do not induce velocity fluctuations. In the Dunn-Lin theory the contrary is true. Velocity fluctuations do not induce temperature fluctuations, but temperature fluctuations induce velocity fluctuations. In other words, the Lees-Lin equations have the four viscous solutions

$$(f_3, g_3, \theta_3) \quad , \quad (f_4, g_4, \theta_4)$$
$$(0, 0, \theta_5) \quad , \quad (0, 0, \theta_6) \tag{16.23}$$

and the Dunn-Lin equations have the solutions

$$(f_3, g_3, 0) \quad , \quad (f_4, g_4, 0)$$
$$(0, g_5, \theta_5) \quad , \quad (0, g_6, \theta_6) \tag{16.24}$$

Consequently, in the Dunn-Lin theory the velocity and temperature boundary conditions must be satisfied simultaneously, and as a result the temperature fluctuations enter into the eigenvalue problem.

If we designate the inviscid solution that satisfies the boundary conditions at infinity by (F , $\bar{\Phi}$, Θ), and eliminate the viscous solutions which become large as $\eta \to \infty$ (subscripts four and six according to the conventional notation), we can write the boundary conditions at $\eta = 0$ as

$$\begin{aligned} F_w + A f_{3w} + B f_{5w} &= 0 \\ \bar{\Phi}_w + A \varphi_{3w} + B \varphi_{5w} &= 0 \\ \Theta_w + A \theta_{3w} + B \theta_{5w} &= 0 \end{aligned} \tag{16.25}$$

In order to have a non-trivial solution of these homogeneous equations for A and B, the determinant must be zero. With θ_3 and f_5 zero from the Dunn-Lin theory, the expansion of the determinant gives

$$\frac{\bar{\Phi}_w}{F_w} \quad \frac{\varphi_{3w}}{f_{3w}} + \frac{\varphi_{5w}}{\theta_{5w}} \frac{\Theta_w}{F_w} \tag{16.26}$$

The inviscid equations given in Section 13.7.1 can be manipulated to yield

$$\frac{\Theta_w}{F_w} = (\gamma-1) c M_1^2 + \left[(\gamma-1) M_1^2 \mathcal{U}_w' - \frac{T_w'}{c} \right] \frac{i \bar{\Phi}_w}{F_w} \tag{16.27}$$

With (16.27) substituted into (16.26), the eigenvalue equation is found to be

$$\frac{\bar{\Phi}_w}{F_w} = \frac{\dfrac{\varphi_{3w}}{f_{3w}} + (\gamma-1) c M_1^2 \dfrac{\varphi_{5w}}{\theta_{5w}}}{1 - \left[(\gamma-1) M_1^2 \mathcal{U}_w' - \dfrac{T_w'}{c} \right] \dfrac{i \varphi_{5w}}{\theta_{5w}}} \tag{16.28}$$

This equation was first obtained by Reshotko (1960), but another equation which reduces to the above for $T_w' = 0$ was derived earlier by Dunn and Lin (private communication). The inviscid terms are on the left-hand side, and the viscous terms are on the right-hand side just as for incompressible flow. In the Lees-Lin theory, (16.28) is replaced by

$$\frac{\mathfrak{D}_w}{F_w} = \frac{\varphi_{3w}}{f_{3w}} \tag{16.29}$$

which is identical to (6.2) in the incompressible theory.

When the temperature fluctuations are unimportant in the sense that the associated velocity fluctuations given by φ_5 are small, (16.28) also reduces to (16.29). For the insulated-wall case, the neutral-stability curve is not influenced by the temperature fluctuations up to about $M_1 = 1.6$. At $M_1 = 2.2$, the neutral-stability curve with temperature fluctuations included is outside of the neutral curve obtained from (16.29). Unfortunately, the neutral-stability curve obtained from numerical integration of the complete stability equations is inside of the neutral curve obtained from (16.29) as will be shown in Section 17.1.

16.3 Lees-Reshotko theory

A further attempt to improve the asymptotic theory was made by Lees and Reshotko (1962), reported first by Reshotko (1960). The separation into inviscid and viscous solutions was retained, but all solutions were calculated by numerical integration of the appropriate equations. Because the viscous solutions were to be obtained by numerical integration, a

more complete system of viscous equations could be used than in the normal asymptotic method. The viscous equations, derived from order-of-magnitude arguments, are

$$f''' + \frac{2}{\mu}\frac{d\mu}{dT}T'f'' + \frac{1}{\mu}\frac{d\mu}{dT}U'\theta'' + \frac{i\alpha R(U-c)}{\nu}\left(\frac{T'}{T}f - f' - \frac{U'}{T}\theta\right) = 0 \tag{16.30}$$

$$\varphi' + if - \frac{T'}{T}\varphi - \frac{i(U-c)}{T}\theta = 0 \tag{16.31}$$

$$\theta'' + \frac{2}{\mu}\frac{d\mu}{dT}T'\theta' + 2(\gamma-1)\sigma M_1^2 U'f' - \frac{i\alpha R\sigma(U-c)}{\nu}\theta = \frac{\alpha R\sigma T'}{\nu}\varphi \tag{16.32}$$

A neutral-stability curve was computed by Lees and Reshotko at $M_1 = 2.2$. It agreed with the Dunn-Lin theory on the upper branch, and on the lower branch was shifted somewhat to the right. Hence there was an improvement over the Dunn-Lin theory, although a small one. An attempt was also made to compute neutral-stability curves at $M_1 = 3.2$ and 5.6, but at these Mach numbers the neutral curve was found to break up into multiple loops of a puzzling nature. These loops have not been explained, but it does appear that they are fundamentally different from the multiple loops to be discussed in the next section, and which can be identified with the multiple inviscid modes already discussed.

17. Viscous Theory - Two-Dimensional Disturbances, Insulated Wall

We now take up the viscous theory to the extent it can be developed from the results obtained from numerical integration of the complete stability equations. With these results, we can assess the accuracy of the asymptotic theories and also find under which circumstances it is possible to make use of the inviscid theory. Further, we can study such things as the influence of the Reynolds number on amplification rates and frequencies of the most unstable disturbances. Finally, we can compute the growth of disturbances of constant frequency as they travel through the boundary layer, and thus be in a position to judge the response of the boundary layer to any particular disturbance spectrum.

17.1 Neutral-stability curves

17.1.1 Comparison with asymptotic theory

Figure 17.1 gives a comparison of three neutral-stability curves for two-dimensional disturbances at $M_1 = 2.2$. The dimensionless frequency, $\omega^* \nu^* / U_1^{*2}$, is plotted against $R = R_x^{1/2}$ (ω^* is referred to as β in the figure). The outermost curve is from Mack (1960) and was obtained from (16.28), the eigenvalue equation of the Dunn-Lin theory which includes the temperature fluctuations. The innermost curve is from the numerical integration of the equations of Section 13.5 according to the method of Mack (1965a). There is seen to be a large discrepancy in the two results. Somewhat better agreement is found by omitting the temperature fluctuations. The intermediate curve was obtained by direct numerical integration of the simplified system of equations given by Dunn and Lin (1955). These equations include, in addition to the inviscid terms, the leading viscous terms

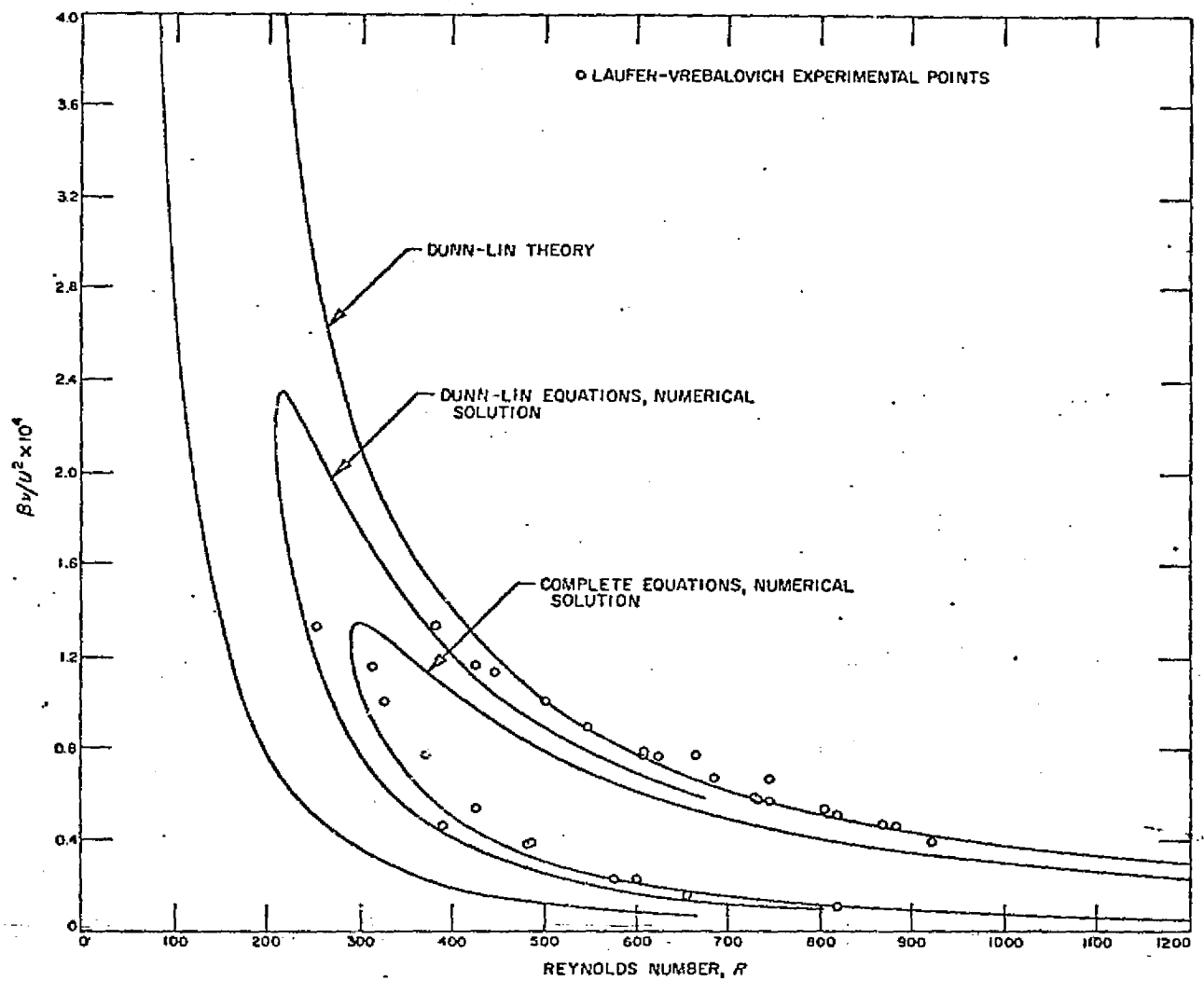

Fig. 17.1 Neutral stability curves of frequency at $M_1 = 2.2$

according to Dunn's order-of-magnitude analysis. There are no dissipation terms in the simplified energy equation.

The asymptotic method is supposed to solve the simplified equations with an error no larger than the error involved in dropping the missing viscous terms. It is obvious from Fig. 17.1 that the equations are better than the method used to solve them. The fact that the Lees-Reshotko neutral-stability curve is in good agreement with the Dunn-Lin neutral curve also indicates that the main source of the failure of the asymptotic theory is not to be found in the equations used. Calculations at lower Mach numbers give good agreement of the three neutral curves at $M_1 = 1.3$, and fair agreement at $M_1 = 1.6$. It can be concluded that the asymptotic method is adequate for two-dimensional disturbances up to $M_1 = 1.6$, and that the refinement of including the temperature fluctuations adds nothing to the adequacy of the theory.

The experimental points shown in Fig. 17.1 were measured by Laufer and Vrebalovich (1960). They are not important in the present context and will be discussed in Section 20.1.

17.1.2 Effect of Mach number

The evolution of the neutral-stability curve with increasing Mach number is of considerable interest. Figure 17.2 gives neutral curves at five Mach numbers from 1.6 to 3.8. The wave number is plotted against $1/R$ to emphasize the high Reynolds number region. At $M_1 = 1.6$, the neutral curve still has the same character as in incompressible flow. There is a weak inviscid instability, and α approaches the inviscid neutral subsonic wave number α_{s1} from above as $R \to \infty$. In the sense of the

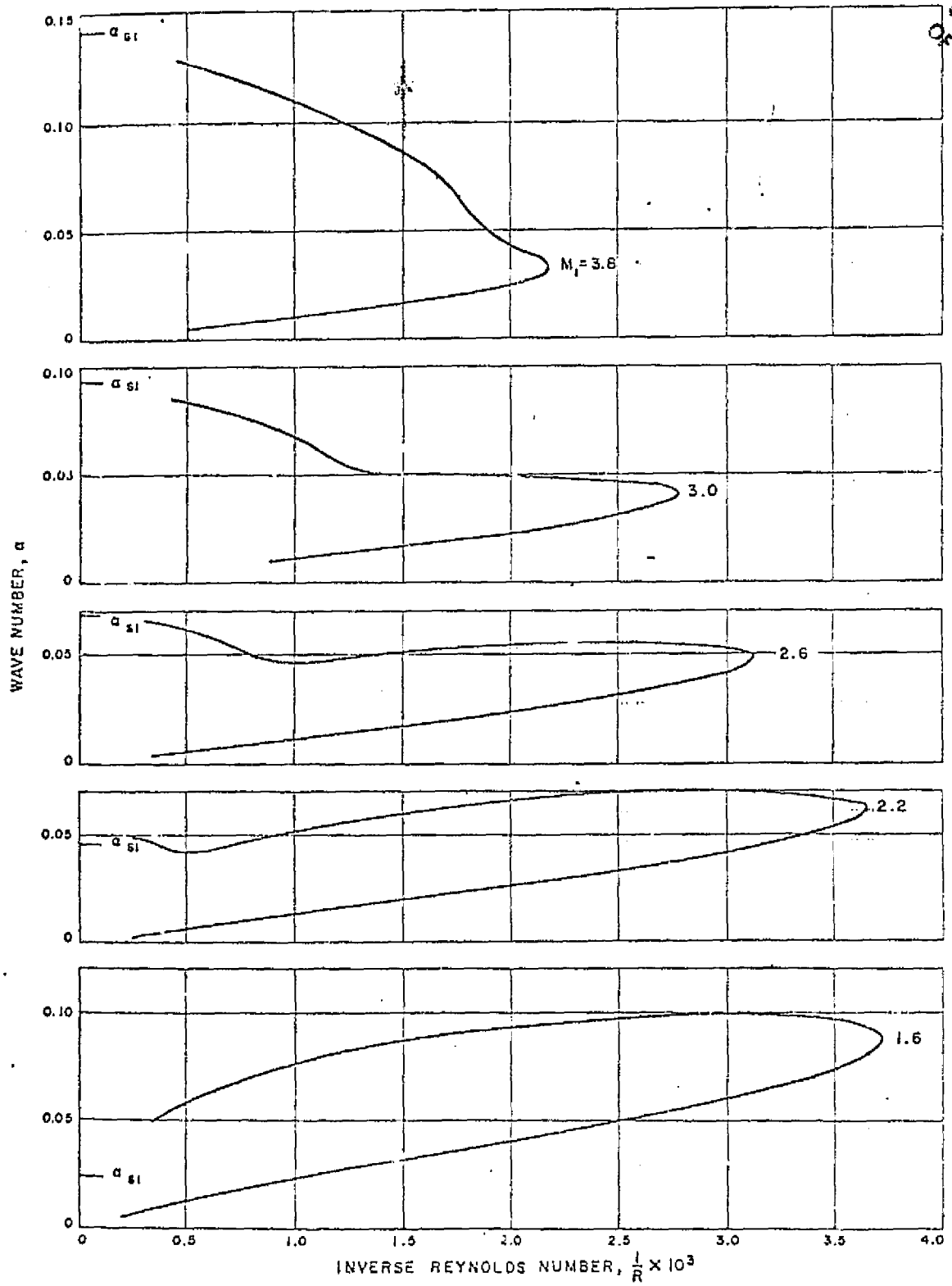

Fig. 17.2 Effect of free-stream Mach number on neutral-stability curve of insulated-wall boundary layer.

definition given in the footnote on p. 75, viscosity has a destabilizing effect with this type of neutral curve.

At $M_1 = 2.2$, a local minimum appears in the upper branch of the neutral curve. This minimum indicates that the effect of viscosity has become stabilizing over a range of high Reynolds numbers. At $M_1 = 2.6$, this minimum is more pronounced and α appears to approach α_{s_1} from below. If this supposition is correct, then viscosity has a stabilizing effect from $R \to \infty$ up to the local minimum. At $M_1 = 3.0$, the minimum has virtually disappeared and α clearly approaches α_{s_1} from below. The effect of viscosity is stabilizing, or almost so, over the entire range of Reynolds numbers. At $M_1 = 3.8$, the minimum has definitely disappeared and the wave number decreases monotonically along the neutral curve from α_{s_1} to $\alpha = 0$. This neutral curve is of the same general type as the one in Fig. 9.2 (p. 74) for the Falkner-Skan separation profile. The maximum instability is inviscid (at $R \to \infty$), and the effect of viscosity is only stabilizing. These statements can all be verified by studying the amplification rate as a function of Reynolds number, as will be done in Section 17.2.1.

The neutral-stability curve at $M_1 = 4.2$, plotted as α vs R, c_r vs R and $\omega^* \nu^* / U_1^{*2}$ vs R, is shown in Fig. 17.3. At this Mach number there are two separate loops, and it is to be expected that the first, or lower, loop is the finite Reynolds number counterpart of the inviscid first mode and the second, or upper, loop is the counterpart of the inviscid second mode. The upper branch of the first loop tends to α_{s_1}, c_{s_1} as $R \to \infty$ while the upper branch of the second loop tends to α_{s_2}, c_{s_2}. The lower

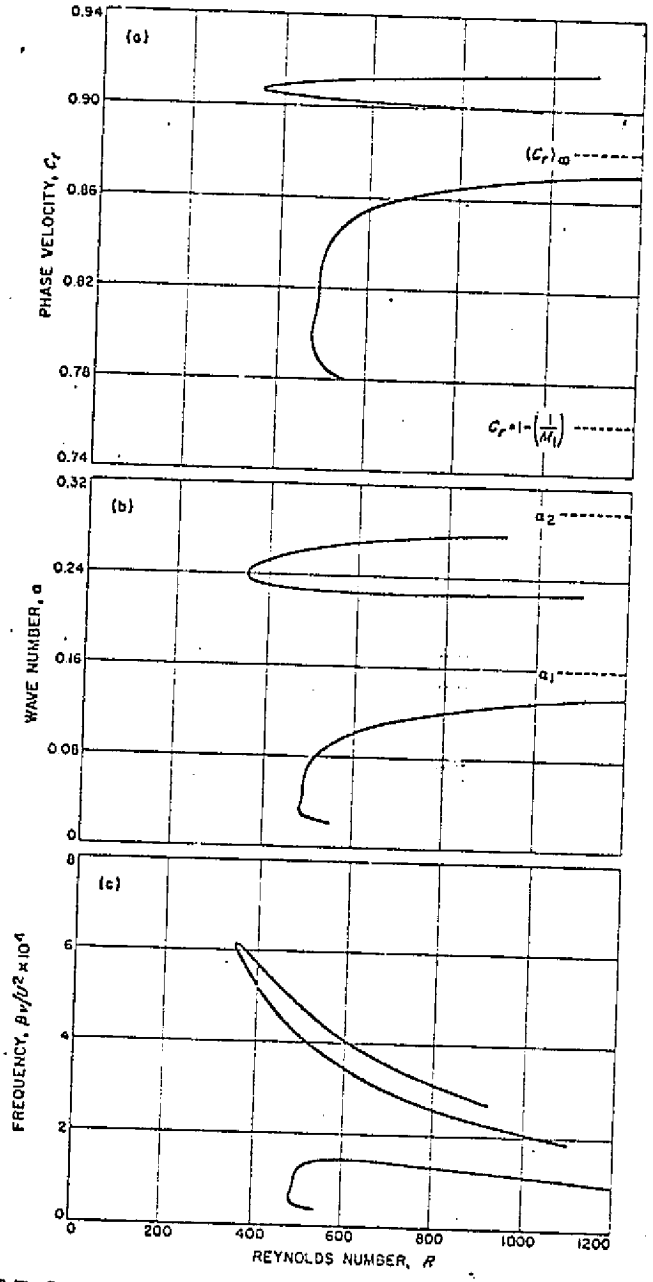

Fig. 17.3 Neutral-stability curves of phase velocity, wave number, and frequency at $M_1 = 4.2$

branch of the first loop tends to $\alpha = 0, c_0$ as $R \to \infty$, and on the upper loop it is not possible to assign a definite limit. These limits fit the identification of the two loops with the first and second modes. If the eigenfunctions of the neutral disturbances are examined, it is found that there is little phase change on the first loop, and a large phase change on the second loop.

The shape of the neutral-stability curve of the second mode indicates that here too viscosity has only a stabilizing influence. The much greater inviscid instability of the second mode as compared to the first mode is reflected in the smaller critical Reynolds number of the second mode. The lowest Mach number at which the second mode has been calculated (because of the αR limitation of the method of numerical integration) is $M_1 = 3.8$, where the critical Reynolds number is $R = 830$, and the wave number is $\alpha = 0.306$ and the phase velocity is $c_r = 0.904$.

Figure 17.4 shows the α vs R neutral curves at $M_1 = 4.5$ and 4.8. At $M_1 = 4.5$ there are still two separate loops as at $M_1 = 4.2$, but at $M_1 = 4.8$ an important change has taken place. The two separate unstable regions have merged into a single unstable region enclosed by a single neutral curve. This single curve starts at the inviscid neutral sonic solution and ends at the inviscid neutral subsonic solution of the second mode. The factor which controls whether there are individual or separate neutral curves is whether α_{i2} is greater than or less than α_{s1}. At $M_1 = 4.5$, $\alpha_{i2} > \alpha_{s1}$ and there are two separate loops. At $M_1 = 4.8$, $\alpha_{i2} < \alpha_{s1}$ and there is a single loop.

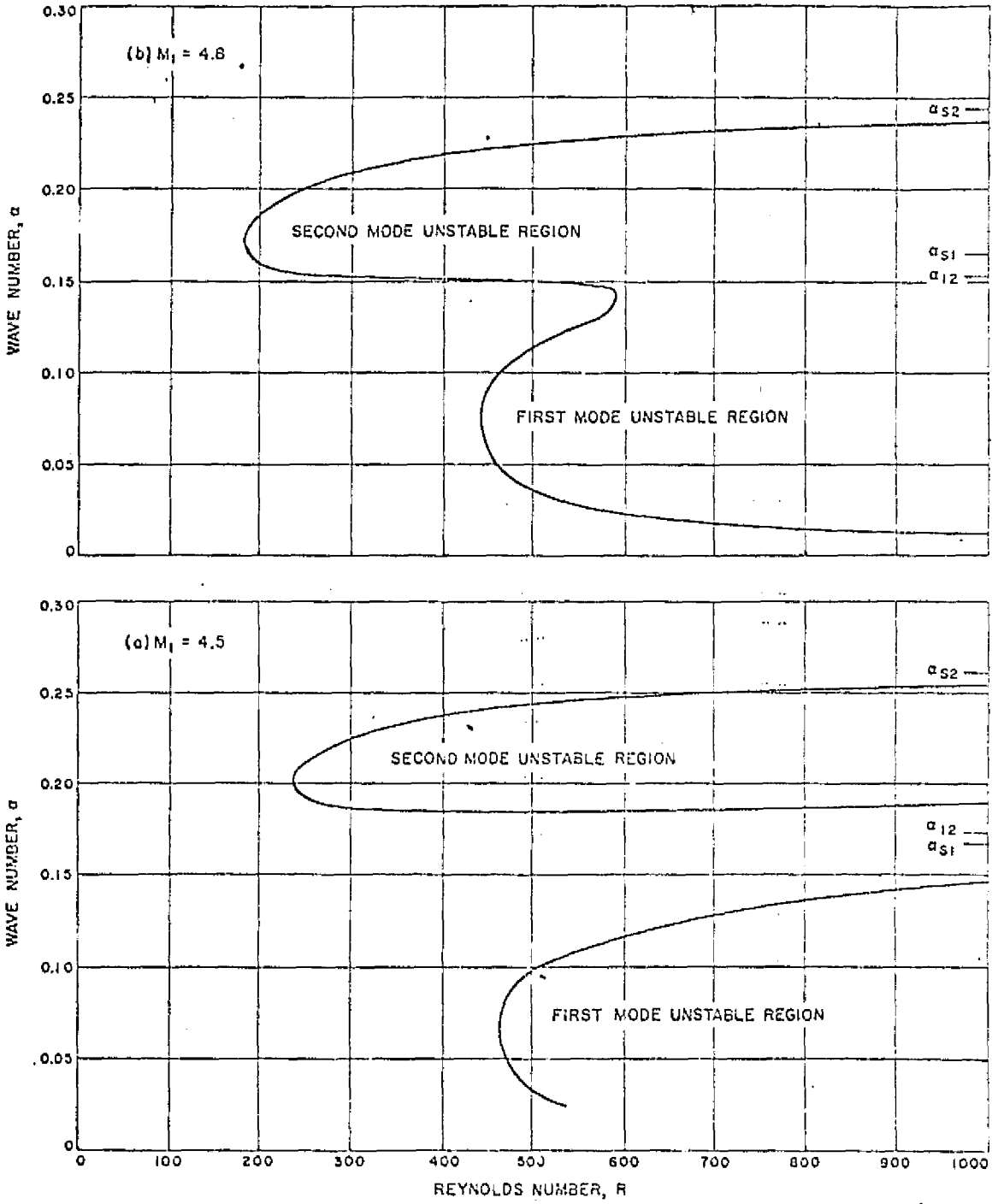

Fig. 17.4 Neutral-stability curve of wave number vs Reynolds number for insulated-wall boundary layer near Mach number at which $\alpha_{12} = \alpha_{s1}$. (a) $M_1 = 4.5$, (b) $M_1 = 4.8$.

At every α, R in the interior of the single neutral curve there is an amplified solution. However, there are multiple viscous solutions, i.e., more than one c for a given α, R, just as there are multiple inviscid solutions, i.e., more than one c for a given α. Hence at the same α, R where there is an amplified solution of one family, there can be a damped or neutral solution of another family. Some examples of multiple viscous solutions are shown in Figs. 19.4 and 19.5.

The neutral-stability curves of α vs R and c_r vs R at $M_1 = 5.8$ are given in Fig. 17.5 together with a few contours of $c_i = \text{const.}$ Although the merger of the two unstable regions is further advanced that at $M_1 = 4.8$, it is seen that these contours still form two distinct families. Consequently, it is still possible to identify disturbances as belonging to the first and second modes even after the merger. There is a rapid change from first-mode to second-mode character at the apparent juncture of the two regions. The fact that both families of contours are open to infinity is another indication that the effect of viscosity is purely destabilizing.

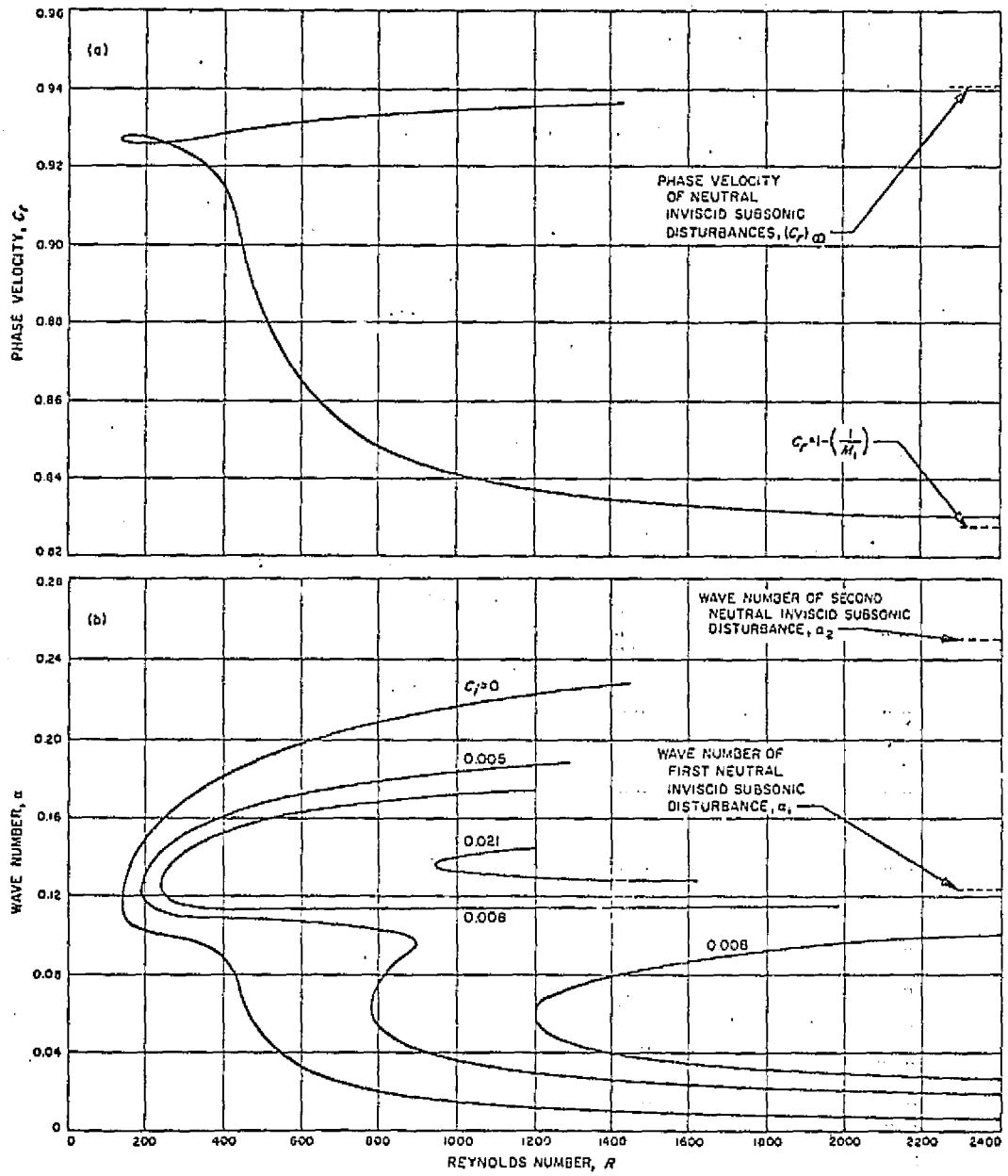

Fig. 17.5 Neutral-stability curves of phase velocity and wave number and contours of amplified disturbances at $M_1 = 5.8$

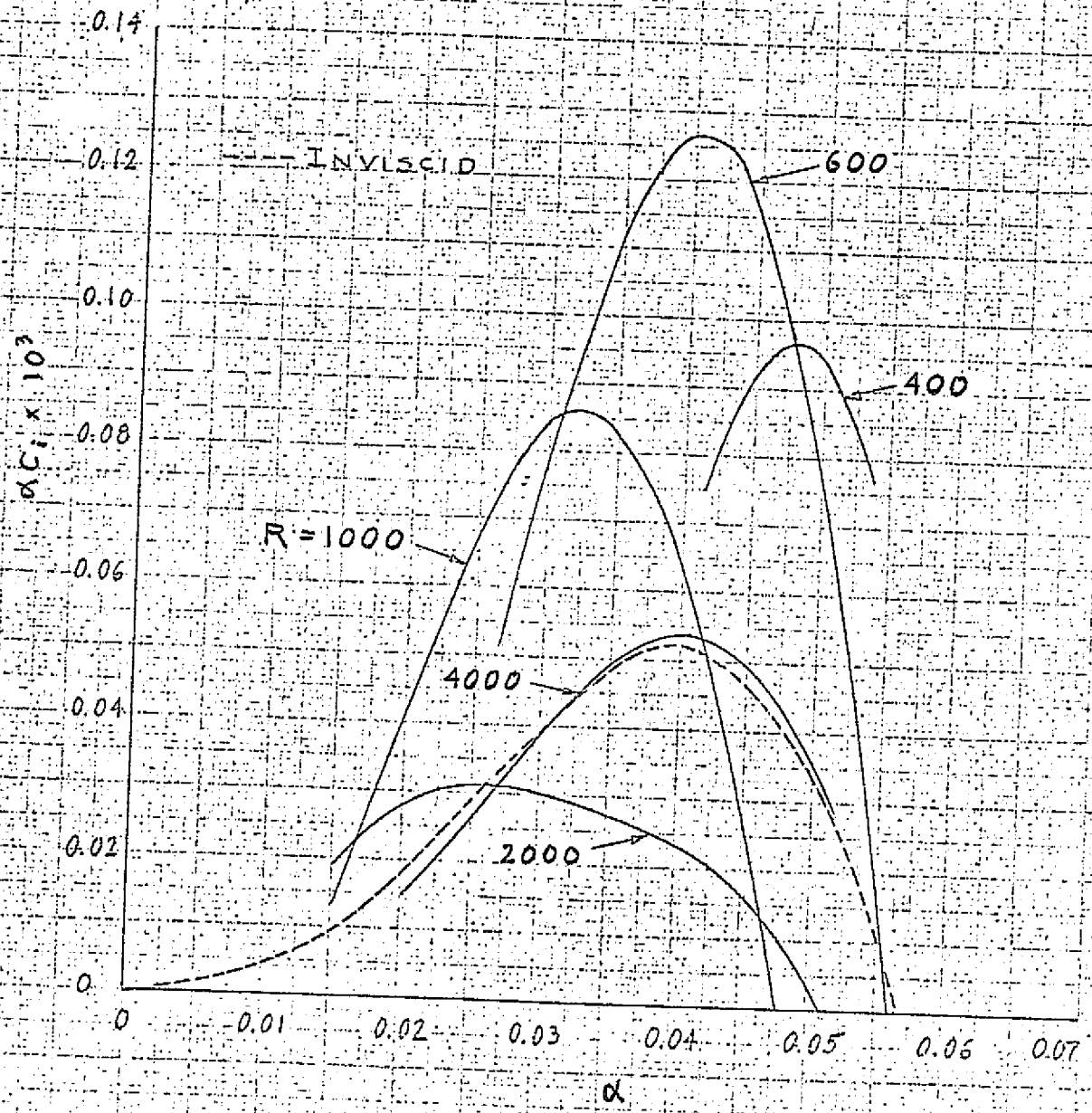

Fig. 17.6 Effect of Reynolds number on amplification rate at $M_1 = 2.4$.

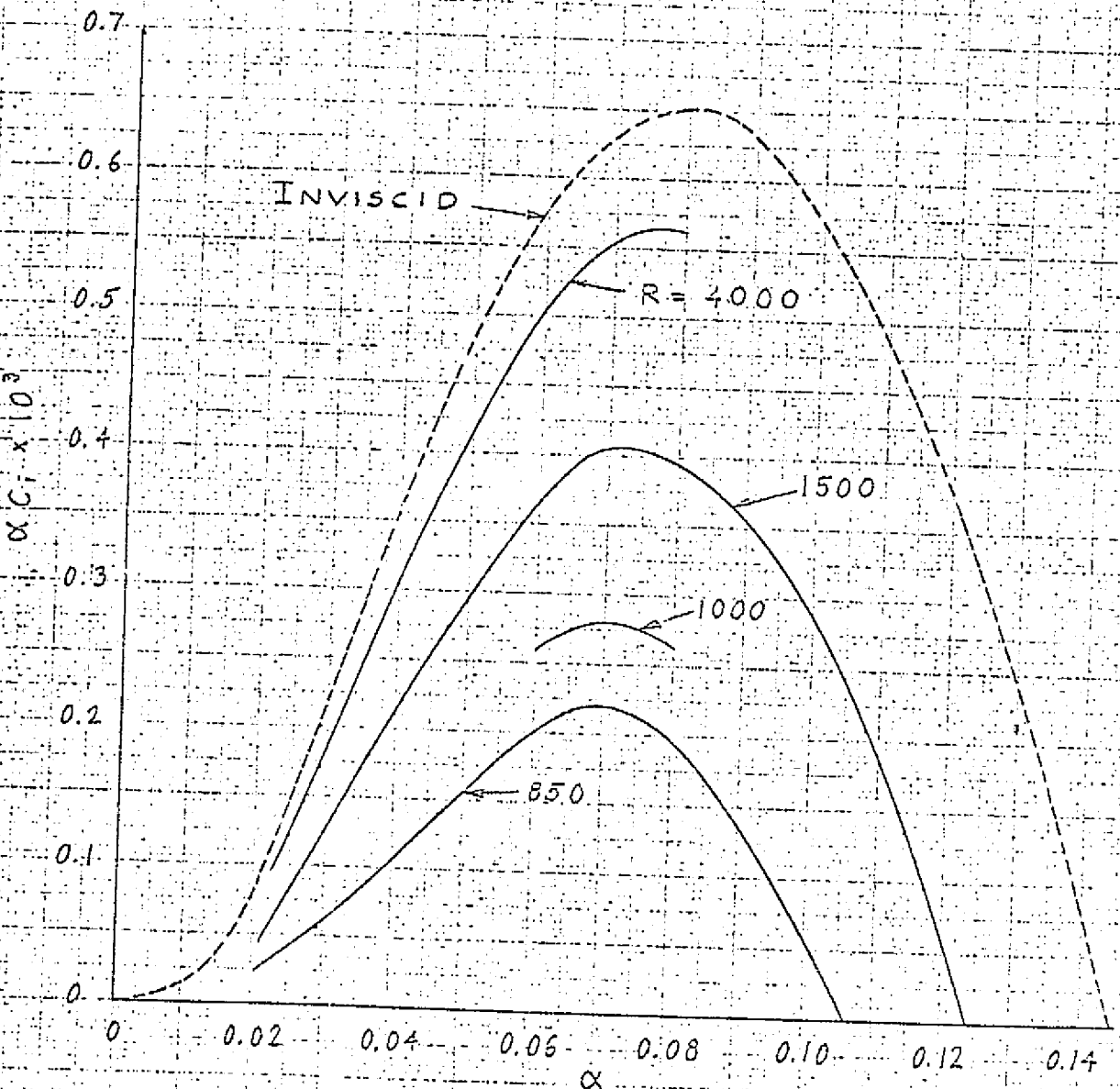

Fig. 17.7 Effect of Reynolds number on amplification rate at $M_1 = 3.8$.

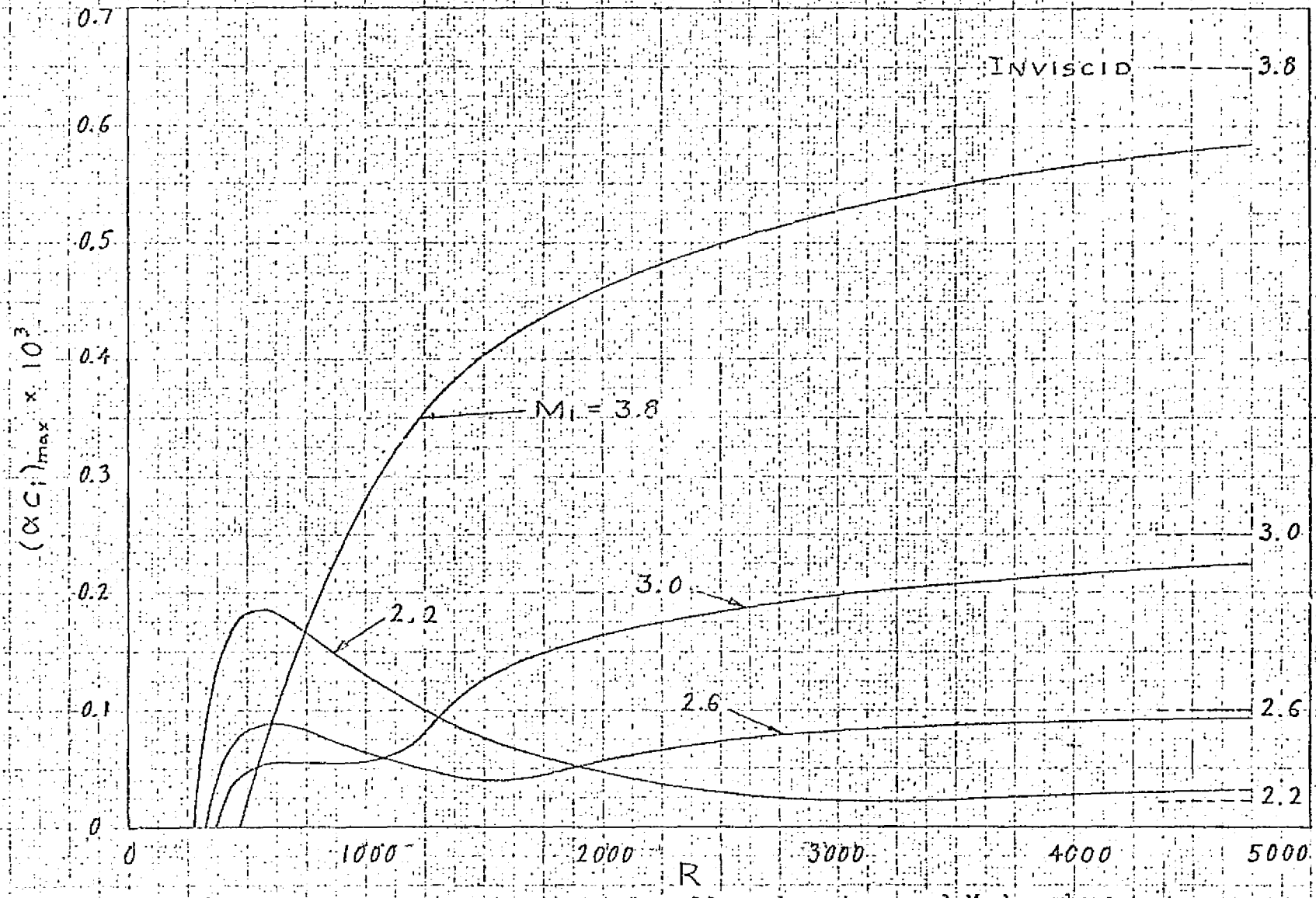

Fig. 17.8 Distribution of $(\alpha c_i)_{max}$ with Reynolds number at several Mach numbers.

VISCOUS THEORY, TWO-DIMENSIONAL DISTURBANCES

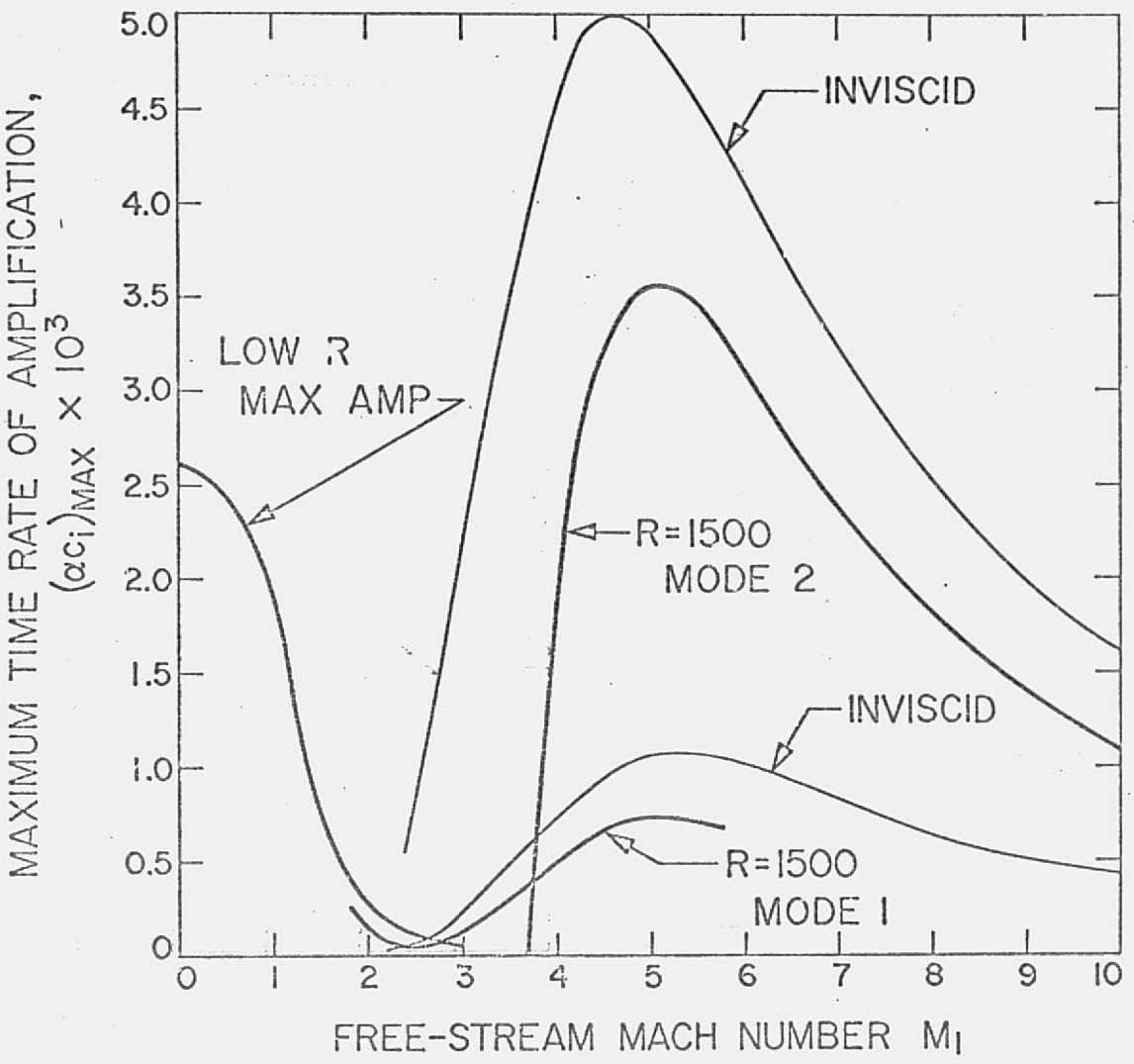

Fig. 17.9 Effect of Mach number on maximum amplification rate of first and second modes at finite Reynolds number.

VISCOUS THEORY, TWO-DIMENSIONAL DISTURBANCES

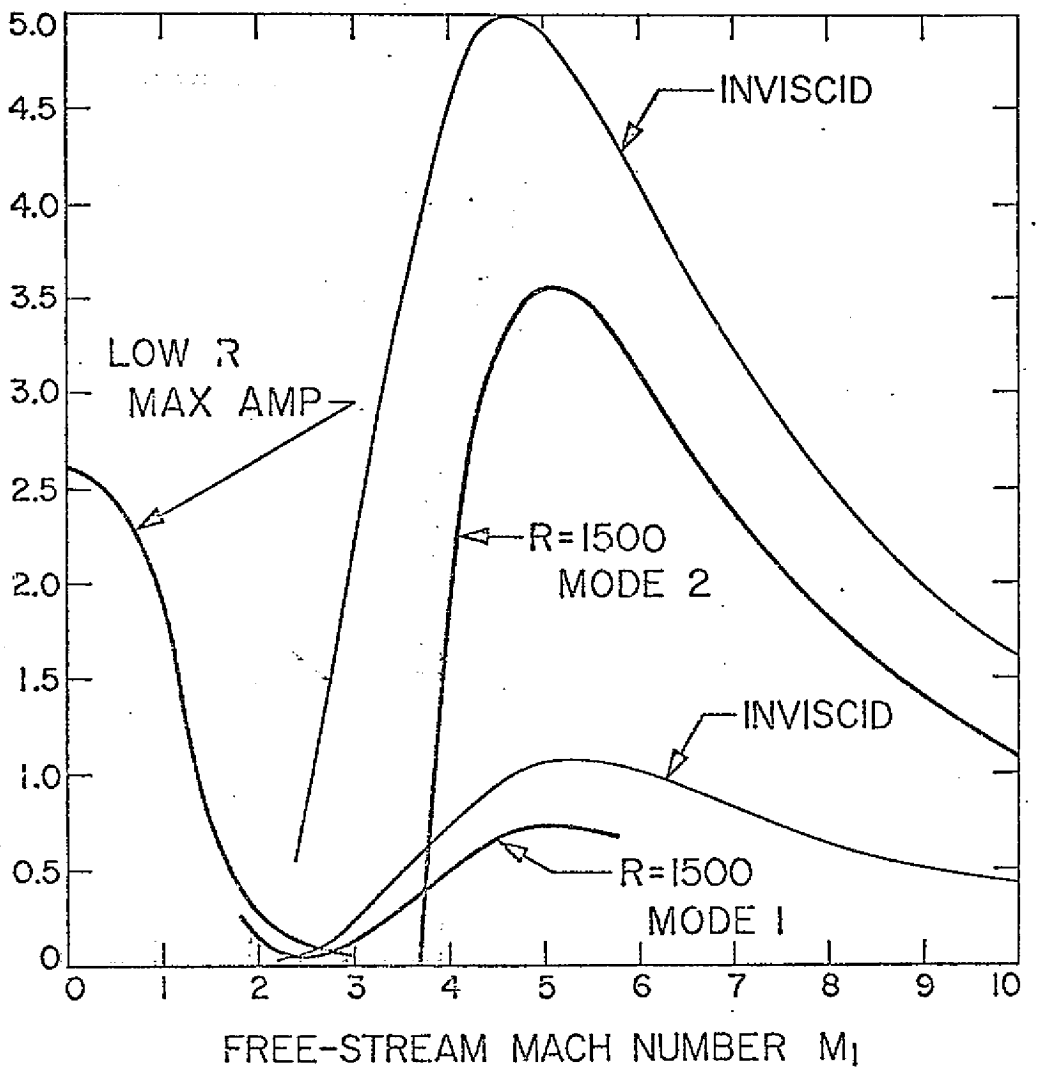

Fig. 17.9 Effect of Mach number on maximum amplification rate of first and second modes at finite Reynolds number.

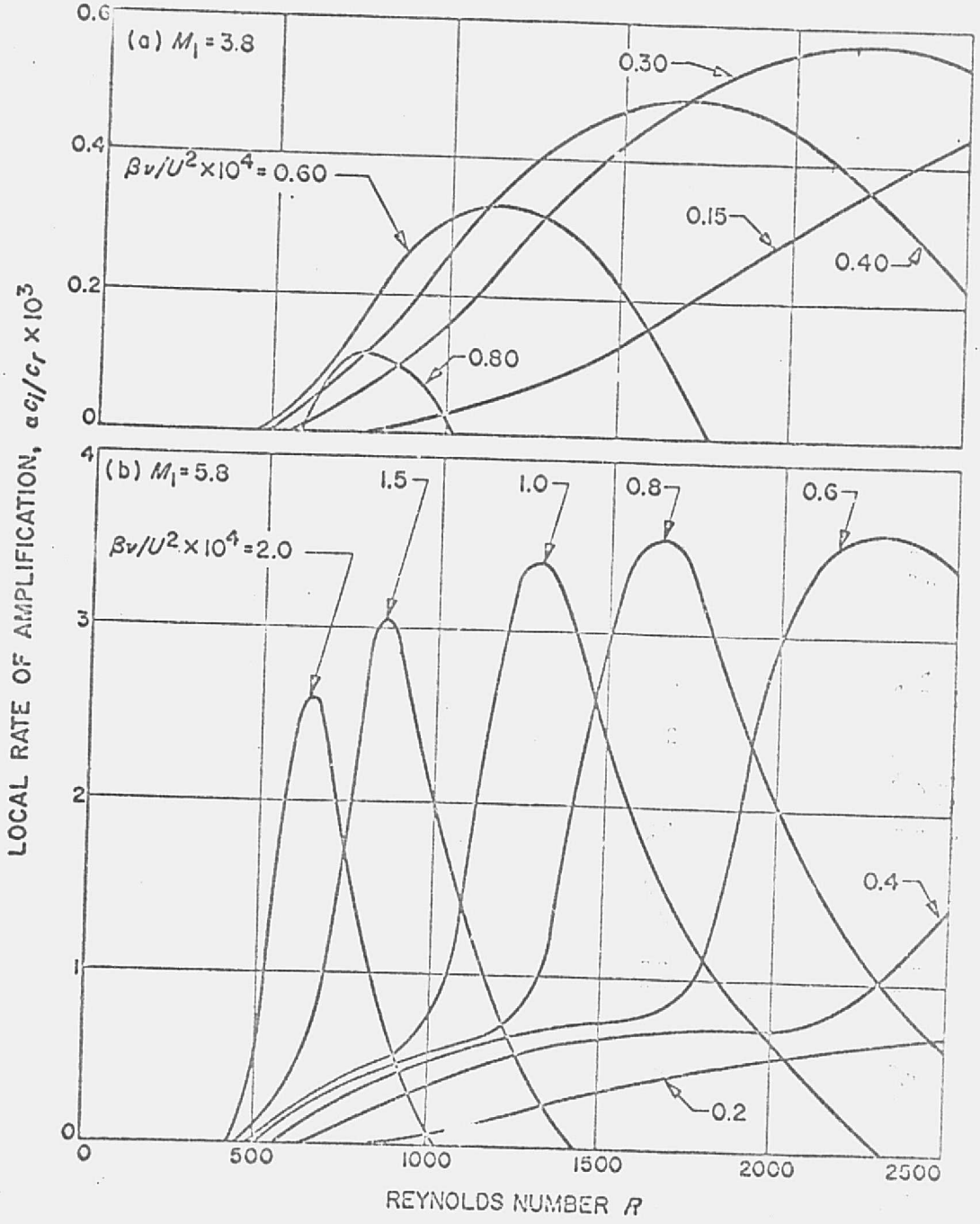

Fig. 17.10 **Local rate of amplification vs Reynolds number for several values of dimensionless frequency at $M_1 = 3.8$ and 5.8**

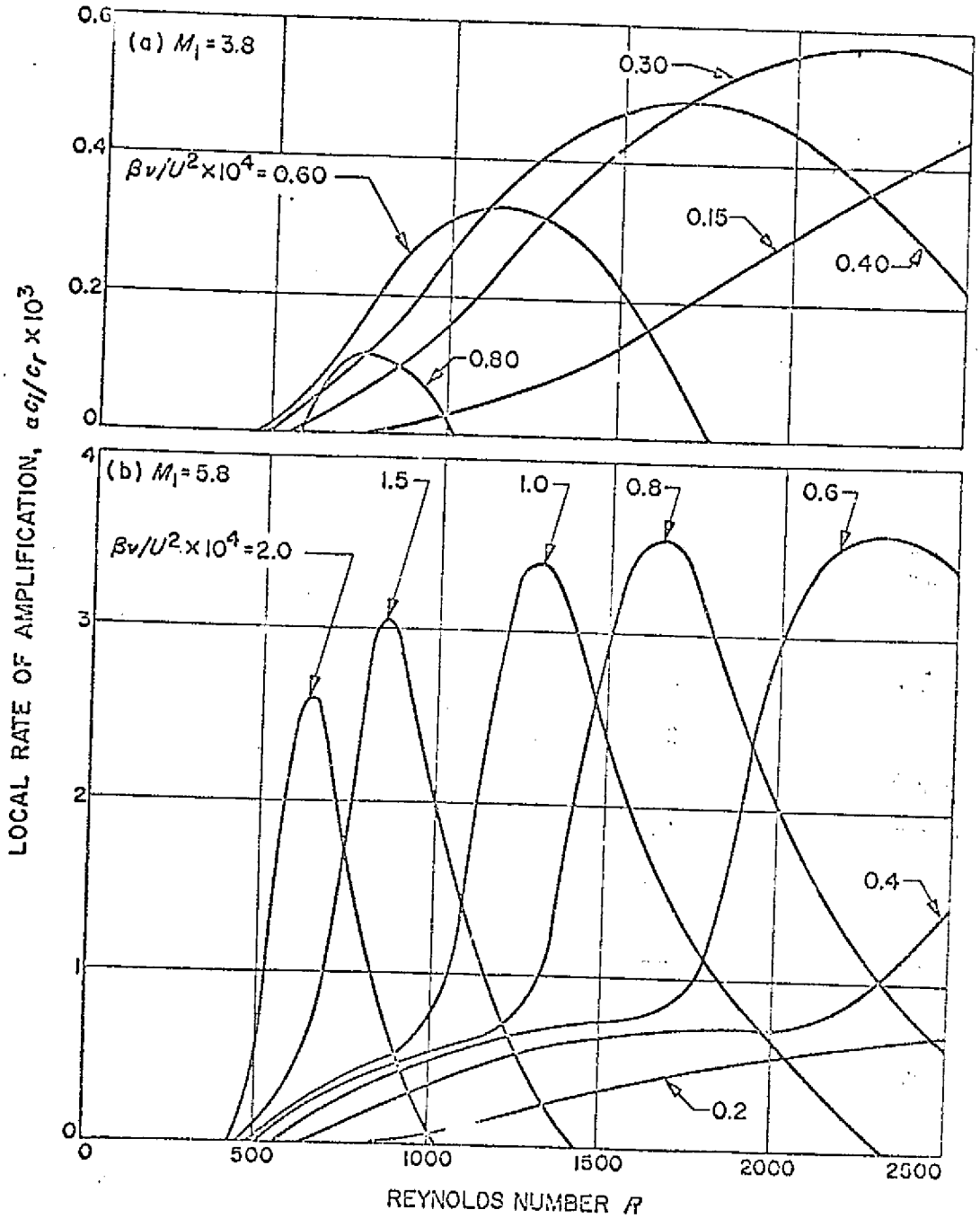

Fig. 17.10 Local rate of amplification vs Reynolds number for several values of dimensionless frequency at $M_1 = 3.8$ and 5.8

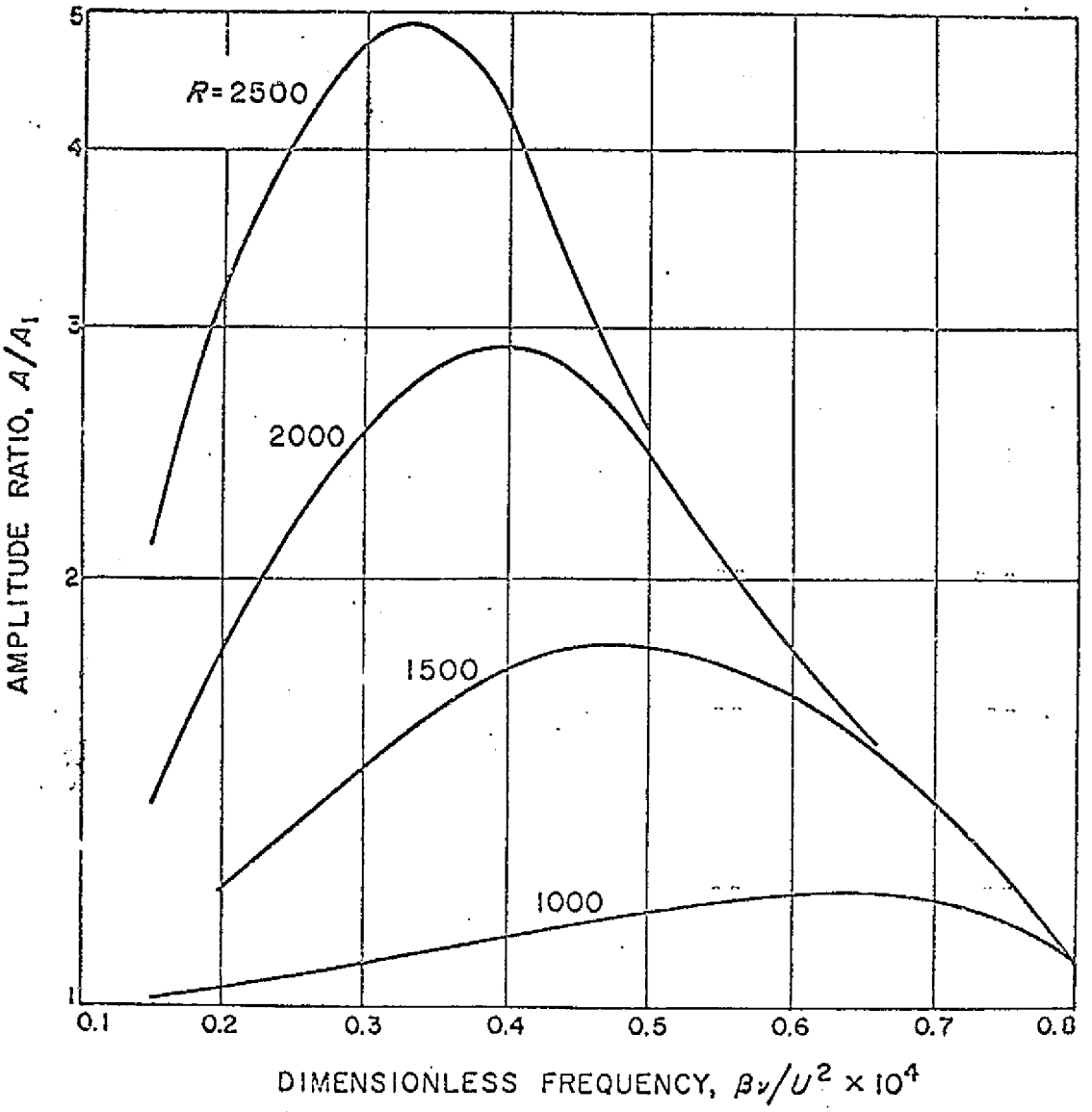

Fig. 17.11 **Amplitude ratio vs dimensionless frequency for four Reynolds numbers at $M_1 = 3.8$**

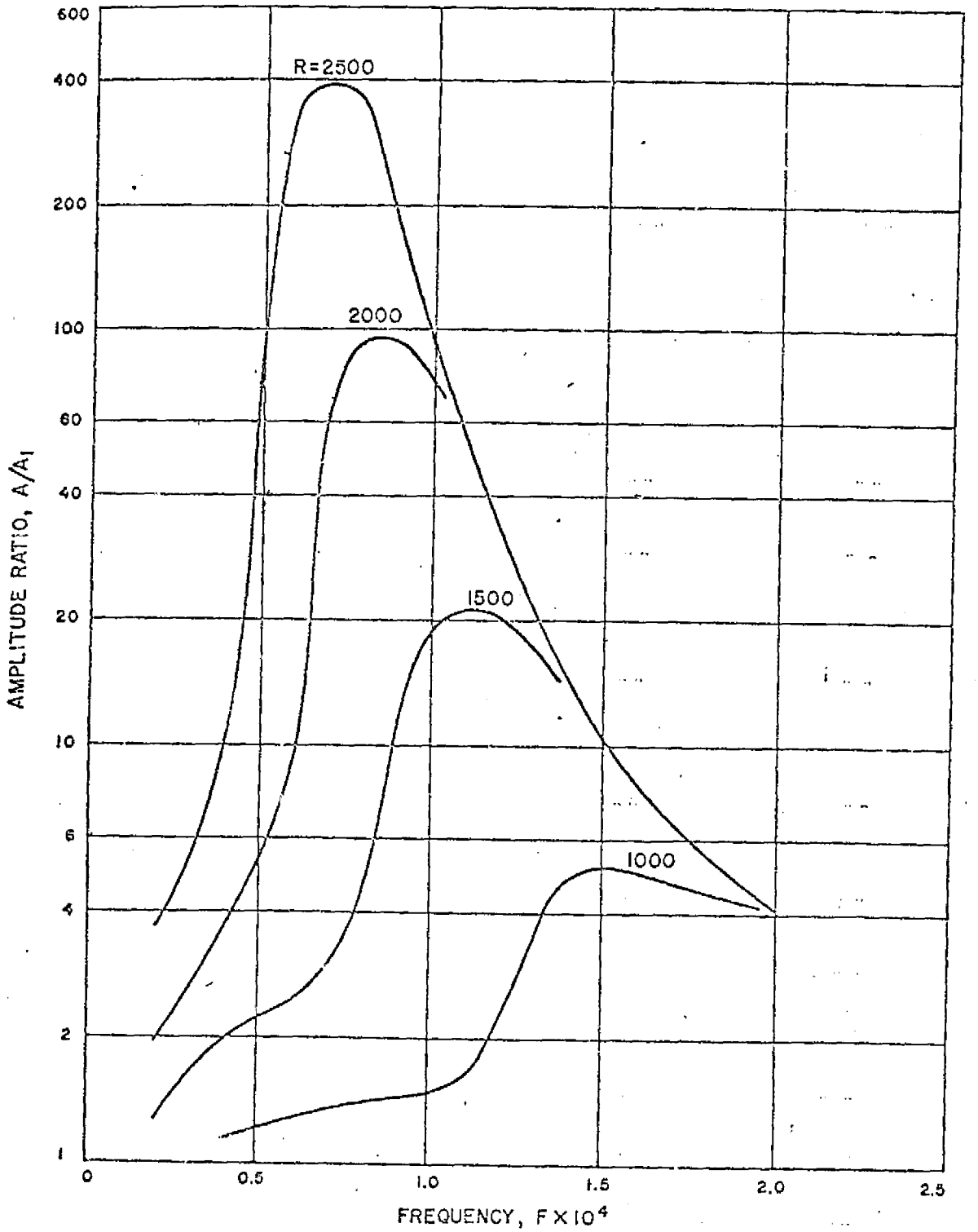

Fig. 17.12 Frequency response of insulated-wall boundary layer at $M_1 = 5.8$.

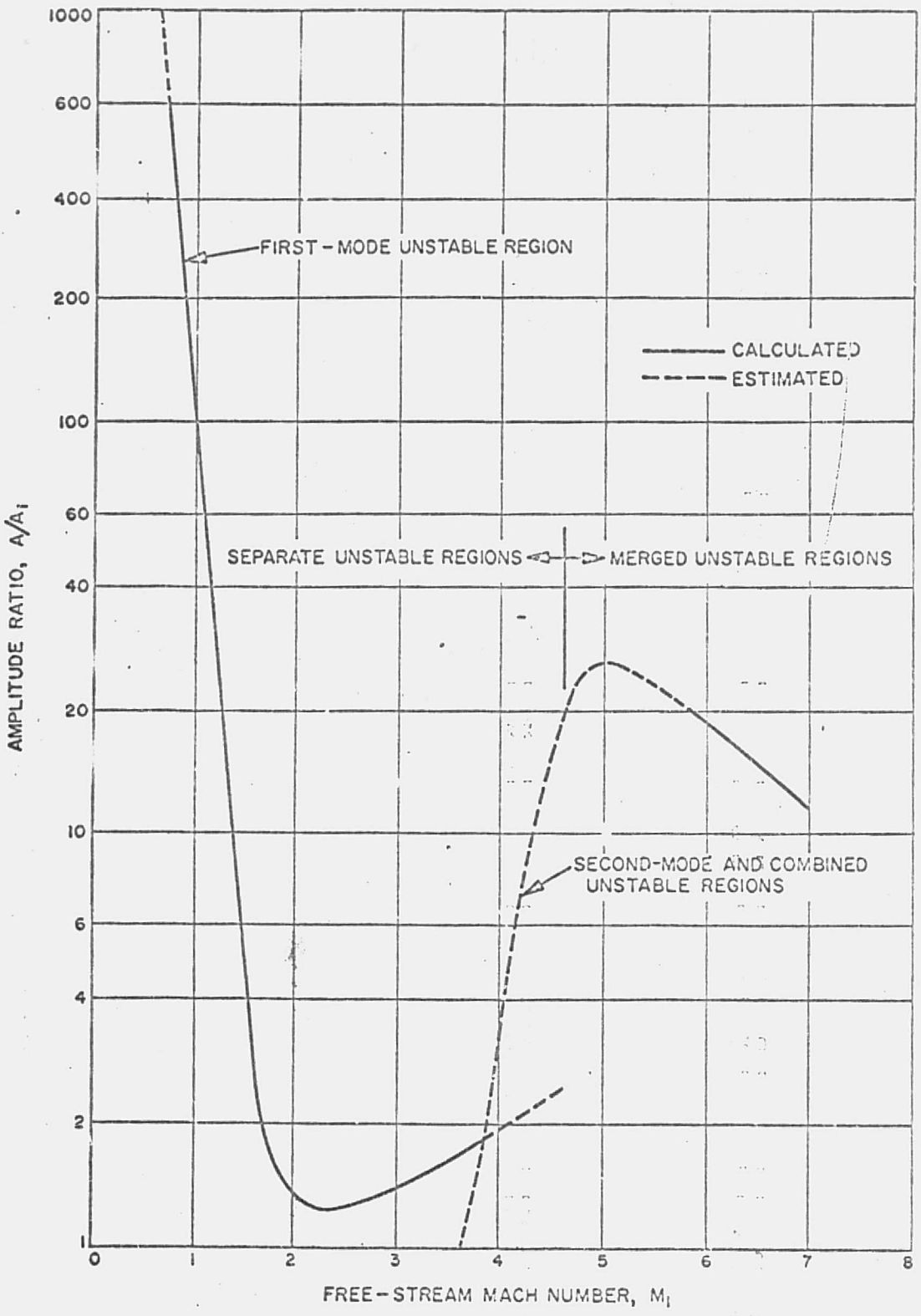

Fig. 17.13 Amplitude ratio of most unstable disturbance at R = 1500 as a function of free-stream Mach number. Insulated-wall boundary layer.

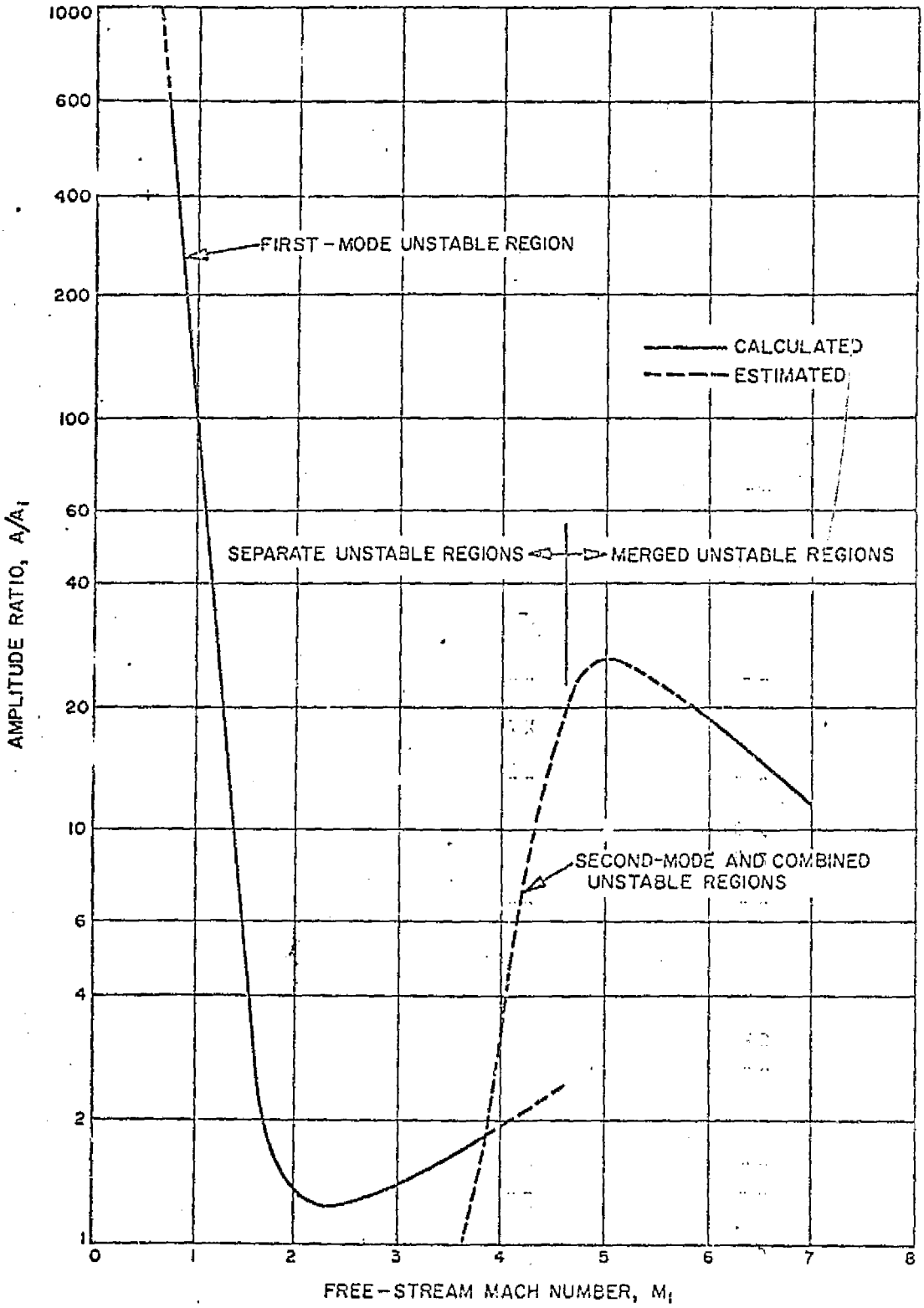

Fig. 17.13 Amplitude ratio of most unstable disturbance at R = 1500 as a function of free-stream Mach number. Insulated-wall boundary layer.

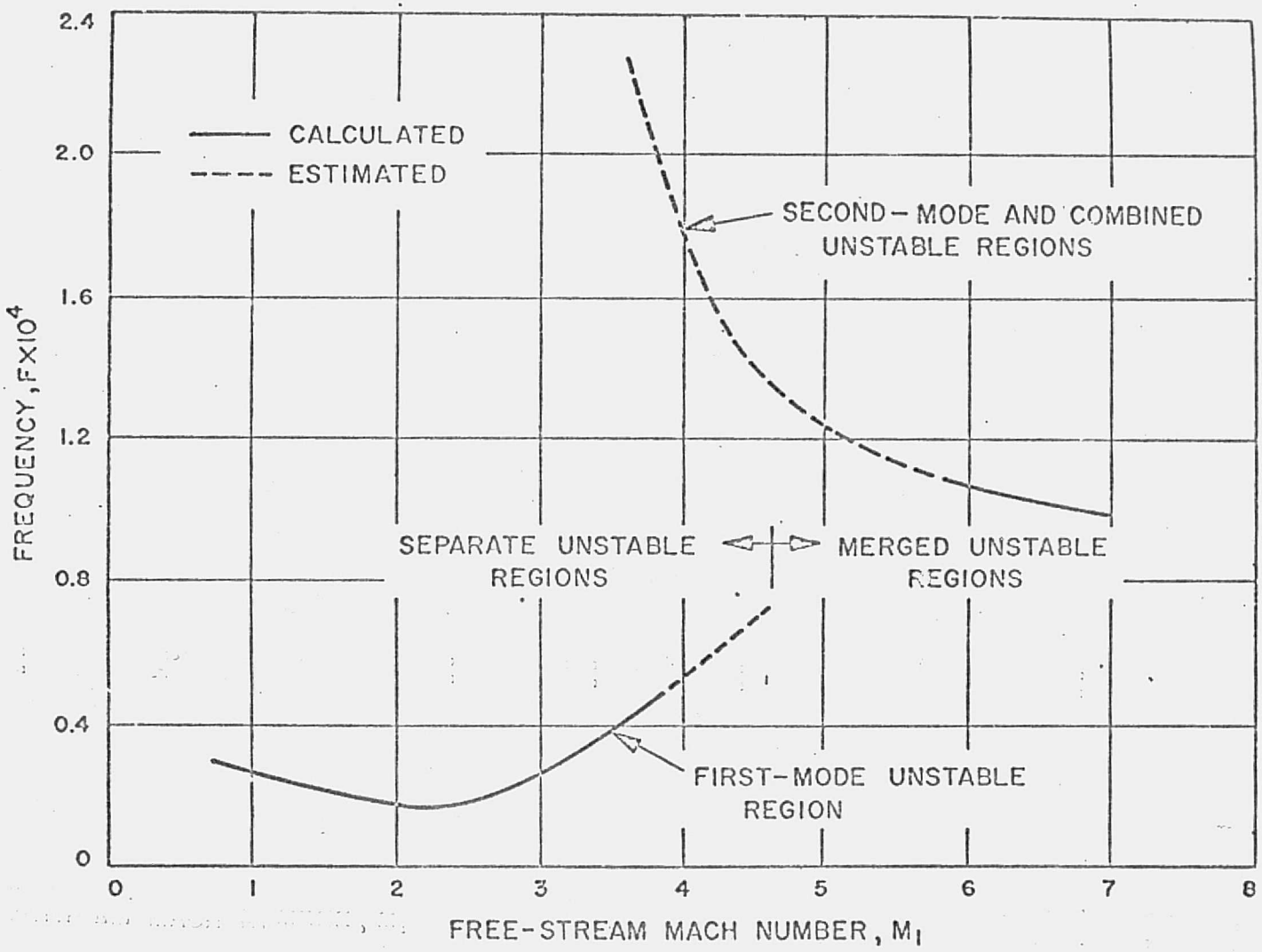

Fig. 17.14 Frequency of most unstable disturbance at R = 1500 as a function of free-stream Mach number. Insulated-wall boundary layer.

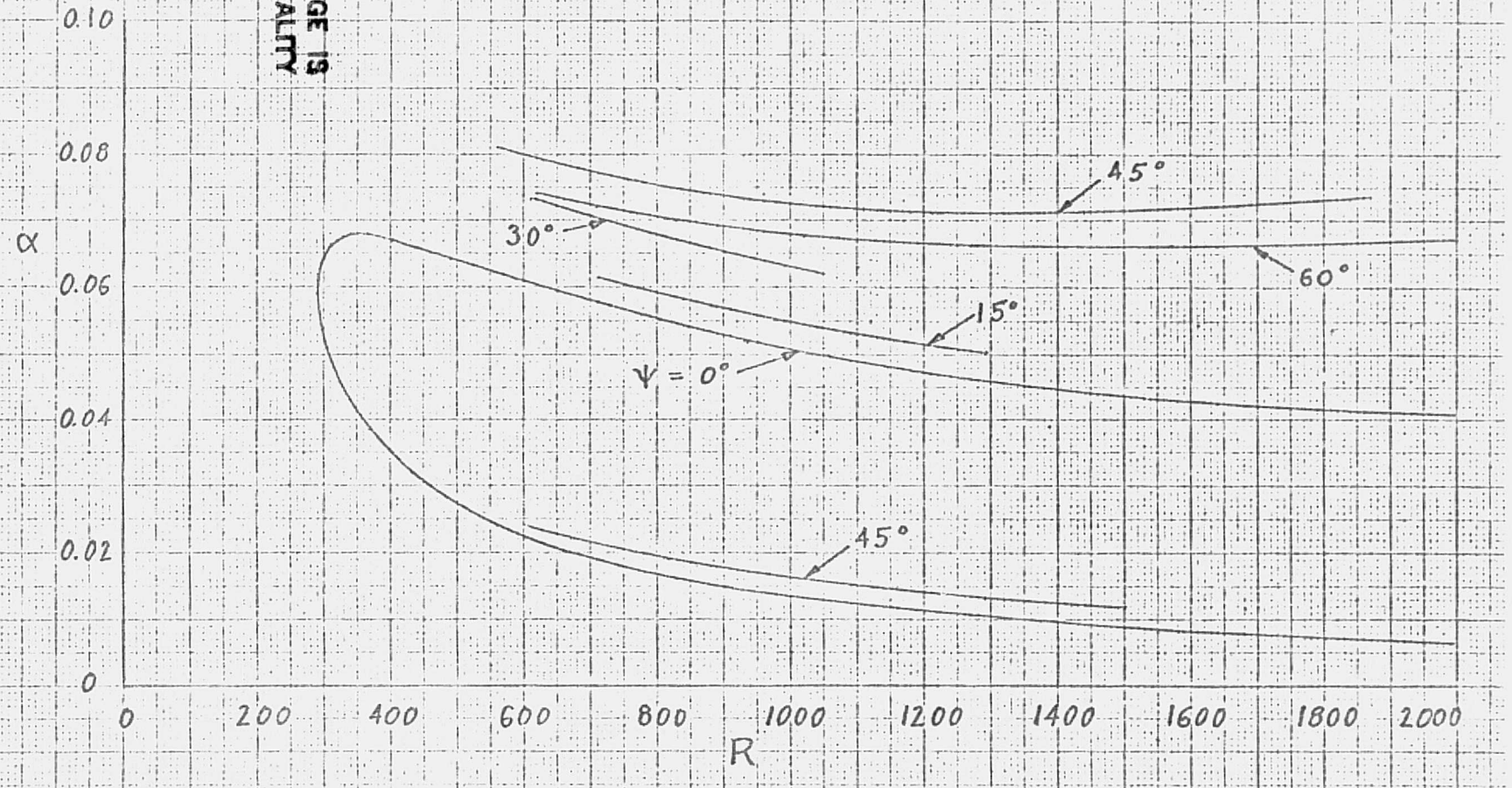

Fig. 18.1 Effect of wave angle on neutral-stability curve at $M_1 = 2.2$ (sixth-order system).

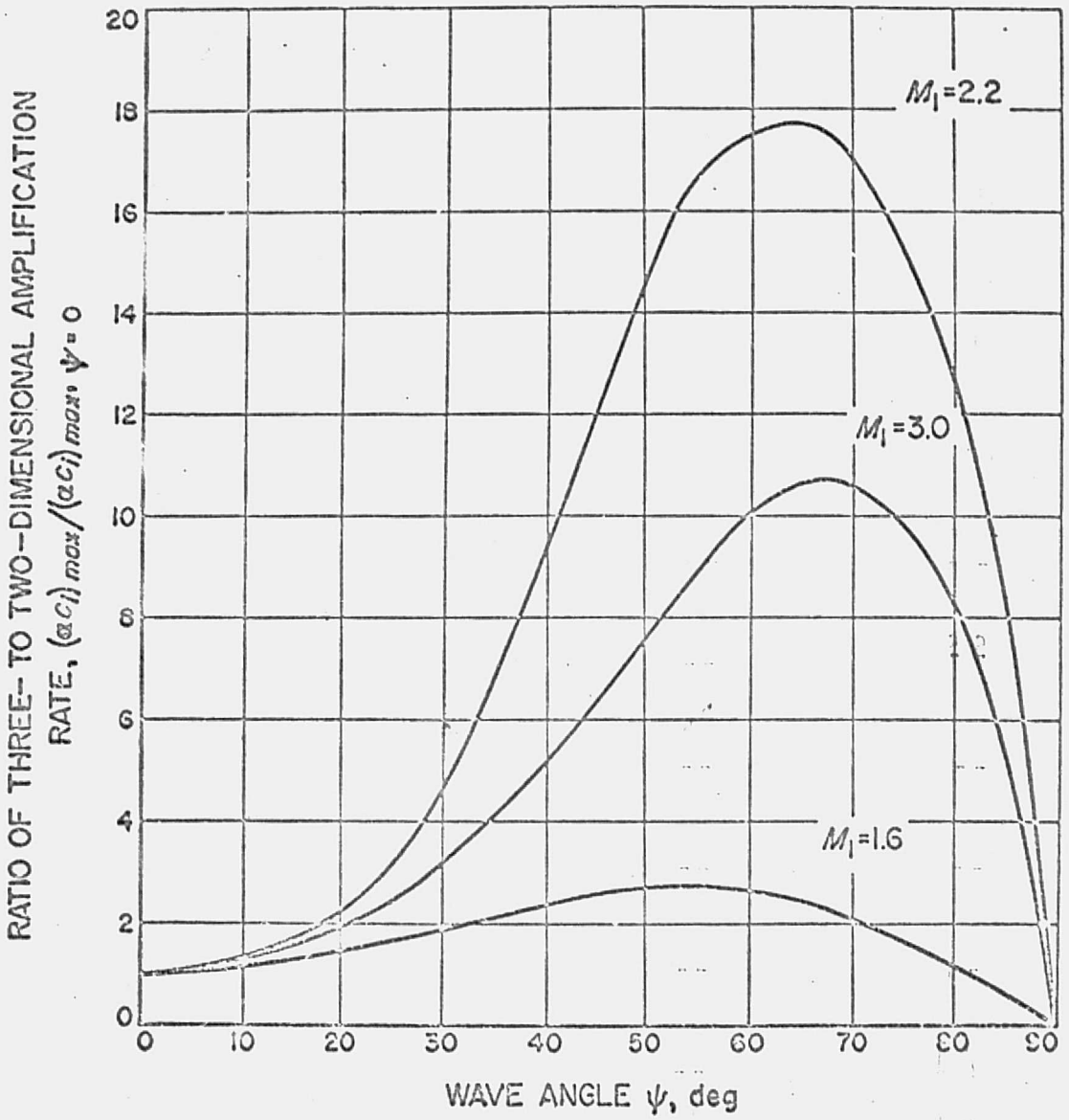

Fig. 18.2 **Effect of wave angle on the amplification rate of first-mode three-dimensional disturbances at $R = 1500$**

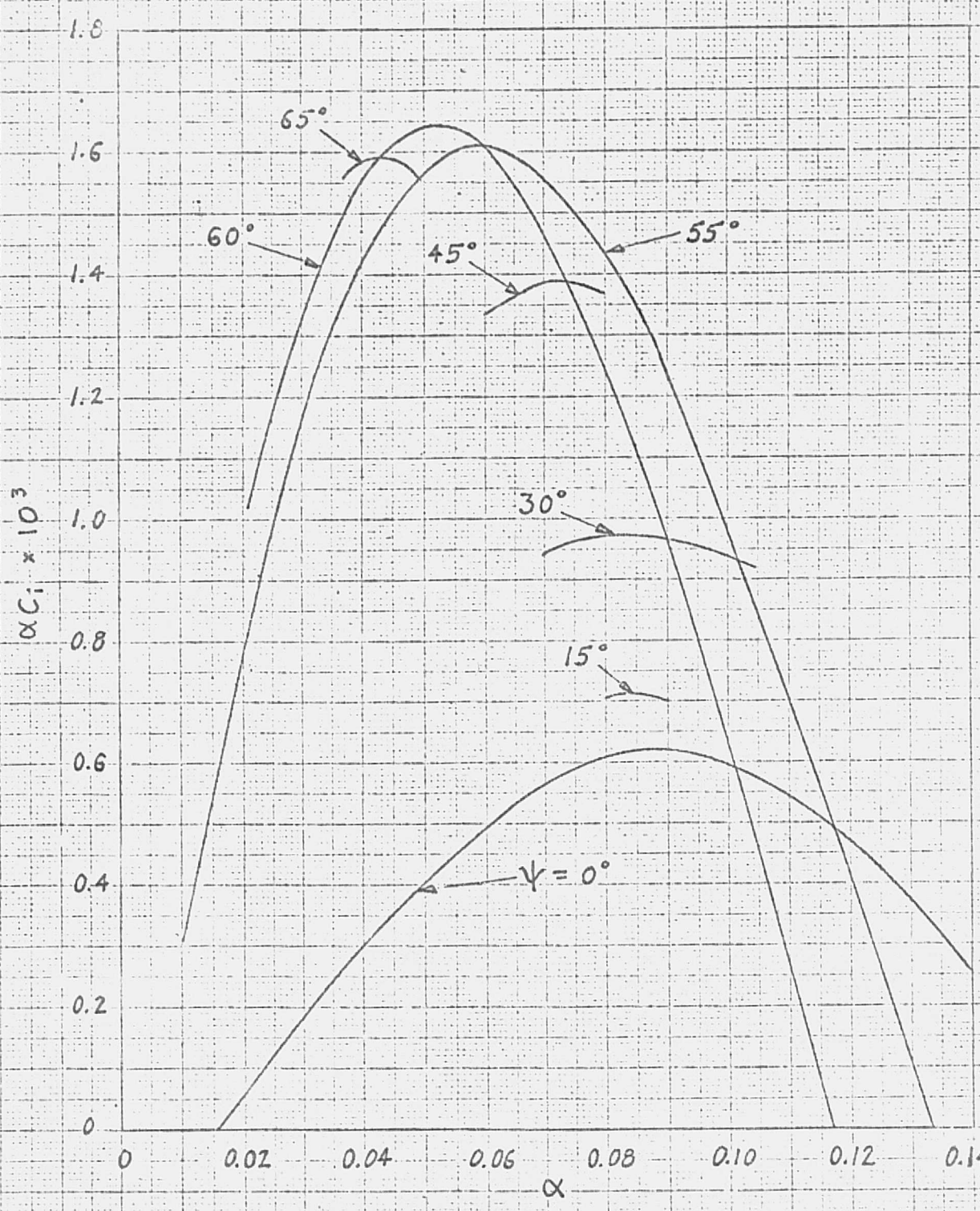

Fig. 18.3 Effect of wave angle on amplification rate at $M_1 = 4.5$ (sixth-order system).

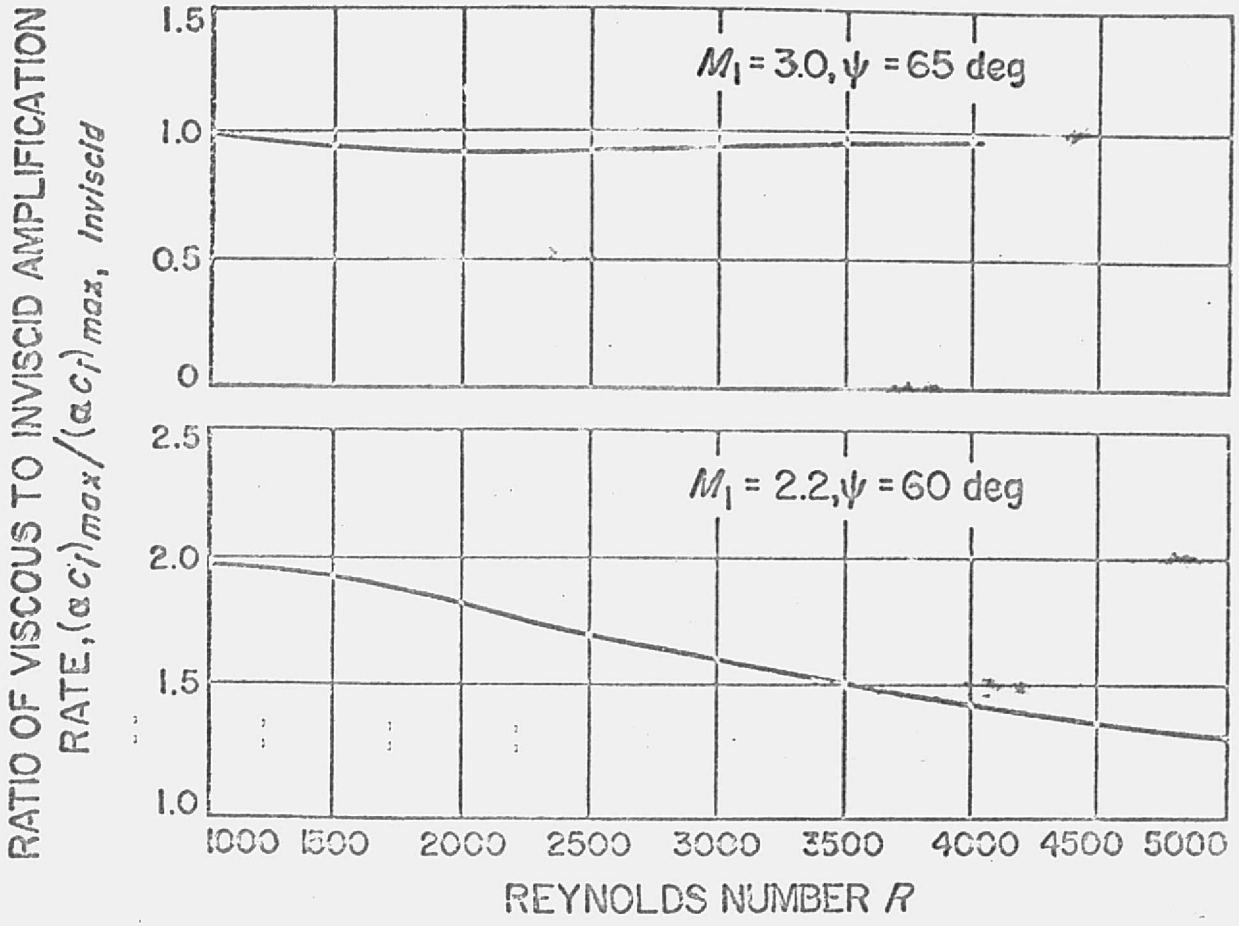

Fig. 18.4 Effect of Reynolds number on the maximum amplification rate of first-mode three-dimensional disturbances

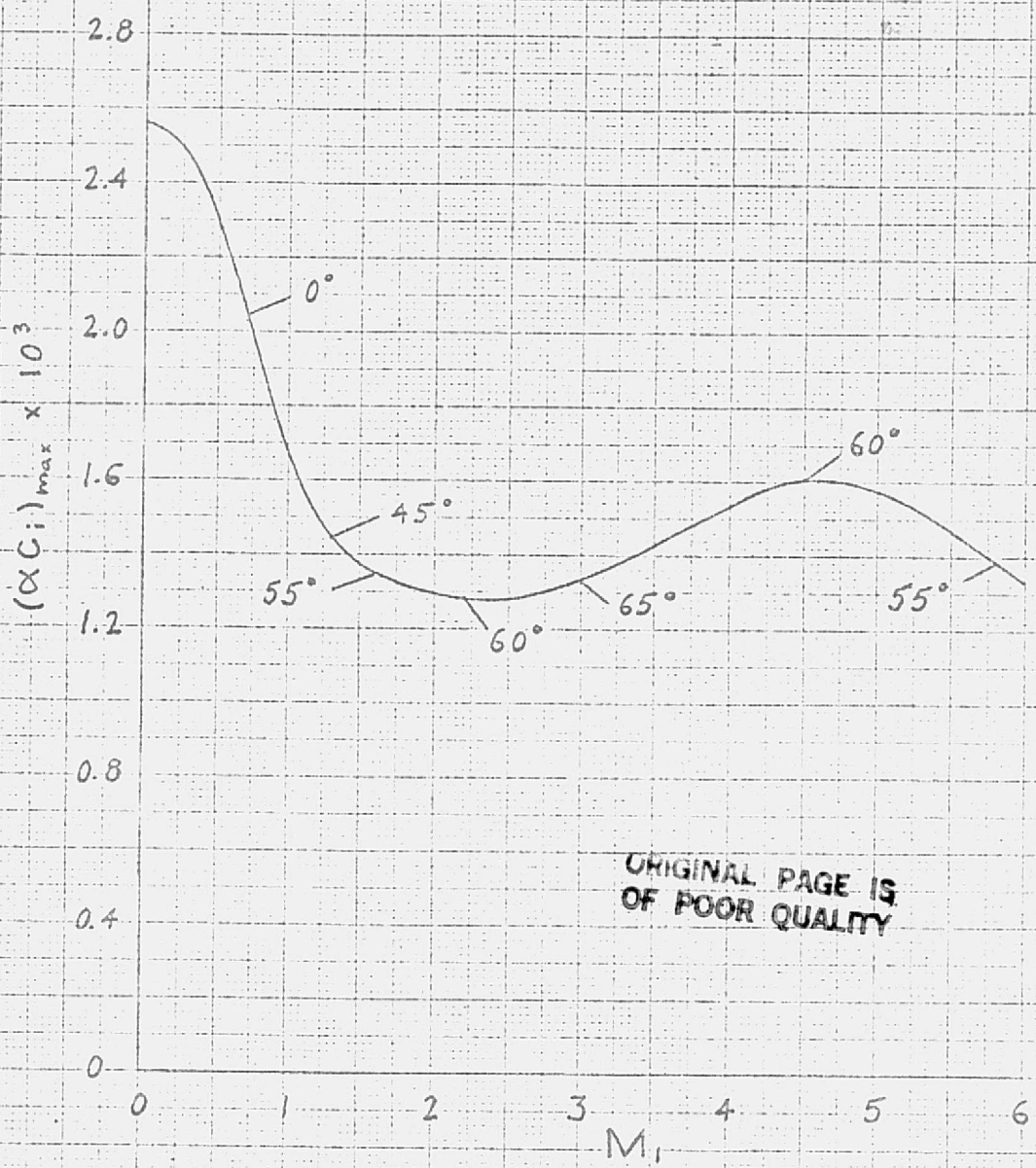

Fig. 18.5 Effect of Mach number on temporal amplification rate and wave angle of most unstable first-mode disturbance at R = 1500.

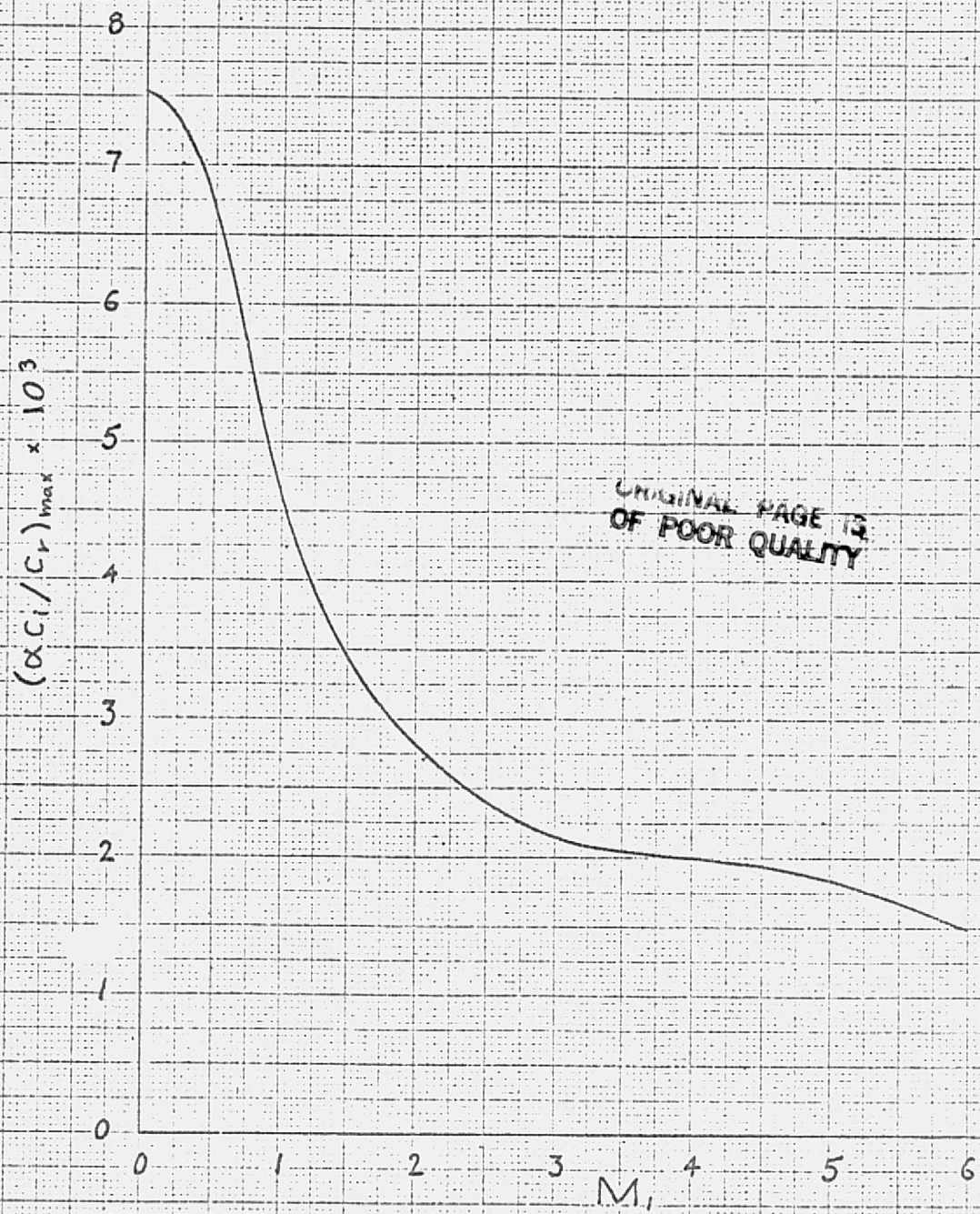

Fig. 18.6 Effect of Mach number on spatial amplification rate of most unstable first-mode disturbance at R = 1500.

M_1	R	α	ψ	6th order $\alpha c_i \times 10^3$	8th order $\alpha c_i \times 10^3$	% difference
1.3	500	0.075	45°	0.883	0.824	7.2
1.3	1500	0.060	45°	1.467	1.445	1.5
1.6	500	0.070	55°	0.974	0.874	11.4
1.6	1500	0.050	55°	1.384	1.346	2.8
2.2	500	0.055	60°	1.198	1.066	12.4
2.2	800	0.045	60°	1.391	1.300	7.0
2.2	1500	0.035	60°	1.325	1.273	4.1
4.5	500	0.045	60°	1.117	1.039	7.5
4.5	1500	0.050	60°	1.641	1.613	1.7
5.8	500	0.050	55°	0.790	0.736	7.3
5.8	1500	0.060	55°	1.403	1.384	1.4
10.0	1500	0.040	55°	0.444	0.434	2.3

Table 18.1 Comparison of amplification rates for three-dimensional disturbances as computed from sixth-order and eighth-order systems of equations at several Mach numbers.

zero term	% change in α_c; $M_1 = 2.2$	5.8	10.0
$2\mu \frac{dU}{dy} \frac{\partial \tilde{u}'}{\partial y}$	+ 1.4	+ 0.7	+ 0.9
$2\mu \frac{dU}{dy} \frac{\partial \tilde{v}'}{\partial \tilde{x}}$	0	- 0.1	- 0.4
$\frac{d\mu}{dT} \left(\frac{dU}{dy}\right)^2 \frac{T'}{\cos^2 \psi}$	- 0.1	- 1.2	- 2.4
$2\mu \frac{dU}{dy} \frac{\partial \tilde{w}'}{\partial y} \tan \psi$	+ 4.1	+ 1.4	+ 2.3
All zero	+ 5.3	+ 0.8	+ 0.4

Table 18.2 Comparison of individual energy-equation dissipation terms on amplification rate at R = 1500 for three Mach numbers.

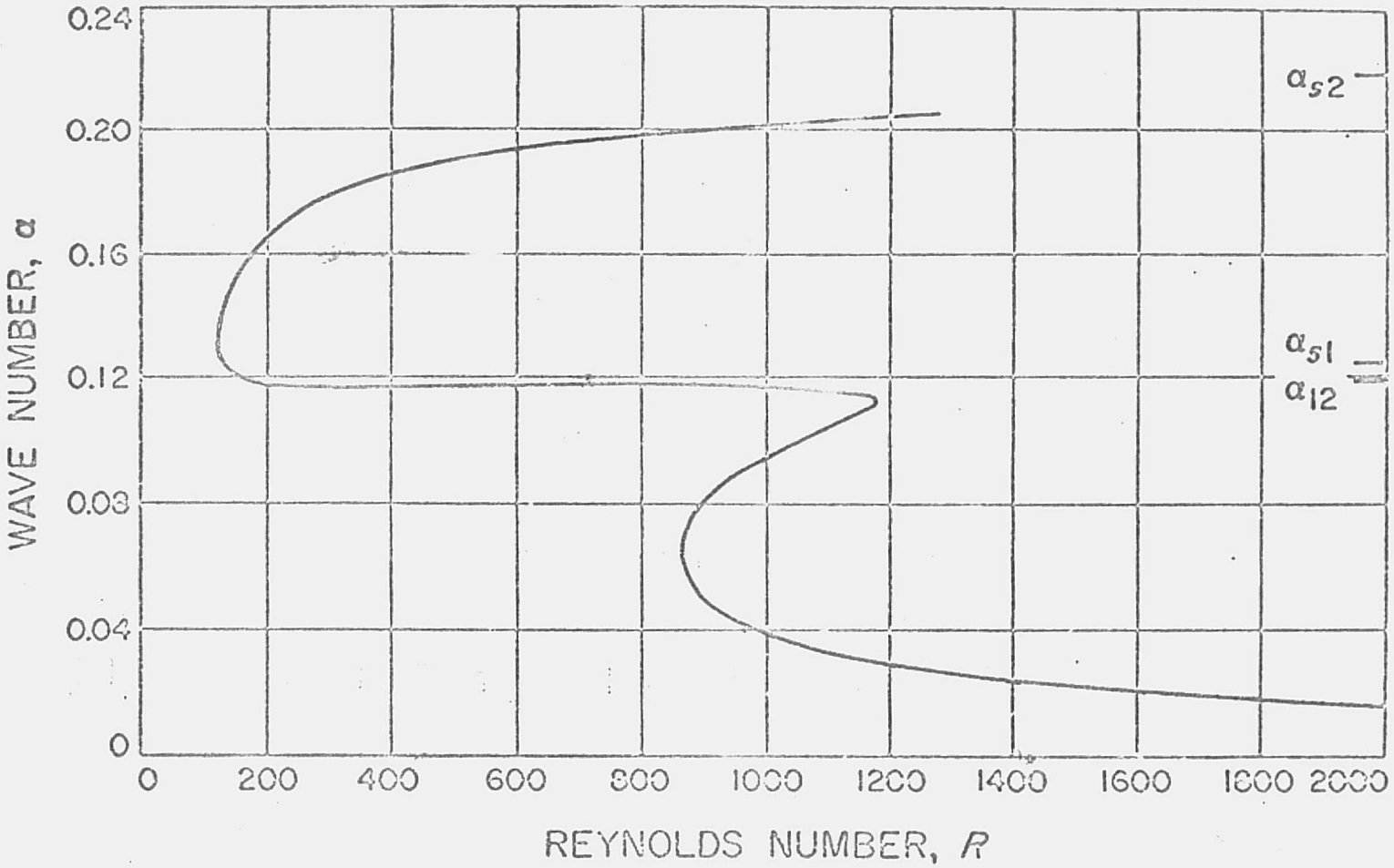

Fig. 19.1 Neutral-stability curve of wave number at $M_1 = 5.8$ (cooled boundary layer; $\theta_w = 0.50$)

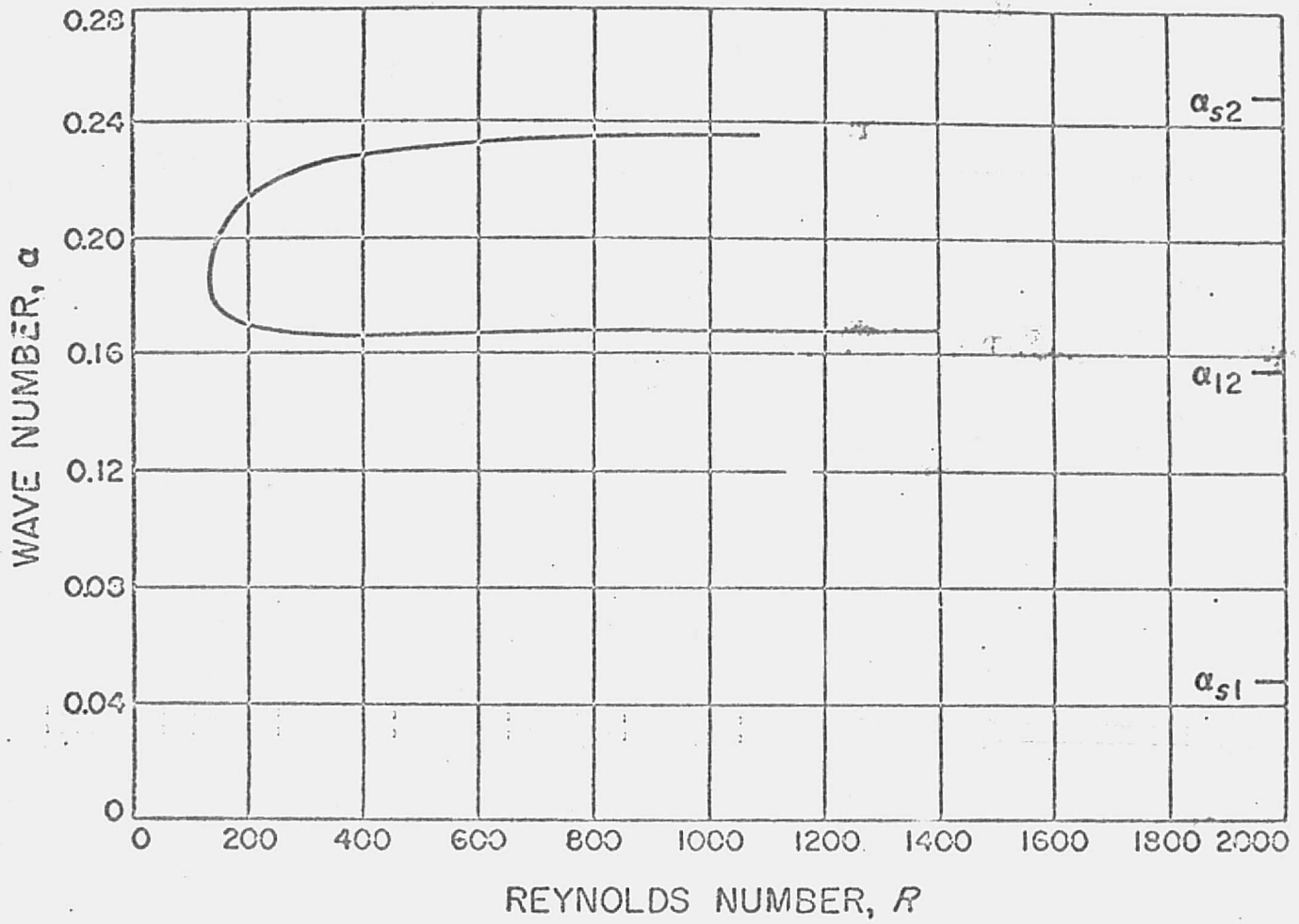

Fig. 19.2 Neutral-stability curve of wave number at $M_1 = 5.8$ (cooled boundary layer; $\theta_w = 0.10$)

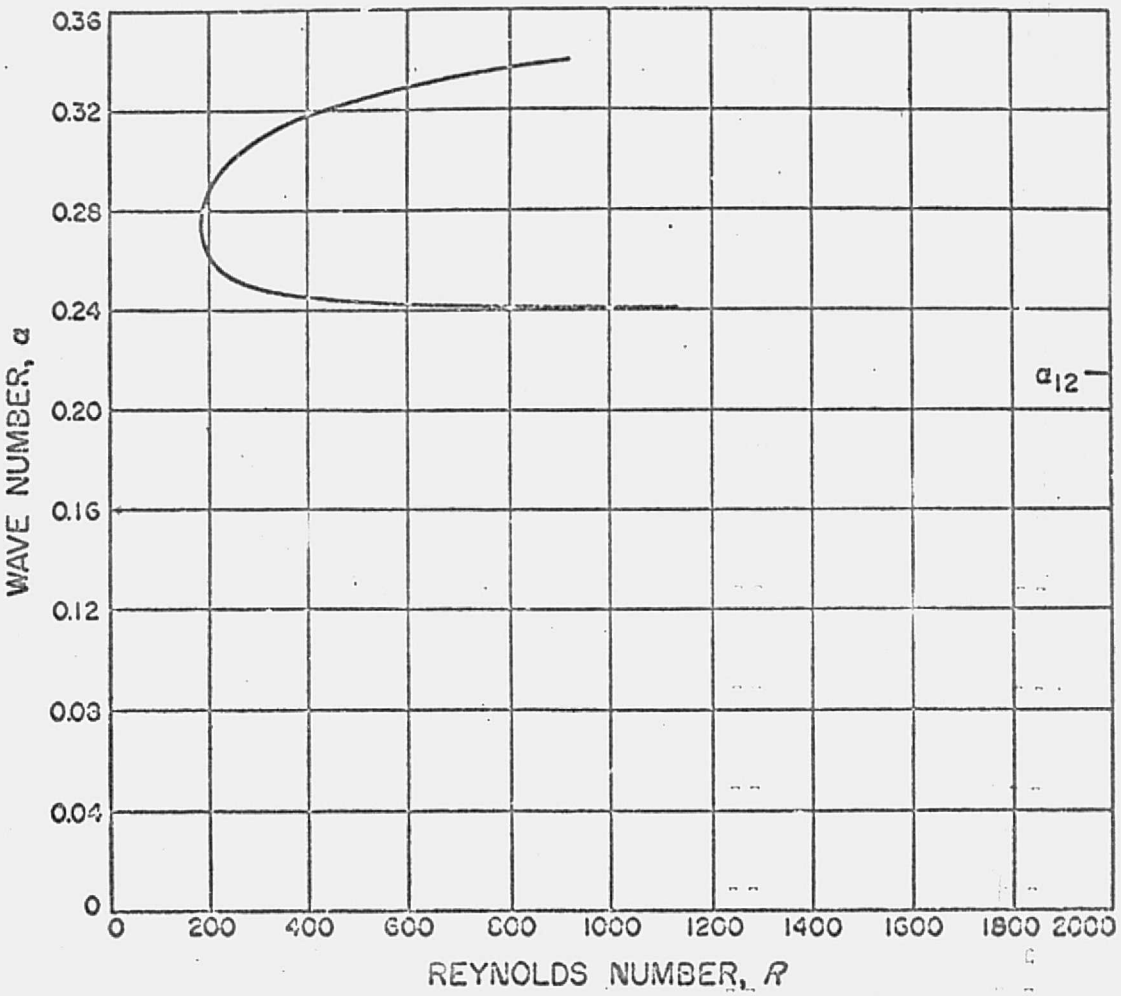

Fig. 19.3 **Neutral-stability curve of wave number at $M_1 = 5.8$ (cooled boundary layer; $\theta_w = -0.10$)**

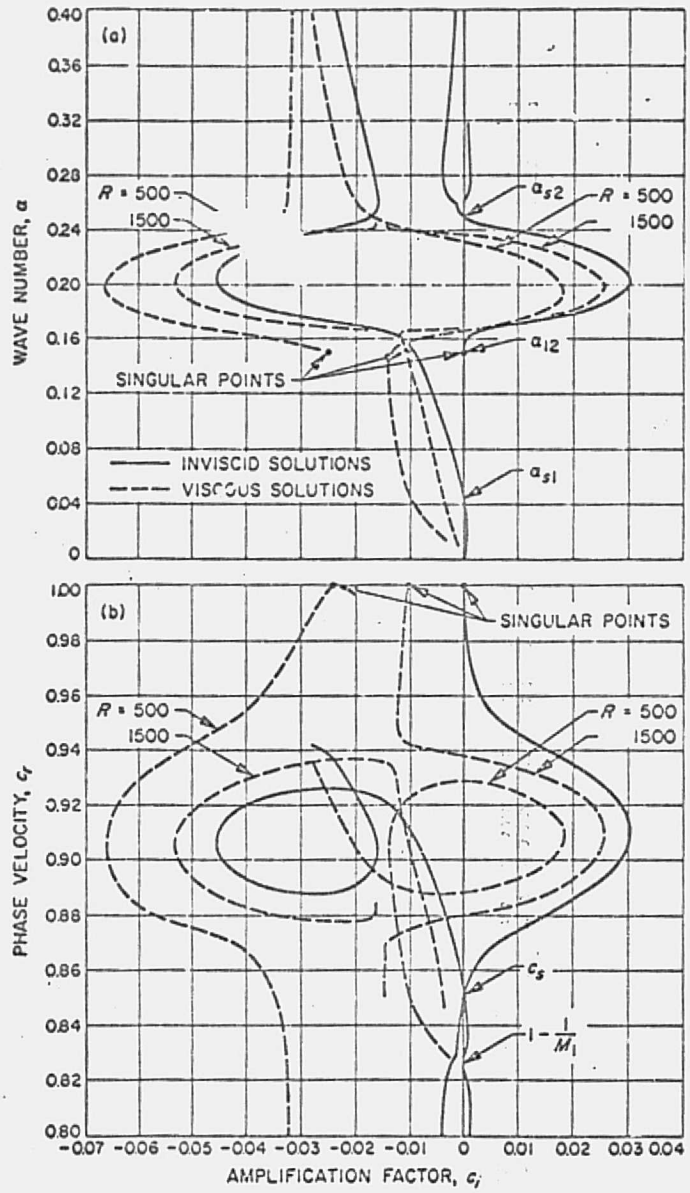

Fig. 19.4 Viscous and inviscid eigenvalues for cooled-wall boundary layer at $M_1 = 5.8$, $T_w/T_r = 0.25$; (a) α vs c_i, (b) c_r vs c_i

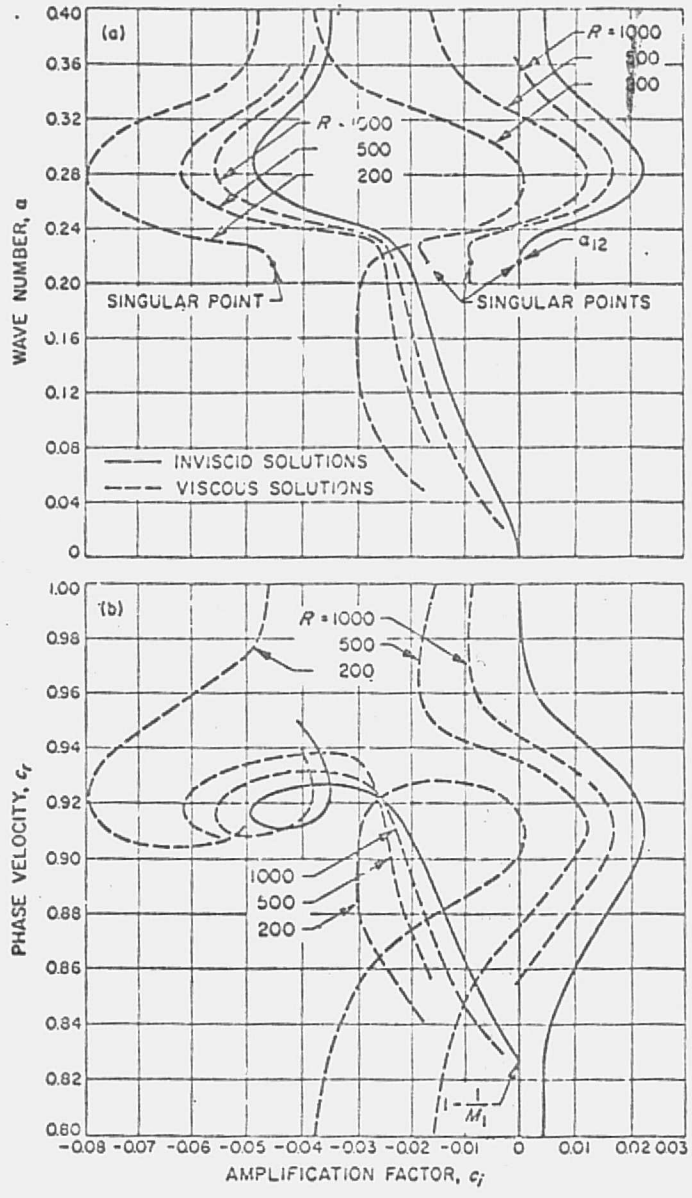

Fig. 19.5 Viscous and inviscid eigenvalues for cooled-wall boundary layers at $M_1 = 5.8$, $T_w/T_r = 0.05$; (a) a vs c_i, (b) c_r vs c_i

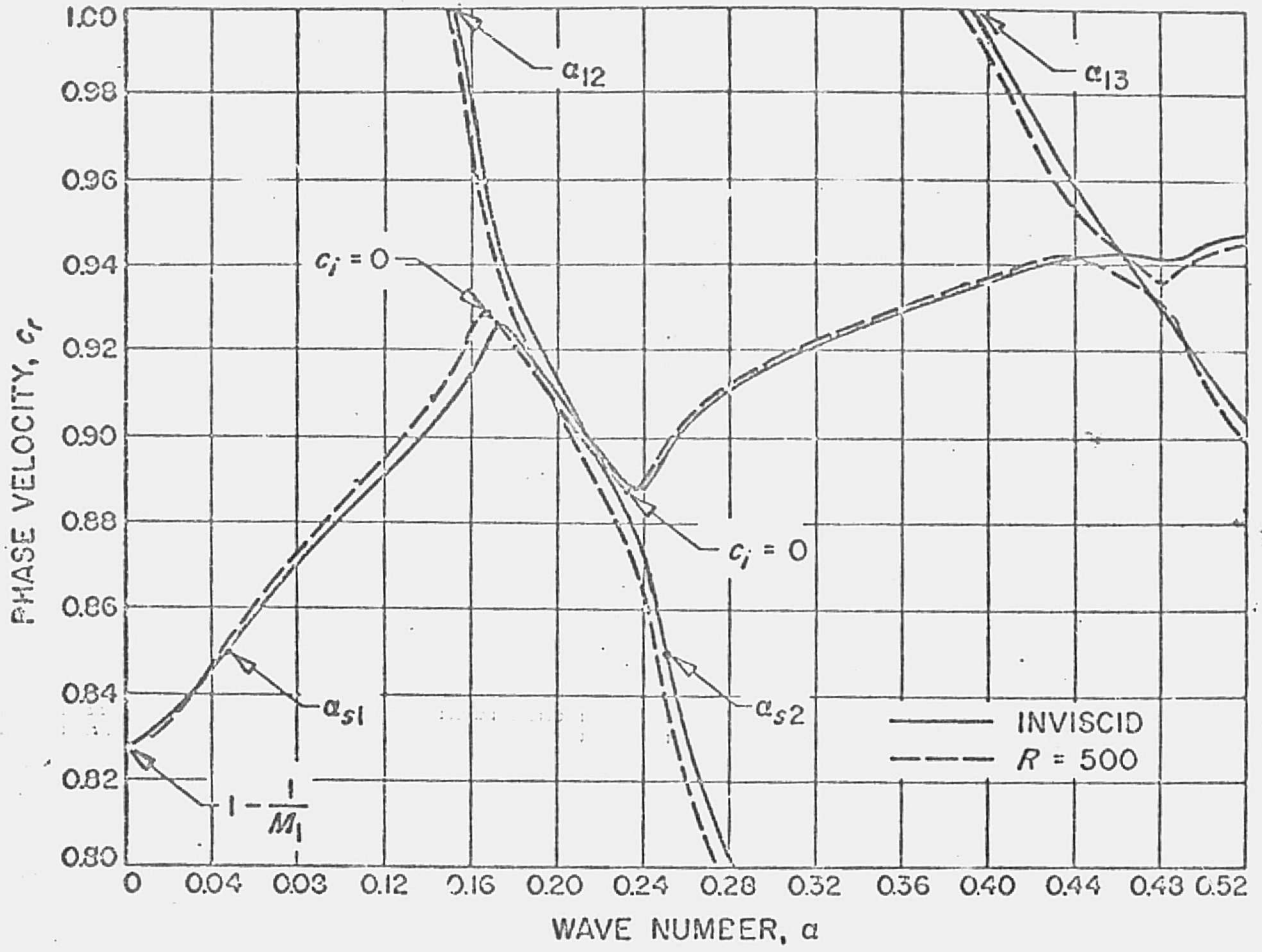

Fig. 19.6 **Phase velocity vs wave number for cooled-wall boundary layer at $M_1 = 5.8$, $T_w/T_r = 0.25$**

Fig. 19.7 EFFECT OF COOLING ON MAXIMUM AMPLIFICATION RATES $M_1 = 5.8$

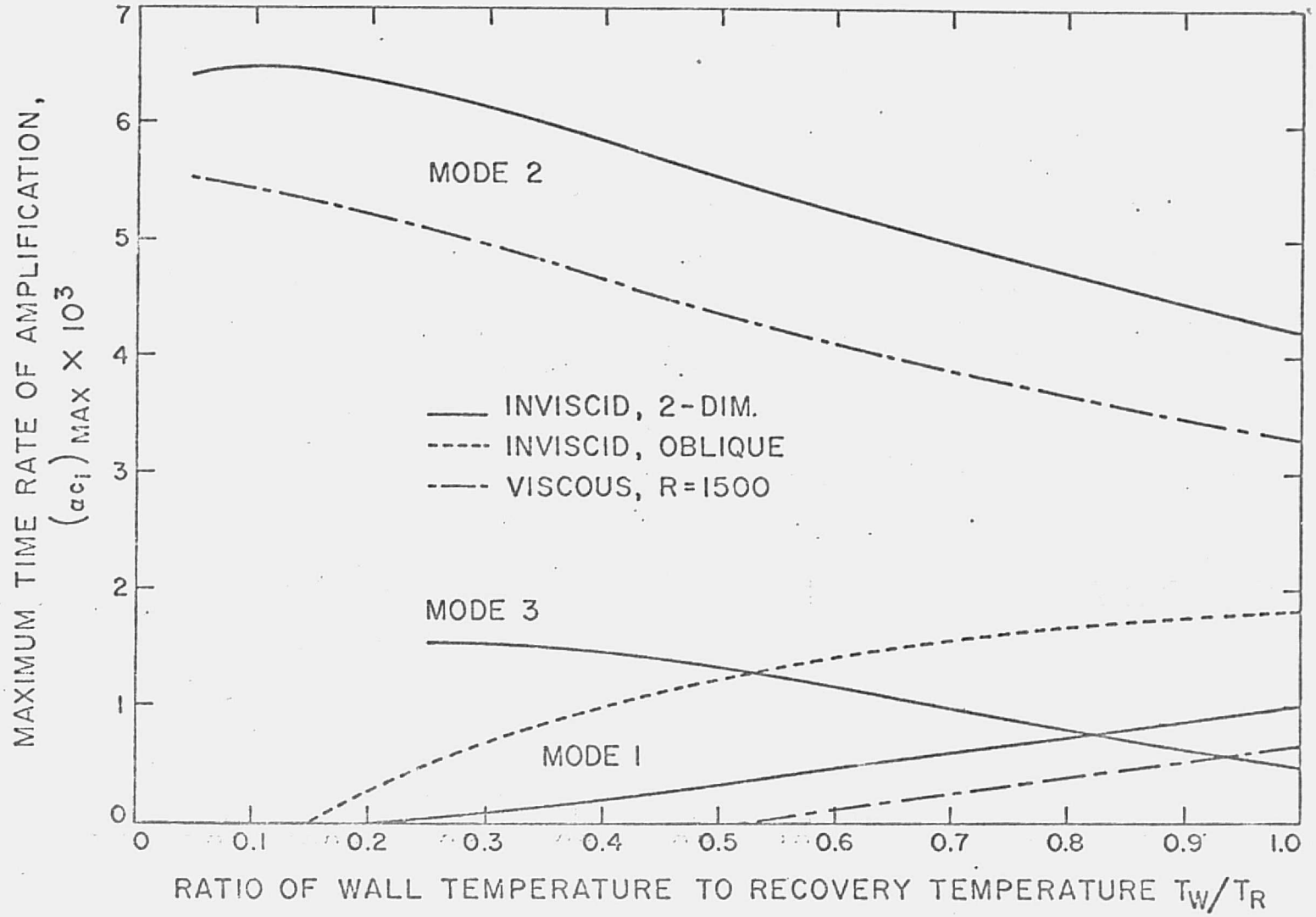

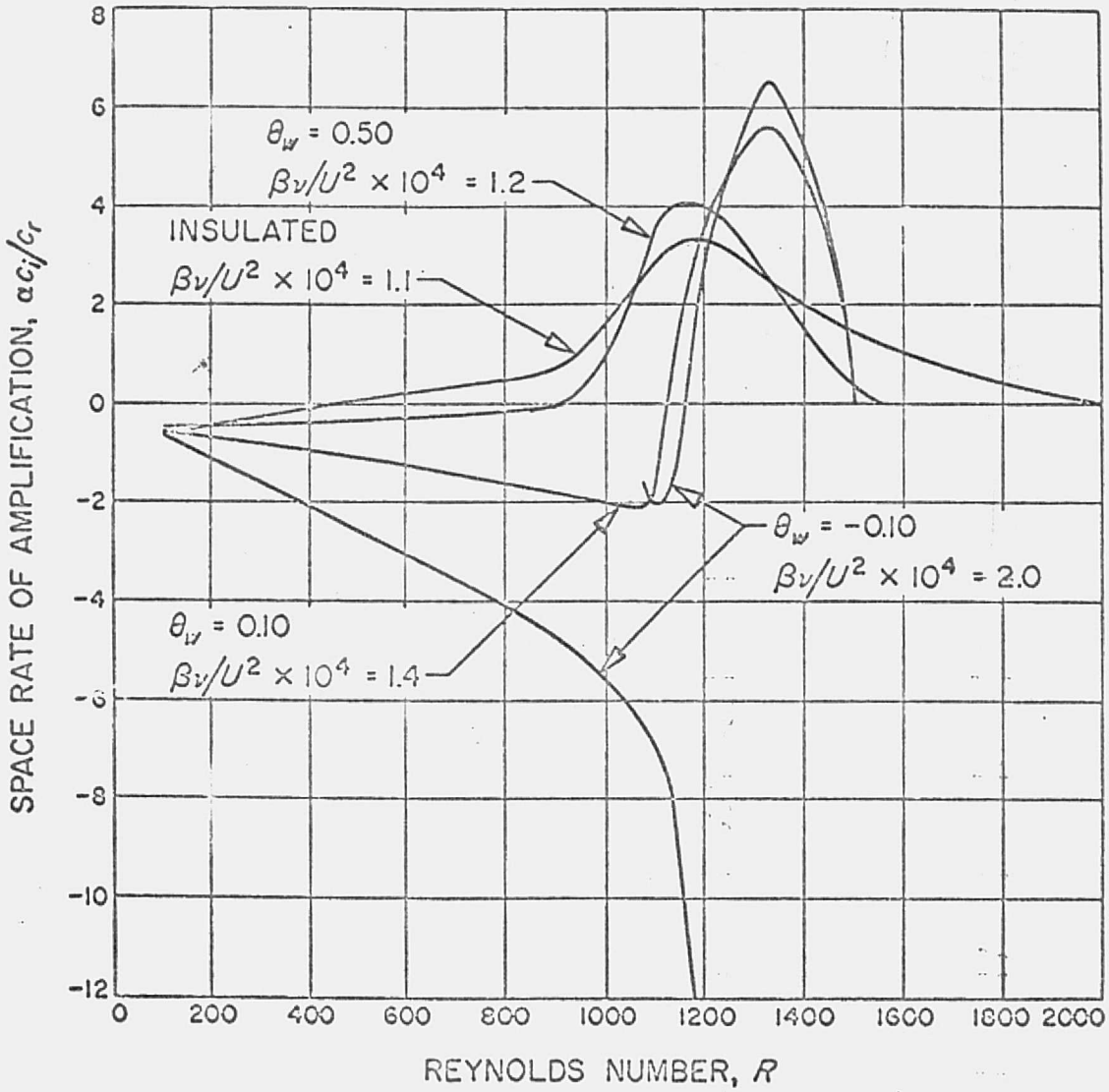

Fig. 19.8 **Amplification rate of the most unstable frequency at $R = 1500$ vs Reynolds Number for the insulated and cooled boundary layers**

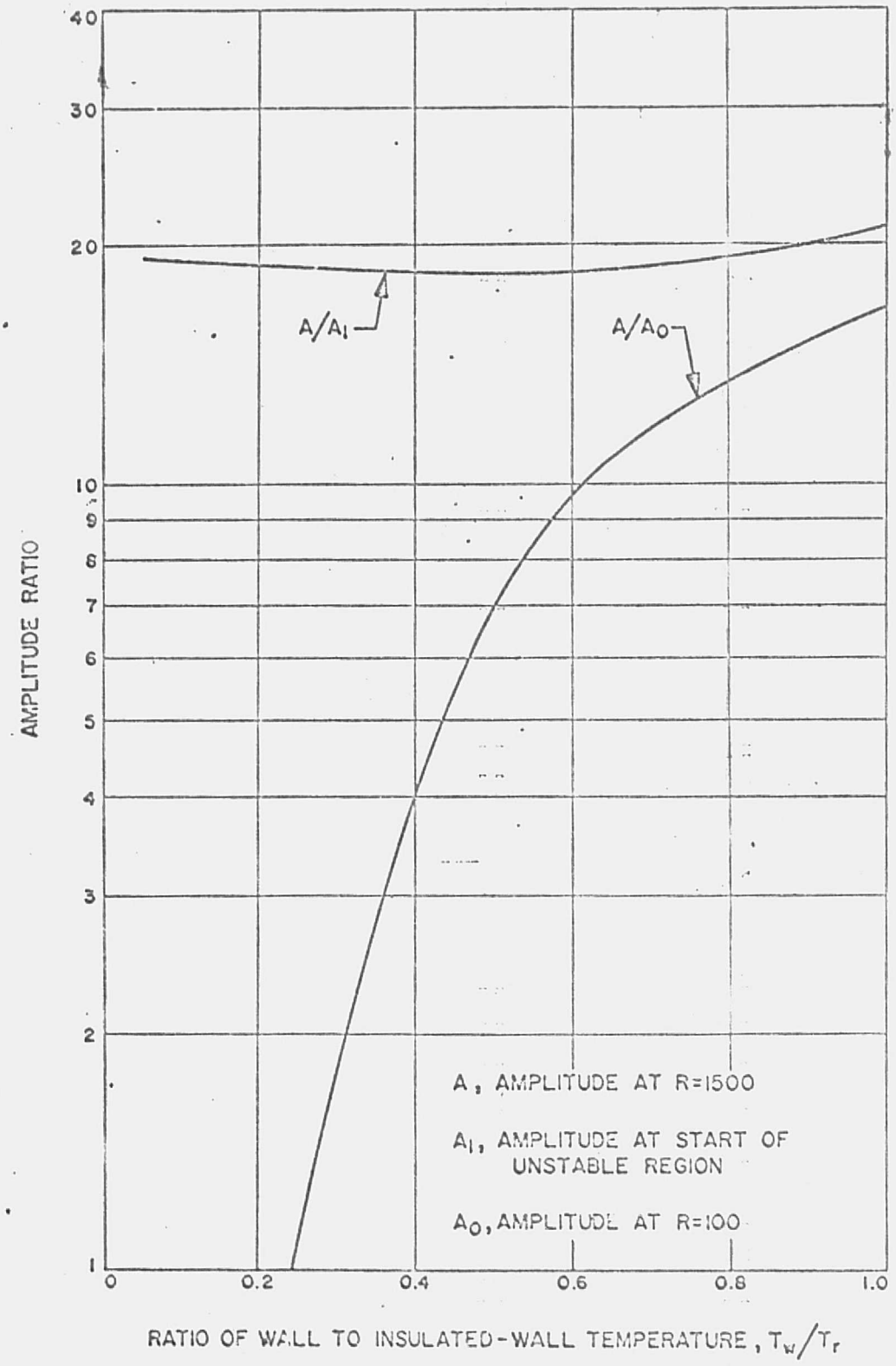

Fig. 19.9 Effect of cooling at $M_1 = 5.8$ on the amplification at $R = 1500$ of two types of disturbances.

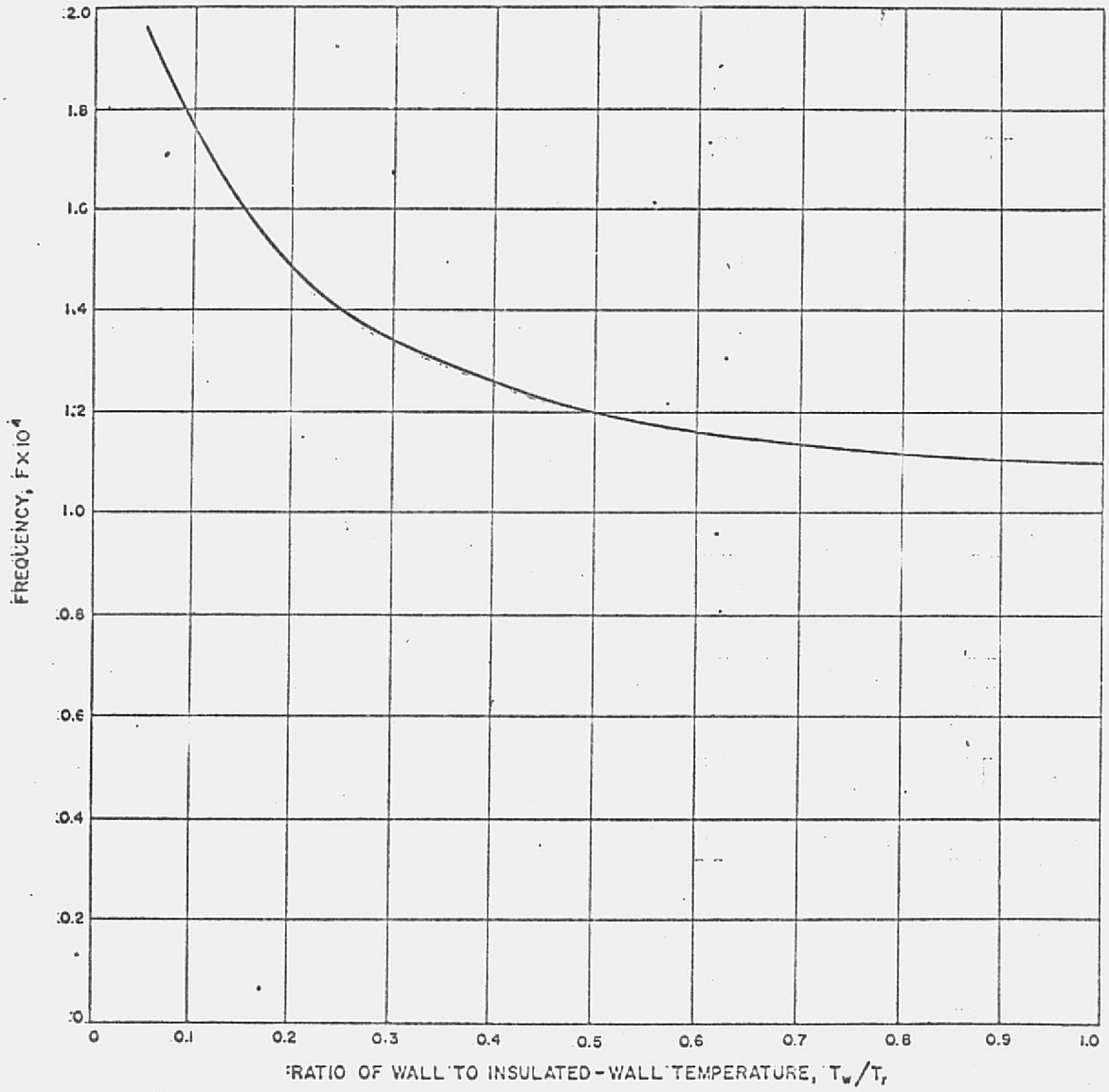

Fig. 19.10 Effect of cooling at $M_1 = 5.8$ on the most unstable frequency at $R = 1500$.

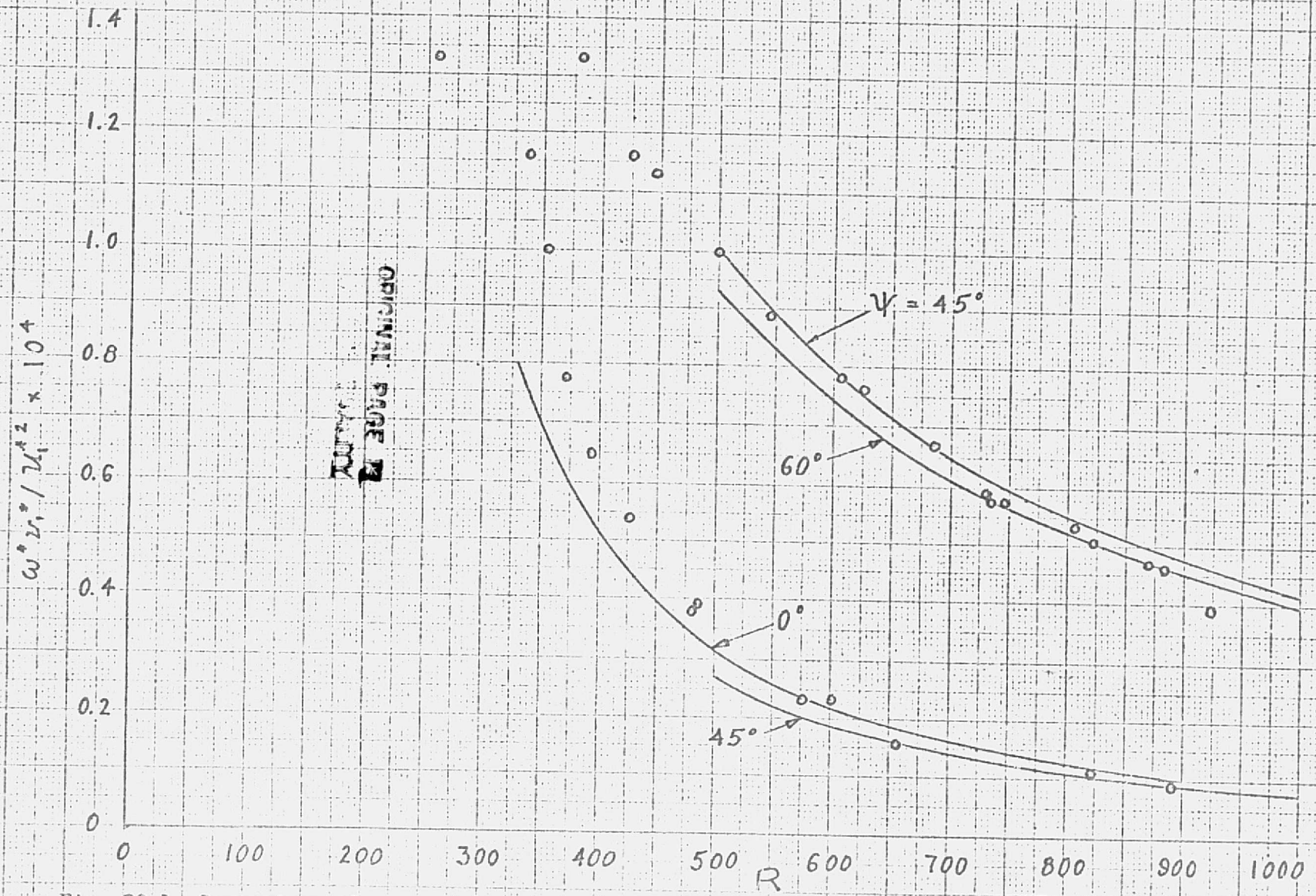

Fig. 20.1 Comparison of approximate neutral stability curves for three-dimensional disturbances at $M_1 = 2.2$ with Laufer and Vrebalovich (1960) experimental points.

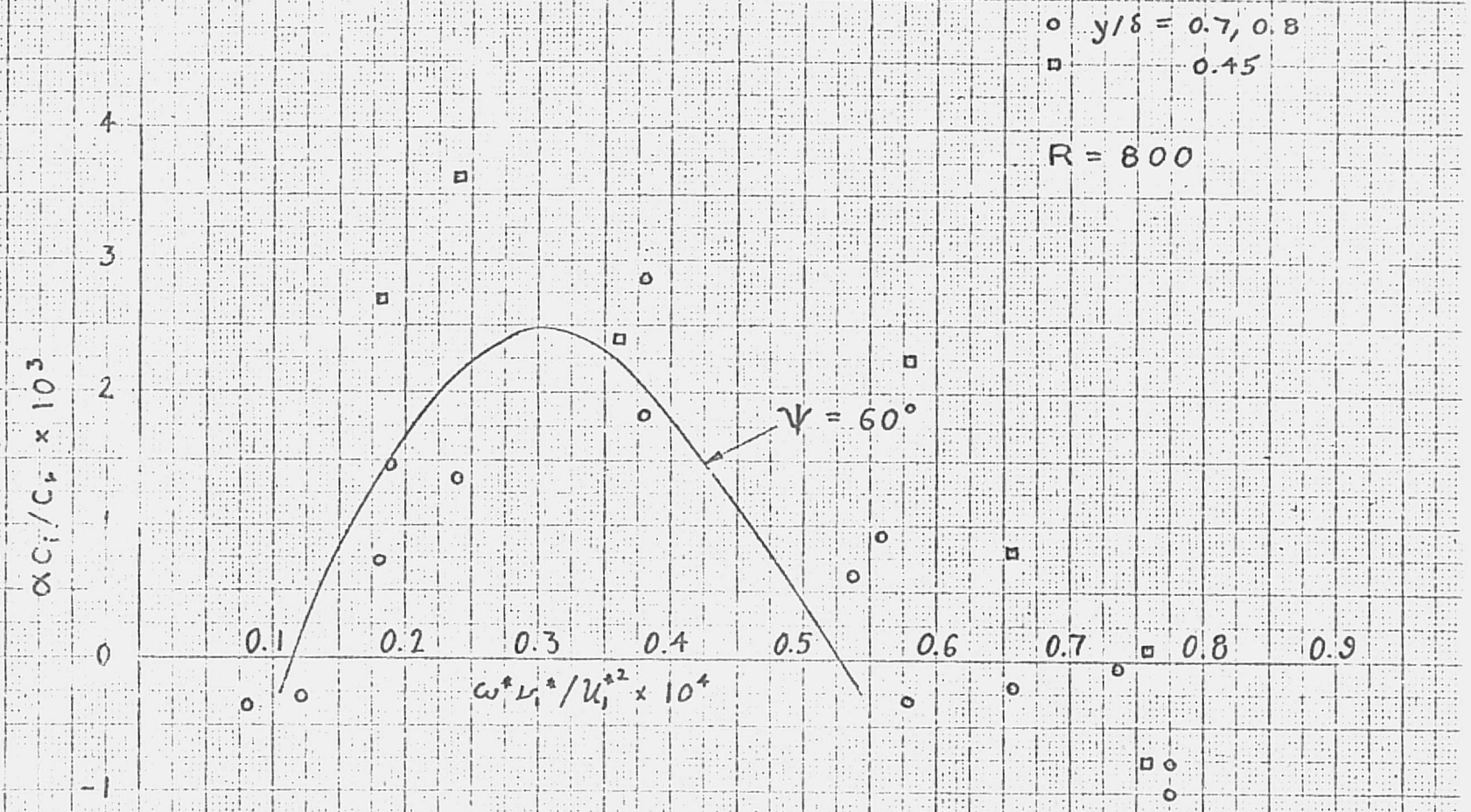

Fig. 20.2 Comparison of calculated spatial amplification rates of 60° wave at $M_1 = 2.2$ with measurements of Laufer and Vrebalovich (1960).

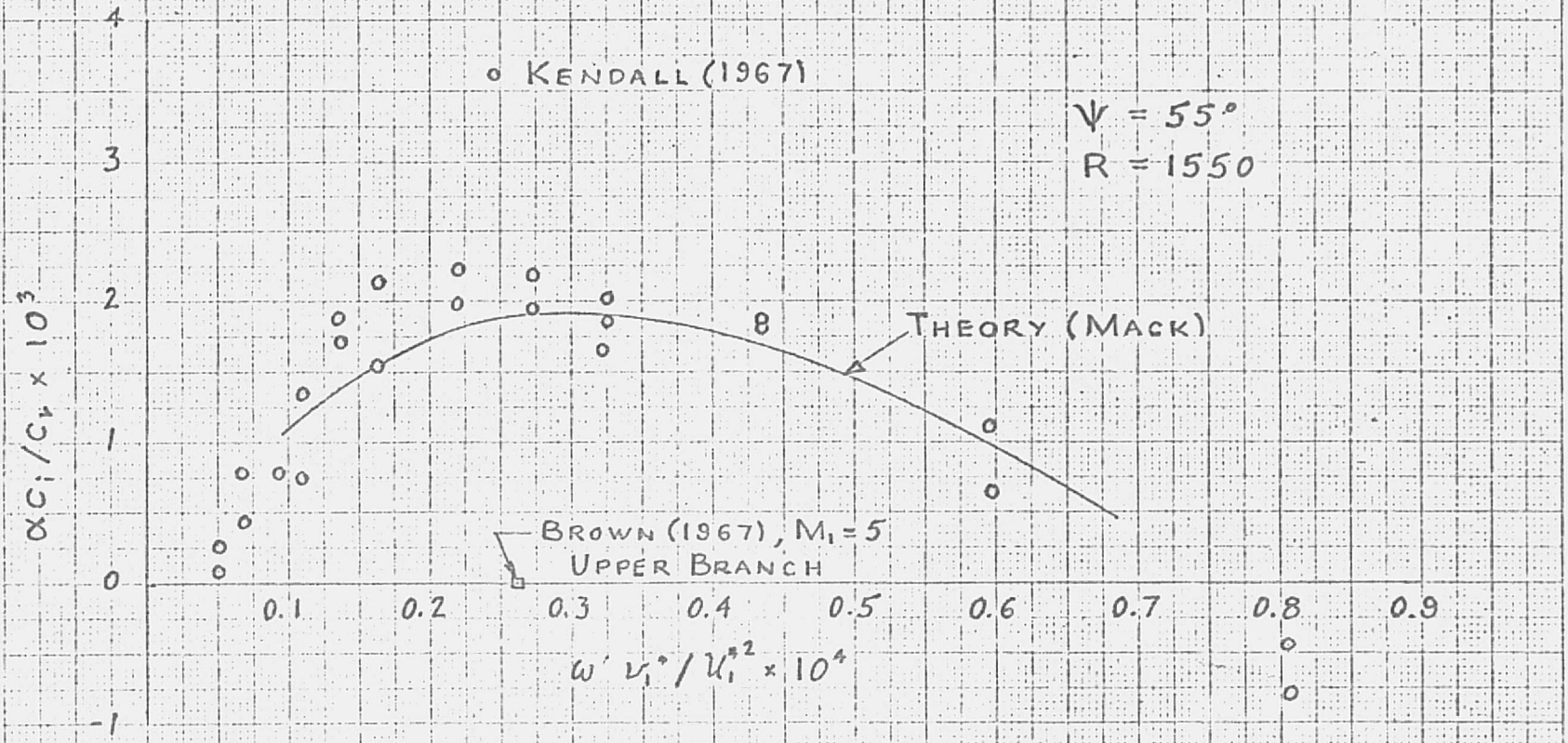

Fig. 20.3 Comparison of calculated first-mode spatial amplification rate at $M_1 = 4.5$ for 55° wave with measurements of Kendall (1967).

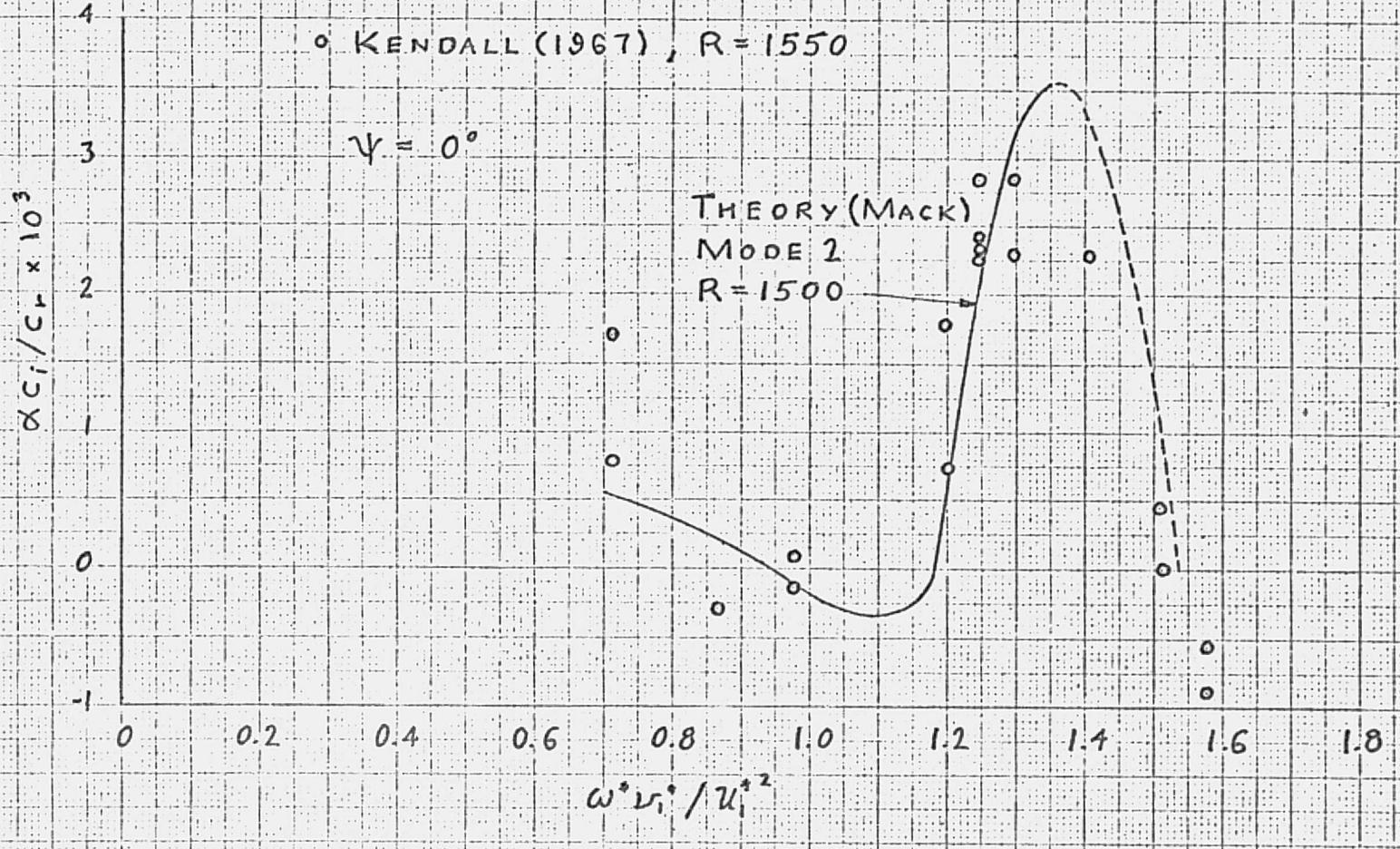

Fig. 20.4 Comparison of calculated second-mode amplification rate at $M_1 = 4.5$ for two-dimensional wave with measurements of Kendall.

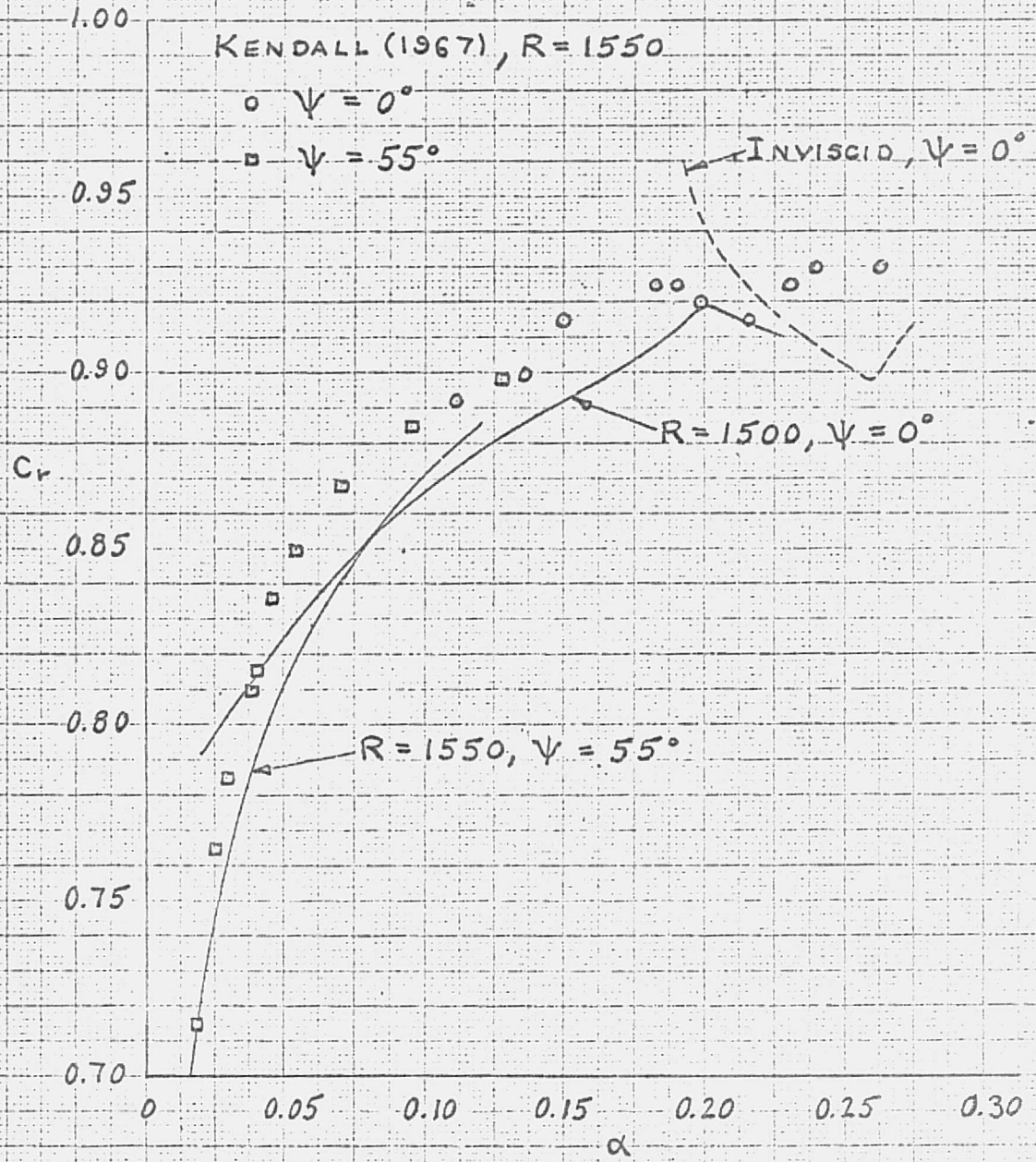

Fig. 20.5 Comparison of theoretical and experimental dispersion relations at $M_1 = 4.5$.

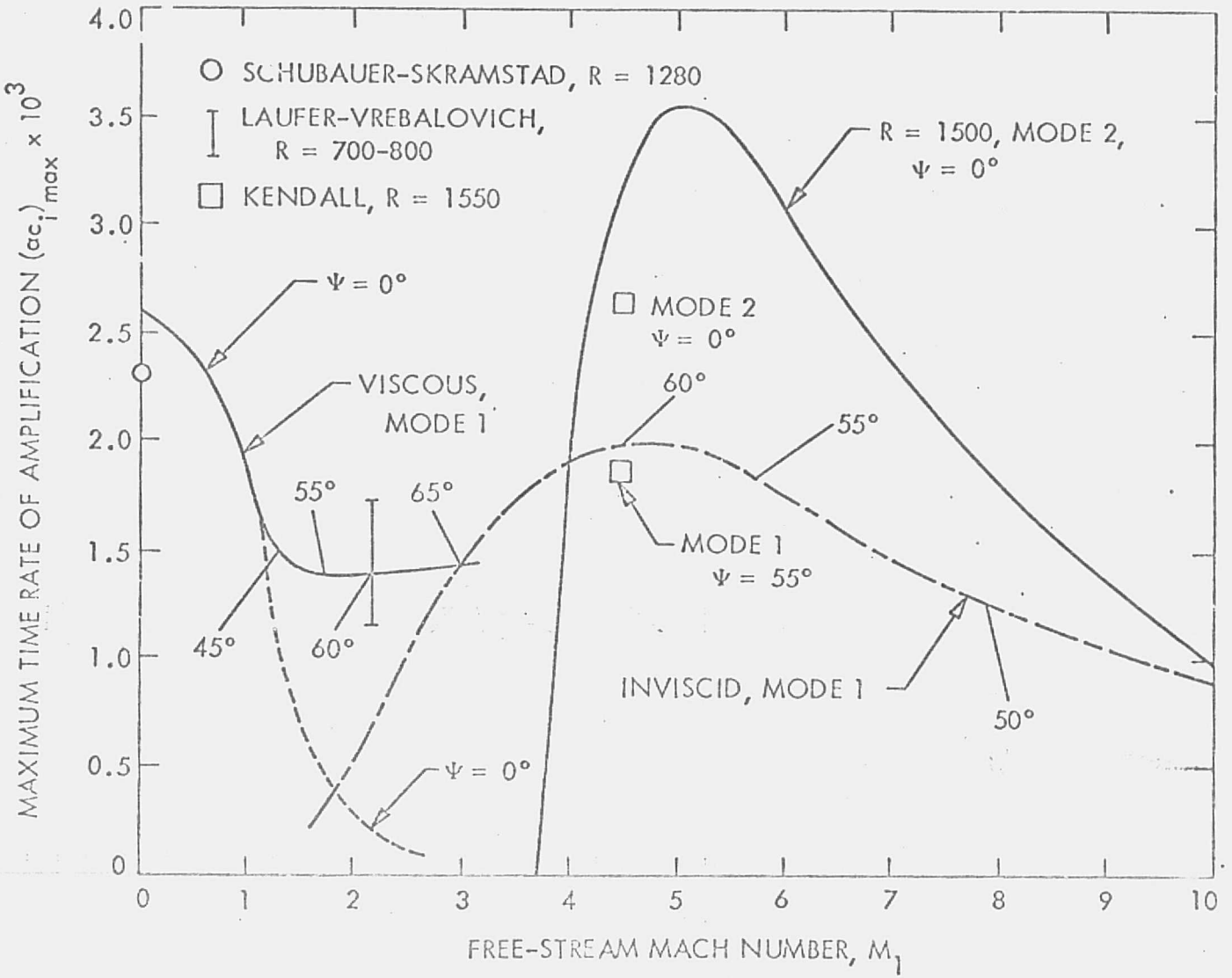

Fig. 20.6 Summary of maximum temporal amplification rates of first and second modes as functions of Mach number.

References

Betchov, R. (1965). Stability of parallel flows with frequency-dependent viscosity. Phys. Fluids 8, 1910-1911.

Bellman, R. E., and Kalaba, R. E. (1965). "Quasilinearization and Boundary-Value Problems." American Elsevier, New York.

Betchov, R., and Criminale, W. O. (1967). "Stability of Parallel Flows." Academic Press, New York.

Brown, W. B., and Sayre, P. H. (1954). An exact solution of the Orr-Sommerfeld stability equation for low Reynolds numbers. Northrop Aircraft Rept. No. BLC-43.

Brown, W. B. (1959). Numerical calculation of the stability of cross flow profiles in laminar boundary layers on a rotating disc and on a swept back wing and an exact calculation of the stability of the Blasius velocity profile. Northrop Aircraft Inc., Rep. NAI 59-5.

Brown, W. B. (1961). Exact solution of the stability equations for laminar boundary layers in compressible flow. In "Boundary Layer and Flow Control" (G. V. Lachmann, ed.), Vol. 2, pp. 1033-1048. Pergamon, London.

Brown, W. B. (1962). Exact numerical solutions of the complete linearized equations for the stability of compressible boundary layers. Northrop Aircraft Inc., Norair Division Rep. NOR-62-15.

Brown, W. B. (1967). Stability of compressible boundary layers. AIAA J. 5, 1753-1759.

Bussmann, K., and Münz, H. (1942). Die Stabilität der laminar Reibungs-schicht mit Absaugung. fb. dtsch. Luftfahrtf. Zbl. wiss. Ber.-Wes I, 35.

Chiarulli, P., and Freeman, J. C. (1948). Stability of the Boundary Layer. Tech. Rep. no. F-TR/1197-1A, Headquarters Air Material Command, Dayton, 104 pp.

Conte, S. O., and Miles, J. W. (1959). On the numerical integration of the Orr-Sommerfeld equation. SIAM J. 7, 361-366.

Demetriades, A. (1958). An experimental investigation of the stability of the hypersonic laminar boundary layer. California Institute of Technology, Guggenheim Aeronautical Laboratory, Hypersonic Research Project, Memo. No. 43.

Drazin, P. G., and Howard, L. N. (1966). Hydrodynamic stability of parallel flow of inviscid fluid. In "Advances in Applied Mechanics" (G. Kuerti, ed.), pp. 1-89. Academic Press, New York and London.

Dunn, D. W. (1953). On the Stability of the Laminar Boundary Layer in a Compressible Fluid. Doctorate dissertation. Massachusetts Institute of Technology.

Dunn, D. W., and Lin, C. C. (1955). On the stability of the laminar boundary layer in a compressible fluid. J. Aero. Sci. 22, 455-477.

Foote, J. R., and Lin, C. C. (1950). Some recent investigations in the theory of hydrodynamic stability. Quart. Appl. Math. 8, 265-80.

Gaster, M. (1963). A note on a relation between temporally increasing and spatially increasing disturbances in hydrodynamic stability. J. Fluid Mech. 14, 222-224.

Gill, A. E. (1965). Instabilities of "top-hat" jets and wakes in compressible fluids. Phys. Fluids 8, 1428-1430.

Hartree, D. R. (1937). On an equation occurring in Falkner and Skan's approximate treatment of the equations of the boundary layer. Proc. Cambridge Phil. Soc. 33, Part II, 223.

Heisenberg, W. (1924). Über Stabilität und Turbulenz von Flüssigkeitsströmen. Ann. Phys. Lpz., (4), 74, 577-627.

Høiland, E. (1953). On two-dimensional perturbations of linear flow. Geofys. Publikasjoner, Norske Videnskaps-Akad. Oslo 18, No. 9, 1-12.

Holstein, H. (1950). Über die äussere und innere Reibungsschicht bei Störungen laminar Strömungen. Z. angew. Math. Mech. 30, 25-49.

Hughes, T. H., and Reid, W. H. (1965). On the stability of the asymptotic suction boundary-layer profile. J. Fluid Mech. 23, 715-735.

Kaplan, R. E. (1964). The stability of laminar incompressible boundary layers in the presence of compliant boundaries. Massachusetts Institute of Technology, Aero-Elastic and Structures Research Laboratory, ASRL-TR 116-1.

Kendall, J. M., Jr. (1967). Supersonic boundary-layer stability experiments. In Proc. of Boundary Layer Transition Study Group Meeting (W. D. McCauley, ed.), Air Force Rept. No. BSD-TR-67-213, Vol. II.

Kuchemann, D. (1938). Störungsbewegungen in einer Gasströmung mit Grenzschicht. ZAMM 18, 207-222.

Kurtz, E. F., Jr. (1961). Study of the stability of laminar parallel flows. Ph. D. Thesis, Massachusetts Institute of Technology.

Kurtz, E. F., Jr., and Crandall, S. H. (1962). Computer-aided analysis of hydrodynamic stability. J. Math. Phys. 41, 264-279.

Laufer, J., and Vrebalovich, T. (1960). Stability and transition of a supersonic laminar boundary layer on an insulated flat plate. J. Fluid Mech. 9, 257-299.

Lees, L. (1947). The stability of the laminar boundary layer in a compressible fluid. N. A. C. A. Tech. Rept. No. 876.

Lees, L. (1952). Instability of laminar flows and transition to turbulence. Consolidated Aircraft Corporation Rep. ZA-7-006, 38 pp. San Diego, California.

Lees, L., and Lin, C. C. (1946). Investigation of the stability of the laminar boundary layer in a compressible fluid. Tech. Notes Nat. Adv. Comm. Aero., Wash., no. 1115, 83 pp.

Lees, L., and Reshotko, E. (1962). Stability of the compressible laminar boundary layer. J. Fluid Mech. 12, 555-590.

Lighthill, M. J. (1953). On boundary layers and upstream influence. Proc. Royal Soc. (A) 217, 344.

Lin, C. C. (1945). On the stability of two-dimensional parallel flows. Parts I, II, III. Quart. Appl. Math. 3, 117-42, 218-34, 277-301.

Lin, C. C. (1954). Some physical aspects of the stability of parallel flows. Proc. Nat. Acad. Sci., Wash., 40, 741-7.

Lin, C. C. (1955). "The Theory of Hydrodynamic Stability." Cambridge Univ. Press., London and New York.

Mack, L. M. (1960). Numerical calculation of the stability of the compressible, laminar boundary layer. California Institute of Technology, Jet Propulsion Laboratory Rept. No. 20-122.

Mack, L. M. (1965a). Computation of the stability of the laminar compressible boundary layer. In "Methods in Computational Physics" (B. Alder, ed.), Vol. 4, pp. 247-299. Academic Press, New York.

Mack, L. M. (1965b). Stability of the compressible layer according to a direct numerical solution. Recent Developments in Boundary Layer Research (AGARDograph 97, part I), 329-362.

Miles, J. W. (1960). The hydrodynamic stability of a thin film of liquid in uniform shearing motion. J. Fluid Mech. 8, 593-610.

Prandtl, L. (1921). Bemerkungen uber die Entstehung der Turbulenz. Z. angew. Math. Mech. 1, 431-436.

Prandtl, L. (1935). Article in Aerodynamic Theory, edited by W. F. Durand, 3, 178-90. Berlin: Julius Springer.

Pretsch, J. (1941). Die Stabilität einer ebenen Laminarströmung bei Druckgefälle und Druckansteig. fb. dtsch. Luftfahrtf. Zbl. Wiss. Ber.-Wes. I, 158-175.

Pretsch, J. (1942). Die Anfachung instabler Störungen in einer laminaren Reibungsschicht. fb. dtsch. Luftfahrtf. pp. 154-71.

Radbill, J. R., and Van Driest, E. R. (1966). A new method for prediction of stability of laminar boundary layers. AFOSR Rept. No. 66-0702.

Reid, W. H. (1965). The stability of parallel flows. In "Basic Developments in Fluid Dynamics" (M. Holt, ed.), Vol. 1, pp. 249-307. Academic Press, New York .

Reshotko, E. (1960). Stability of the compressible laminar boundary layer. California Institute of Technology, Guggenheim Aeronautical Laboratory, GALCIT Memo. No. 52.

Reshotko, E. (1962). Stability of three-dimensional compressible boundary layers. N. A. S. A. Tech. Note D-1220.

Schlichting, H. (1933a). Zur Entstehung der Turbulenz bei der Plattenströmung. Gesellschaft der Wissenschaften. Göttingen. Mathematisch-Physikalische Klasse. Nachrichten, 181-208.

Schlichting, H. (1933b). Berechnung der Anfachung kleiner Störungen bei der Plattenströmung. Z. Angew. Math. Mech. 13, 171-174.

Schlichting, H. (1935). Amplitudenverteilung und Energiebilanz der kleinen Störungen bei der Plattengrenzschicht. Gesellschaft der Wissenschatten. Göttingen. Mathematisch-Naturwissenschattliche Klasse, 1, 47-78.

Schlichting, H. (1940). Über die theoretische Berechnung der kritischen Reynoldschen Zahl einer Reibungsschicht in beschleunigter und verzögerter Strömung. Jb. d. dt. Luftfahrtforschung I, 97.

Schlichting, H. (1960). "Boundary Layer Theory," 4th. ed. McGraw-Hill, New York.

Schlichting, H., and Ulrich, A. (1942). Über die Berechnung der Umschlagsstelle laminar-turbulent. f. dtsch. Luftfahrtf. I, 8-35.

Schubauer, G. B., and Skramstad, H. K. (1947). Laminar boundary layer oscillations and transition on a flat plate. J. Aero. Sci. 14, pp. 69-78.

Shen, S. F. (1954). Stability of Laminar Flows. "Theory of Laminar Flows" (High Speed Aerodynamics and Jet Propulsion, Vol. 4), Section G. Princeton Univ. Press, Princeton, New Jersey.

Squire, H. B. (1933). On the stability of three-dimensional disturbances of viscous flow between parallel walls. Proc. Roy. Soc. (London) A142, 621-628.

Smith, A. M. O. (1954). Improved solutions of the Falkner and Skan boundary layer equation. Sherman Fairchild Fund Paper No. FF-10. Inst. of Aero. Sci.

Stuart, J. T. (1963). Hydrodynamic stability. In "Laminar Boundary Layers" (L. Rosenhead, ed.), pp. 629-670. Oxford Univ. Press (Clarendon), London and New York.

Stuart, J. T. (1956). On the role of Reynolds stresses in stability theory. J. Aero. Sci. 23, 86-88.

Taylor, G. I. (1915). Eddy motion in the atmosphere. Phil. Trans. Roy. Soc. (A), 215, 1-26.

Taylor, G. I. (1938). Some recent developments in the study of turbulence. Proc. 5th Int. Congr. Appl. Mech., Cambridge, U.S.A., pp. 294-310.

Tietjens, O. (1925). Beiträge zur Entstehung der Turbulenz. Z. Angew. Math. Mech. 5, 200-217.

Thomas, L. H. (1953). The stability of plane Poiseuille flow. Phys. Rev. 91, 780-783.

Timman, R., Zaat, J. A., and Burgenhout, T. J. (1956). Stability diagrams for laminar boundary-layer flow. Amsterdam, Nationaal Luchtvaart Laboratorium, Tech. Note F-193.

Tollmien, W. (1929). Über die Entstehung der Turbulenz. Gesellschaft der Wissenschaften. Göttingen. Mathematisch-Naturwissenschaftliche Klasse. Nachrichten, 21-44.

Tollmien, W. (1935). Ein allgemeines Kriterium der Instabilität laminarer Geschwindigkeitsverteilungen. Gesellschaft der Wissenschaften. Göttingen. Mathematisch-Naturwissenschaftliche Klasse, Nachrichten, 50, 79-114.

Tollmien, W. (1947). Asymptotische Integration der Störungsdifferentialgleichung ebener laminarer Strömungen bei hohen Reynoldschen Zahlen. Z. Angew. Math. Mech. 25/27, 33-50, 70-83.

Wazzan, A. R., Okamura, T., and Smith, A. M. O. (1966). Spatial stability study of some Falkner-Skan similarity profiles. Proc. Fifth U. S. Natl. Congr. Appl. Mech. p. 836. A.S.M.E., University of Minnesota, June 1966.

Wasow, W. (1948). The complex asymptotic theory of a fourth order differential equation of hydrodynamics. Ann. Math. (2), 49, 852-71.

Wasow, W. (1953). Asymptotic solution of the differential equation of hydrodynamic stability in a domain containing a transition point. Ann. Math. 58, 222-52.

Zaat, J. A. (1958). Numerical contribution to the stability theory of boundary layers (in German). International Union of Theoretical and Applied Mechanics. Grenzschichtforschung Symp. pp. 127-138. Springer, Berlin.